Thermochemical valorization of Acrocomia aculeata endocarp : solid and liquid pyrolysis products analysis

Shirley Duarte Chavez

Thèse de doctorat

NNT: 2021UPAST012

Thermochemical valorization of *Acrocomia aculeata* endocarp: solid and liquid pyrolysis products analysis

Thèse de doctorat de l'Université Paris-Saclay et de Universidad Nacional de Asunción

École doctorale n° 579: Sciences mécaniques et énergétiques, matériaux et géosciences (SMEMAG)
Spécialité de doctorat: Génie des Procédeés
Unité de recherche : Université Paris-Saclay, CentraleSupélec, Laboratoire de Génie des Procédés et Matériaux, 91190, Gif-sur-Yvette, France.
Référent: CentraleSupélec

Thèse présentée et soutenue à Asunción, le 22 janvier 2021, par

Shirley Johanna Magalí Duarte Chávez

Composition du jury:

M. Marcelo CASTIER Professeur, Universidad Paraguayo Alemana de Asunción Professeur, Texas A&M University at Qatar	Président & Rapporteur
M. Gérald DEBENEST Professeur, Institut National Polytechnique de Toulouse	Rapporteur & Examinateur
Simone FAVARO Maitre de Conferences, Agricultural Research Corporation (EMBRAPA)	Examinatrice
Mme. Giana ALMEIDA Maitre de Conferences, AgroParisTech	Examinatrice
M. Sergio MOTOIKE Professeur, Universidade Federal de Viçosa, Brazil	Examinateur
M. Patrick PERRÉ Professeur (HDR), CentraleSupélec	Directeur
M. Dario ALVISO Professeur, Universidad Nacional de Asunción Universidad de Buenos Aires	Codirecteur
M. Pin LU Ingénieur de recherche, CentraleSupélec	Coencadrante
Juan Carlos ROLÓN Professeur (HDR), CentraleSupélec (retraité) Professeur, Universidad Nacional de Asunción (retraité)	Invité
Juan Francisco FACETTI Professeur, Universidad Nacional de Asunción	Invité

université PARIS-SACLAY | ÉCOLE DOCTORALE Sciences mécaniques et énergétiques, matériaux et géosciences (SMEMAG)

Titre: Valorisation thermochimique de l'endocarpe de noix de coco —Acrocomia aculeata— : analyse des produits solides et liquides de pyrolyse

Mots clés: Endocarpe de noix de coco, Biomasse lignocellulosique, Bio-huile, Charbon de bois, Pyrolyse, Modéle cinétique, Combustion, Substituts, Gazéification

Résumé: La mise en place d'une industrie biosourcée robuste avec des produits chimiques, des matériaux et des carburants de grande valeur a pour objectif économique de fournir l'incitation financière nécessaire pour stimuler son expansion. L'endocarpe de noix de coco d'Acrocomia aculeata est un déchet agro-industriel intéressant qui peut être utilisé comme matière première pour la production de ces produits à haute valeur ajoutée, dans le contexte des bio-raffineries de lignocellulose. En raison de sa faible teneur en humidité et de sa teneur élevée en lignine, l'endocarpe peut être traité via des traitements thermochimiques tels que la pyrolyse et la gazéification. En plus des matières premières, la distribution des produits dépend aussi des paramètres du procédé. L'étude de la pyrolyse de la biomasse ainsi que des caractéristiques de ses produits dans différentes conditions est essentielle afin d'identifier le traitement le plus efficace. Le but de ce travail est d'étudier la pyrolyse de l'endocarpe d'A. Aculeata en tant que matière première pour la production de biocarburants ou de matériaux tels que la bio-huile et le charbon de bois. Afin d'atteindre cet objectif, les modifications des propriétés de la biomasse ont été évaluées avant et après 2 heures de pyrolyse isotherme entre 250 et 550 °C. Différentes méthodes analytiques ont été utilisées pour évaluer les altérations du produit: analyse élémentaire, analyses de la surface et de la taille des pores, visualisation ESEM et SEM/FEG et détermination de la sorption dynamique à la vapeur. Des mesures de perte de masse anhydre ont été effectuées à l'échelle microscopique pour avoir un aperçu des mécanismes de réaction. Un modèle cinétique basé sur la méthode de l'énergie d'activation distribuée a été utilisé pour reproduire la perte de masse observée et pour déterminer les paramètres cinétiques du processus. La pyrolyse lente et gazéification de l'endocarpe de noix de coco et de ses carbonisés a été réalisée dans différentes conditions, en évaluant expérimentalement le taux de conversion et les modifications de la porosité et de la surface au cours du procédé. De la même manière, des études expérimentales et numériques de combustion de la bio-huile de pyrolyse de l'endocarpe de noix de coco ont été conduites. La pyrolyse a été effectuée sur un endocarpe de noix de coco torréfié et les bio-huiles recueillies ont été analysées par chromatographie en phase gazeuse (GC)/spectrométrie de masse (MS). Sur la base de l'analyse GC/MS, trois mélanges différents de toluène, d'éthanol et d'acide acétique, représentatifs de la chimie du carburant réel, ont été proposés comme substituts pour mener des études de combustion numérique. Un mécanisme de cinétique chimique pour l'oxydation des mélanges toluène/éthanol/acide acétique a été développé. Pour ce faire, une combinaison du modèle chimique de Huang et al (2017) pour le toluène et celui de Christensen et al (2016) pour les réactions éthanol/acide acétique a été proposée. La modélisation cinétique de l'oxydation de la bio-huile a été réalisée à l'aide du code REGATH. Le modèle combiné comprend 180 espèces et 1495 réactions. Afin de valider le modèle proposé, les travaux se concentrent sur des études numériques de la combustion de mélanges toluène/éthanol/acide acétique utilisant une auto-inflammation à volume constant 0D ainsi que des configurations de flammes prémélangées gazeuses 1D à propagation libre. Différentes conditions de fonctionnement des flammes, telles que les rapports d'équivalence, la pression et la température, ont été étudiées. Nos résultats montrent l'intérêt de l'endocarpe de noix de coco et de ses carbonates en tant que combustible solide ou comme matière première pour la bio-huile ou dans un procédé de gazéification.

Title: Thermochemical valorization of —Acrocomia aculeata— endocarp: solid and liquid pyrolysis products analysis

Keywords: Coconut endocarp, Lignocellulosic biomass, Bio-oil, Char, Pyrolysis, Kinetic model, Combustion, Surrogates and Gasification.

Abstract: The development of a robust bio-based industry with high value chemicals, materials and fuels is of major technical and economical interest. In the context of the so-called lignocellulose bio-refinery, coconut endocarp of Acrocomia aculeata is an interesting agro-industrial waste that can be used as feedstock for the production of these high value-added products. Because of its low-moisture and high lignin contents, it can be processed using thermo-chemical treatments, such as pyrolysis and gasification. However, the product distribution depends on the reactor type, the process parameters as well as the feedstocks. The evaluation of biomass pyrolysis behavior as well as its products characteristics under different conditions is essential, in order to propose the most efficient processes. The aim of this work is to investigate the pyrolysis of endocarp of A. aculeata as potential feedstock to produce biofuel or materials such as bio-oil and charcoal. In order to achieve this goal, alterations of its fundamental properties were evaluated before and after 2h of isothermal pyrolysis between 250 and 550 °C. Different analytical methods were used to assess the product alterations: elemental analysis, surface area and pore size analyses, ESEM and SEM/FEG visualization and dynamic vapor sorption determination. Anhydrous weight loss measurements have been performed at the microscale to have an insight into the reaction mechanisms. A kinetic model based on the Distributed Activation Energy Method has been used to reproduce the observed mass loss and to determine the process kinetic parameters. Moreover, the slow pyrolysis/gasification of the coconut endocarp and its chars were carried out under different conditions, experimentally assessing the conversion rate and the changes of porosity and surface area during the process. In addition, experimental and numerical combustion studies of pyrolysis bio-oil from coconut endocarp were conducted. Pyrolysis was performed on torrefied coconut endocarp and the collected bio-oils were analyzed by gas chromatography/mass spectrometry. Based on the GC/MS analysis, three different blends of toluene, ethanol and acetic acid representative of the real fuel chemistry were proposed as the surrogates to carry out numerical combustion studies. A chemical kinetics mechanism for toluene/ethanol/acetic-acid blends oxidation was developed. This will be done by combining the chemical model of Huang et al (2017) for toluene, and that of Christensen et al (2016) for ethanol/acetic-acid reactions. The kinetic modeling for bio-oil oxidation was performed using the REGATH code. The combined model consists of 180 species and 1495 reactions. In order to validate the proposed model, the work focuses on numerical studies of the combustion of toluene/ethanol/acetic-acid blends using 0-D constant-volume auto-ignition as well as 1-D freely-propagating gaseous premixed flame configurations. Different flames operating conditions such as equivalence ratios, pressure and temperature were studied. In conclusion, our results provide sufficient evidence for long-term application of this feedstock and its chars as a solid fuel or raw material for bio-oil, or in the gasification process.

Université Paris-Saclay
Espace Technologique / Immeuble Discovery
Route de l'Orme aux Merisiers RD 128 / 91190 Saint-Aubin, France

General Preamble

The present work aims to contribute towards the transition to a sustainable bio-economy. It is important to continue with research studies using *Acrocomia aculeata* as a promising crop to be used in productive systems. This work focuses on the generation of higher value-added products from *A. aculeata* fruit processing wastes (coconut endocarp), using thermo-chemical treatments and analyzing its products by means of experimental techniques and numerical modelling. We focus on this feed-stock, since its fruits have a great current relevance as a raw material for the sustainable generation of vegetable oil of prominent quality and quantity, biofuels and others bio-products.

This thesis has been carried out in collaboration between the Laboratoire de Génie des Procédés et Matériaux (LGPM, CentraleSupélec - Université Paris Saclay, France) and Laboratorio de Mecánica y Energía (LAMEEN, FIUNA - Facultad de Ingeniería de la Universidad Nacional de Asunción, Paraguay).

This manuscript is written in an article-based form. Two publications therefore constitute chapters 3 and 6, with unpublished supplementary information included in chapters 4 and 5. The content of the publications have been slightly modified from the published versions, according to the general format of the manuscript and mainly in the Introduction and Materials and Methods sections of the articles, in order to avoid redundant information to the reader.

The references to the publications are as follows:

- Shirley Duarte, Pin Lu, Giana Almeida, Juan Carlos Rolón, Patrick Perré. Alteration of physico-chemical characteristics of coconut endocarp —*Acrocomia aculeata*— by isothermal pyrolysis in the range 250 - 550 °C. Journal of Analytical and Applied Pyrolysis. Volume 126, July 2017, Pages 88-98.

DOI: https://doi.org/10.1016/j.jaap.2017.06.021

- Dario Alviso, Shirley Duarte, Nelson Alvarenga, Juan Carlos Rolón, Nasser Darabiha. Chemical Kinetic Mechanism for Pyrolysis Bio-oil Surrogate. Energy Fuels. Volume 32, Issue 10, August 2018, Pages 10984-10998.

  <DOI:https://doi.org/10.1021/acs.energyfuels.8b02219>

- Shirley Duarte, Pin LU, Patrick Perré. Kinetic parameters estimation for coconut endocarp pyrolysis.

  To be submitted to *Current Opinion in Green and Sustainable Chemistry.*

The references of presentations at international conferences and its conference proceedings are as follows:

- Shirley Duarte, Pin Lu, Juan Rolon, Gonçalo Monteiro, Patrick Perré. Pag. 209. PYRO2016 Conference (21st International Symposium on Analytical and Applied Pyrolysis), in Nancy, France, on May 9-12, 2016.

  <Conference book: PYRO2016>

- Shirley Duarte, Dario Alviso, Nelson Alvarenga, Juan Carlos Rolón. 25TH European Biomass Conference Exhibition, in Stockholm, Sweden, on June 12-15, 2017.

  <Conference book: EUBCE2017>

- Shirley Duarte, Cassandra Giesbrecht, Pin Lu, Patrick Perré. P2.26. 5th Green and Sustainable Chemistry Conference, ONLINE, on Nov 10-11, 2020.

  <Abstracts: GREN2020>

Contents

List of Tables

List of Figures

Introduction

The world is moving towards a bio-based economy, where the gradual but sustainable introduction of biofuels and bioproducts into the global market is sought. There is a progressive replacement of fossil fuels and petroleum products, for example, by using mixtures of liquid biofuels for transportation purposes and others.

Biomass takes an increasingly important role in this transition to a bio-based economy. This is because it is the main source of renewable raw material for the generation of these products. The concept of bio-economy, is expected to gradually affect all industries, where a continuous changeover to more complex bio-renewable feedstocks like agricultural residues will occur.

The increase in the quality of life and the growth of any nation, means an increase in its energy requirements, which also leads to an increase in the world oil price [29]. Biofuels, referred to any solid, liquid or gaseous fuels generates from biomass, emerges as an alternative to cover these high requirements [30].

The Acrocomia endocarp has the advantage of being a second generation feedstock. This agro-industrial waste is generated in great quantity, about 7 ton per/ha/year [31] during the almond and pulp oils production from *A. aculeata* fruit. High oil yields (about 4-6 ton oil/ha) and oil properties similar to palm oil (*Elaeis guineensis*) [32, 33], which has the 40 % of the market of plant oils [34], have attracted the attention of Acrocomia palm. In addition, the pulp oil, can be used for biodiesel production and cosmetic applications (pulp of fruits presented a fat content of about 25.1-32.1 %) and the almond oil for cosmetic and as edible oil (has a mean fat content of about 59.3-68.9 %) [35, 36, 37].

Another great advantage of *A. aculeata* plant is that it can even grow in mixed crops and does not require large amounts of water. It can grow in degraded land or nutrient-poor sandy soils. It may also serve as a carbon sink and enrich the soil with organic matter during its productive lifetime of about 70 years. In addition, it is an alternative to the deforestation from the generation

of charcoal with high energy density, from the waste of the processing of its fruits [34, 36, 38].

Research Motivation

In recent decades, several investigations have been carried out with different purposes related to *A. aculeata* [39, 18]. Most of these works have focused on the performance and quality of the oils extracted from their pulp and almonds [37]. Other reports focus on the combustible properties of the by-products generated during the processing of their fruit [40, 41, 42]. Concerning biofuels production, the focus of the researches were on bio-diesel generation and its properties from pulp oil, but no in the liquid product of the pyrolysis of its process residues [1].

However, there is a lack of scientific research related to the evaluation of the by-products of *A. aculeata* fruit processing, specifically "coconut endocarp". Larger scientific research is needed to evaluate the diversity of potential end products for a biorefinery. In this sense, there is a gap in the literature related to the evolution in chemical and structural properties of coconut endocarp during its isothermal pyrolysis. In particular, the charcoal properties will indicate the more appropriate uses for this material (i.e. as solid fuel, a raw material for the gasification process, or others).

Furthermore, kinetic parameters of Acrocomia endocarp pyrolysis process were not yet determined. Pyrolysis process can be carried out with the main purpose of obtaining bio-oil. Physical properties of bio-oils from coconut endocarp have been analyzed in our previous work [6]. However, its chemical composition was not yet analyzed, and its combustion chemical kinetics mechanism was not yet proposed. Finally, the activated carbon generated from Acrocomia endocarp have shown very high surface area, and to the best of our knowledge this is the first time that water vapor has been used as pyrolysis and gasification agent simultaneously for this feedstock.

Objectives and Layout

This thesis has the following main objectives:

To evaluate the evolution in chemical and structural properties of coconut endocarp —*Acrocomia aculeata*— during its isothermal pyrolysis.

To determine the kinetic parameters of the pyrolysis process, using at least five temperatures simultaneously.

To evaluate the surface area and porosity of activated carbons obtained under different slow-pyrolysis/gasification conditions.

To determine the chemical composition of the bio-oil produced from torrefied coconut endocarp —*Acrocomia aculeata*—.

To propose a chemical kinetic mechanic for the bio-oil combustion based in a surrogate selected from its chemical composition.

Manuscript outline

To achieve the objectives of this work, the general structure of this manuscript has been organized as follows:

A non-exhaustive review of biomass as a sustainable resource, emphasizing the potential of Acrocomia palm as a new feedstock for biorefinery is presented in Chapter 1. The general concept of thermochemical process: pyrolysis, combustion and gasification are presented, where it is included a short review about the use of bio-oil as a non-conventional fuel and its combustion characteristics.

Chapter 2 details the experimental procedure, the facilities and the analytical techniques used to obtain the results of the physicochemical evolution along the thermal decomposition of the endocarp of *Acrocomia aculeata* fruit samples and the kinetic mechanic model for the bio-oil combustion of coconut endocarp.

Chapter 3 presents the experimental procedure and results obtained along the thermal decomposition of the endocarp of *Acrocomia aculeata* fruit samples, before and after 2 h of isothermal pyrolysis in the range 250 to 550 °C. The physicochemical evolution measured by techniques as differential thermogravimetric (DTG) analysis, elemental analysis, surface area and pore size analyses, ESEM and SEM/FEG observation and dynamic vapor sorption evaluation.

Two complementary studies are developed in Chapter 4 and Chapter 5. The first one is to determinate the kinetic parameters of the pyrolysis process and the second is to observe the gasification rate and the porosity's properties of the activated carbon obtained under different conditions.

Finally, Chapter 6 presents the chemical composition of the coconut endocarp bio-oil and the numerical simulation using REGATH. A chemical kinetic model for its combustion is proposed. To validate the model, the work focuses on numerical studies of the combustion of toluene/ethanol/acetic-acid blends using 0-D constant-volume auto-ignition as well as 1-D freely-propagating gaseous premixed flame configurations.

Chapter 1

Overview

This chapter provides a review of the lignocellulosic biomass structure, the potential of Acrocomia palm as a sustainable source of feedstock for biorefinery and the physico-chemical properties of coconut endocarp. The general concept of thermo-chemical processes: pyrolysis, combustion and gasification are also presented, with its respective theoretical, fundamental and typical product composition. Moreover, a non-exhaustive review about the use of bio-oil as a non-conventional fuel and its combustion characteristics are presented.

1.1 World energy demand and biofuel policies

The growth of any nation is directly related to energy consumption. According to the International Energy Outlook 2018 (IEO2018) the world energy consumption will grow by 21% between 2020 and 2040, which would represent from 643.5 quadrillion kJ in 2020 to 697.4 quadrillion kJ in 2030 and 779.7 quadrillion kJ in 2040 (Fig. 1.1), with more than half of the increase attributed to countries outside the OECD (Organization for Economic Cooperation and Development), including China and India, where strong economic growth drives increasing demand for energy [29].

This entails an increase in the world oil price, from its current price of about 60 US-dollars per barrel to more than double by 2040 [29].

Giving the world energy demand forecast, the focus all over the globe is starting to blend biofuels (bioalcohols, vegetable oils (bio-oils), biodiesels and biocrude and synthetic oils), with petroleum fuels. Bio-fuels also refers to the

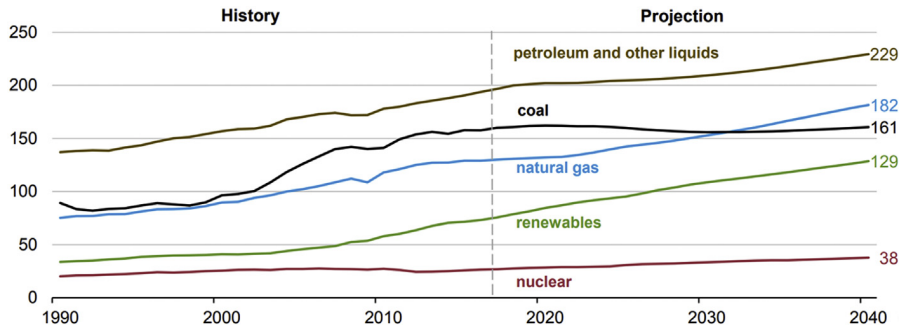

Figure 1.1: World energy consumption by fuel type, 1990-2040 (quadrillion British thermal units "Btu", 1 Btu = 1.055 kJ). Source: International Energy Outlook 2018 - IEO 2018 [14].

solid or gaseous fuels that are produced from biomass [30].

Thereby, the United States and the European Union have renewable fuel standards and bio-fuel policies, which have been implemented to promote a smooth transition to a bio-based economy. The main standards are, Renewable Fuel Standards (RFSs) by the Unites States, which establish a minimum volume of biofuels to be used in the national transportation fuel supply [43], and the European Union (EU) Biofuel Policy [44].

1.2 Biomass as a sustainable resource

Biomass is any biological material that derives from living matter or that was recently alive, that is, from animals, plants or plant derived materials and were produced directly or indirectly by photosynthesis [45]. Lignocellulosic biomass refers to plant stems, whose main constituents are cellulose hemicellulose and lignin (Fig. 1.2) as wood and agricultural residues [15].

Global biomass production is estimated approximately between 100 and 220 billion tons per year and lignocellulosic biomass is one of the most abundant renewable resource [46]. Biomass can be converted in liquid, solid and gaseous fuels in contrast with other renewable sources giving heat and power. Therefore, the main potential of lignocellulosic biomass as renowable source is to produce heat, electricity, fuels, chemicals, and other products.

1.2.1 Lignocellulosic biomass structure

The basic components of the lignocellulosic biomass, also called second-generation feedstocks, are cellulose, hemicelluloses and lignins (see Fig. 1.2). Apart from wood produced in forest, the most important world production, they are mostly derived from agricultural processes, such as wastes (e.g. corn cobs and stover, wheat straw, rice hulls, etc.) and usually they are combusted in boilers for heat and electricity, for forage or into croplands [47, 48].

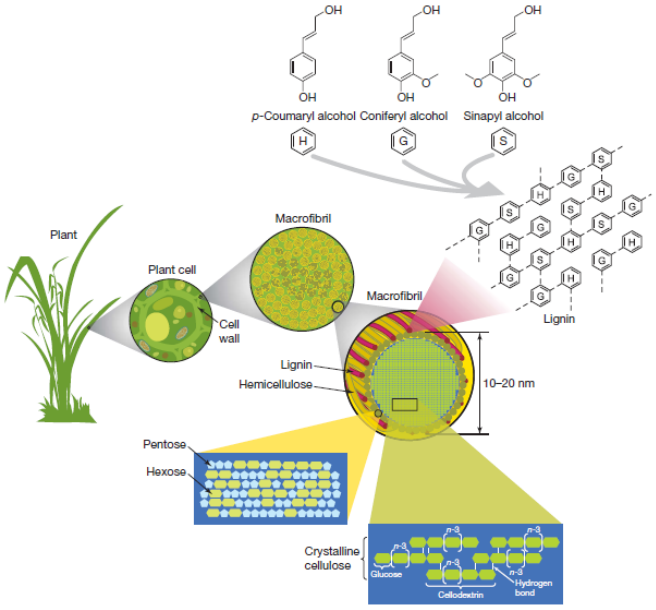

Figure 1.2: Main components of lignocellulose Biomass (reprinted from Rubin [15] with permission).

The plant biomass comprises an enormous variety of polymeric substances with multifunctional molecular structures. Concerning the chemical structure of the main components, we can state:

Cellulose: it is a linear homogeneous structural polysaccharide composed of D-glucose units in the $^4C_1$ conformation, with a high molecular-weight (more than 100), being the number of repeating saccharide monomers between 5000-10000 and the basic repeating unit consists of two glucose anhydride units called cellobiose unit. Cellulose can be amorphous or crystalline, the latter form being more resistant to thermal decomposition than hemicellulose. Normally comprising between 40-50 % wt of dry wood, thus it is the primary component and its fibrous and insoluble nature gives the strength to the cell wall [49, 17].

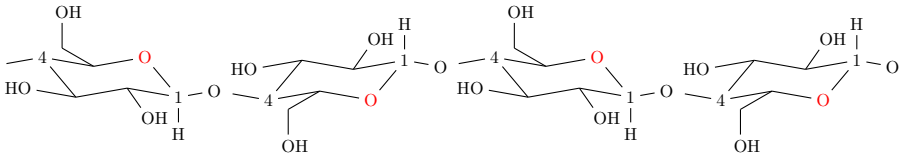

Figure 1.3: Chemical structure of cellulose.

Hemicellulose or polyose: it is considered the second major wood chemical constituent (usually between 25-35 % wt of dry wood), is a ramified heterogeneous structural polysaccharides composed of a mixture units of D-xylose, L-arabinose, D-mannose, D-galactose, D-glucose, $4-O-$methyl glucuronic acid and galacturonic acid residues. The number of repeating saccharide monomers is lower than cellulose, only about 150. The monosaccharidic composition, depends on the phylogenetic origins of the plant species [50].

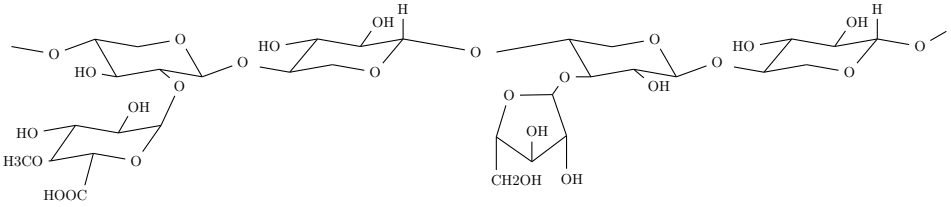

Figure 1.4: Chemical structure of hemicellulose

Lignin: the third major component of wood is lignin. Lignin derives primarily from three hydroxycinnamyl alcohols, p-coumaryl, coniferyl and sinapyl alcohols. It is a phenyl propanoid three-dimensional, highly branched polymer, composed of syringil (S), guaiacyl (G) and *p*-hydroxyphenyl (H) units. The internal structure consists of an irregular array of variously bonded "hydroxy-" and "methoxy" substituted phenylpropane units, which exhibit the *p*-coumaryl, coniferyl and sinaphyl structures [51, 52].

Many factors such as type of plants, tissues, cell-type, stages of growth, and also the environmental conditions can influence in the content, composition, and structure of the lignin. Lignin compositions from three *A. aculeata* fruit parts selected (stalk, epicarp and endocarp) have been studied by [16] using two-dimensional nuclear magnetic resonance (2D-NMR) spectroscopy and analytical pyrolysis coupled to gas chromatography and mass spectrometry (Py-GC/MS) (Fig. 1.5).

Lignocellulosic biomass also contains other constituents in less proportion, such as pectins, soluble sugars, starch, proteins, which are commonly

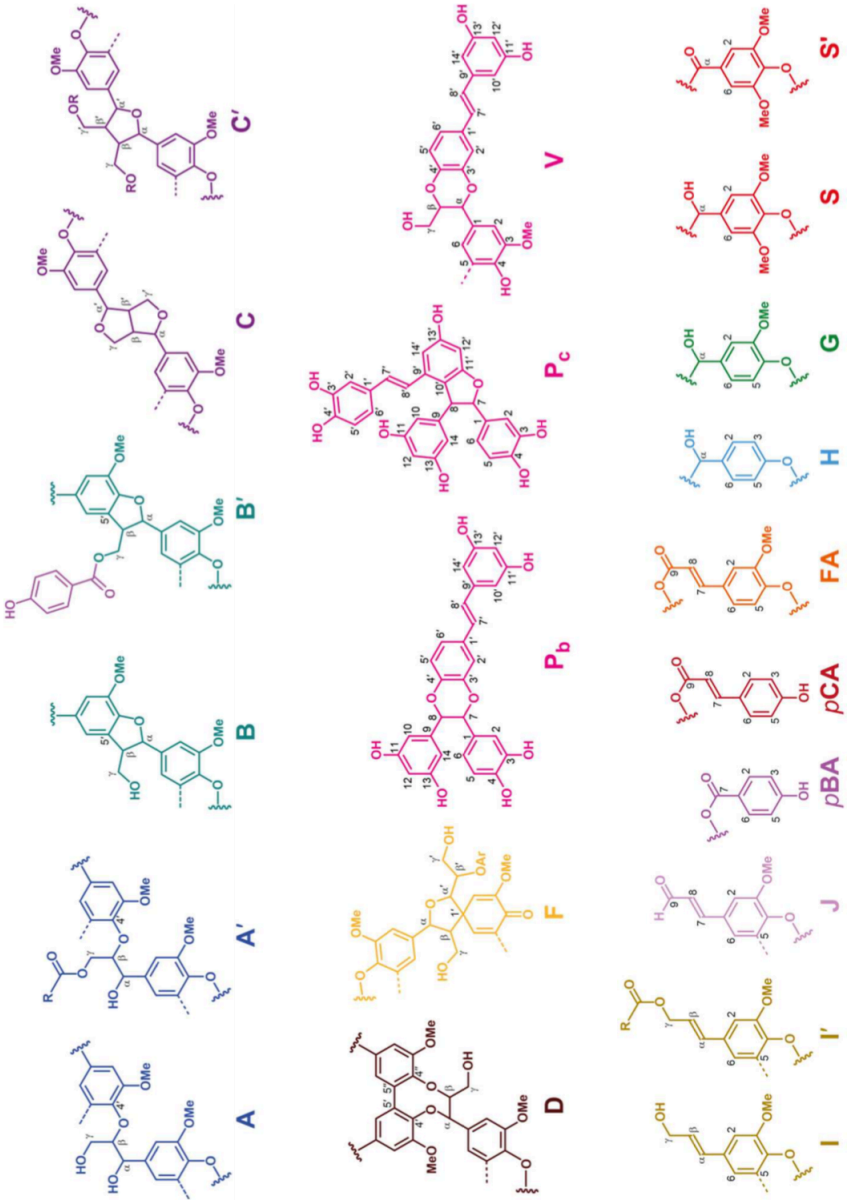

Figure 1.5: Main structures present in the lignins from three parts of *A. aculeata* fruit by 2D HSQC NMR (reprinted from del Río [16] with permission). **A**: $\beta - ethers$; **A'**: $\beta - ether$ structures with acylated (by acetate, benzoate, $p-$hydroxybenzoate or $p-$coumarate) $\gamma - OH$; **B**: phenylcoumaran; **B'**: phenylcoumarans with $p-$hydroxybenzoates acylating the $\gamma - OH$; **C**: resinols; **C'**: tetrahydrofuran structures formed by $\beta - \beta'$-coupling of monolignols acylated at the $\gamma - OH$; **D**: dibenzodioxocins; **F**: spirodienones; **P_b**: benzodioxane $-$ type piceatannol dimeric structures; **P_c**: phenylcoumaran$-$type piceatannol dimeric structures; **V**: benzodioxane structures formed by cross$-$coupling of piceatannol and a monolignol; **I**: cinnamyl alcohol end$-$groups; **I'**: cinnamyl alcohol end$-$groups acylated at the $\gamma - OH$; **J**: cinnamaldehyde $end - groups$; ***p*BA**: $p-$hydroxybenzoates; ***p*CA**: $p-$coumarates; **FA**: ferulates; **H**: $p-$hydroxyphenyl units; **G**: guaiacyl units; **S**: syringyl units; **S'**: C$\alpha-$oxidized syringyl units.

called as organic extractives, and small mineral content.

1.2.2 Processes for biomass conversion

Several processes can be used to convert biomass to energy or more value materials such as chemicals. The concept of biorefinery consists in using biomass instead of oil for producing energy and chemicals (Fig. 1.6) [53].

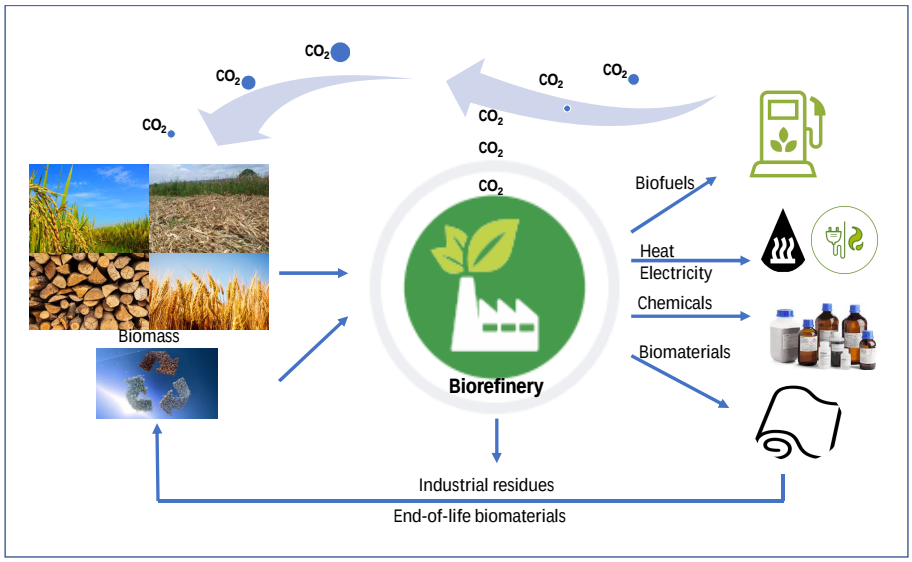

Figure 1.6: Main products of a biorefinery.

The biomass conversion methods are several, such as mechanical (e.g. biomass size reduction), chemical (e.g. hydrolysis and transesterification), biochemical and thermochemical processes [53, 17].

In general the biochemical processes (e.g. fermentation and anaerobic digestion) are more commonly used to produce products as alcohols, organic acids or biogas for example. However, the removal of lignin is usually a pretreatment to improve the conversion of sugars [54, 55].

The thermochemical methods (combustion/incineration, liquefaction, gasification, and pyrolysis) have important advantages as these methods use the entire biomass. Thus, reducing pretreatment costs (acid hydrolysis, enzyme hydrolysis) and the products can be obtained quickly (in a few seconds to an hour or two) [17].

1.2.3 Thermochemical Biorefinery

Several biorefinery concepts have been proposed as three-phase, whole-crop, green, lignocellulosic feedstock, integrated, two-platform and hybrid biorefineries [56]. Thermochemical biorefinery concept is seen to be a multiproduct plant based on a platform chemical. The main advantage is its capability to be combined or slightly modified to achieve multiproduct generation [56, 57].

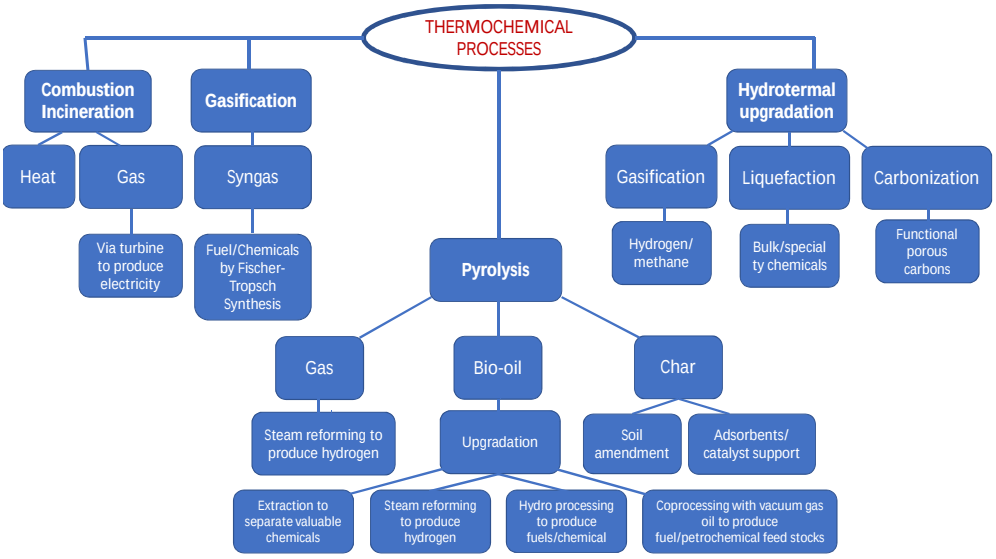

Figure 1.7: Products from thermochemical biorefineries. Adapted from [17].

In this type of biorefinery, thermochemical methods can be used isolated or integrated with others thermochemical methods, being the latter able to produce more value hydrocarbons than in an isolated manner [17].

The main products, both chemicals and energy carriers, from a thermochemical biorefinery are:

Syngas: is a mixture of gases (CO and H_2) from which is possible to produce chemicals (e.g. hydrocarbons C_1 to C_{50}) by Fischer-Tropsch reaction or biohydrogen [58].

Bio-oil: is a dark liquid, frequently considered as a microemulsion, obtained from the condensed vapors effluents from the pyrolysis process. Bio-oil has thousand compounds, most of which are oxygenated and very reactive. Chemically, it is a complex mixture of water, guaiacols, catecols, syringols, vanillins, furancarboxaldehydes, isoeugenol, pyrones, acetic acid, formid acid, other carboxilic acids, hydroxyaldehydes, hydroxyketones, sugars and phenolics compounds [59, 60].

Char, Charcoal or Bio-char: is defined as charred organic matter that has many applications depending on its physical and chemical properties. It can be used as an energy carrier, as an adsorbent and for improvement of the soil properties [61].

1.3 Biofuels and bio based products — An opportunity

The current trend is towards an increase in the requirements of primary energy in the world (EIA, 2018) [29]. In this regard, biofuels emerge as a sustainable alternative to hydrocarbons in the transport sector.

The conversion of biomass (an abundant carbon-neutral renewable resource) to solid, liquid and gases biofuels, promotes a gradual transition from a petroleum-based to a bio-based society and economy in which, biomass is the only renewable resource of carbon (compared to the others: solar, wind, water and geothermal) from which chemicals, materials, and fuels can be produced.

In addition, the establishment of a robust biobased industry (bio refinery) with high value biobased chemicals and materials has an economic goal providing the necessary financial incentive to stimulate its expansion.

1.3.1 Generation of biofuels

First-generation biofuels: they are mainly bioethanol, biodiesel and biogas, derived from edible materials such as sugar, starch, vegetable oil or animal fats. However, biogas can be also derived from feedstocks which are not in competition with the food and feed industry, such as waste and residues, in these cases it can be categorized as 2nd generation biofuel. The main producer countries of these first-generation biofuels are USA, Brazil and the European Union (Germany, France, Italy, Austria and Sweden) [62, 63]. Despite the advantages in terms of the production of these biofuels (high sugar and oil content of the raw materials and their relatively easy conversion into biofuel) there are other environmental issues (air pollution, acidification, eutrophication, ozone depletion, land use, etc) to be analyzed. The main problems of these biofuels, are that there is a direct competition with food for their feedstock and fertile land and also the high energy and water input required for crop cultivation and conversion which raises questions about the effective savings of CO_2 emissions and fossil energy consumption [53, 64, 65].

Second-generation biofuels: they are mainly gases (e.g. CO, CO_2, CH_4 and H_2 from lignocellulosic biomass) or synthetic liquid biofuels (e.g. Fisher Tropsch (FT)-diesel from biomass, bio-oil and bioethanol from lignocellulosic feedstock) derived from non-edible materials such as agricultural and forest residues and crops grown for biofuel purposes such as perennial grasses, Jatropha curcas L.) [66, 67, 68].

Finally briefly, the **Third-generation biofuels** are those derived from aquatic biomass such as algae and the **Fourth-generation biofuels** are derived from engineered plants and microorganisms [49].

1.3.2 Generation of bio-based products

Nowadays, only about 5% of all chemicals are bio-based [69]. The most common **bio-based chemicals** are: Succinic, Fumaric and Malic acids; 2,5-Furan dicarboxylic acid; 3-Hydroxypropionic acid; Aspartic acid; Glucaric acid; Glutamic acid; Itaconic acid; Levulinic acid; 3-Hydroxybutyrolactone; Glycerol; Sorbitol; Xylitol/Arabinitol [70]. Its characteristic of high value, lower volume bio-based chemicals contributes to a bio-based economy since only biofuels would not provide the necessary economic incentives.

With respect to high value materials, the most common **bio-based plastics** from biomass are: vinyl polymers, polyesters, polyamides, polyurethanes,

and synthetic rubbers. Harmsen et al, 2014 [71] have investigated the possible routes to produce polymers from biomass, such as those based in lactic acid and succinic acid. They can be well produced, since the oxygen atoms needed for these building blocks are already present in the biomass [71]. Producing these materials from biomass instead of fossil resources significantly contributes to the development of the bio-based economy.

1.4 *Acrocomia aculeata*: an alternative oil crop and feedstock for biorefinery

The South-American palm species *Acrocomia aculeata*, commonly known as mbocayá, macaw, macauba or just coconut palm, has attracted the attention of researchers in recent years, mainly for its great potential as a sustainable oil crop [40, 41, 42, 37]. Although *Acrocomia aculeata* is a native species of South America, its distribution spans the tropics and subtropics of Mexico and Central America as well. *Acrocomia aculeata* grows in regions that extend from Mexico to Argentina. In Paraguay, 23 palm species have been identified [18], and the *A. aculeata* specie fruit (coconut) has been processed since 1940 [39]. At present, no other country processes the fruit. Its many potential uses are shown in Fig. 1.8.

Concerning vegetable oils demand, it is continuously growing in the food, energy and chemical sectors. Compared to the oil palm—*Elaeis guineensis*—, which has 40 % of the market of plant oils [34], *A. aculeata* is a promising candidate for the production of plant oils from its high oil yields (about 4-6 Tm oil/ha) and from its oil properties similar to oil palm [32, 33]. The main commodities are the pulp oil produced in the mesocarp and the kernel or almond oil produced in the endosperm. On average, the pulp of fruits presented a fat content of about 25.1-32.1 %, whereas the almond had a mean fat content of about 59.3-68.9 % and the time for begin its production yield from its first harvest is around 4-6 years [35, 72, 37].

Most oil plants (palm, soybean, rapeseed, sunflower, etc.) compete for land area with rainforest [34]. To this context, *Acrocomia aculeata* is an alternative oil crops, it grows on a diversity of soils (it has been cultivated on degraded land or nutrient-poor sandy soils), the plant may also serve as a carbon sink and enrich the soil with organic matter during its productive lifetime of 60 to 70 years, it has potential for a sustainable expansion of plant oil production area, can even be grown in mixed cultures [72], and it does not compete with rainforest or fertile land (in Henderson et al. (1995) and Lorenzi et al. (2010), cited by [38]). Also, it has another advantages: it can be processed in

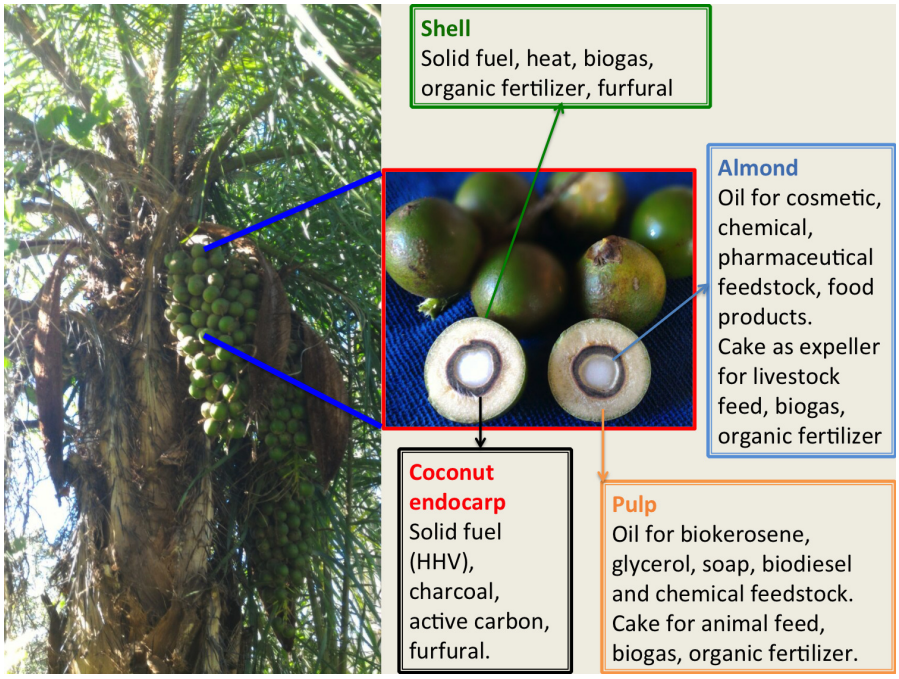

Figure 1.8: Potential uses of Acrocomia fruit.

small quantities, its storage stability (higher than *Elaeis* fruits), its processing technology is comparably simple and already cost-efficient at a scale of 5000 Tm of fruits per year, its average yield is 20 Tm of fruits per hectare and year, and a range of valuable by-products with local and international markets [39].

1.4.1 Industrialization of *A. aculeata* fruit in Paraguay

Five terrestrial ecoregions are recognized to be present in Paraguay (Fig. 1.9a) [18]. *A. aculeata* palms are distributed mainly in open areas as Savannah (Cerrado), and it constitutes the ecoregion with the highest palm species diversity [18].

The distribution of *A. aculeata* occurring naturally along the Eastern region of Paraguay in almost all kinds of vegetation. Figure 2.9b shows the extent of occurrence and area of occupancy of *A. aculeata*. It is possible to observe a predominance in the growth density of the *A. aculeata* in the following regions: Central, Paraguarí, Cordillera and Guairá, which matches with the observations of Bertoni (1941) and Markley (1955) [73, 74].

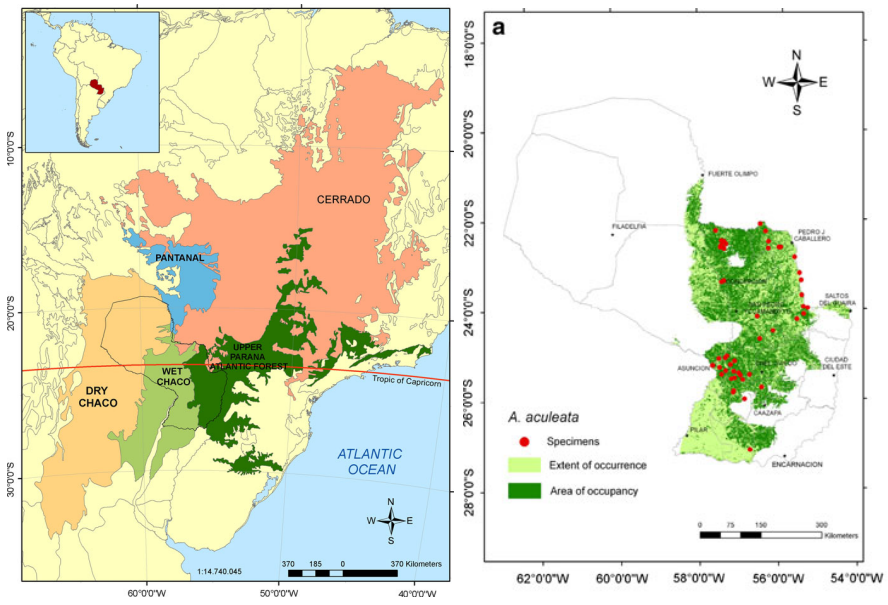

(a) (b)

Figure 1.9: Distribution of A. aculeata in Paraguay. Five terrestrial ecoregions present in Paraguay (a) and extent of occurrence and area of occupancy of Acrocomia aculeata palm. Adapted from Gauto et al. [18].

From the economic and productive point of view, the importance of this indigenous palm that has for the country is unquestionable. Since the beginning of the 20th century, the almond oil has been used in Paraguay for the manufacture of soap. However, the beginnings of the commercial exploitation for oil is not known with certainty. Even more, the oil was also known in Europe prior to 1900 and results of chemical examinations of the kernel oil were reported since 1896 [74]. In the 50's, the production of almond oil reached 2849 Tm and 1125 Tm for pulp oil annually [74].

By 1965, the production of almond oil reached 5100 Tm and pulp oil at 5000 Tm [75]. Currently, there are at least five coconut oil industries working in Paraguay (Fig. 1.10), most of which are concentrated in three departments: Central, Cordillera and Paraguarí [75]. However, they are operating at 60% of their capacity as presented in Table 1.1 and others were closing due to the shortage of raw material. Until today, practically the same production of about 5000 Tm, for both almond and pulp oil, are kept.

Figure 1.10: Visit to OISA S.A. factory in August 2020, with the COO Carin Daher.

The main reason for the decrease in the supply of raw materials is the low price that collectors receive for each box of coconut. The price paid for a box of about 45 kg ranges between 2 and 3 USD approximately.

The production process of almond and pulp oil is quite simple and is presented together with details of industrial yields in the following Fig. 1.11.

Table 1.1: Main coconut oil industries in Paraguay

Factory name	Coconut fruit volume (amount of boxes per year)*	Operation over its capacity (%)	Installed capacity volume (amount of boxes per year)
Aceitera Km. 45†	65000	60	108.333
Aceites Vegetales del Paraguay S.A. (TROVATO)‡	800.000	85-90	870.000
Base Industrial Salinas (BISA) S.A.	290.000	48	600.000
Cocotera San Isidro§	80.000	100	80.000
Cocotero San Roque S.A. (INCA))¶	380.000	50	760.000
Fidu S.A.‖	125.000	30	417.000
INDHOR S.A.**	132.000	38	350.000
Industrial Aceitera S.A.C. (CAVALLARO)	150.000 ††	50	300.000
Oleaginosas Industrializadas S.A. (O.I.S.A)	210.000 ‡‡	60	350.000
INDUPALMA S.A.	190000	55	350000

*corresponding to the year 2006 extracted from [75]
†Closed
‡Closed
§It is not currently working
¶It currently belongs to the BISA S.A
‖Closed
**It is not currently working
††According to the Industrial Manager Agric. Eng. Juan Lionel Vera Benítez, from verbal communication in August 2019
‡‡According to the COO Lawyer Carin Daher, from verbal communication in August 2020

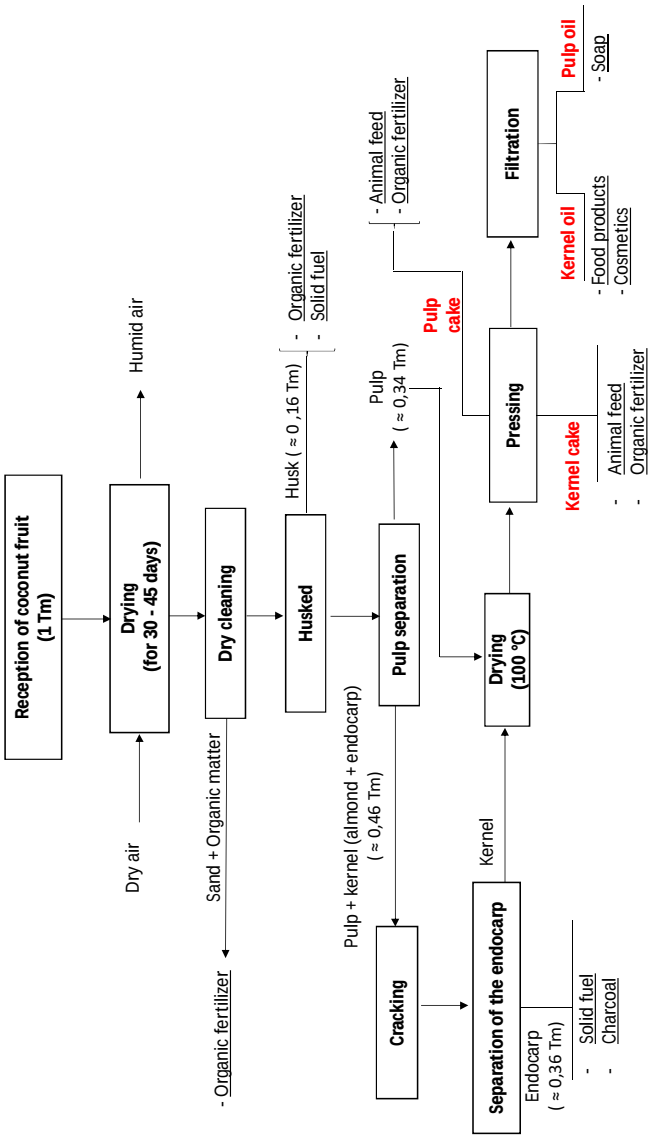

Figure 1.11: Processing of A. aculeata in Paraguay.

The process illustrated in the Fig. 1.11 was detailed by the Agric. Eng. Juan Lionel Vera Benítez [1] and corresponds to the one used by the Paraguayan

[1] Industrial Manager of Industrial Aceitera S.A.C., from personal communication in Au-

company "Industrial Aceitera S.A.C."[2], which began its operation in 1964 and has a processing capacity of 60 Tm of fruit per day. However, it currently operates at 50% of its capacity due to the shortage of raw material.

The reception of the raw material is carried out in boxes of about 50 kg, at a rate of approximately 500 boxes per day. The fruits are arranged in a barn for drying by natural convection for 30-40 days, in order to facilitate the detachment of the pericarp. Then, the dried fruit is sent through a conveyor belt to a table vibratory, in order to remove impurities that accompany the fruits and fall through its gratings.

The clean and dry fruit is recovered and sent to a pallet system that separates the husk from the rest of the fruit. The husk is used to feed the boiler and its ashes are used as a mineral load in one of the by-products "organic fertilizer" of the process.

Subsequently, the pulp is separated from the kernel by means of a knife mill. The pulp is then sent to cookers that operate at 100 °C below atmospheric pressure, to dry the pulp, and then extract its oil by pressing and filtering using press filters (Fig. 1.12). Finally, the pulp oil is stored in tanks in order to maintain its temperature above 20 °C.

In another line of the process, the endocarp is broken by roller mills. Then, the almond grain separation is done by density difference, in a mixture of water and kaolin. The less dense almond is separated from the mixture by means of collectors and they are directed to the cookers that operate in a vacuum at 100 °C, for drying. Almond oil is extracted by pressing and subsequently is filtered and storage in heated tanks. The almond and pulp expeller are used to feed cattle.

As we can see, the endocarp is used in boilers to provide heat in different parts of the process (Fig. 1.13). However, the amount of endocarp produced is greater than that required and due to its composition, there is a potential to employ it as raw material for the pyrolysis and gasification process and to obtain high value products and biofuels.

1.4.2 Coconut endocarp as second generation feedstocks

Relevant aspects of feedstocks for a biorefinery are its quality and quantity available and the required process to convert them efficiently in high value

gust 2019

[2] www.iasa.com.py

Figure 1.12: Oil extraction by hot pressing. Courtesy of OISA S.A.

products. To this context, similarly biofuels, biomass is classified as first, second and third generation feedstocks, where the second-generation feedstocks refers to the non-edible and comprise of raw materials derived from lignocellulosic biomass and crop waste from agricultural and forestry processes [17, 76, 77].

The process of oil extraction, of both the almond and the pulp of the coconut fruit, generates important quantities of by-products such as the coconut shell and endocarp (about 7 Tm of dry matter per hectare per year) [31]. However, there is a lack of scientific research to evaluate the by-products of Acrocomia fruit processing. Even more, scientific research is needed to evaluate the diversity of potential end products for a biorefinery.

The endocarp of *A.aculeata* has high calorific value and high lignin content, so it can be used in many application (syngas devices, in steel and metallurgical operations and for domestic use and feedstocks for activated carbon) [1]. Table 1.2 shows the higher calorific value of some oil species and typical

Figure 1.13: Coconut endocarp to be used in boilers. Courtesy of OISA S.A.

solids fuels, compared to the epicarp, mesocarp and endocarp of *A. aculeata*.

Table 1.2: Higher calorific value of some oil species and typical solids fuels, compared with the epicarp, mesocarp and endocarp of *A. aculeata*. Source: [1, 2].

Species	Higher calorific value* ($MJkg^{-1}$)
Acrocomia aculeata epicarp	18.33
Acrocomia aculeata mesocarp	15.85
Acrocomia aculeata endocarp	18.33
Sun flower (cake)	7.12
Soybean (cake)	9.21
Oil palm (cake)	18.00
Castor oil (cake)	18.84
Coconut shell	14.65
Lignite (mineral origin)	18.38
Bituminous coal (mineral origin)	35.63

*on the dry basis.

To this context, there is a gap in the literature related to the evolution in chemical and structural properties of coconut endocarp—*Acrocomia aculeata*—during its isothermal pyrolysis. In particular, the char properties will indicate the more appropriate uses for this material (i.e. as solid fuel, raw material for the gasification process or others).

Besides, pyrolysis process can be carried out with the main purpose of

obtaining bio-oil, considering its many possible applications.

Physical properties of bio-oils from coconut endocarp *A. aculeata* have been analyzed in a previous work [6], showing water content levels higher than 50 w %, as well as the presence of suspended solids, relative density of about 1.07, viscosity of about 1.55 cSt, pH 2.4 and a higher heating value (HHV) of about 13 $MJkg^{-1}$. However, the chemical composition of the pyrolysis bio-oils of *A. aculeata* was not yet analyzed as well as its combustion chemical kinetics mechanism.

1.5 Processes for the conversion of biomass: Thermochemical processes

Biomass can be converted into energy, bioproducts and biopowers using several technologies, such as total or partial combustion (fuel gas), biochemical processes (biogas), fermentation (bioalcohol), transesterification (biodiesel), pyrolysis (bio-oil) and gasification (syngas, from which chemicals and fuels can be synthesized).

Such methods are divided into biological (anaerobic digestion and fermentation) and thermal. The main difference is that the thermochemical conversion process uses the entire content of biomass, unlike the biochemical and biological processes where mostly pretreatments are required before processing [78].

The thermo-chemical processes for conversion of biomass are pyrolysis, liquefaction, gasification and combustion. However, only pyrolysis process can convert various types of biomass into solid, liquid, and gaseous fuels, but the product distribution depends on the process parameters (as pyrolysis environment, heating rate, final temperature, vapor residence time). Also, combining pyrolysis with other technologies such as charcoal extraction, bio-oil and gaseous intermediates upgrading, important chemicals can be obtained.

Because of the tremendous diversity of biomass feedstocks, the selection of a suitable conversion technology will depend on the physical and chemical characteristics of these materials. An exhaustive list of the compositional analysis among various types of feedstock is found in [79].

These chemical and physical properties will affect the product distribution and quality of the end product in the thermochemical conversion process. Further, pretreatment processes can be necessary depending on the chemical composition and properties of the biomass feedstocks.

To this context, feedstock properties/composition such as bulk density, moisture content, and organic, ash content in biomass and storage will determine the most efficient conversion process to be applied to produce biobased fuels and coproducts.

In this regard, biomass with high-moisture are processed by hydrothermal treatment, where the water is used as one of the reactants and the drying of feedstock is not necessary. Pyrolysis, combustion and gasification are more suitable for biomass with a moisture content less than 11 %.

1.5.1 Pyrolysis

Torrefaction, pyrolysis and carbonization are all parts of the decomposition process of biomass as it is heated in an inert atmosphere. However, it is important to consider their main differences concerning the heating rate, temperature range of heating, physical and chemical changes that govern the decomposition process and the major motivation of each process.

Concerning the process, even though carbonization is similar to torrefaction as both require slow rates of heating, the main differences between them are the process temperatures and the characteristics of the final products. Torrefaction takes place at a narrow low temperature range (200-300 °C), while carbonization takes place at higher temperature range (>300-600 °C). Carbonization drives away much of the volatiles, but torrefaction retains most of it, driving away only the low energy dense compounds and chemically bound moisture. Thus, carbonization produces solid fuels with high energy density (by increasing its carbon content while decreasing its oxygen and hydrogen content) than torrefaction, but it has a much lower energy yield, indeed a progressive effect between torrefaction and carbonization was observed [80].

Pyrolysis is also carried out in absence of air or oxygen at a certain temperature, known as the pyrolysis temperature, but usually a higher heating rate than torrefaction and carbonization. Normally, the process is holding at the pyrolysis temperature for a specified time, to convert organic materials (biomass or other feedstock) into usable final products. The pyrolysis process can be adjusted to favor non-condensable gases, solid char and liquid product, but generally the latter is of primary interest in this process.

1.5.1.1 Pyrolysis products and characterization

Pyrolysis involves a breakage of large complex molecules into several smaller molecules (see Fig. 1.14).

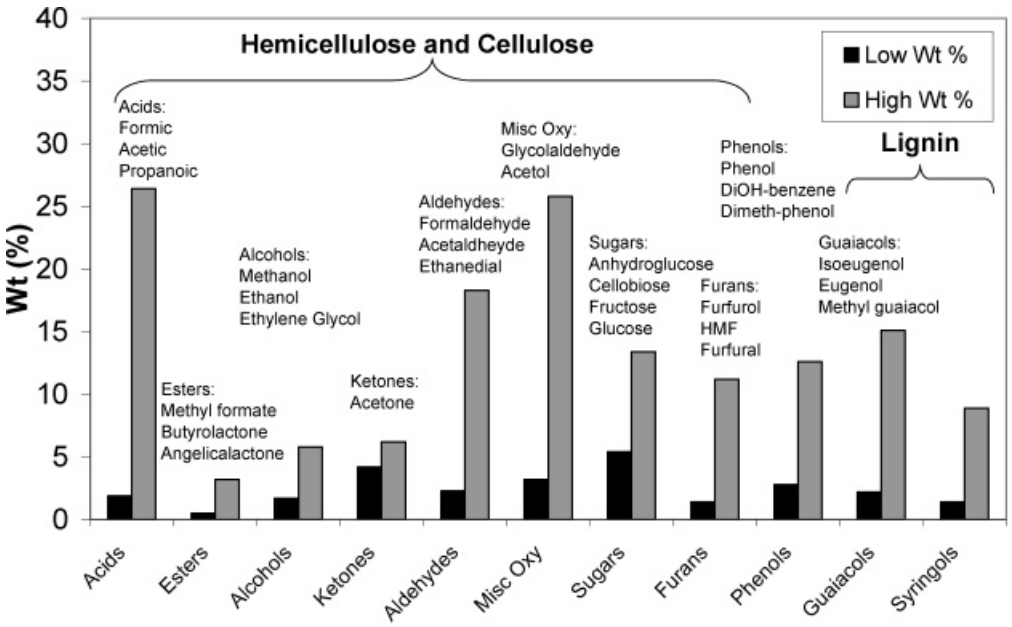

Figure 1.14: Product distribution of pyrolytic oil. Adapted from [19], with permission.

The figure shows the range of compositions that can be found in bio-oils and the most abundant molecules of each of the components (High Wt %) and the biomass fraction from which the components were derived.

Pyrolysis products are classified into three principal types:

Liquid (tars, heavier hydrocarbons, and water): known as "bio-oil", "tar" or "biocrude", is a mixture of complex hydrocarbons with large amounts of oxygen and water, produced by a rapid and simultaneous depolymerization and fragmentation of the hydrocarbons components of biomass followed by an immediate quenching to freeze the intermediate pyrolysis products.

Concerning the properties of coconut endocarp, its high lignin and volatile matter contents (Table 2.1), suggest that this agroindustrial waste could be

considered as feedstock for bio-oil with appreciable yields in the liquid fuel.

Lignin is the second most abundant natural polymer and stores more than half of lignocellulosic biomass energy content [81; 82]. Several studies were carried out to understand the structure of lignin [83; 84] in order to eliminate or modify it from the lignocellulosic biomass and thus to improve the yield of the liquid fuel produced from the hydrolysis of its carbohydrates.

Through pyrolysis, it is possible to obtain highest yield of another liquid fuels, i.e. Bio-oil, without the need to eliminate lignin previously [85; 86; 6].

The chemical and physical properties normally evaluated of bio-oil and its respectively standard methods are showed in Table 1.3.

The Bio-oil can be fractionated using a column chromatography or a liquid-liquid extraction (LLE) based on the water addition. Then, the major bio-oil chemical compounds can be determined by gas chromatograph/mass spectrometer (GC-MS) using an appropriate mass spectral data base as NIST98 [5]. Thousand of chemical compounds in bio-oil were found, which can be grouped into the following categories [60, 3]:

- Hydroxyaldehydes
- Hydroxyketones
- Sugars and dehydrosugars
- Carboxylic acids
- Phenolic compounds

Solid (mostly char or carbon): the highly carbonaceous solid material yield of pyrolysis is known as charcoal. Charcoal is defined as the residue of solid non-agglomerated organic matter, of vegetable or animal origin, that results from carbonization by heat in the absence of air at a temperature above 300 °C. If the heat-treatment temperature (HTT) is above 800 °C, charcoals are referred to as "carbonized charcoals" [87, 88].

Concerning its physical properties, charcoal can be a good (or poor) electrical conductor, can have a high (or low) specific surface area, and depending on the initial feedstock and the HTT employed, it can have variable densities [88,89]. As biomass is carbon neutral, the combustion of biochar is considered more environmentally friendly than coal. Also, it has a large number on non-fuel use such as adsorption of chemicals and carbon storage in ground [90].

Table 1.3: Properties of bio-oil and standard methods used in the analysis [3, 4, 5, 6]

Property	Standard method
Density	ASTM D 1298
Relative density using a Gay-Lussac pycnometer	ASTM D4052
pH	by pHmeter
Water content by Karl Fischer method	ASTM D 1744
Ash content	ASTM D 482
Sulphur content	IP 336
Carbon residue by Condradson carbon residue	ASTM D 189
Viscosity by Saybold viscosity	ASTM D 88
Viscosity by Ostwald or Brookfield rotational viscometer	ASTM D-445
Flash point	ASTM D 93
Heating value using a LECOAC 350 instrument	ASTM D 3286-91a
Heating value by bomb calorimeter	ASTM D240-02
Total acid value	ASTM D 974
Pour point	ASTM D 97
Elemental analysis using a CARLO ERBA 1106 instrument	ASTM D 5373
Elemental analysis using a E 2400 II CHNS/O analyzer	ASTM D 3176
Functional group composition	by FTIR analysis *

*Fourier transform infrared (FTIR) spectroscopic analysis

The chemical and physical properties normally evaluated on charcoal and its respectively standard methods are presented in Table 1.4

Also the porosity, total pore volume and surface area can be measured by using an mercury intrusion porosimeter or a model surface area meter, SEM micrographs can be obtaining by using a Scanning Electron Microscope. The functional group by FTIR analysis (Fourier transform infrared spectroscopic analysis) [91].

While biomass is strongly hygroscopic, biochar is characterized by its hydrophobicity. To evaluate the hygroscopic transformation, equilibrium moisture content and contact angle can be evaluated [92]. The equilibrium moisture content (EMC) can be determined using a dynamic vapor sorption apparatus (DVS) at ambient temperature [23]. The measurement of the contact angle can be based on the sessile drop method [93]. This method consists of observing the profile of a deposited drop on a solid surface, using an optical contact angle apparatus, which consisted of a video measuring system and a high-resolution CCD camera [92].

Concerning its chemical structure, biochar is primarily carbon ($\sim 85\%$), but it can also contain some oxygen and hydrogen and some inorganic ash depending on the temperature of preparation and also on the nature of the initial material [88,90].

Gases products: the non-condensable gases (e.g., CO_2, H_2O, CO, C_2H_2, C_2H_4, C_2H_6, C_6H_6) are produced from the decomposition cracking reactions, which occur partly through gas-phase reactions and partly through gas-solid-phase thermal reactions. The relative amounts of these products depend also on the operating conditions such as heating rate, pyrolysis temperature, sweeping gas flow rate, vapor residence time, etc. [90].

It is possible to detect and identify these gases through an appropriate evolved gas analysis (EGA) equipment such as infrared (IR) analysis and mass spectroscopy (MS) [94, 95]. Consequently, the TGA instrument needs to be coupled with a gas chromatography/mass spectroscopy (GC/MS) and the evolving volatile species are separated by GC and identified by MS [54]. Through the application of those coupled techniques, the chemical compositions of released volatiles from biomass can be correlated to its biopolymer components [96, 97].

Table 1.4: Properties of charcoal and standard methods used in the analysis [3, 7]

Property	Analytical method
Heating value by bomb calorimeter	ASTM E 71
(usually in the range $25 - 32\ MJkg^{-1}$ dry basis)	
Heating value using a IKA Calorimeter C 7000 model instrument	ASTM D 3286-91a
or using a LECOAC 350 instrument	
Particle size distribution	ASTM E828
Bulk density	ASTM E873, Weight of char at 15 °C
	which covers a vacancy of 10 cm^3
Proximate analysis	
Moisture content	ASTM E871
	ASTM-D 4442
Ash	ASTM E830 (575 °C)
	ASTM D1102 (600 °C)
	ASTM-E 1755
	ASTM D 3174-89
Volatile matter	ASTM E 872
	ASTM E872/E897
	ASTM D 3175-89a
Fixed carbon	by difference
Elemental analysis using a CARLO ERBA 1106 instrument or	ASTM D 5373
E 2400 II CHNS/O analyzer	
Ultimate elemental	
C, H	ASTM E777
N	ASTM E778
S	ASTM E775
Sulphur content by means of a LECO SC 32 instrument	ASTM D 4239-93
Cl	ASTM E776
Ash elemental	ASTM D3682
	ASTM D2795
	ASTM D4278
	AOAC 14.7
Ash fusibility	ASTM E953/D1857
Chemical composition	ASTM D 3176
Metals	ASTM E885

1.5.1.2 Reaction schemes of biomass pyrolysis

Based on experimental composition of the pyrolysis products, several reaction schemes were proposed to predict them.

One of the most commonly employed to describe the product composition of biomass pyrolysis is the competitive schemes proposed by Shafizadeh and Chin [98]. In these schemes, only a competition between the formation of char, tar and gas products are considered, from the primary pyrolysis. However, primary tar can react in a secondary reaction to product secondary char and permanent gases, such as proposed by [99] and shown in Fig. 1.15.

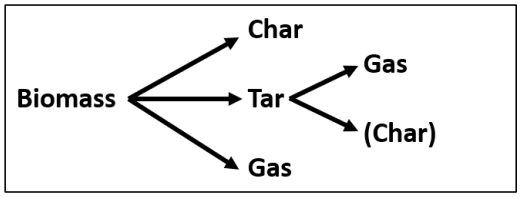

Figure 1.15: Competitive biomass pyrolysis scheme.

However, the secondary production of char in the competitive scheme corresponds to its production at high temperatures from tar cracking. The competitive scheme only predicts differences in char yield at different heating rates or different constant temperatures. They lack the ability to predict the product composition at different conditions from the ones from which the kinetic data were derived, therefore efforts are needed to propose more detailed schemes in the future as explained in [100].

1.5.2 Combustion

Combustion is the chemical reaction of any ignitable matter such as biomass, in the presence of oxygen. It is defined as a rapid oxidation generating heat or heat and light, also slow oxidation to produce relatively little heat and no light [101]. This irreversible and strongly exothermic reaction can be represented for any fuel characterized by $C_xH_yO_z$ as follow:

$$C_xH_yO_z + a(O_2 + 3.76N_2) \rightarrow xCO_2 + (y/2)H_2O + 3.76aN_2, \tag{1.1}$$

where

$$a = x + y/4 - z/2.$$

Combustion has been the most widely applied conversion method for biomass, which provides heat and light energy for the human population worldwide. The amount of heat released will depend on the feedstocks properties as well as on the conversion efficiency of the reaction. Usually the lignin-rich feedstocks are preferred for combustion process due to its energy content [79].

There is a growing motivation for use carbon neutral biomass to replace fossil fuels in the industries (steam power plants, cement industries, and iron making) because it could reduce carbon footprint. To this context, the liquid product of biomass pyrolysis "bio-oil", is also considered a carbon-neutral alternative to hydrocarbons and has been of interest to replacing fuel-oils in turbines, furnaces, and boilers for heat and power generation systems. Also, because of their inherently high volumetric energy density, liquid fuels are often an ideal choice for transportation uses [90, 102].

In this work we will address the combustion of bio-oil and its comparison regarding other liquid fuels. Therefore, aspects related to the liquid fuels combustion are presented below.

1.5.2.1 Types of flames

The thin reaction zone where the molecular decomposition and recombination occurs, presenting huge gradients of temperature and pressure, is commonly refers as a flame. According to the condition of the mixedness of the reactants prior to the combustion reaction, the flames are typically categorized broadly as either premixed or diffusion flames. A premixed flame is one in which the fuel and oxidizer are uniformly mixed at the molecular level prior to any significant reaction, whereas a non-premixed (or diffusion flame) is one in which the fuel and oxidizer are initially separated, and reaction occurs only at the interface between the fuel and oxidizer [101, 103].

Laminar premixed flames are considered kinetically limited, while laminar diffusion flames are considered mass transfer limited. When turbulence is introduced to a premixed flame, burning velocities are increased because the turbulent eddies in the flow wrinkle the reaction sheet, giving it more surface area and allowing it to propagate more rapidly . In a non-premixed turbulent flame, overall flame speeds are increased from those in a laminar diffusion flame, predominately because the turbulence serves to increase mass transfer rates between the fuel and oxidizer [101].

1.5.2.2 Important combustion characteristics

Stoichiometric air-fuel ratio: The reactants can be mixed in different proportions, where the air-fuel ratio is represented as (A/F).

If the quantity of oxidizer is just that amount needed to burn a quantity of fuel, the mixture is stoichiometric. However if more than a stoichiometric quantity of oxidizer is supplied, the mixture is said to be fuel lean, or just lean, whereas if is supplied less quantity than the stoichiometric oxidizer, the mixture is fuel rich or rich.

Assuming that the simplified composition for air is 21 percent O_2 and 79 percent N_2 (by volume), then the stoichiometric air-fuel ratio can be found as:

$$(\frac{A}{F})_{stoic} = (\frac{m_{air}}{m_{fuel}})_{stoic} = \frac{4.76a}{1}\frac{MW_{air}}{MW_{fuel}}, \tag{1.2}$$

where MW_{air} and MW_{fuel} are the molecular weights of the air and fuel respectively.

Equivalence ratio: In many combustion applications, the equivalence ratio is the single most important factor in determining a system's performance. The equivalence ratio, Φ, is defined as:

$$\Phi = \frac{(\frac{A}{F})_{stoic}}{(\frac{A}{F})} = \frac{(\frac{F}{A})}{(\frac{F}{A})_{stoic}} \tag{1.3}$$

The equivalence ratio, Φ, is more commonly used to indicate is the mixtures are fuel-rich ($\Phi > 1$), fuel-lean ($\Phi < 1$) or stoichiometric ($\Phi = 1$).

Flame speed: A flame is a self-sustaining propagation of a localized combustion zone at subsonic velocities. Considering a flame which occupies only a small portion of the combustible mixture at any one time, the premixed flame propagation velocity "S_L" (Fig. 1.16), is defined as the speed of displacement of a flat flame front in the direction of unconsumed reactants [104].

Some factors that influence the flame velocity are the temperature, pressure, equivalence ratio and the fuel type. The laminar flame speed has a strong temperature dependence, in this way when unburned gas temperature increases,

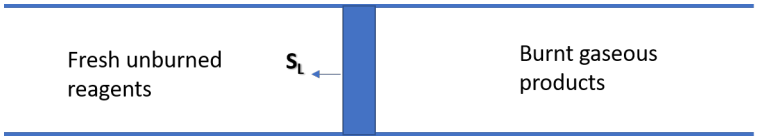

Figure 1.16: Scheme of a flame front propagation towards reactants.

also the flame speed increases, however the burned gas temperature will also increase [101].

Andrews and Bradley [105] and Law [106], provide experimental correlations, which generally show a negative dependence of pressure for the following fuels: H_2, CH_4, C_2H_2, C_2H_4, C_2H_6 and C_3H_8 for a range of pressure up to 5 atm. Flame speeds increase rapidly when the temperature of the fresh gases increases but decrease when pressure increases [107].

Other more recent studies carried out on different fuels, at high temperatures and pressures are reported in Refs. [108, 109, 110, 111, 112].

Concerning the effect of the equivalence ratio on the flame speed for similar fuels (except for very rich mixtures), a maximum of flame speed is expected, for a slightly rich mixture, as a result of how this parameter affects flame temperatures [101]. Lawes et al. (2005) [113] have found that for the same fuel, the equivalence ratio for peak turbulent burning velocity proved not always coincident with that for laminar burning velocity.

Another factor is the fuel type (e.g. H_2, CH_4, paraffins, olefins, acetylenes, etc.). Several authors have studied the effect of the nature of various pure fuel and mixtures on the laminar flame speed [106, 114] and in the equivalence ratio [115].

In this sense, several factors combined can increase a fuel flame speed, such as its thermal and mass diffusivity and the reaction kinetics. Generally the hydrocarbons follow the same trend as a function of flame temperature and H_2 has a maximum flame speed many times greater than that of propane for example [101]. The effect of fuel structure on combustion efficiency and emissions was studied by [108].

In consequence, the flame speed provides information about the combustion properties and oxidation process for a fuel or a mixture of fuels, so it is used as parameter for validation of a chemical kinetic mechanism [116].

Auto-ignition delay: combustion can occur in either a flame or non-flame mode. Auto-ignition occurs under certain conditions, namely when the

mass of the reactants reaches the autoignition temperature and ignites without the need for an external source of heat, this is explained by a very rapid combustion or a rapid oxidation reaction in the entire volume of the unburned gas [101].

However, when the autoignition temperature is reached, the fuel mixture does not burn instantly, but rather it ignites after a brief period of time known as "auto-ignition delay". This delay time has two components: due to physical phenomena such as formation, heating and evaporation of fuel droplets and another due to chemical phenomena due to the kinetics of chemical reactions that occur during combustion [117].

Hernández et al. (2010) [118] have studied the ignition delay in three-stage of oxidation (low-, intermediate-, and high-temperature range) of a diesel fuel under homogeneous charge compression ignition (HCCI) conditions. They have assuming an Arrhenius-type equations and considering the effect of the main parameters affecting the auto-ignition time, i.e. pressure, temperature, and equivalence fuel/air ratio.

Recent work on ignition of alternative aviation fuels (Fischer-Tropsch (F-T) jet fuels synthesized in gas-to-liquid processes, the produced from plant oil sources, animal fats through hydroprocessing, alcohol-to-jet fuels and others) are reported in Refs. [119, 120, 121]. A comparison of conventional and alternative fuels has been reported by [122]. This study reveals similar orders of magnitude of ignition delay data and small but evident differences in the activation energy among these fuels.

In particular, for alternative aviation fuels, alcohol-to-jet fuels were found to be generally less reactive than Fischer-Tropsch paraffinic kerosenes or hydro-processed renewable jet fuels and respect to the conventional fuels [122]. The overall ignition delays of alternative jet fuels are all seen to be much shorter than that of Jet-A, and their pressure rises due to ignition are higher than that of Jet-A [120]. Shorter ignition delay time usually is related to a higher cetane number and more complete combustion of the fuel charge in the combustion chamber, which translates into a smoother running, better performing engine with more power and fewer harmful emissions [120].

The auto-ignition delay is a key characteristic of the combustion chemistry and specific for a fuel or its mixtures, therefore it is used as parameter for the kinetic mechanic validation [123]. Experimental and theoretical studies of ignition delay times and laminar burning velocities, have already used to describe the oxidation of bio-fuels considered as possible alternatives of transportation fuels [109].

1.5.2.3 Properties of a liquid fuel

The more typical liquid fuel characteristics are heating value, viscosity, density, molar weight, C/H ratio (w/w), cetane number, flash point, cloud and pour point. These fuel properties along with others have influences in: the efficiency of the combustion processes, NOx emission and combustion design, the vaporization and spray behavior of liquid fuels, problems of deposits in the combustion chamber and other characteristics. A comparison of these properties for typical liquid fuel and bio-fuels are shown in the Table 1.5 [8, 9].

Pyrolysis-oil composition and properties depend significantly on the biomass feedstock, processes, and operating conditions. Pyrolysis liquid are more dense and viscous that light petroleum-based fuels and other bio-fuels [3], but regarding heavy fuel-oil, it's at least 9 times less viscous [9]. In addition, they are acidic, unstable (high oxygen content), highly polar with a large amount of chemically dissolved water and can contain solids or may be classified as solids-free pyrolysis liquids after a treatment [9].

As regards to the cetane number, the predicted value for pyrolysis liquids were evaluated between 13 and 14 by Chiaramonti et al. (2007) [9] and only as 10 by others authors (Table 1.5). The authors classify it as non-flammable, non-distillable, possess only limited volatility, and ignite only at high temperatures, unlike petroleum-based fuels. However, once ignited, pyrolysis liquid can be burned steadily [136].

According to its water content, the heating value, density, and viscosity of pyrolysis liquids can vary. Typical values are between 20-30 w %. If the water content is very high (above 30 w %) the liquid separates into two phases of differing properties [9]. The water content of pyrolysis liquids must be regulated because it affects the combustion properties.

Because the bio-oil properties are completely different, compared to conventional liquid fuels or mineral oils, it is necessary to establish standards that allow the successful introduction of this product into the market.

Oasmaa et al. (2015) [136], presents the two fuel oil grades for fast pyrolysis bio-oil (FPBO) established by ASTM (Table 1.6), being the main differences between the two grades concern the maximum solids and ash content in the bio-oil.

Also, EN standards are needed and a European Commission is driving the development of standards for FPBO.

To this context, five different qualities of FPBO were foreseen, depending on its application [136]:

(1) A European Standard for FPBO replacing heavy fuel oil;

[3] Light fuel oil consists mainly of saturated olefinic and aromatic hydrocarbons (C9-C25) that are immiscible with highly polar pyrolysis liquids.

Table 1.5: Liquid fuels and bio-fuels characteristics [8, 9].

Property	Diesel [127]	JET-A [128,129,9]	Straight vegetable oils [130,125,131]	Bio-diesel [124,125,126, 132,128,133,134,135]	Bio-ethanol [68, 135, 129]	Bio-methanol [8]	Pyrolysis oil [68,124,129,9]
Density (kg/m^3)	827.4	807	900-940	860-900	794-810	796	984-1250
Kinematic viscosity (cSt at 40 °C)	1.7283	0.88	30-40	3.5-5	1.4-1.7	1.4-1.7	32-45
Flash point (° C)	44	38	230-280	120-180	13	11	56-130
Cloud point (° C)	-6	-	-4 to 12	-3 to -12	-	-	-
Pour point (° C)	-16	-47	-12 to 10	-15 to 5	-117	-161	-35 to -10
Lower calorific value (MJ/kg)	43	43.23	38-39	39-41	25-26	20	13-18
Ignition temperature (° C)	250	220	325-370	177	423	463	580
Cetane no.	45-55	55	37-42	48-60	8	5	10
Stoichiometric air/fuel ratio	14.6	14	13.8	13.8	9.79	6:1	34:1
Carbon (%, w/w)	80.33	80-83	76.11	77.81	52.2	37.5	32-48
H_2(%, w/w)	14	10-14	-	12	13.1	12.6	7-8.5
N_2(%, w/w)	1.76	-	0	0.03	-	-	<0.4
O_2(%, w/w)	1.19	-	11	9-11	34.8	49.9	44-60
Sulfur (%, w/w)	<0.4	<0.4	0	<0.3	-	-	<0.05

Table 1.6: ASTM Burner Fuel Standard D 7544 for Fast Pyrolysis Bio-oil [10,11]

Property	Grade G	Grade D
Gross heat of combustion, min (MJ/kg)	15	15
Water content, max (w %)	30	30
Pyrolysis solids content, max (w %)	2.5	0.25
Kinematic viscosity at 40 °C, max (cSt)	125	125
Density at 20 °C (kg/dm^3)	1100-1300	1.1-1.3
Sulfur content, max (w %)	0.05	0.05
Ash content, max (w %)	0.25	0.15
pH	Report	Report
Flash point, min (° C)	45	45
Pour point, max (° C)	-9	-9

(2) A European Standard for FPBO replacing light fuel oil;

(3) A Technical Specification for the quality of FPBO replacing fuel oils in stationary internal combustion engines;

(4) A Technical Specification for a quality specification of FPBO suitable for gasification feedstock for the production of syngas and synthetic biofuels; and

(5) A Technical Specification for FPBO suitable for mineral oil refinery co-processing.

It was anticipated that all these EU Standards, should be effective in 2017. However, at the time of writing this manuscript, it is known the CEN/TC 19/WG[4] is still developing the first three standards (for replacement of heavy fuel oil, light fuel oil and for use of bio-oils in stationary combustion engines). Also, it is expected that two further technical specifications may also be introduced for use of fast pyrolysis oils as gasification feedstocks and for mineral oil refinery co-processing.

1.5.2.4 Modelling Combustion Chemistry

Combustion is a highly complex phenomenon that encompasses a great diversity of areas such as fluid mechanics, transport phenomena, thermodynamics and chemical kinetics [101, 137].

In a generic way, the combustion of a fuel F for a product P can be expressed

[4]Working Group established under the technical committee, "Gaseous and Liquid Fuels, Lubricants and Related Products of Petroleum, Synthetic and Biological Origin" of the European Standardisation body

with the global reaction:

$$F + \alpha O_2 \longrightarrow \beta P \tag{1.4}$$

During combustion, fuels are oxidized by a series of chain reactions (elementary reactions), which involves the formation of a large number of intermediate species (highly reactive radicals, such as $\dot{O}$, $\dot{OH}$, and $\dot{H}$) that are not indicated in the global equation [101].

The set of elementary reactions necessary to describe a global chemical process that leads from reactants to products is called the reaction mechanism and can be expressed as:

$$\sum_{j=1}^{N} v_{ij}^{'} X_j \longleftrightarrow \sum_{j=1}^{N} v_{ij}^{''} X_j, \quad \text{for } i = 1, 2, \ldots, L \tag{1.5}$$

where L is the number of reversible chemical reactions considered, N the total number of species, X_j the $j-th$ chemical species, $v_{ij}^{'}$ and $v_{ij}^{''}$ constitute the elements (i, j) of the matrices of stoichiometric coefficients of reagents and products, respectively.

The reaction mechanism that follows the combustion of a substance depends on the nature of the reactants, richness, presence of catalysts and the conditions of temperature and pressure [101].

The chemical kinetic allows determining at what rate in a molecular level, reactants are transformed into products, through intermediate species, and the residence time necessary to reach equilibrium concentrations, while thermodynamics indicates which is the maximum amount of reagent that can be converted into a product under certain conditions of temperature and pressure.

A chemical kinetic mechanism is a comprehensive list of elementary chemical reactions with corresponding reaction rates [138], and significantly affects the release of energy, generation of pollutants, and the formation, color and extinction of the flame [101].

The net rate of reaction of each species in a multi-step mechanism is expressed in the following equation:

$$\dot{\Omega}_j = \sum_{i=1}^{L} (v_{ij}^{''} - v_{ij}^{'}) \left\{ k_{f_i} \Pi_{j=1}^{N} C_j^{v_{ij}^{'}} - k_{r_i} \Pi_{j=1}^{N} C_j^{v_{ij}^{''}} \right\} \tag{1.6}$$

where $\dot{\Omega}_j$ is the rate of change of the molar concentration of species j with respect to time, k_{fi} and k_{ri} are the constants of direct and inverse velocity of reaction i, and

C_j the molar concentration of species j. This expression indicates that the speeds of the direct and inverse reactions are proportional to the molar concentrations of the reactants, elevated to their respective stoichiometric coefficients. The velocity constants are determined by the Arrhenius equation of three parameters.

$$k(T) = AT^b e^{\left(\frac{-E}{RT}\right)} \tag{1.7}$$

where A is the pre-exponential factor, b an empirical exponent of the temperature and E the activation energy of the reaction.

To model a combustion phenomena, the balance equations (mass, energy, chemical species, momentum) are taken into account; as well as equations to estimate transport coefficients and properties. Solving these equations requires using a computer application in order to simulate the experimental configuration [139]. Then, the data obtained from the simulation must be validated. This will be detailed in Section 2.3.3.

1.5.2.5 Overview of the bio-oil combustion

Bio-oil is composed of thousand of compounds, mostly oxygenated [140]. The chemical and physical properties of bio-oils are completely different from petroleum fuels affecting the combustion process. Its high oxygen and water content confers high internal chemical reactivity (its properties change over time) and difficulties in ignition delay time, however for spray combustion applications it will expect enhances in the atomization properties [141].

Bio-oil is considered a carbon-neutral alternative to hydrocarbons in the transport sector. Pyrolysis oil has been used in boilers, turbine, and diesel engines with some issues as acidity, ignition characteristics, coking/clogging tendency, and particulate emissions [9, 142]. Thus, initially this fuel would be used in boilers or gas turbines, rather than in internal combustion engines, or for domestic heating applications [143].

Concerning bio-oil combustion, several studies have been carried out in the last decade. A study of chemical kinetics and combustion characteristics of multi-component bio-oil/kerosene droplets was done by [144]. An experimental and numerical simulation study of bio-oil fast pyrolysis oxycombustion from lignocellulosic biomass was realized by Wu and Yang [145]. This study examined the chemical kinetics and combustion characteristics of multi-component bio-droplets. Specifically, spark ignition was employed to examine the combustion characteristics of kerosene/aqueous phase bio-oil and kerosene/oil phase bio-oil droplets by using thermogravimetric analysis and gas chromatography-mass spectrometry.

Experimental measurements and numerical simulations were conducted to examine the effects of varying O_2 concentrations, oxidant velocity (V_o) levels, and bio-oil proportions on the combustion characteristics of the bio-oil/kerosene mixtures.

Droplet combustion and thermal characteristics of pinewood bio-oil from slow pyrolysis was studied by Yang and Wu [146]. The combustion properties of droplets with different butanol/bio-oil proportions were determined and compared.

1.5.3 Gasification

Gasification is the conversion of a carbonaceous solid, liquid, or even gaseous fuel into desired gaseous products with usable heating value. These gaseous products can be used as either fuel or for production of value-added chemicals. However, gasification process can be directed also to the production of activated carbon through a partial gasification.

Unlike combustion, which releases energy from breaking the chemical bonds, gasification stores energy into chemical bonds in the product gases. Generally gasification produces gases with a higher hydrogen-to-carbon (H/C) ratio through the addition of hydrogen and the removing of carbon from the hydrocarbon feed-stock, while combustion oxidizes the hydrogen and carbon into water and carbon dioxide, respectively.

It is necessary to recognize the importance that many types of carbon have in our society. The two main crystallography forms of the carbon are graphite and diamond. Carbonaceous solids can be produced from many organic precursors as woody biomass feed-stock or even from harmful waste materials [147], which in addition to carbon contain also hetero-atoms and possibly inorganic elements in its structure. Upon thermal treatments at elevated temperatures, as pyrolysis and gasification, these heteroatoms and some inorganic materials, to some extent, they are lost during the process, yielding a solid with higher carbon content. The final structure of the solid product, depends on both, the initial organic solid precursor and the specific thermal treatment applied to obtain it. In this way, the nature of the intermediate phase formed during the carbonization process, to produce then activated carbon, it is of the utmost importance [148].

1.5.3.1 Carbon gasification reactions

The gasifying medium is of importance to obtain the desired products along the process. Oxygen, steam and air, are the main gasifying agents used. The nature and amount of the gasifying used, determines the heating value and composition of the gas produced.

Different structural properties of activated carbon are produced according to the selected gasification agents employed.

A general equation for a gasification process using air ($1O_2 + 3.76N_2$) as gasifi-

cation agent is [149]:

$$\begin{aligned} Feedstock(C_nH_xO_yN_z) + m(O_2 + 3.76N_2) \rightarrow \\ x_1H_2 + x_2CO + x_3CO_2 + x_4H_2O + x_5CH_4 + x_6C + (z/2 + 3.76m)N_2 \end{aligned} \tag{1.8}$$

The reaction considers the production of six main products during the process including three energy carriers (H_2, CH_4 and CO). The fraction of carbon in the feedstock that remains after the process is also included as a free carbon.

Some important gasification reactions we can consider are [150, 151, 90]:

Carbon reactions:

$$\begin{aligned} C + CO_2 &\Longleftrightarrow 2CO \ (\Delta H = +172kJ/mol) \\ C + H_2O &\Longleftrightarrow CO + H_2 \ (\Delta H = +131kJ/mol) \\ C + 2H &\Longleftrightarrow CH_4 \ (\Delta H = -74.8kJ/mol) \\ C + 0.5O_2 &\Longleftrightarrow CO \ (\Delta H = -111kJ/mol) \end{aligned} \tag{1.9}$$

Oxidation reactions:

Shift reaction

$$CO + H_2O \Longleftrightarrow CO_2 + H_2 \ (\Delta H = -41.2kJ/mol) \tag{1.10}$$

Methanation reactions

$$\begin{aligned} 2CO + 2H_2 &\Longleftrightarrow CH_4 + CO_2 \ (\Delta H = -247kJ/mol) \\ CO + 3H_2 &\Longleftrightarrow CH_4 + H_2O \ (\Delta H = -206kJ/mol) \\ CO_2 + 4H_2 &\Longleftrightarrow CH_4 + 2H_2O \ (\Delta H = -165kJ/mol) \end{aligned} \tag{1.11}$$

Steam-Reforming reactions

$$\begin{aligned} CH_4 + H_2O &\Longleftrightarrow CO + 3H_2 \ (\Delta H = +206kJ/mol) \\ CH_4 + 0.5O_2 &\Longleftrightarrow CO + 2H_2 \ (\Delta H = -36kJ/mol) \end{aligned} \tag{1.12}$$

1.5.3.2 Production of Syn-Gas

The gasification process directed towards the production of syn-gas (H_2 + CO) has been an important commercial process for several decades. In South Africa the production on commercial scale of synthetic fuels from coal gasification via Fischer-Tropsch

technology is known since 1950's. The raw synthesis gas from gasifier must be purified and may require desulfurization and the adjustment of the hydrogen-to-carbon monoxide ratio.

On the other hand, it is possible to use the gas directly to fuel combustion turbine in a combined cycle power plant, with the inherent advantages of both its high efficiency and extremely low rates of atmospheric emissions [152].

1.5.3.3 Production of activated carbon

Activated carbon has been produced from several feedstocks as agroindustrial waste and sludge, scrap tyres, bituminous wastes, biomass fly ash, waste particleboard, sewage sludge.

Physical activation is a partial gasification at temperatures around 800-1000 °C. During the process, the disorganized materials are removed first, which entails an increase in the pore volume and this allows the development of the porosity by the activated agent, with increasing the burn-off[5]. Three variables were defined as the most important in the activation process, from the point of view of porosity development: the activated agent, the final burn-off reached and the presence of inorganic impurities that catalyze or inhibit the gasification reaction [148, 153].

1.6 Knowledge gap

From this short literature review, there is currently a knowledge gap on the following issues:

- Although there are several studies about compositions and other properties of several lignocellulosic biomass, this novel feedstock, coconut endocarp, lacks a detailed analysis in terms of its properties and those of its products obtained using different thermochemical treatments. In this context, there is a gap in the literature related to the evolution in chemical and structural properties of coconut endocarp—*Acrocomia aculeata*— during the isothermal pyrolysis. In particular, the char properties will indicate the more appropriate uses for this material (i.e. as solid fuel, raw material for the gasification process or others).
- Regarding bio-oil production, the physical properties of bio-oils from coconut endocarp *Acrocomia aculeata* have been analyzed in a previous work [6]. However, the chemical composition of the pyrolysis bio-oils of *A. aculeata* as well as its combustion chemical kinetics mechanism were not yet analyzed.
- Although there are extensive studies on the mechanisms of biomass pyrolysis and several kinetic models [154, 155, 156], none of them evaluated this specific

[5] Defined as the weight loss between the activated carbon and the char, in percentage

feedstock. To the best of our knowledge, it has not yet been proposed a set of kinetic parameters for simulating the heat treatment of coconut endocarp using a set of temperatures representative of pyrolysis conditions, simultaneously.

- Regarding high value added products produced from agroindustrial wastes, activated carbon is one of the most interesting one, considering its many applications. Therefore, we propose slow pyrolysis/gasification of coconut endocarp in different conditions to evaluate its gasification rate as well as the products characteristics obtained.
- The major focus of this study is the experimental characterization of the coconut endocarp and its chars, obtained from a variety of isothermal pyrolysis conditions. It is important to propose the more relevant uses of coconut endocarp and its chars, as *Acrocomia aculeata* is a potential feedstock for a biorefinery.

Chapter 2

Experimental approach

This chapter presents the experimental procedure and the facilities to obtain the results about the physicochemical evolution along the thermal decomposition of the endocarp of Acrocomia aculeata fruit samples and about the kinetic mechanic model for the bio-oil of coconut endocarp. The measurement techniques used were: differential thermogravimetric (DTG) analysis, elemental analysis, surface area and pore size analyses, ESEM, SEM/FEG observation and dynamic vapor sorption evaluation and the bio-oil chemical characterization by Gas Cromatography and Mass Spectroscopy

.

2.1 Study system

Experimentally, our work focuses on the study of the thermal degradation of coconut endocarp (Fig. 2.1), a solid waste from the agroindustrial companies in Paraguay, showing potential as solid or liquid fuel or as adsorbent material.

Table 2.1 presents the general properties of this materials determined by different authors.

Coconut endocarp has high lignin content, which has been considered as a hindrance in cellulosic bioethanol production in biochemical conversion processes, since biodegradation of lignin is lower than cellulose. However, for thermochemical process as combustion, gasification, and pyrolysis, is a suitable feedstock [163].

Respect its relatively high volatile matter content and fixed carbon content, it is expected a high amount extracted of hydrocarbon species from biomass pyrolysis, but also an important generation of charcoal.

Table 2.1: Properties of coconut endocarp —*Acrocomia aculeata*—

Origin	Ref.	HHV * ($MJkg^{-1}$)	elemental analysis (%wt)					proximate analysis (%wt)			Density (gcm^{-3})
			C	H	O	N	S	Ash	VM†	FC‡	
Paraguay(Paraguar)	6	19.28						1.75	75.25	17.9	
Paraguay (Central)	157					0.36		3.26			
Brazil (Botucatu, SP)	158	18.33									
Brazil§	159							0,97			
Brazil	160	21.55									
Brazil (North region, Minas Gerais)	161										1,325
Brazil (Mirabela , Minas Gerais)	40	20.45	48.00	6.19		0.56		1.54	76.00	22.45	1,325

Compositional analysis

Origin	Ref.	Lignine (%wt)	Cellulose (%wt)	Hemicellulose (%wt)	Holocellulose (%wt)	Extractives (%wt)
Brazil¶	159	24.60			69.00	6.40
Brazil (Mirabela, MG)	16	39.8				
Brazil (Mirabela , Minas Gerais)	40	31.67				
Brazil (Mirabela , Minas Gerais)	162	39.8				

*Higher heating value
†Volatile matters
‡Fixed carbon
§ —*Acrocomia sclerocarpa*—
¶ —*Acrocomia sclerocarpa*—

Figure 2.1: Coconut endocarp (on the left) and grinded fine particles of coconut endocarp (on the right).

Also, recently Rencoret et al. (2017) [16], have determined the composition of neutral monosaccharides (as percentages of total neutral carbohydrates) in the coconut endocarp as follow: arabinose (0.9%), mannose (0.8%), galactose (0.8%), xylose (45.3%), glucose (52.2%). Respect to the lignin composition, they also have reported high levels of phenol from the endocarp (24.8% and 51.3% in CW[1] and its MWL[2]). However, significant amounts of intact 4-hydroxybenzoic acid, were also released from the endocarp cell walls (20.8% of all phenolics). Estimatively, the endocarp lignin presents an intermediate S/G ratio of around $0.9 - 1.5$ [16].

Although several properties of the coconut endocarp have been determined, to the best of our knowledge none evaluated the physical and chemical alterations and the mass loss of this material, produced by isothermal pyrolysis. In addition, we carried out for the first time, the chemical characterization of the liquid product of the pyrolysis of coconut endocarp and from this results a numerical proposal of its chemical kinetic mechanism for it combustion process.

The work has then an experimental approach and a numerical approach as presented in the following sections.

2.2 Coconut endocarp physico-chemical alterations by pyrolysis and its kinetic analysis

The design of any thermochemical process to deeper understanding of the physico-chemical properties of lignocellulosic biomass are required, as they significantly influence the process conversion performance and associated supply chain network for material handing and transport [163].

Although there is information in the literature about certain important prop-

[1] cell-walls
[2] "milled wood" lignin

erties of coconut endocarp (Table 2.1). To the best of our knowledge, this is the first time the alterations of the coconut endocarp are measured during its pyrolysis in a wide range of 250 - 550 °C, by different physical and chemical properties.

From an experimental point of view, it is relatively difficult to control the external variables that can affect the measurements. In addition, biomass pyrolysis produces an appreciable amount of tar during the process, which can cause secondary reactions in homogeneous and heterogeneous phase and further complicate the reproducibility of the results, and this is more remarkable when the process is carried out at higher scales (e.g. reactor and pilot scales). Also a rapid cooling system is required, which allows the thermoactivated reactions in the sample to be inhibited once the pyrolysis time is over. Thus, a thermogravimetric analysis unit was chosen to carried out the experiments.

Thermogravimetic analysis (TGA) is a thermal analytical technique in which the changes in the mass of a sample is measured as a function of time or temperature as it is subjected to a controlled temperature program in a controlled atmosphere [164]. It consists of a sample pan placed in a furnace where the heating temperature and environment are controlled. Also, because the sample pan is supported by a precision balance, the mass of the sample is continuously measured and recorded during the experiment [163].

Although the main use of TGA is for kinetic analysis of lignocellulosic biomass pyrolysis, where, according to Cai et al. (2017), it was reported over 1300 papers dating from 2000, it is also an useful tool to perform the proximate analysis of solid fuels. Besides, using TGA some chemical reactions as dehydration stage and decomposition of biopolymer components (e.g. hemicellulose, cellulose, and lignin), and also physical transitions can be analyzed [163].

The first part of the work then deals with the study of the main physical and chemical changes that occur in the raw material during its pyrolysis and was carried out entirely at the Laboratoire de Génie des Procédés et Matériaux (LGPM).

Additionally in Chapther 4 and Chapter 5, are presented as complementary results, the kinetic analysis of the pyrolysis process and the gasification process of the coconut endocarp to obtain activated carbon.

Regarding the kinetic analysis we have used the results of thermogravimetric mass loss to determine the kinetic parameters of the pyrolysis process and was carried out partly at the Laboratorio de Mecánica y Energía (LAMEEN, FIUNA). The explanation of the kinetic models and its solutions and optimization are presented in Chapther 4.

Regarding the gasification process (Chapter 5), we have employed the thermal analysis devices of section 2.2.1, but with a water vapor furnace as described in section 5.2.1 to obtain the characteristic curves of the process and the conversation rate. Besides, for the activated carbon obtained the surface area and porosity were determined using the analysis technique described in section 2.2.2.

2.2.1 Thermogravimetric analysis unit

We have used the thermal analyzer STA F3 Jupiter of NETZSCH (Fig. 2.2) to obtain the curves of loss of mass in function to the time and to prepare the sample for the respective analyzes required after the heat treatment.

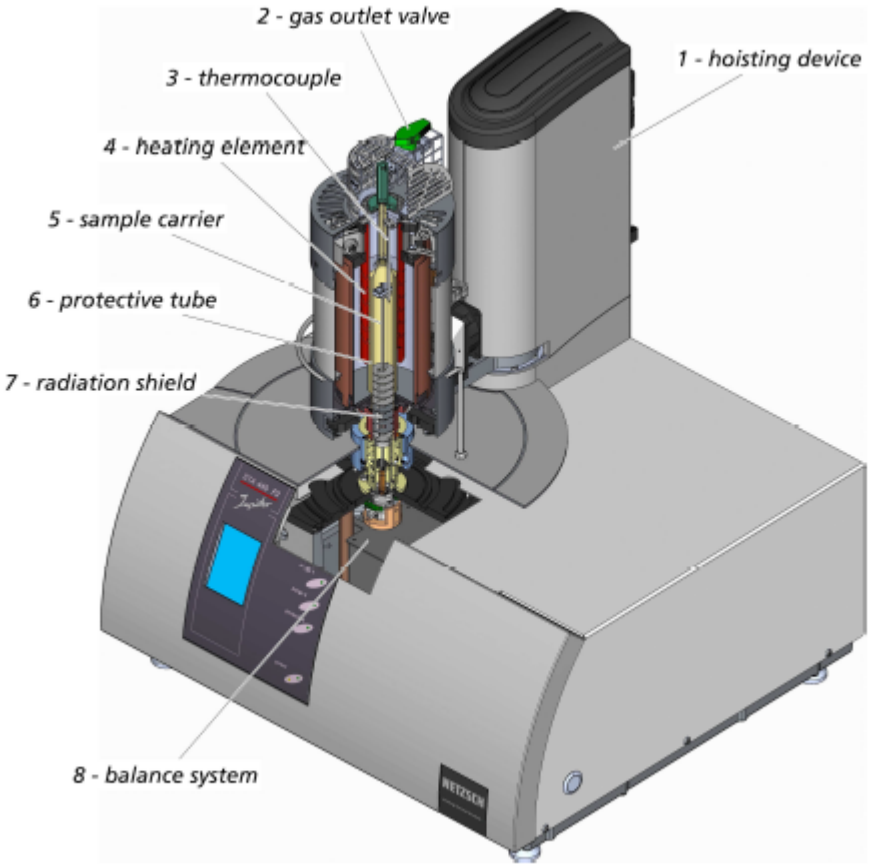

Figure 2.2: Thermal analyzer STA F3 Jupiter of NETZSCH
(Source: NETZSCH, Operating Instructions Simultaneous TG-DTA/DSC Apparatus STA 449 F3 Jupiter)

The device consists of a silicon carbide furnace that allows operating temperatures up to 1600 °C. The sample was placed inside a alumina crucible. The crucible was placed on the balance, a platform through which the thermocouples are connected. In addition to the sample, an empty crucible of reference was placed on the balance. The temperature of the thermogravimetric analysis was measured in this reference crucible.

The heating program used to perform the thermal degradation analysis of coconut pyrolysis is presented in Fig. 2.3 and called isothermal heating program [165]. The drag force is corrected with an empty crucible submitted to the same thermal program as the sample.

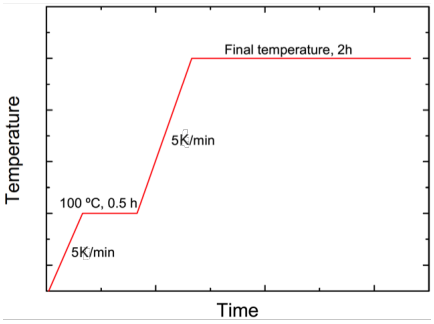

Figure 2.3: Heating program used to perform the thermal degradation analysis

To analyze the curves, it was necessary to remove the dehydration stage. For this, we just take a constant temperature as the end temperature (T_0) of the dehydration stage, which was maintained for a certain period of time. For example, 105 °C as the end temperature of the dehydration stage for 1 hour. This method was selected because it was observed a mass loss plateau (refers to a region of mass−time curve with a relatively constant mass) at the final of this stage, after several tests

2.2.2 Analysis techniques used

The structure of a char, which influences its physical characteristics, depends on both the feedstock and the pyrolysis process used. In most cases, the original biomass structure strongly influences the final char structure, its eventual physical characteristics, and its eventual interaction with the soil if it will be used as biochar. Most typically, pyrolysis reactions lead to a number of structural or physical changes including loss of volatile organics and structural shrinkage. So, it is important to verify the physical, structural and chemical changes that occur during its pyrolysis [61].

Besides, the characteristic properties of char indicate its different uses. Some important aspects that make it suitable as a solid fuel, adsorbent or as catalyst, are its hygroscopicity and specified surface area. When planing to use the char in a gasification process, in particular to obtain activated carbon or syn-gas, its porosity, moisture content and chemical composition, are important characteristics that result from the process, to maximize a particular product.

The measurement techniques used in this work to characterizate the porous solid materials, were: differential thermogravimetric (DTG) analysis, elemental analysis, surface area and pore size analyses, ESEM, SEM/FEG observation and dynamic vapor sorption evaluation, are presented below.

- *Environmental Scanning Electron Microscopy (ESEM)*: is a analysis technique that utilizes focused beams of electrons to magnification with high-resolution images (Fig. 2.4).

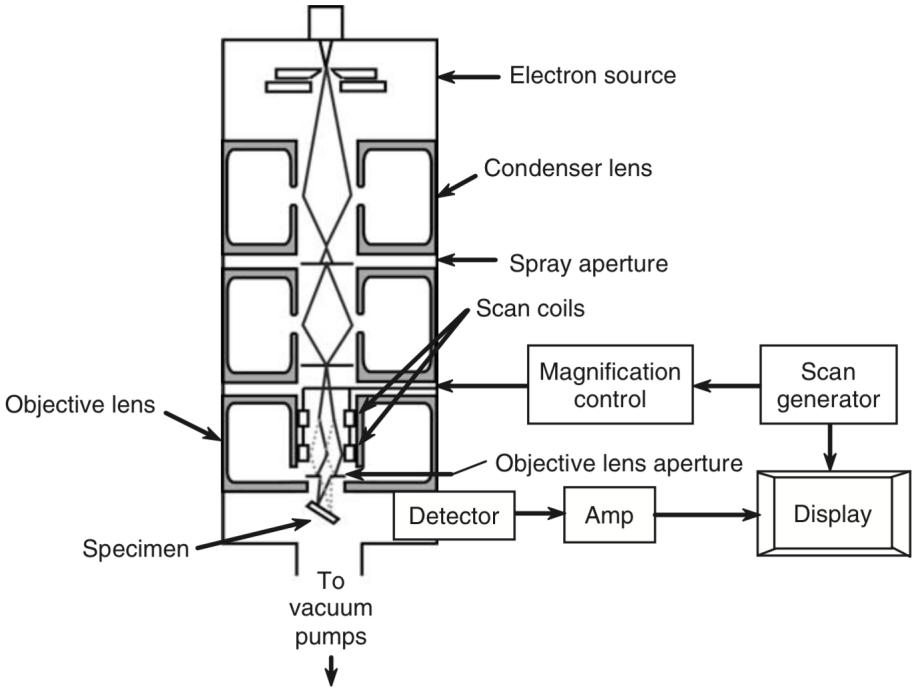

Figure 2.4: Simplified schematic diagram of the basic components of an SEM. Adapted from [20].

Environmental SEM are designed to image sample with a quite high gaseous pressure in the chamber. Using water vapour as chamber gas, the sample can be observed without coating and at different equilibrium moisture contents.

The analysis provide topographical, morphological and compositional information. Usually, it is employed to observe the morphology of biomass chars, to obtain details about the pore dimensions, phase changes during thermal treatments and the general structure of the cell walls (like clusters, fibrous, voids) [166]. This is important for gasification process where for example, the fine voids of biomass char, allow explains the more uniform gas transfer and that the high gasification reactivity is maintained and increased with the elapsed time [167].

- *Elemental analysis:* This analysis allows quantities of organic elements, CHNSO, present in a sample, giving the composition as a percentage of the sample weight. The basic principle is the rapid high oxidation of the sample to then direct the CHNS/O elements to chromatographically separate the combustion gases and then detect them in a highly sensitive TCD (thermoconductivity detector).

  This analysis is very useful to evaluate in function of the chemical composition of the sample, the energy intensification of a solid or liquid fuel, using the

van Krevelen diagram (Fig. 2.5) and the relation in the O/C and H/C ratios respectively [21].

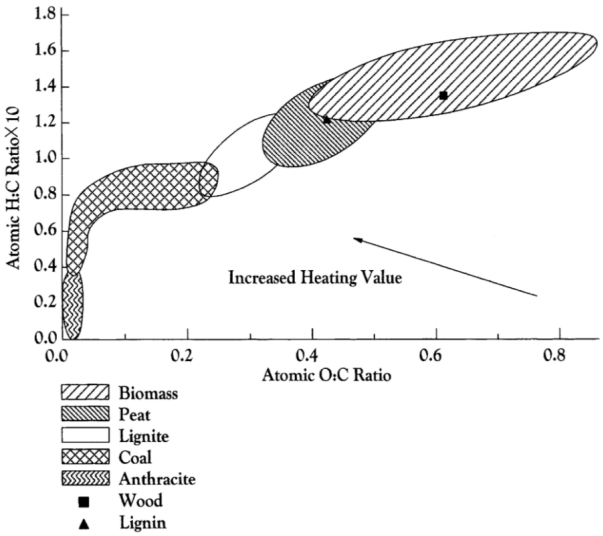

Figure 2.5: Van Krevelen diagram of biomass. Adapted from [21].

- *Surface area BET and pore size analysis:* surface adsorption can occur via two mechanics: physisorption (physical interaction between the molecule and surface, as van der Walls forces) and chemisorption (intermolecular attraction by chemical bonding). Surface area, pore size and pore size distribution are derived from physisorption analysis [22].

  According the Brunauer, Deming, Deming and Teller (BDDT) classification and the International Union of Pure and Applied Chemistry (IUPAC) classification, commonly eight gas adsorption isotherms (Fig. 2.6) can be observed based on the physicochemical conditions of the interactions. Detailed information about the isotherms can be found in [22, 168, 169].

  Surface area or external surface area (including surface attributable to pores), is one of the major importance analysis for the characterisation of a wide range of porous materials as char/charcoal, biochar and activated carbon. The area covered may be calculated by considering the amount of gas/vapour used to form the monolayer as well as the dimensions and the number of molecules 22.

  This technique is based in a gas adsorption, as nitrogen at 77 K by a porous material, where a continuous or discontinuous manometric techniques is employed for nitrogen adsorption measurements.

  The Brunauer−Emmett−Teller (BET) equation, as shown below, is the most commonly used method to determine the monolayer and specific area values in various physicochemical areas.

$$\frac{x}{V(1-x)} = \frac{1}{V_m c_{BET}} + \frac{x(c_{BET}-1)}{V_m c_{BET}} \tag{2.1}$$

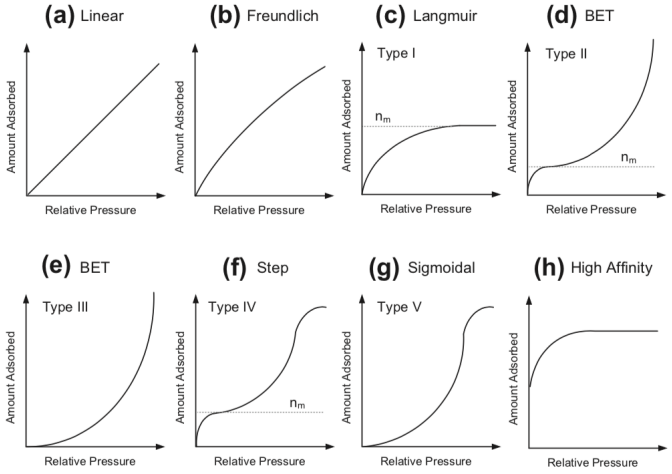

Figure 2.6: Schematic diagrams of eight commonly observed adsorption isotherms. Adapted from [22].

where V is the volume of adsorbed molecules, V_m is the monolayer volume, c_{BET} is the BET constant, and x is the relative pressure (P/P_0).

BET equation is considered a standard evaluation of monolayer values for adsorbate activity of between 5% and 35% P/P_0 and there can be no doubt in the universality or importance of the nitrogen BET method at low temperatures [22].

- *Dynamic vapor sorption:* is a gravimetric technique based on the mass changes sensitivity of a ultra-microbalance with the experiments performed at ambient temperature and ambient pressure.

  This technique allows relatively low surface areas "as BET surface area" to be measured and is applied also to obtain some information on the water sorption capacity. These are a very useful means of determining accurate sorption isotherms using water vapor in a range of pre-set relative humidity (RH) values.

  Therefore, as lignocellulosic materials derives from the numerous hydroxyl (OH) groups associated with the cell wall macromolecules, its hygroscopic properties can be determined. The hygroscopic characteristic depend of the OH content of its main components and its accessibility to the water molecules. Cellulose and hemicelluloses, has the highest $OH - carbon$ ratio, but not all of the OH content is accessible. Even more, there is a swelling of the cell wall as it absorbs water, which involves expansion of the $lignin - hemicellulose$ matrix in which the microfibrils are embedded.

  Figure 2.7 shows a schematic of dynamic vapour sorption apparatus.

  As explained in [23], the apparatus contains two measurement pans (sample and reference holders) suspended from the arms of a ultra-sensitive microbalance. The sample and reference holders were connected to the microbalance by

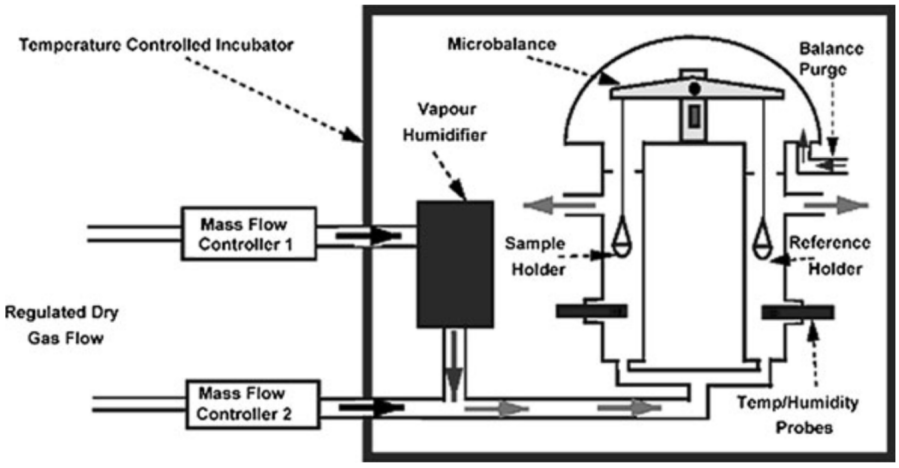

Figure 2.7: Dynamic vapour sorption device as a Surface Measurement Systems. Adapted from [23].

hanging wires sitting in a linked double chamber which is located in a thermostatically controlled cabinet. A constant flow of dry nitrogen gas, into which is mixed another nitrogen stream containing water vapour, passes through the measurement chamber to maintain a set RH. A typical run started at 0% RH and then increased in RH steps of 5 or 10% RH), before decreasing to 0% RH in the reverse order. The instrument maintained a constant RH until the sample moisture content change per minute (dm/dt) was almost constant (less than 0.002% per minute) over a period of time (usually 10 min).

When exposed to an atmosphere at constant RH, the cell wall has an associated moisture content (MC) which is in equilibrium with the atmosphere; but the situation is one of the dynamic equilibrium with there being a balance with the flux of water molecules exiting the cell wall being equal to the flux of water molecules entering the cell wall. The moisture content at the point, where this dynamic equilibrium occurs, is usually referred to as the equilibrium moisture content (EMC) [23].

2.3 Numerical approach: "bio-oil combustion kinetics"

In this part of the work, we focus on the numerical approach to propose a chemical kinetic mechanism for the bio-oil oxidation process. In addition, the bio-oil production unit and the bio-oil chemical composition, to examine it as liquid fuel for combustion process (e.g. as an alternative to fuel-oil used in boiler) are presented.

Power generation from different bio-oils has already been studied by several

authors and its combustion have been demonstrated empirically [9, 142, 143]. To the best of our knowledge, this thesis presents the first chemical kinetic mechanism for bio-oil oxidation, which seeks to better understand its combustion phenomena. In adittion, the first chemical characterization of coconut endocarp —*Acrocomia aculeata*— bio-oil is presented.

2.3.1 Bio-oil production unit

A pretreatment "torrefaction" was performed to the raw material, mainly to reduce the bio-oil water content [170, 171, 172], which is around 50% w/w for this specific feedstock [6] and to improve its grindability properties (biomass loses its tenacious nature) [173].

The devices used for both, torrefaction and pyrolysis process are: an electric oven, a nitrogen balloon, a fixed bed reactor, a vertical condenser of concentric tubes and a condensate collector (Fig. 2.8).

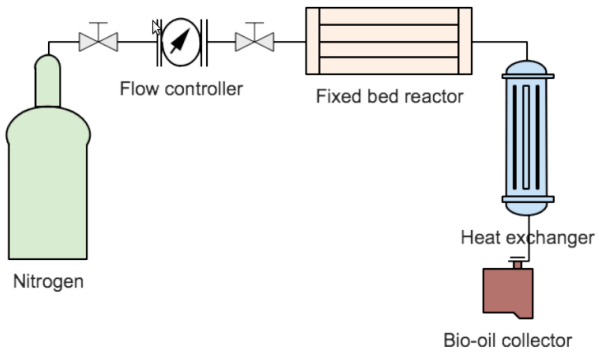

Figure 2.8: Schematic of the experimental process.

The reactor consists of a stainless steel tube AISI 304 of 15 cm length; 3.81cm outer diameter and 3.54 cm inner diameter; and at the end of it, two segments of wire mesh Tyler No. 300, in order to support the bed and allow gases to flow through the reactor. The reactor is horizontally supported, inside an electric furnace, to a pipe section of the same material as the reactor, through which nitrogen gas is transported. As the products of pyrolysis are volatilized in the reactor, the nitrogen stream enters the reactor, and drags them out of it (Fig. 2.9).

At the reactor outlet it is installed as a condenser, which consists of two concentric tubes of 3.81 cm and 2.54 cm diameter and 30 cm length, with water at room temperature flowing counter-current as a cooling fluid. The condensate collector col-

(a) (b)

Figure 2.9: (a) Stainless steel reactor. (b) Tubular furnace to pyrolysis process. [18].

lects most of condensed that can condense at room temperature. The non-condensed gases leave through a lateral connection.

The charge of the reactor was introduced into the furnace before each experiment. The system purging was performed with nitrogen gas at 2 L/min flow rate for a 10 min period. The pyrolysis was carried out under a non-linear heating rate, with 18.0 °C/min average rate. During pyrolysis process, nitrogen gas flow was kept constant, performing two functions: to maintain the anaerobic conditions and to flush fluid for the products that are formed by controlling the gases residence time.

2.3.2 Composition analysis of bio-oil

Bio-oil characterization is very difficult due to the presence of the pyrolytic lignin and the huge complexity of its components (mixtures of hundreds of organic oxygen-containing components as carboxylic acids, phenols, alcohols, aldehydes, ketones, ethers, esters, furans, sugars, and water), with a wide distribution of boiling points and molecular weights and with a different polarity and solubility [140].

Moreover, many of the bio-oil compounds are present in very low concentrations and only approximately 40 wt % of components, which are detectable by gas chromatography, 15 wt % of nonvolatile components are detectable by liquid chromatography and approximately 15 wt % of high-molecular (residual) components cannot be detected by chromatographic methods [174]. Therefore, detailed analysis requires the combination of several analytical methods.

Several authors have proposed, a pretreatment in order to achieve more detailed information about their chemical composition. Typical fractionation by liquid-liquid extraction (LLE) based on the water addition was used [140, 175, 176]. Then, Bio-oil composition is analyzed with Gas Chromatography and Mass Spectrometry (GC-MS) technique.

The objective of these measurements is to obtain the chemical composition of studied bio-oil, in order to estimate the equivalence ratio of different bio-oil flames.

Furthermore, different surrogates will be proposed in function of blends of the major components determined by GC-MS. This surrogates must to have equivalent formulas and ratios H/C and O/C very close to those of bio-oil. The equivalent formula will be calculated in function of the number of atoms presents in the major components and its corresponding mole fractions

2.3.3 Simulation of bio-oil combustion

Due to the large amount of information necessary to describe complex phenomena, such as combustion, the simulation is performed on computers using softwares including data libraries of thermodynamic and transport properties, as well as differential equation resolution codes. Some of these software are Regath, Aspen Plus, Therm, Quarry, Ansys, Cantera and Chemkin. Regath is a Fortran 90 package which includes thermodynamics and chemical routines (Transport and Chemkin). It also includes a $0-D$ reactor solver as well as a $1-D$ freely-propagating flame solver and a counterflow solver [177].

One important combustion tool is the chemical kinetic mechanism. These mechanisms can be used to predict ignition properties, heat release rate, amount of emissions, and the types and levels of intermediate species in any combustion system.

In order to consider a mechanism accurate, the data obtained from the simulation must be validated. In the validation usually, the temperature, velocity and concentration profiles of experimentally measured species are compared with those predicted by the simulation [178]. In addition, two extremely important macroscopic parameters constitute the auto-ignition delay and the propagation speed of the premixed flame. Both parameters are characteristic for a given fuel and depend on the chemical processes that occur during combustion [179].

2.3.3.1 Developing and validating Chemical Kinetic Mechanisms

The steps necessary to develop and validate chemical kinetic models was established by Frenklach et al. (1992) [180], which then was summarized by Simmie (2003) [181]:

1. Generate a comprehensive list of elementary chemical reactions,

2. Determine reaction rate constants for each elementary reaction using literature data or estimation, treating temperature and pressure dependencies in a consistent manner. Evaluate error limits and thermodynamic data to calculate equilibrium reverse rate constants,

3. Carry out and/or find in the literature reliable experiments that can be used to validate the reactions and rate parameters given in the model,
4. Solve the reaction mechanism kinetics and transport equations using a computer application in order to simulate the experimental configuration. Conduct a sensitivity analysis to determine how the model rate constants affect the final result,
5. Make a comparison of the model predicted values with the experimental results. Optimize reaction rate parameters that have the largest impact on fitting the experimental results.

In the present work, only numerical simulations of the combustion will be carried out. Experimental tests will not be performed for the validation of the numerical results, due to lack of necessary equipment.

First, we have chosen among all the reaction mechanisms available in the literature for the chosen surrogate fuel (the chosen of this surrogate is detailed in 6.2.4), the one best suited to our case (items 1 and 2 on the list). Then, we focus on items 3 and 4 on the list, for which, the REGATH software, developed in the EM2C laboratory (Laboratoire de Energetique Moleculaire et Macroscopique, Combustion, Centrale Supelec, France) was used, considering the reaction mechanism and thermodynamic and transport properties.

Finally, concerning item 5, we have conducted a numerical validation due to the impossibility of performing an experimental validation. Thus, the developed mechanism is validated by analyzing important parameters of the main bio-oil components and comparing results obtained using both the developed scheme and others mechanisms and experimental data from the literature.

2.3.3.2 Surrogate chosen

In this section, the objective is to carry out bio-oil combustion studies.

For experimental studies associated with numerical simulations, the complex and varying composition of bio-oil makes the number of possible reaction pathways in the chemical reaction to increase drastically [86, 182]. Development of models that represent all of these components is prohibitive because the model would be too large for current computational resources [183].

In order to avoid these difficulties, simplified synthetic fuels, called "surrogate fuels", with shorter chain lengths and known physical chemical properties are chosen to carry combustion studies. The term surrogate refers to a simplified representation of a real complex fuel [183].

The purpose of using surrogates is to simplify the combustion mechanism by using a single fuel molecule or a blend of relatively small molecules to represent the real fuel. Numerically, the use of surrogate fuels reduces significantly the number of

possible chemical reactions in the kinetic scheme, while still representing the main properties of the real fuel [178].

Mueller et al. (2012) [184], have indicated the steps to follow for the selection of the substitute of a specific fuel,

- Select the target fuel.
- Choose the property you want to reproduce.
- Identify the compounds that could form the substitute.
- Determine the concentrations of each component.

In this work, torrefied coconut endocarp is used to produce pyrolysis bio-oil, which is selected as the complex target fuel. An equivalent formula and the ratios H/C and O/C very close to those of bio-oil are selected as the parameters to be reproduced. Then, the auto ignition delay along with the propagation speed of premixed flames can be determined.

Usually, the chemical composition of bio-oils is analyzed by chromatography analysis (GC/MS) [185, 171]. Consequently, the compounds that will form the substitute will be the three major components obtained from this GC/MS analysis, together with their respective concentrations.

In numerical studies of combustion, several surrogates were proposed for fossil fuels and more recently for biofuels. Thus, as substitutes for gasoline, which is a complex mixture of linear, branched and cyclic alkanes; the n-heptane, iso-octane and toluene compounds, were used [186]. To biodiesel, which is formed by different types of methyl esters, were proposed the methyl butanoate, methyl decanoate, methyl 9-decenoate, n-hexadecane and others as substitutes [178]. Different mixtures of n-heptane, toluene, ethanol, dimethylether, ethane, and phenol were employed for simulation of diesel engine to describe the combustion chemistry of typical biofuels [187].

Recently, several surrogates for biomass-derived fuels have been proposed. Anisole (or methoxybenzene) was used as a substitute of lignocellulosic biomass pyrolytic oil due to its typhical composition rich in phenolic species to study its decomposition under pyrolysis and oxidative conditions [188]. Also, the combustion kinetics of ethyl levulinate (Ethyl 4-oxopentanoate), a liquid fuel that may be easily obtained from lignocellulosic biomass, have been investigated. For the kinetic model, was used the thermochemical-kinetic analogies to 2-butanone, for the ethyl levulinate ketone functionality, and to ethyl propanoate for the ethyl ester functionality [189].

The objective of this work is to propose a surrogate fuel that represent the real complex composition of torrefied coconut endocarp bio-oil and numerical studies to obtain fundamental parameters of this bio-oil fuel combustion.

2.3.3.3 Autoignition delay simulation

Autoignition delay simulations are performed using 0-D constant-volume reactor solver of REGATH package, which have included the detailed thermochemical and transport properties for the fuel compounds and have developed at EM2C laboratory [190, 191].

In this configuration a transient, closed system of constant volume and perfectly mixed is considered that initially contains a reactive mixture at a certain pressure and temperature.

These considerations affect the following terms of the conservation equations.

In a closed system (there is no convective transport of species or energy)

$$\rho_j \vec{v} = 0 \tag{2.2}$$

$$\rho \vec{v} h^s = 0 \tag{2.3}$$

The temperature and the composition of the species does not vary with respect to the spatial dimensions, only with respect to time. Therefore, the gradients of these variables are zero, and there is no diffusion of energy or species.

$$\vec{J}^{(h)} = 0 \tag{2.4}$$

$$\vec{J}_j = 0 \tag{2.5}$$

The degradation of the mechanical energy to thermal is neglected.

$$(\tau : \nabla \vec{v}) = 0 \tag{2.6}$$

It is considered a mixture of ideal gases, therefore the enthalpy depends only on the temperature and the term $\frac{DP}{Dt}$ is not included in the energy balance.

The species conservation equation is as follows

$$\frac{dY_j}{dt} = \frac{M_j \dot{\Omega}_j}{\rho} \tag{2.7}$$

where Yj is the mass fraction of the species j.

The energy balance for the system is then

$$\frac{dT}{dt} = \frac{-\sum_{j=1}^{N} h_{fj}^{0} M_j \dot{\Omega}_j}{\rho c_p} \tag{2.8}$$

Thus we have two differential equations of the first order. The initial conditions of the temperature and mass fractions of each species are given as:

Equations (2.7) and (2.8) are discretized by finite differences and the resulting algebraic equations are solved using Newton's Method [192]. Equation (2.8) allows the temperature profile of the system over time to be obtained. With this information, the program calculates the auto-ignition delay as the time that elapses from the start of the simulation to the point where the maximum rate of temperature change is reached (190).

$$\tau = t|_{\frac{dT}{dt}=max} \tag{2.9}$$

2.3.3.4 Freely propagating premixed flames

The laminar burning velocity is a physicochemical property dependent on the temperature, pressure, and mixture composition (fuel type, equivalence ratio, and amount of diluents) [101]. As a result, the laminar burning velocity provides invaluable information on the combustion properties and the underlying oxidation chemistry of the given fuel [116]. It is also an important parameter in the design of engines, burners and other equipment where combustion is involved.

Several experimental setups can be used to measure the laminar burning velocity of fuels: flat flame burners, combustion chambers, counterflow burners, etc. [193].

It is found that a detailed knowledge of laminar premixed flames will provide insights into such properties as heat release rate, flammability limits, propagation rates, quenching and emissions characteristics. It is also common to use measured burning velocities to validate chemical kinetic schemes [186].

Although the majority of fuel is probably burnt in turbulent combustion, data on laminar burning velocities are still needed as input to many turbulent combustion models. Also, in internal combustion engines the initial combustion is laminar, so again there is a need for the laminar burning velocity [194].

For our system, we consider a steady, isobaric, quasi-one-dimensional flame propagation configuration. A bio-oil/air mixture is injected from one side, and a premixed flame propagates freely towards fresh gases with the corresponding laminar flame velocity. In order to get a stabilized flame (instead of a propagating flame) one must inject fresh gases with a velocity equal to the laminar flame velocity.

Gaseous phase are described by the following balance equations (mass, energy and species, respectively). It must be noted that there is one species conservation equation for each species present in the numerical model (N_{sp}).

$$\frac{\partial \rho_g v_g}{\partial z} = 0, \tag{2.10}$$

$$\rho_g v_g c_{p_g} \frac{\partial T_g}{\partial z} = \frac{\partial}{\partial z}\left(\lambda_g \frac{\partial T_g}{\partial z}\right) - \sum_{k=1}^{K} h_k W_k \Omega_k - \left(\sum_{k=1}^{K} \rho_g Y_k V_{kz} c_{p_{gk}}\right) \frac{\partial T_g}{\partial z}, \tag{2.11}$$

$$\rho_g v_g \frac{\partial Y_k}{\partial z} = -\frac{\partial}{\partial z}\left(\rho_g Y_k V_{kz}\right) + W_k \Omega_k, \qquad k = 1, ...N_{sp} \tag{2.12}$$

The solutions have the form: gas density $\rho_g = \rho_g(z)$, gas axial velocity $v_g = v_g(z)$, gas temperature $T_g = T_g(z)$ and species mass fractions $Y_k = Y_k(z)$, $k = 1, ..N_{sp}$ (N_{sp} is the number of species).

In these equations $c_{p_{gk}}$ and c_{p_g} are the heat capacity at local constant pressure of species k and of the mixture respectively. h_k, W_k, Ω_k are the specific enthalpy, the molar weight and the molar chemical production rate of the k^{th} species respectively and V_{kz} is the diffusion velocity of the k^{th} species in the axial direction.

The above system of equations is completed by the ideal gas equation.

2.3.3.5 Solution method

The governing equations are solved using a Newton solver, that evaluates the chemical kinetic, thermodynamic, and transport properties in each differential element in function of time [195].

REGATH package provides modelling of a wide range of combustion configurations, including 1-D premixed flames, gas and spray counterflow for both diffusion and premixed flames, and perfectly stirred reactors.

In order to carry the simulations, three information files must be provided: the chemical kinetic database, the thermodynamic database and the transport database.

Chemical kinetic mechanisms are coupled with thermochemical data for all the species in the mechanism to calculate forward and reverse reaction rates.

Transport properties for the species are also included in combustion processes in which transport phenomena are important (e.g. premixed counterflow flames).

2.3.3.6 Summary

The use of pyrolysis oil as a transportation fuel is limited due to its high acidity, low thermal stability, low calorific value, high water content, high viscosity and poor lubrication characteristics. Therefore, to improve certain characteristics of bio-oil, blends with petroleum fuel and alcohols are a viable short-term alternative to utilize an important fraction of these oils [196, 197].

Consequently, the second part of the work is about the numerical studies of bio-oil surrogates oxidation in 0-D and 1-D gaseous premixed flames. The goal is to develop a chemical kinetic mechanism for its major components blends oxidation by carefully merging appropriate chemical kinetics mechanisms from the literature. For this, simulations are used, taking into account detailed chemical kinetics and multi-component transport properties and are performed using the REGATH package of EM2C laboratory [190, 198, 199].

Thus, once the developed bio-oil surrogate chemical kinetic model has been experimentally validated, it would be possible to use it to carry out simulations and more complex experiments with mixtures (e.g. bio-oil/diesel/n-butanol).

Chapter 3

Alteration of physico-chemical characteristics of coconut endocarp –Acrocomia aculeata– by isothermal pyrolysis: micro experiments

This chapter presents the experimental procedure and results obtained by physicochemical evolution along the thermal decomposition of the endocarp of Acrocomia aculeata fruit samples, evaluated before and after 2 h of isothermal pyrolysis in the range 250 to 550 °C. The measurement techniques used were: differential thermogravimetric (DTG) analysis, elemental analysis, surface area and pore size analyses, ESEM and SEM/FEG observation and dynamic vapor sorption evaluation.

3.1 Introduction

The endocarp represents about 21% of the overall residue mass generated after processing the mbocayá —*Acrocomia aculeata*— fruit [40]. In addition, it has higher values of fixed carbon, lignin content and energy density than other parts of the fruit [40; 6]. These characteristic properties allow us to consider endocarp as potential feedstock to produce biofuel or materials like charcoal and activated carbon for a variety of applications; the thermochemical conversions, pyrolysis and gasification, could be promising methods to accomplish this.

During pyrolysis, thermal decomposition of biomass components (cellulose, hemi-

cellulose and lignin) takes place. In general, the char produced is expected to have higher carbon content and heating value. Its chemical structure and physical properties such as density, specific surface area, water content, and electrical conduction, changes according to the pyrolysis conditions and feedstocks [89; 88; 200].

In order to produce different fuels and chemicals from pyrolysis, the composition of raw material and thermal decomposition mechanism should be determined. Although there are extensive studies on the mechanisms of biomass pyrolysis [154; 155; 156], none is specific to this feedstock or the kinetic progress of its thermal decomposition.

In this study, mass loss as a function of time, in static conditions, were used to explain kinetic pyrolysis in the coconut endocarp. Three decomposition rates were observed from the mass loss vs time curves, related to the three main components' degradation. These measurements serves as the basis for future work in developing a kinetic model for biomasses of this type.

The major focus of this study is the experimental characterization of the coconut endocarp and its chars, obtained from a variety of isothermal pyrolysis conditions. It is important to propose the more relevant use of coconut endocarp and its chars, as *Acrocomia aculeata* is a potential feedstock for a biorefinery, likely to reduce deforestation and pollution.

3.2 Materials and pyrolysis conditions

A. aculeata, indigenous to Paraguay, is usually found in areas situated between the latitudes 19 and 27 south and longitudes 54 and 62 west. The solid and woody residue inside the fruit, referred to as 'coconut endocarp", was used in this study. The availability of the coconut endocarp, as agroindustrial waste in Paraguay, is about 7 tonnes of dry matter per hectare per year [31]. The feedstock was cleaned with water and dried in air flow at room temperature. Sample particles, between 0.2-0.63 mm selected from a previous work [6], were obtained using a grinder (IKA M20 Universal mill) and subsequently sieved.

The pyrolysis was carried out by a STA 449 F3 Jupiter, NETZSCH at atmospheric pressure. Each sample with an initial weigh of 10 ± 2 mg was placed in an alumina crucible and heated at 5 °C min^{-1} under a nitrogen flow of 50 mL min^{-1} (STP). Initially, samples were heated from ambient temperature to 100 °C, and dried for 30 minutes. The temperature was then increased to a final temperature (250 °C, 300 °C, 350 °C, 400 °C, 450 °C, 500 °C, 550 °C) and was observed, thereafter, for 2 hours.

The percentage mass loss "ml" defined as the instantaneous anhydrous mass

loss as a function of time, was calculated with the following equation 3.1.

$$ml = \frac{m_i - m_t}{m_i} \times 100 \tag{3.1}$$

where m_i is the anhydrous mass at the beginning of the thermal degradation (after they were dried at 100 °C for 30 min) and m_t is the anhydrous mass of the char residue (thermal treated sample) in the instant t of the thermal degradation. The final mass loss "fml" is measured at the end of the plateau for each selected temperature. This method was employed following previous testing in this lab which indicated that 30 min at 100 °C was enough time to release the moisture content in powder wood samples [201].

The term "char" in this study, refers to the solid residue that remains in the crucible after each treatment. This term, and its associated temperature, are used to refer to the char obtained after each pyrolysis treatment obtained at a specific temperature, for example, "350 °C-char", represents the char obtained after the pyrolysis of coconut endocarp at 350 °C for 2 h in the condition described above.

In addition, derivative thermogravimetric (DTG) curves were plotted for the cases of untreated endocarp and char samples in order to check for the characteristic DTG peaks normally found in carbohydrate decomposition (cellulose, hemicellulose and lignin). The heating rate employed was 10 °C/min under the nitrogen gas flow of 50 ml/min. The initial mass sample remained between 3 and 4 mg. All experiments were performed in triplicate and several blank tests were made to correct the effects of buoyancy forces.

3.3 Analytical methods

3.3.1 Elemental analysis

The evolution of the elemental composition was measured by Thermo Scientific FLASH 2000 CHNS/O analyzers. In order to determine carbon, hydrogen, nitrogen and sulfur (CHNS), the standard reactants were used: BBOT (2,5-(Bis(5-tert-butyl-2-benzo-oxazol-2-yl) thiophene), methionine, and cysteine. Additionally, vanadium oxide (V_2O_5) was added in order to ensure good resolution of the peaks. BBOT and benzoic acid were used to determine the oxygen (O) content. All the samples were dried at 103 ± 2 °C and stored in a desiccator until the analysis and the experiments were performed in triplicate.

Since lignocellulosic biomass are composed of three main chemical components (cellulose, hemicellulose, lignin), a review of its elemental and proximate analyses is shown in Table 3.1 for comparison proposes.

Table 3.1: Elemental and proximate analyses of the main components of biomasses

components		Ref. *	elemental analysis (%wt)			proximate analysis (%wt)		
			C	H	O	Ash	VM†	FC‡
Cellulose	Micro-crystalline cellulose	202	44.4	5.8	49.3	0	94.8	5.2
	Sigmacell micro-crystalline cellulose		44.5	5.6	49.5	0	94.1	5.9
	Micro-crystalline cellulose powder	203	39.99	5.8	54.2	0.51	98.7	0.8
	Pure cellulose	204	42.06	6.06	46.38	-	89.20	5.30
Hemicellulose	Xylan from birchwood	202	46.7	5.7	47.4	4.1	73.3	22.6
	Xylan from beechwood		44.3	5.4	49.9	4.8	75.3	19.9
	Xylan from oat spelts		44.8	5.6	49.5	10.1	71.1	18.8
Lignin	Alkali lignin	202	56.6	4.2	37.1	10	49.9	40.1
	Lignin from Borregaard		65	4.9	28.7	13.5	45	41.5
	Lignin from Meadwestvaco		66.7	5.6	26.1	2.4	58.9	38.7
	Organic-solved lignin	203	49.53	4.39	46.07	1.71	93.8	4.5
	Pure Lignin	204	47.65	4.30	19.60	12.35	35.74	38.81
	Alkali Lignin	166	66.5	5.8	25.3	5.7	-	-

*Differences between the results presented by each author, are attributed to different extraction methods and the origin of raw material
†Volatile matters
‡Fixed carbon

3.3.2 Surface area BET analysis and porosity characteristics

The surface area evolution of the samples was evaluated by the adsorption of nitrogen at 77 K in the Micromeritics 3Flex surface characterization analyzer. Prior to analysis, the samples were outgassed at 80 °C until achieving a residual pressure of 10^{-4} mmHg, which lasted for different periods of time according to the surface area of each sample. BET surface area, from the isotherms, was calculated using the Brunauer-Emmett-Teller (BET) equation. The relative pressure (P/P_0) range that was considered was 0.01 to 0.30 and was assumed to be 0.162 nm^2, which is the cross-sectional area for a nitrogen molecule. The total mass of the samples used was enough to achieve a good isotherm plot without mathematical smoothing. The pore size distribution was calculated using the Density Functional Theory (DFT) and the total pore volumes were determined from a single adsorption point at a relative pressure $P/P_0 \geq 0.95$. The experiments were performed in triplicate.

3.3.3 Environmental scanning electron microscopy (ESEM) and scanning electron microscopy with a field emission gun (SEM-FEG)

Two microscopy analyses were conducted. First, particles (2 mm size), before and after the treatment at 250 °C and 550 °C were evaluated using a FEI Quanta 200 to observe the global changes, under low vacuum, at 0.6 Torr and 12.5 kV. Second, the char residues were recovered from the thermo-gravimetric devices with tungsten and observed, using the Leo 1530 (SEM-FEG) at 2.00 kV and high vacuum, in order to see the main morphological changes in the cellular wall.

3.3.3.1 Water vapor sorption properties of untreated (control) and treated samples

Sorption isotherms and hysteresis were measured using a dynamic vapor sorption apparatus (DVS; Surface Measurement Systems Ltd, London, UK) at a temperature of 25 °C. Detailed information about the apparatus can be found in [23]. All of the samples had similar weights 22.2 ± 0.6 mg and were weighed using a sample pan and a micro-balance, which measured the change in the mass under dry nitrogen. The relative humidity (RH) was increased from 0 to 90% in 10% increments. The RH was raised to the next step when the change in sample mass was below 0.002% min^{-1} and remained so for 10 min. After a constant mass was achieved at 90%, the RH was lowered back to zero in the same configuration as each step. Absolute hysteresis was calculated as the difference between the equilibrium moisture content (EMC) during the desorption ($EMC_{desorption}$) and adsorption ($EMC_{adsorption}$) [205]. The experiments were performed in triplicate.

3.4 Results and Discussion

3.4.1 Mass change profile as a function of time

When biomass is pyrolyzed, different depolymerization and devolatilization reactions take place from the polysaccarides and organic polymers decomposition. Anhydrous mass loss during pyrolysis is a consequence of these decompositions and is depicted in Fig. 3.1.

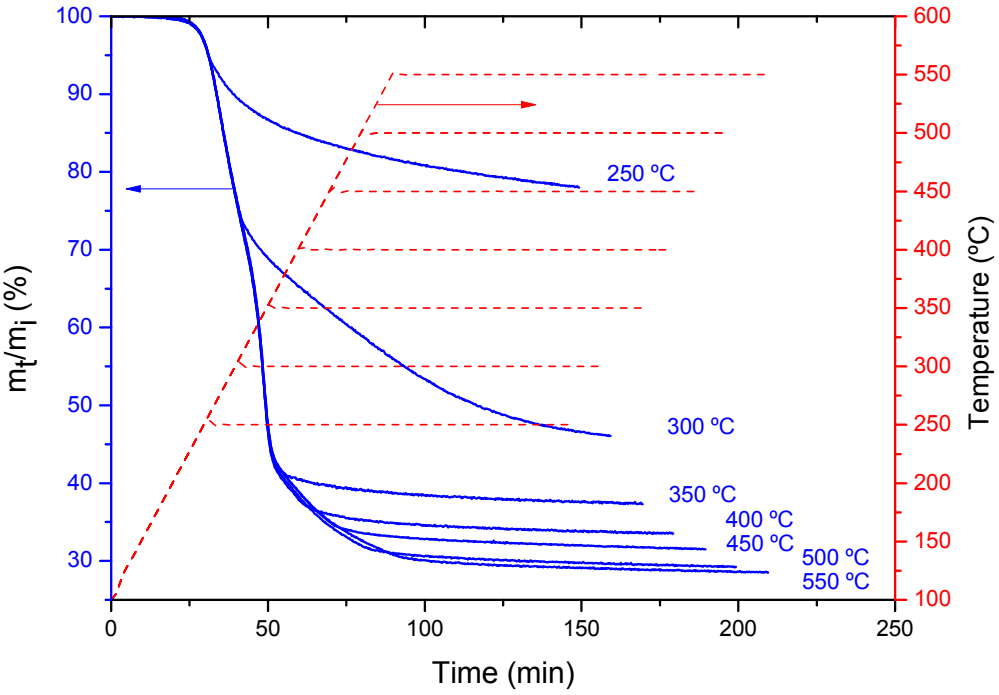

Figure 3.1: Anhydrous mass loss of coconut endocarp, as a function of time, for each pyrolysis treatment. The red lines indicate the temperature evolution as function of time.

We can clearly observe three behaviors, which are related to the three main components degradation. The first behavior occurs during the treatment at 250 °C, with a "*fml*" of about 25%. For this level of temperature, the decomposition of hemicellulose and the release of high-volatility compounds and gases (majorly: H_2O, CO, CO_2 and acid compounds) is expected [206; 207].

The second behavior is observed in the sample treated at 300 °C. It is mainly the consequence of both hemicellulose and cellulose thermal decomposition. Cellulose degradation is usually explained as a two-step process: an initial reaction step that leads to the formation of "active cellulose", which then undergoes some competitive reactions that produce char plus permanent gases and volatiles (tar) [208; 209; 210]. It

is well known that from 300 to 400 °C, cellulose thermal decomposition occurs with a higher decomposition rate that lignin, which decomposes in a wide temperature range (250-500 °C) [211; 212]. The slope in the TG curve, nevertheless exhibits a significant decrease at 350 °C, indicating perhaps, that cellulose has been completely degraded at this temperature level.

The third observed behavior occurs from 350 °C until 550 °C, where the increment in fml was only 19% of the fml observed until 350 °C. This behavior is expected because from 350 °C, the main components in the char residue should be lignin and the degradation solid products derived from the carbohydrates decomposition. This slow mass decrease was observed in woody biomass [203; 213] as a second stage due the lignin decomposition.

Figure 3.2 illustrates the DTG curves for untreated and char samples. DTG of coconut endocarp shows two well-defined peaks with a maximum mass-loss rate of 4.84 %wt min^{-1} at 293 °C for the hemicellulose and 9.53 %wt min^{-1} at 365 °C for cellulose decomposition.

This double-peak was already observed for lignocellulosic biomass with high lignin contents, such as coconut endocarp (*C. nucifera*) [84; 214]. These authors also explained this double peak by high S/G ratios[1]. Therefore, we expect similar S/G ratio and the presence of p-hydroxybenzoates, proposed as authentic lignin precursors by [215], for our coconut endocarp lignin structure and composition as presented in [84]. However, the S/G ratios for the isolated lignin of coconut endocarp (*C. nucifera*) exhibits different values. These discrepancies could be due the extraction techniques employed [84; 83].

All other peaks, such as hemicellulose and cellulose peaks, were not well-separated in other lignocellulose biomass [211; 216; 217]. A little characteristic shoulder between 350 and 550 °C for lignin which apparently continues until 900 °C according to [213], showed a very slow mass loss that reached 1.40 %wt min^{-1} at 416 °C maximum.

DTG curves for 250 °C-char also depicts the sharp and shoulder peaks for cellulose and lignin, respectively. But the 300 °C-char, exhibited only the characteristic shoulder for lignin on the DTG curve, which indicated that the degradation of cellulose and hemicellulose were completed. This led us to suppose that at most 54 %wt of the coconut endocarp is composed of holocellulose, considering that the lignin decomposed slower than the other components, which is also in accordance with the results presented in [159].

The same shoulder, but at higher temperatures (550 °C), appears for 350 °C-char DTG curve. As lignin is resilient to pyrolysis, its relative content increases with pyrolysis temperature at similar residence time. So, as suggested in [214] higher lignin content can be expected for higher pyrolysis temperatures.

In the chars treated at 450 and 550 °C, this marking shoulder has apparently disappeared.

[1] syringyl- and guaiacyl- lignin units ratio

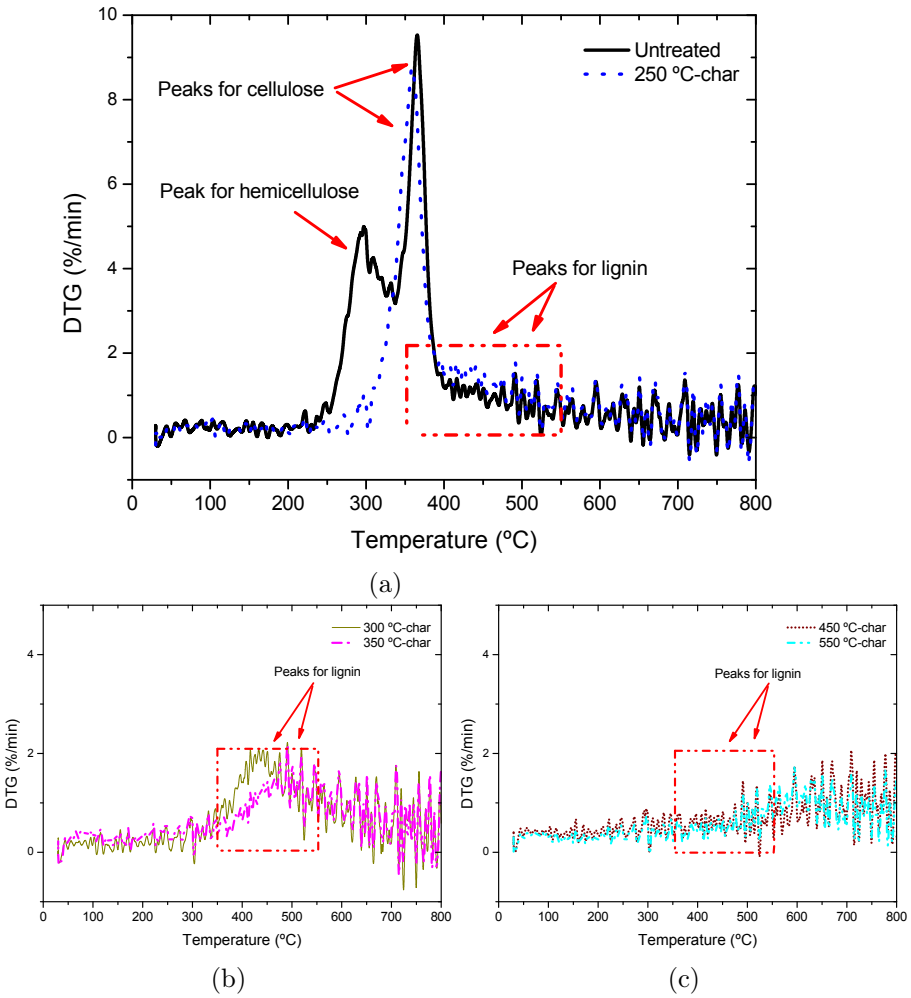

Figure 3.2: Comparison of DTG curves for (a) untreated and 250 °C-char, (b) 300 °C-char and 350 °C-char, and (c) 450 °C-char and 550 °C-char.

Mass loss results from numerous competitive reactions and this thermogravimetric curves can give us insight about the reaction mechanisms for the coconut endocarp pyrolysis.

3.4.2 Elemental composition

Elemental and surface analyses for the untreated and char samples are given in Table 3.2. Note that sulfur was not detected in any sample.

Coconut endocarp has a high lignin composition with amounts of carbon (C)

Table 3.2: Elemental composition and physical properties for untreated and char samples

	fml	elemental analysis (%wt)*					surface area	total pores volume	micropore volume
	(%wt)	C	H	N	O	S	BET (m^2/g)	(cc/g) $\times 10^{-3}$	(cc/g) $\times 10^{-3}$
Untreated	——	51.1	5.53	0.37	42.6	0.00	0.28	0.603	0.014
250 °C-char	22.0	56.9	4.95	0.40	38.6	0.00	0.30	0.322	0.079
300 °C-char	53.9	68.9	4.11	0.25	24.5	0.00	0.44	0.439	0.108
350 °C-char	62.7	71.9	3.75	0.26	21.1	0.00	0.52	0.457	0.138
400 °C-char	66.5	75.1	3.34	0.27	18.1	0.00	0.57	0.520	0.175
450 °C-char	68.5	78.2	3.02	0.28	13.6	0.00	5.95	2.56	2.06
500 °C-char	70.7	82.1	2.78	0.31	9.10	0.00	108	45.7	42.3
550 °C-char	71.5	85.7	2.55	0.59	6.08	0.00	216	89.1	84.2

*For an analyzer detection limit of 0.01% (100 ppm).

higher than 50% and oxygen (O) lower than 43%, in comparison to values reported in Table 3.1. These results are expected since the coconut endocarp has in average a high lignin content of approximately 35% and hollocelulose content of approximately 53% [40; 159].

Another important observation is that the sum (C + H + N + O) is not equal to 100% from 300 °C-char. This is due to char fraction contains inorganic materials (ash) and its proportion increases with the pyrolysis temperature [218; 219].

The most important thermochemical reactions can be visualized from the van Krevelen diagram (Fig. 3.3a). Overall, dehydration and decarboxylation reactions, led coconut endocarp to become more lignin-like, even from the first treatment at 250 °C.

Notable oxygen reduction from the initial oxygen content occurs for the sample treated at 300 °C ($\approx$ 24 %), which is expected from the hemicellulose and cellulose decomposition and the devolatilization of low molecular mass products at this temperature.

Considering the oxygen reduction, the low sulfur content and the lignin-like characteristic of char obtained at 250 °C and 300 °C, an interesting output could be the production of high-quality bio-oil for power generation or to produce phenolic-based chemicals.

The slow lignin decomposition explains the low additional oxygen reduction (about 6%) of the samples treated at 400 °C compared with those treated at 300 °C. There is an increase in the mass-loss rate from 400 until 550 °C, in accordance with the DTG curves (Fig. 3.2) and hence it observed a small increment in oxygen reduction (9%) was observed between the samples treated at 400 and 500 °C.

For the higher thermal treatment of 550 °C, 85.7% of the initial oxygen content has been removed with just 71% of fml. It is not trivial to predict the chemical structure of the 6% of oxygen that remains, which should be highly aromatic considering its carbon enrichment. More explanations about the chemical structure of carbonized charcoal can be found in [88].

Charcoal could be used as a reductant, in the production of chemicals, refining of metals, production of activated carbon or just as domestic cooking and heating [220]. The quality of the charcoals depends on the end use. The yields of charcoal obtained in our standard experiment seem promising because the treatment is almost uniform and leads to optimum yields [221; 222].

The van Krevelen diagram demonstrates the energy intensification with a linear correlation, H/C $\approx$ 1.64 (O/C) + 0.26 (R^2 = 0.999), see Fig. 3.3a. Elementary composition resembles a peat for the treatment at 250 °C and from 300 °C it goes from characteristic charcoal towards anthracite at the higher temperature [223; 224].

Furthermore, Fig. 3.3b shows a decrease of O/C and H/C ratios as a function of fml. A good polynomial approximation can be found for both ratios: O/C $\approx$ 0.62 –

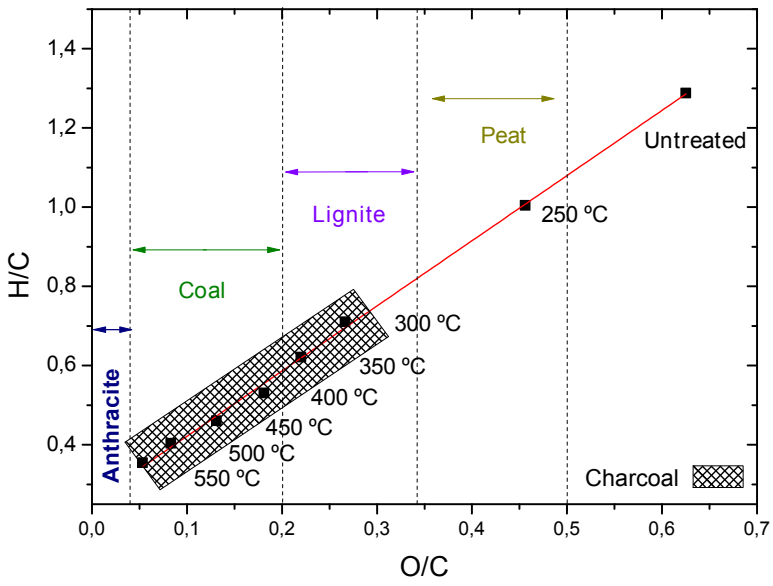

(a)

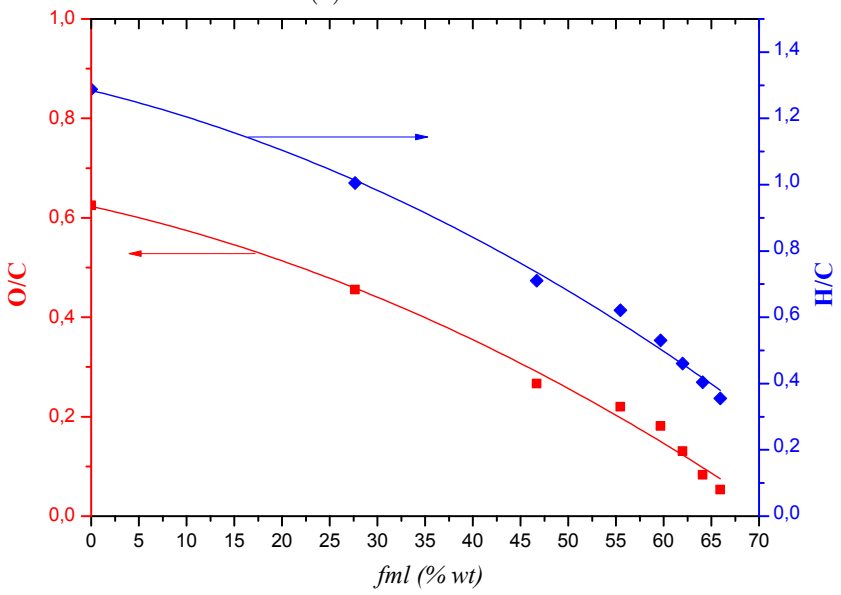

(b)

Figure 3.3: (a) van Krevelen plot. (b) O/C and H/C ratios as function of the fml.

$4\times10^{-3}(fml)-6.18\times10^{-5}(fml)^2$ with $R^2=0.986$ and H/C $\approx 1.28-7\times10^{-3}(fml)-1.02\times10^{-4}(fml)^2$ with $R^2=0.993$. These results show potential feasible application of the charcoals for electric power generation, for example, via biomass integrated gasification gas turbine (BIG/GT) technologies [220; 21], that could compete with

fossil fuels, also fewer emission and gas cleaning problems (from its lower nitrogen, sulfur and ash contents) are expected.

Physicochemical properties such oxidation stability and moisture sorption capacity can be predicted from the H/C and O/C ratios. Indeed, a considerable reduction in the number of polar sites from the O/C ratio reduction is expected and therefore a lower hygroscopicity in such chars. In [225], it was proposed for a first time a parameter "Z", $(Z = 2(O/C) - (H/C))$ to computed the average carbon oxidation state. The Z values computed as in [225], displays negative values for all chars here, in agreement with a reduced states of carbon (lignin is most reduced), which has a pronounced effect on its chemical reactivity.

3.4.3 Surface area and pore size analysis

Table 3.2 also displays the specific BET surface area and pore volume for the untreated and char samples. The untreated and char, obtained up to 400 °C, had very low surface areas, lower than 0.6 m^2/g, and a total pore volume lower than 0.52×10^{-3} cc/g. This behavior is explained by considering the high lignin content in the coconut endocarp, which could obstruct the pores since alkali lignin pyrolysis displayed a melting even at low temperatures of 250 °C [166; 226], resulting in low surface area until 350 °C, where the primary devolatilization process is less pronounced.

The low surface area of 400 °C-char could be attributed to coke formation as a consequence of tar cracking by the secondary heterogeneously reactions [227; 228], which may occur even in the pores of the particles [155]. Others authors [88] also justify the low surface area for carbonized charcoal of melt carbons (at 950 °C) as consequence of this liquid phase ocurring during pyrolysis. The 450 °C-char exhibits an exponential increase in the surface area, reaching a value of 216 m^2/g and total pore volume of 0.089 cc/g for the higher thermal treatment of 550 °C, which represents an increment of more than a thousand times the untreated sample.

Coconut endocarp presented typical adsorption isotherm type II (Fig. 3.4a), in accordance with the Brunauer classifications. In addition, char obtained until 400 °C showed the same type II isotherms, but less pronounced than those that were left untreated. From 450 °C, the adsorption isotherms change from Type II to Type I, characteristic of microporous materials, with at least 80% of total pore volume adsorbed ($\approx 2.56 \times 10^{-3} cc/g$) corresponding to microporous volume ($\approx 2.06 \times 10^{-3} cc/g$).

Furthermore, the pore size distribution (PSD) in the chars, Fig. 3.4b, shows that the exponential increment in the surface area is a consequence of the micropore development, with a pore width between 10 and 20 Å. To put this value in perspective, the diameter of the glucose molecule is 80 Å. Considering the microfibrils are composed of many chain of cellulose, the diameter of the microfibrils is more than 500 Å.

A zoom of the PSD for untreated and char samples until 400 °C, is presented in Fig. 3.4c and 3.4d. Although these samples are not microporous, the small peaks detected between 10-25 Å of the pore width, match with the size of micro-voids nat-

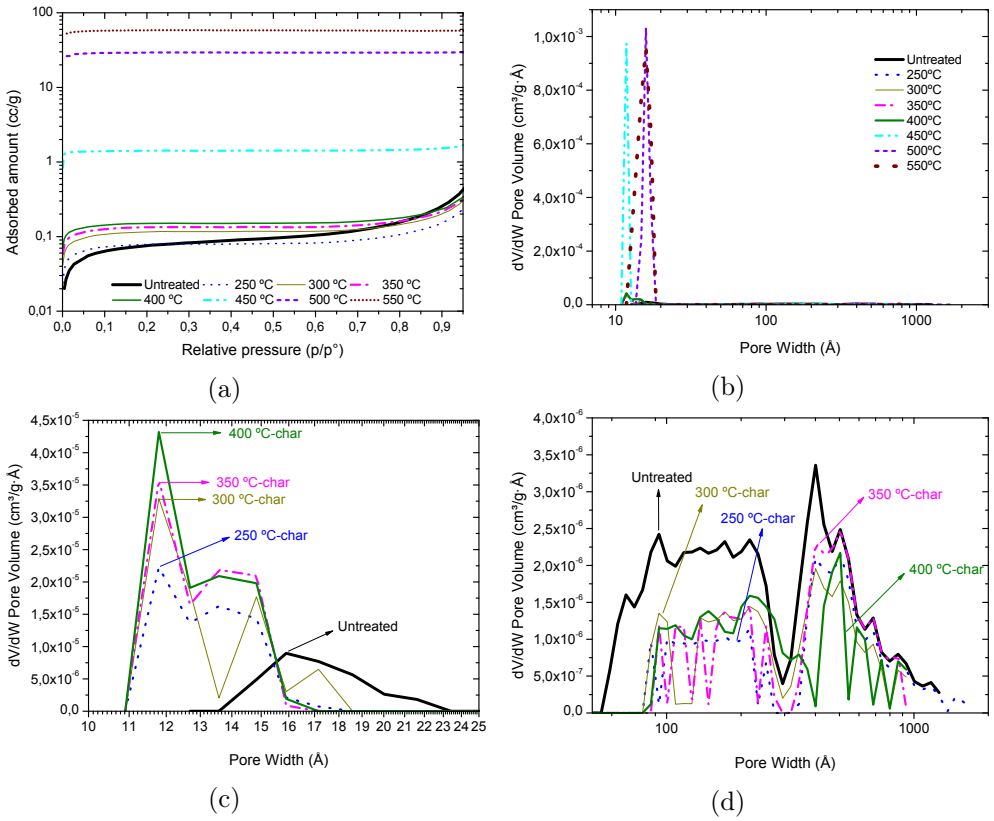

Figure 3.4: (a) Adsorption isotherms for the untreated and treated samples. (b) Pore size distribution (PSD) by Density functional theory (DFT) for untreated and treated samples (Below). (c) Amplification of PSD for the untreated and chars treated until 400 °C, from 10 to 15 Å, and (d) from 25 until 200 Å.

urally presented in the cell walls of cellulose samples [229], which apparently suffers a little contraction with thermal treatment. In addition, peaks were detected in the range corresponding to mesoporous and macroporous materials (Fig. 3.4d), with reduced intensity as a consequence of the thermal treatment until reaching 400 °C. These peaks, detected between 100-2000 Å of pore width, could represent simple pores, presented naturally in the scleroids cell walls and as will be seen later in the results of the SEM/FEG micrographs.

From its microporous structure, surface area and carbon content, the 500 °C-char and 550 °C-char are proposed as a raw material for activated carbon or syngas production from the gasification process, due to its expected more uniform gas transfer, which should maintain the gasification reactivity with elapsed time [167].

Finally, these results clearly show that the coconut endocarp undergoes chemical changes as a consequence of the primary decomposition, but not major changes in the porous structure until 450 °C.

3.4.4 ESEM and SEM-FEG visualization

Morphological changes of a single particle, as a consequence of the lower (250 °C) and higher (550 °C) temperature of treatment, are displayed in Figure 3.5. Simple pores, of about 1 μm of pore width, naturally present in cell walls, are observed in the untreated samples. It is possible to observe that the initial physical shape of the cell wall remains, even for the more intense treatments at 550 °C (Fig. 3.5d), but with a significant contraction in the structure of the sample, which is apparently submerged in a molten fibrous mass.

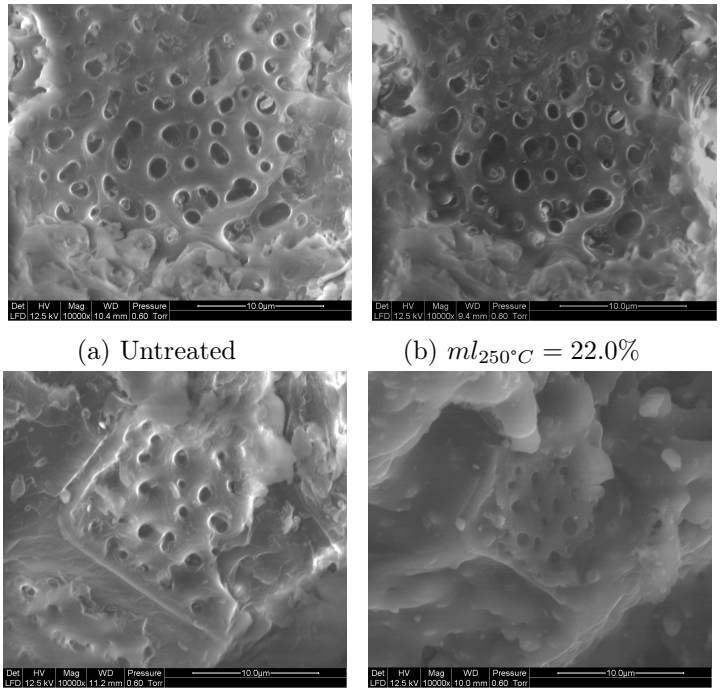

(a) Untreated (b) $ml_{250°C} = 22.0\%$

(c) Untreated (d) $ml_{550°C} = 71.5\%$

Figure 3.5: Morphological and structural changes over a single particle for the lower (a-b) and higher (c-d) temperature of treatment.

Figure 3.6 illustrate the SEM/FEG micrographs for untreated and char samples, obtained at 250 °C, 350 °C, and 550 °C. Apparently, an initial softening in the chars treated at 250 °C and 350 °C, is observed (Fig. 3.6b and 3.6c). As the intensity of treatment increases, the 550 °C-char appears to melt as displayed in the Figure 3.6d. These results are consistent with observations in lignin chars obtained in the same range of temperatures [166] and allow us to suppose that the low surface areas in the chars until 400 °C, could be a consequence of this softening.

Other SEM/FEG visualizations, not displayed here, allowed us to see the fibrous structure of the cell walls, which are composed of sclereid cells [41; 230]. The sclereids appear as columnar cells, with about 20 μm of diameter and variable depth. The

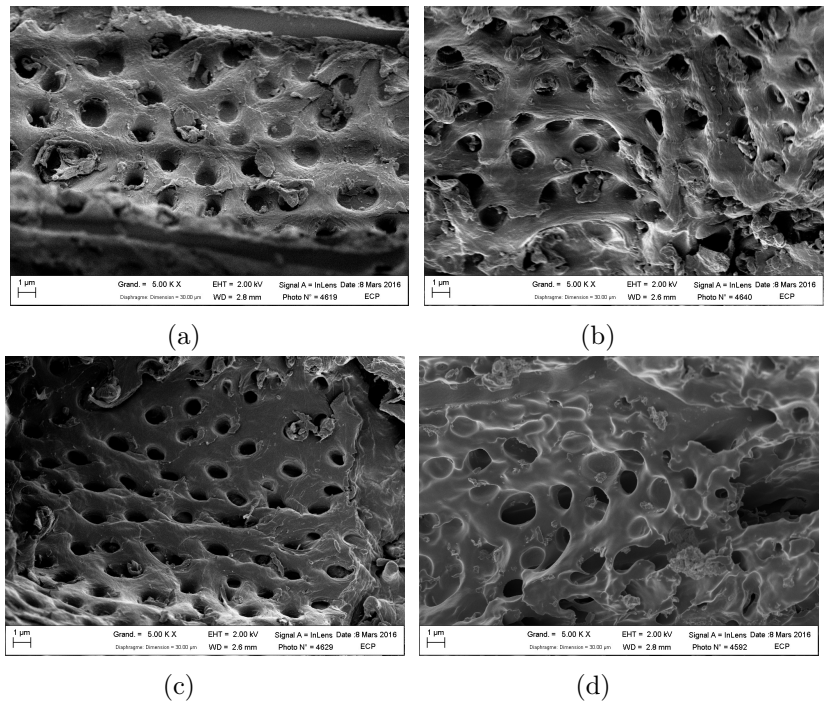

Figure 3.6: SEM/FEG micrographs of (a) coconut endocarp and its chars obtaining at (b) 250 °C, (c) 350 °C and (d) 550 °C.

longest dimension of the fiber bundle was difficult to define, but it was possible to observe that the fiber was longer than 50 μm, with a thickness higher than 500 Å, which is in agreement with the microfibrils diameter.

3.4.5 Dynamic vapor sorption isotherms

An important factor in the moisture sorption properties of polymers is the hydroxyl groups (OH) accessibility, termed as sorption sites, because these OH-groups have strong hydrogen bond-interaction with water molecules.

Although cellulose has many OH-groups, only 33% of these are accessible, whereas the surface of the microfibrils are considered sorption sites [231]. Estimation of these sorption sites in wood, based on the molecular mass of its main components, had a very high water-accessible OH concentration for Xylan and Glucomannan [231] in comparison with cellulose and lignin concentrations.

Figure 4.2 shows the sorption isotherms for the coconut endocarp and chars samples. It should be noted that the EMC in the coconut endocarp was lower than the typical values presented for wood samples The coconut endocarp also contains about 53% of holocellulose [159], of which less than 22% is hemicellulose from the fml

and DTG of the 250 °C-char. These results are presented in Table 3.2 and Fig. 3.2. Its composition, together with the random distribution of its highly lignified sclereids cells [41], is responsible for its natural, more hydrophobic character, which explain its low values of EMC. In all cases, charring resulted in a decrease of the average EMC.

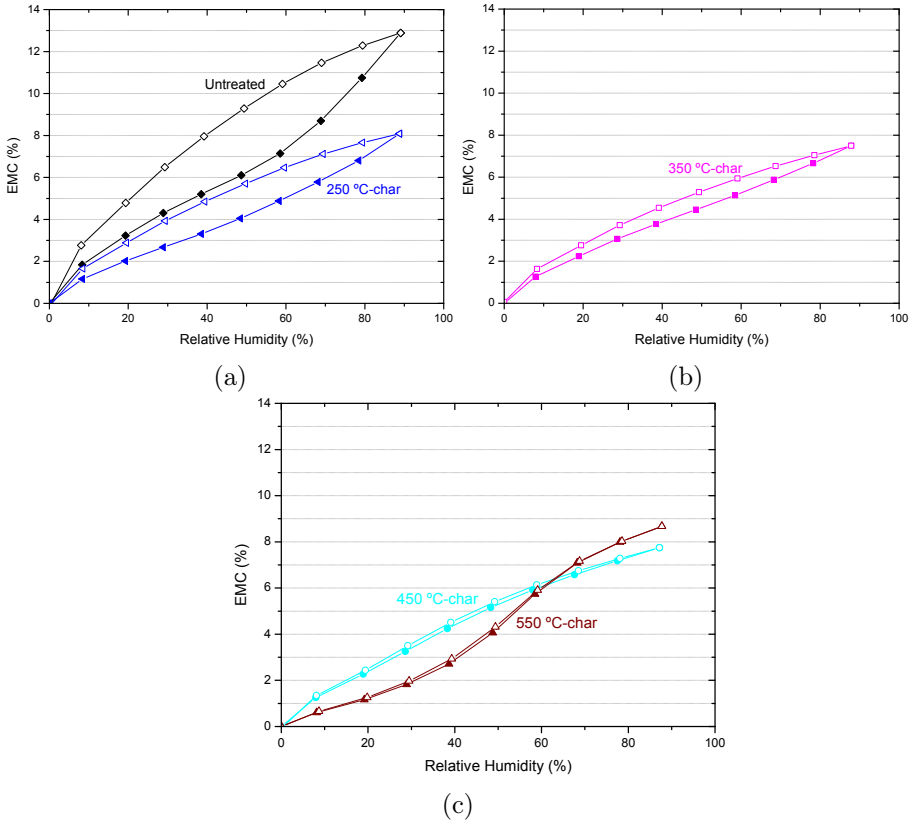

Figure 3.7: Dynamic vapor sorption isotherms for: (a) untreated and 250 °C-char, (b) 350 °C-char, (c) 450 °C-char and 550 °C-char.

It is also possible to observe the changes in the isotherm shape during pyrolysis. Typical sigmoidal type II curves for cellulosic materials are presented. Both the untreated sample (Fig. 3.7a) and 250 °C-char exhibit this sigmoid shape as a result of their cellulose content and based on the fact that hemicellulose was decomposed at this temperature (Fig. 3.2). The isotherms going through a combination of type I and type II for 350 °C-char (Fig. 4.2b), because no more cellulose remains and, as expected, there is a higher lignin fraction (Fig. 3.2) and do not show a microporous structure, unlike the 450 °C-char which exhibits the characteristic type I isotherm (Fig. 4.2c).

The pronounced curve type V for the char obtained at 550 °C (Fig. 4.2c) is explained by its higher carbon content of about 86%. The charcoal has a particular water adsorption behavior, which was already explained by [232]. This behavior is considered an initial weak uni-molecular attraction between the carbon-water molecules at low RH values. As soon as the water molecules become adsorbed and the RH in-

creases, the next strongest interaction between water molecules happens more easily within the micro-voids until they are filled.

At relative humidity values higher than 60% RH, the EMC for the 550 °C-char increases with respect to the 450 °C-char; this is a consequence of its high microvoids number (Fig. 4.2c). The micro-porous volume is indicative of the micro-void quantities present in the charcoal structure which, for the 550 °C-char, is forty times more than that for 450 °C-char. Then, the isotherm type V would be in effect a type I isotherm, considering its microporous structure, which matches with our previous results of N_2 type I adsorption isotherms.

Similar sorption behaviors were obtained for torrefied and charcoal wood up to 450 °C but with different holding times at each peak temperature.

Figure 3.8 shows that absolute hysteresis decreases as the pyrolysis intensity increases; this is a consequence of overall decreases on the hygroscopicity. The higher value of 3.32% was found in coconut endocarp at 60% RH.

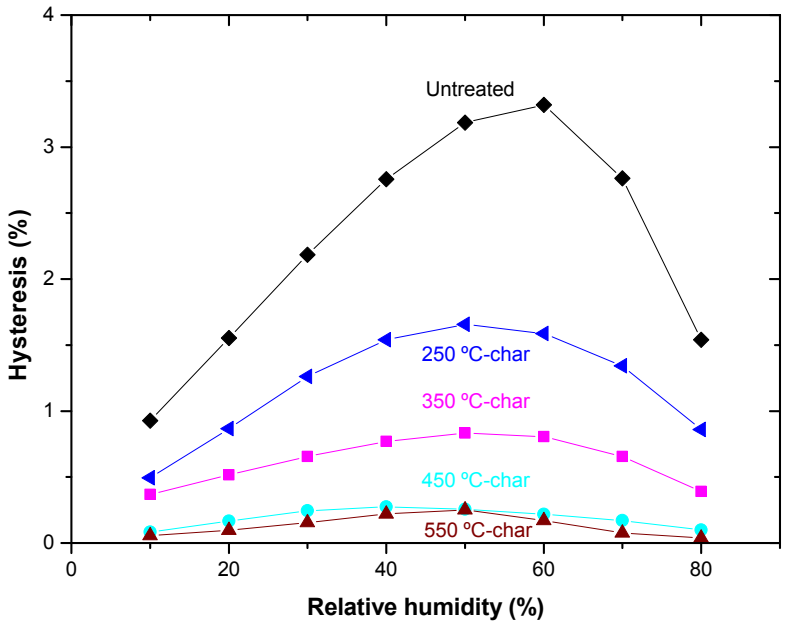

Figure 3.8: Absolute hysteresis of coconut endocarp and its chars at 0-90 % of RH.

The hysteresis ratio agreed with the results obtained in the mild thermal treatment of wood [233]. The small increases in hysteresis ratio is explained by the authors as a product of the stiffness increases with the higher times of treatment.

The pore geometry has influence over the hysteresis, thus capillary condensation in mesopores with narrow necks and wide bodies could occur, in the multilayer adsorp-

tion range or in micropores with narrow slip-like pores materials [169]. A hysteresis model has been proposed in [234] as result of different states (expansion and collapse of nanoporous in the cell-walls matrix) of the material in which the adsorption and desorption process will take place.

The microcapillaries or microvoids measure a diameter of 2-10 nm in wood samples [229]. The pore size distribution shown in Fig. 3.4c, for the untreated and chars until 400 °C, match this range. The desorption process takes place in a swelling matrix, resulting from the hydrogen-bonds and hemicellulose, within the microcapillaries. A pore collapse could occur during the desorption process for an untreated sample.

Similarly, hysteresis in 250 °C-char and 350 °C-char is explained by the water retention inside the collapse matrix, which will be less due at the lower sorption sites in cellulose. The lignin content could present a higher deformation facility to accomodate water, so, we expect that in the desorption process, its deformation capacity could avoid the matrix collapse, thus reducing the hysteresis.

Char obtained at 450 °C and 550 °C present with negligible hysteresis. Both, have significant microporosity, which was confirmed by the exponential increases in the surface area BET and the pore size distribution (Table 3.2 and Fig. 3.4b). Microporous charcoals from different feedstock show hysteresis [88] for nitrogen adsorption, which was explained to be the result of pore shape, like narrow slit-shaped pores, that impede the diffusion of adsorbate [235]. Also, microporous activated carbon shown a significantly high hysteresis as consequence of its functional groups, which increases the interaction with the water molecules [236].

Recently, the loss of hysteresis for charcoal of wood was explained as consequence of inaccessible internal porosity or negligible micropore formation which consequently increases in stiffness that avoids the micropore creation/destruction mechanism We wish to suggest an alternative explanation. Given sufficient time, water will enter pores smaller than 4-5 Å with dimensions comparable to that of the water molecules [237]. The lack of hysteresis in these two charcoals is most likely related to diffusional aspects. For example, as a consequence of the geometrical pore shape that is more suitable to the mechanism of egress of water molecules; and the poor interaction between the water molecules and the substrate, which facilitates its release during the desorption process.

3.5 Conclusion

Prior work emphasized the enormous potential of coconut endocarp as raw material to produce biofuel, charcoal or activated carbon. However, these studies were not focused on its physicochemical evolution along the thermal decomposition. In the present work, different analytical methods were used to assess the product alterations due to pyrolysis: elemental analysis, surface area and pore size analyses, ESEM and SEM/FEG observation and dynamic vapor sorption determination.

At low temperature, the main effect is on the oxygen content, with a gradual shift from native biomass to charcoal, which is preferable as solid fuel or as feedstock to high-quality bio-oil. DTG curves indicate that the product becomes lignin-like from a thermal treatment at 300 °C. At higher temperature, this trend continues, shifting towards fixed carbon and above 450 °C, the chars acquire microporous materials characteristics with an exponential increase of the specific surface and low hygroscopicity values. This allows such treated products to be considered as raw materials in a gasification process to produce syngas or activated carbon.

In addition, we proposed expressions for O/C and H/C ratios as a function of the mass loss that can be used for prediction purposes. To our knowledge, this is the first investigation of the sorption properties, BET surface area and morphology evolution along the thermal decomposition of coconut endocarp —*Acrocomia aculeata* —.

Our results provide sufficient evidence for the long-term application of this feedstock and its chars as solid fuel or raw material in the gasification process. However, the combustion characteristics and gasification conditions still need be tested.

Chapter 4

Kinetic parameters estimation for coconut endocarp —*Acrocomia aculeata*— thermal degradation in the temperature range of 250-400 °C

Kinetic parameters for the pyrolysis of coconut endocarp Acrocomia aculeata were determined under isothermal conditions, via thermogravimetric analysis techniques at low heating rates. Multi-step kinetic models and the Distributed Activation Energy model based on mass loss residues, assuming a 1st order reaction model fitting, were used to study the thermal degradation to estimate the kinetic parameters of isothermal pyrolysis with 2 h of residence time. Four temperature levels were considered (250, 300, 350 and 400 °C). The parameters of the resulting set of differential equations were adjusted by solving a non linear least square optimization problem. The computational solutions of the models were derived using the optimal parameters, which allow the exact conditions undergone by the sample to be used as input parameters. Overall we find reactions models that provide very good accuracy for reproducing the mass loss from this lignocellulosic biomass under pyrolysis conditions. To the best of our knowledge, this is the first determination of kinetics parameters for this specific raw material using multi-step and DAE models at different temperatures levels.

4.1 Introduction

Currently, the coconut endocarp of *Acrocomia aculeata* fruit, present in the central-eastern region of south America, is an agro-industrial waste and a potential substitute for conventional fuels [18, 39]. A major feature of this biomass, is its high calorific value (HHV) of approximately 19.3 MJ/kg. This HHV is higher than other agricultural residues used for energy generation [40], which enables an enormous potential of industrialization of coconut fruit in biorefinery to obtain fuels, materials and chemicals, which justifies a thorough study [40, 41, 42, 37]. All the more, coconut endocarp can be transformed into solid fuel, charcoal, active carbon, furfural, bio-oil by pyrolysis or into syngas by gasification. In the case of pyrolysis or gasification process, it is expected that torrefied biomass presents better grindability properties and higher energy density [238].

The important role of biomass feedstock in the pyrolysis process is well known. The composition and physical properties of the pyrolysis products depend on the raw material properties. The physico-chemical properties of coconut endocarp were analysed by Duarte et al. [6, 238], Evaristo et al. [40], Reis et al. [41], Mazzottini-dos-Santos et al. [230].

The first step in designing a biomass torrefaction reactor is the kinetic study of the thermal degradation process. This includes analyzing different reaction mechanisms, determining kinetic parameters and evaluating the applicability of these parameters for different operation conditions.

Thermal analysis such as thermogravimetry and calorimetry are widely used to study lignocellulosic material kinetics. In the previous chapter 3, the thermogravimetric and differential thermogravimetric curves were used to obtain information about the decomposition of the main components of coconut endocarp. We found that chars can yield three products, depending on the treatment temperature: bio-oil from treatment at 250-300 °C, charcoal from treatment at 350-450 °C and feedstock for gasification from treatment at temperatures above 500 °C.

In this study, mass loss as a function of time, in isothermal conditions, was used to explain pyrolysis kinetics of coconut endocarp under long residence time. To the best of our knowledge, this is the first time that an evaluation of the applicability of these kinetic models and their parameters estimation are made for this specific feedstock.

4.1.1 Models for lignocellulosic biomass

Many kinetic models were used to describe biomass decomposition. Model-based (model-fitting) and iso-conversional (model-free) methods are two main mathematical approaches used to obtain the kinetic data [239, 100]. In this work, model-fitting methods were used, where a reaction model must be postulated first. Models with the assumption that reactions occur in one or more steps are widely applied in ex-

periments with a constant heating rate increasing temperatures above 400 °C [240]. Another model, the Distributed Activation Energy Model (DAEM), considers many independent reactions taking place simultaneously with different activation energies representing different bond strengths. A complete review of DAEM and its application to pyrolysis of lignocellulosic biomass is presented by Cai et al. 2013 [241].

In this work, multi-step models and the Distributed Activation Energy model were used. These models are shown in Table 4.1.

Usually in the biomass community, the method most commonly employed to fit experimental data and evaluate the Arrhenius parameters is the nonlinear least squares fitting. Then, on the basis of the quality of the regression fit, it can be selected as the most appropriate reaction model [100].

4.2 Experiment

4.2.1 Samples

Solid and woody biomass inside the *Acrocomia aculeata* fruit, referred to as 'coconut endocarp", were obtained as agroindustrial residue from Cavallaro Company [1]. This feedstock was cleaned with water and dried in air flow at room temperature. Sample particles between 0.1-0.2 mm were obtained using a grinder (IKA M20 Universal mill), which were subsequently sieved.

The moisture content of the samples was less than 4% m/m. However all the samples were dried completely before the start of the thermal decomposition. Other physico-chemical characteristics of this feedstock are showed in Table 3.2.

4.2.2 Thermogravimetric experiments

.

The TGA measurements were carried out using a STA 449 F3 Jupiter, NETZSCH as it was described in section 3.2. The kinetic parameters are determined using available models in the literature as multi-step series and DAE kinetic models, to asses the kinetic rates under essentially isothermal conditions.

4.2.3 Solutions and optimization of the kinetic models

Multiple step models

[1] https://www.cavallaro.com.py

Table 4.1: Kinetic models for lignocellulosic biomass.

Biomass	Model	References
Locus, Spruce, Eucalyptus	One-step model	Cavagnol et al. [240]
Wood		Wendlandt [242]
	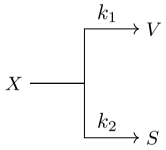	
Avicel cellulose		Varhegyi et al. [243]
Locus, Spruce, Eucalyptus	Two-step model	[240]
	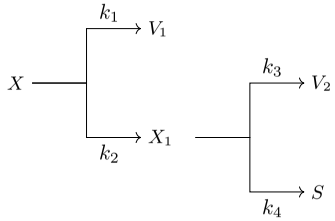	
Locus, Spruce, Eucalyptus	Three-step model	[240]
	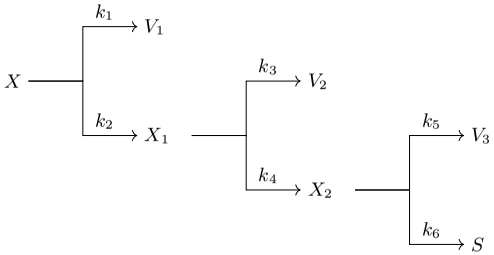	
Corn stover, cotton stalk, palm oil husk, pine wood, red oak, sugarcane bagasse, switch-grass and wheat straw	DAEM $\frac{V}{V_i^\infty} = 1 - exp\left[-\int_0^t A_i exp(-E_i/RT)dt\right]$	[244]
	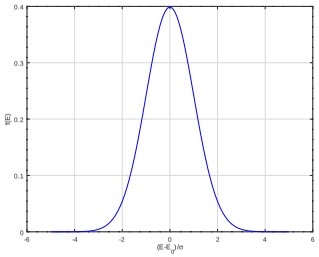	
Locus, Spruce, Eucalyptus		[240]
Wheat, Oat, Barley and Brassica carinata Straws	$f(E) = \frac{1}{\sigma\sqrt{2\pi}} exp\left(-\frac{(E-E_0)^2}{2\sigma^2}\right)$	[245]

Numerical solutions for multiple step models are similar. The mass balance equations for the 3-step reactions are detailed in the matrix form below. Here, $[X]$ is the initial mass of the raw material, $[X_i]$ are the masses of the intermediary components, V_i are the volatile masses and k_i the kinetic constants. The reactions are supposed to be of first order and the kinetic constants are defined by the Arrhenius equation.

$$\begin{bmatrix} d[X]/dt \\ d[X_1]/dt \\ d[X_2]/dt \\ d[V_1]/dt \\ d[V_2]/dt \\ d[V_3]/dt \end{bmatrix} = \begin{bmatrix} -(k_1+k_2) & 0 & 0 & 0 & 0 & 0 & 0 \\ k_2 & -(k_3+k_4) & 0 & 0 & 0 & 0 & 0 \\ 0 & k_4 & -(k_5+k_6) & 0 & 0 & 0 & 0 \\ k_1 & 0 & 0 & 0 & 0 & 0 & 0 \\ 0 & k_3 & 0 & 0 & 0 & 0 & 0 \\ 0 & 0 & k_5 & 0 & 0 & 0 & 0 \end{bmatrix} * \begin{bmatrix} X \\ X_1 \\ X_2 \\ V_1 \\ V_2 \\ V_3 \end{bmatrix}$$

Although isothermal conditions were adopted in this work, the mass loss during the heating phase to the final temperature is considerable Table 4.2 as it was reported by [240] for different lignocellulosic biomasses.

Table 4.2: Anhydrous mass loss during the heating phase.

Temperature	**Mass loss (%)**	**Total mass loss (%)**
250°C	3.1	20.2
300°C	21.4	50.0
350°C	48.6	58.0
400°C	57.2	61.2
450°C	59.8	63.0
500°C	62.6	65.2
550°C	64.1	66.3

In this way, as the kinetic constants are function of temperature, they will be computed for each instant of time.

The initial values are equal to zero for all quantities except for X, the initial mass, which was measured experimentally.

The kinetic modeling is an inverse problem, where the parameters are optimized by iteration, solving the set of differential equations at each step, using the implicit Euler method.

4.2.4 Distributed Activation Energy Model - DAEM

The DAEM assumes a continuous set of parallel reactions simultaneously with different activation energies, these energies are modeled by a distribution functions $f(E)$.

Several $f(E)$ has been proposed in the literature as Gaussian, Weibull, Gamma, logistic and pseudo-nth-order distributions [246, 247, 248, 249, 250]. In this work, as a first approach, we have used the Gaussian distribution function. This has the advantage of being a simple symmetric shape easy to optimize, however the activation energy distribution of the phenomenon might not be symmetric [251].

For numerical calculations, it is necessary to discretize the amount of reactions considered. This is done by considering a finite amount of activation energies as follows

$$E_i = E_0 - n\sigma + (i - 0,5)\Delta E, \qquad i = 1, ..., 2nm, \tag{4.1}$$

where E_0 is the mean of the distribution, E_i is the energy activation for the $i-$th reaction and $\Delta E = \sigma/m$, n and m are positive integers. In this work, we have used $n = 4$ and $m = 3$, since the improvement in the results with higher values is not big enough to justify the increase in computational time [240].

After the discretization of the activation energy, we obtain the Gaussian distribution function as follows:

$$f_i(E_i) = \frac{1}{S} exp\left(-\frac{(E_i - E_0)^2}{2\sigma^2}\right), \tag{4.2}$$

where

$$S = \sum_{i=1}^{2nm} exp\left(-\frac{(E_i - E_0)^2}{2\sigma^2}\right). \tag{4.3}$$

Note that the sum of all f_i is equal to 1.

Assuming first-order reactions and kinetic constants given by the Arrhenius equation, the amount of volatiles emitted for each activation energy is:

$$V_i = V_i^{\infty}\left[1 - exp\left(-\int_{t_0}^{t} k_i(T(t))dt\right)\right], \tag{4.4}$$

with

$$k_i = Aexp\left(-\frac{E_i}{RT(t)}\right), \qquad V_i^{\infty} = f_i V^{\infty}, \qquad V_i(0) = 0.$$

The pre-exponential factor A is assumed to be constant for all reactions, although there are other methods which express as a function of temperature [241, 252,

253] or is assumed to follow a compensation effect [241]. The numerical solution of the integral is done with the trapezoidal rule.

The total volatiles are then,

$$V(t) = \sum_{i=1}^{2nm} V_i(t) \tag{4.5}$$

It is possible to consider the existence of several Gaussian curves with different values of E_0, σ and A. In this case, the sum of the total volatiles includes all the V_i calculated for all the E curves considered, and

$$V_i^{j,\infty} = \alpha^j f_i^j V^\infty, \tag{4.6}$$

where j is the considered Gaussian curve and α^j is the weight that is given to it. In this work, the model was evaluated using two and three Gaussian curves.

4.2.5 Optimization Problem

The parameter estimation for both models were performed with a similar approach used in the work of Cavagnol et al. [240]. In each model we define a set of parameters to be determined such that an error function has to be minimized. In the case of multi-step models, the parameters are the pre-exponential factors $A_1, A_2 \dots A_i$ and activation energies $E_1, E_2 \dots E_i$ corresponding to $k_1, k_2, \dots, k_i$, respectively, where i is the number of reactions in the model. On the other hand, for the Gaussian DAEM the parameters are A, E_0 and σ, with discretization values $n = 4$ and $m = 3$. Therefore, for the two and three parallel DAEM reactions, besides the parameters A, E_0 and σ for each Gaussian, we introduce the value α_i in order to maintain the unity area over the two and three Gaussian curves respectively.

The optimization method used was the interior points using constraint on the alpha.

The error function or objective function is defined as follows,

$$Error = \sqrt{\frac{\sum_{i=1}^{N}(m_{i,observed} - m_{i,calculated})^2}{N(m_0)^2}}, \tag{4.7}$$

[1]The effect of an increase of E_0 is partially or completely offset by a "compensatory" increase in A.

where $m_{i,observed}$ is the measured mass loss, $m_{i,calculated}$ the corresponding calculated mass loss, N the number of measured data and m_0 the initial anhydrous mass.

4.3 Results and discussion

The aim of this study is to propose a set of kinetic parameters for the thermal decomposition of coconut endocarp employing the multi-step models and DAEM and using a similar approach as Cavagnol et al. [240] for the optimization process.

The mass change profile as a function of time, that is the thermogravimetric curves, can give us insight about the reaction mechanisms for the coconut endocarp pyrolysis. Anhydrous mass loss, depicted in Fig. 3.1, is the consequence of numerous competitive reactions of depolymerization and devolatilization.

As reported in the previous section 3.4.1, there are three behaviors, according to the slope in the curve, which are related to the three main components degradation: the hemicellulose, cellulose and lignin.

4.3.1 Kinetic parameters estimation

Several kinetics models were developed for cellulose, hemicellulose and lignin. The model proposed for Varhegyil et al. [243] was widely used to describe the cellulose decomposition. For hemicellulose, several two and three step kinetic mechanisms have provided accurate predictions. According to Cavagnol et al. [240], the single-step first order reaction was the only kinetic model proposed for lignin.

4.3.1.1 Three-step model

In this work, we have considered only the three step model, because the composition of the lignocellulosic biomass and considering the wide range of temperatures of treatment employed in our experiments. The model take into account more steps for the biomass degradation and gives the proportion of volatiles for each irreversible first order reaction. Figure 4.1 shows the curve fitting for the three-step model.

It is observed that the model only adjusts relatively well the data at lower temperatures of treatment, until 300 °C. At temperatures lower than 300 °C occurs the decomposition of the hemicellulose. Besides considering 2 h of isothermal treatment, the cellulose and even lignin decomposition could have an important contribution to the mass loss at this level of temperature as explained in the previous section 3.4.1.

This result may indicate that a three-stage model is able to better describe reactions at low temperatures. For higher temperatures, where pyrolysis of cellulose

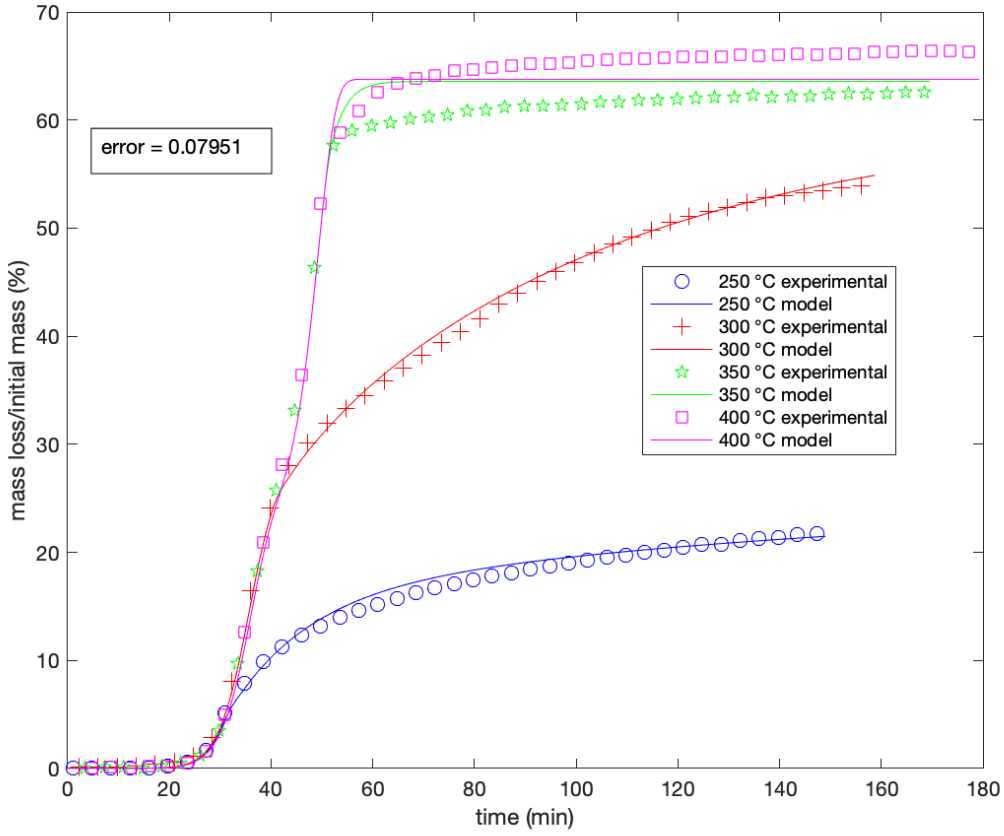

Figure 4.1: Three-step model fitting

and lignin predominantly occurs with an important mass loss, it would be necessary to test more complex models.

The Table 4.3 display the results of the kinetic parameters estimated for the model and the *error*, which was defined in section 4.2.5.

Table 4.3: Kinetic parameters estimated for the multi-step models.

Kinetic parameters	**Three-step model**
$E_1(kJmol^{-1})$	146.3
$E_2(kJmol^{-1})$	112.8
$E_3(kJmol^{-1})$	134.0
$E_4(kJmol^{-1})$	108.6
$E_5(kJmol^{-1})$	196.4
$E_6(kJmol^{-1})$	187.2
$A_1(s^{-1})$	7.5880e+10
$A_2(s^{-1})$	1.6592e+8
$A_3(s^{-1})$	3.1742e+8
$A_4(s^{-1})$	1.0052e+7
$A_5(s^{-1})$	8.3333e+13
$A_6(s^{-1})$	1.6543e13
error	0.07951

As can be seen in Table 4.3, the values of the activation energy are low but similar to those reported in the literature for other lignocellulosic biomass [240, 155].

Figure 4.2a presents the curves of the different fractions X, X_1, X_2, V_1, V_2, V_3 and S of the model as a function of time. It is noted that for 250 °C the amount of volatiles and an intermediate solid X_i and V_i has been distributed between the first two steps (Table 4.4), and the amount of S and V_3 are very low. It is also observed that for the greater isotherm, the decomposition is rapid, the intermediate solid fractions disappear completely.

At this temperature the decomposition of lignin is a considerable contribution to degradation, and secondary reactions of the primary decomposition products. This does not occur at low temperatures: rather there is an apparent competition between volatiles and solid products formed, favoring the formation of volatiles as the temperature increases.

4.3.1.2 Distributed activation energy model

Through the three-step model, we find a set of parameters that does not adjust very well the experimental data. The distributed activation energy model (DAEM) assumes that the decomposition mechanisms involve a large number of independent, parallel, first order or nth-order reactions with different activation energies as the variations in

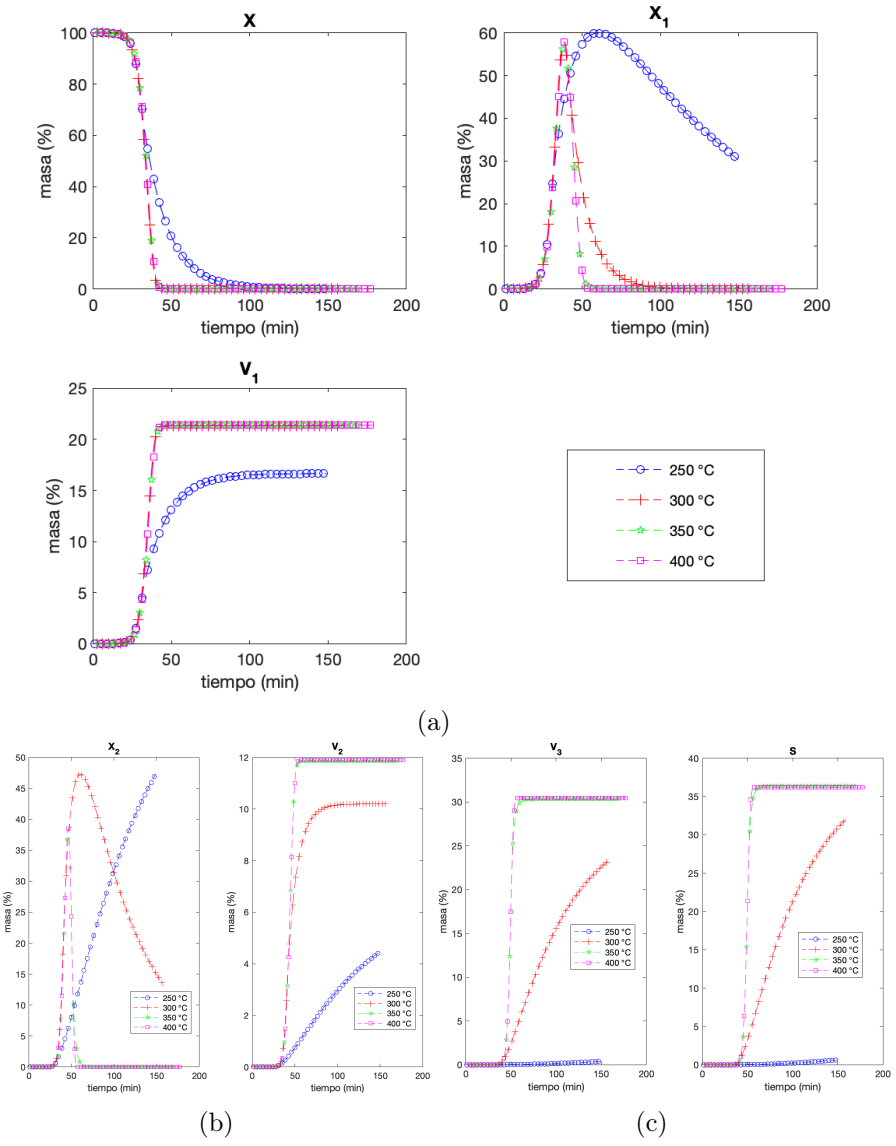

Figure 4.2: Different fractions of 3-step model.

the bond strengths of species. The efforts on DAEM for the pyrolysis of lignocellulosic biomass indicate that the model consisting of three parallel DAEM reactions, is the most accurate and up-date approach for modeling the pyrolysis kinetics of lignocellulosic biomass [241]. Therefore, to fit our experiments, we have selected to test the results obtained using two and three Gaussian DAEM distributions.

Two Gaussian DAEM distributions

The DAEM for the coconut endocarp was applied for the total amount of

Table 4.4: Total volatiles released for the three-step model.

Temperature °C	**Step 1** V_1 %	**Step 2** V_2 %	**Step 3** V_3 %
250	77.5	20.7	1.8
300	38.8	18.6	42.6
350	33.6	18.7	47.7
400	33.5	18.7	47,8

volatiles released during the thermal treatment. Fig.4.3 shows the curve adjustment considering a Gaussian distribution of the activation energy, discretized in 48 fractions.

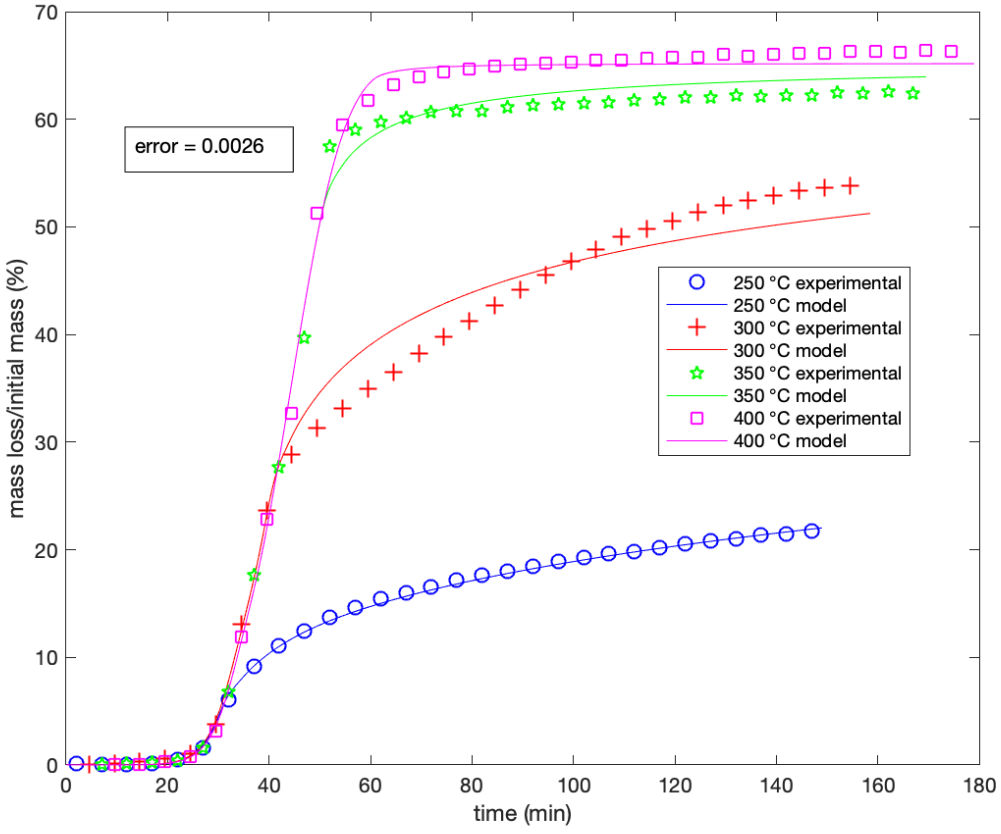

Figure 4.3: (a) Curve adjustment considering two Gaussian distribution model.

Figure 4.4 shows the volatiles of each Gaussian curve, for each isotherm.

It can be seen that the second Gaussian curve has a greater influence at higher temperatures. This is reasonable, because its activation energy is greater. The different amounts of volatiles associated to the two curves indicate that the main compo-

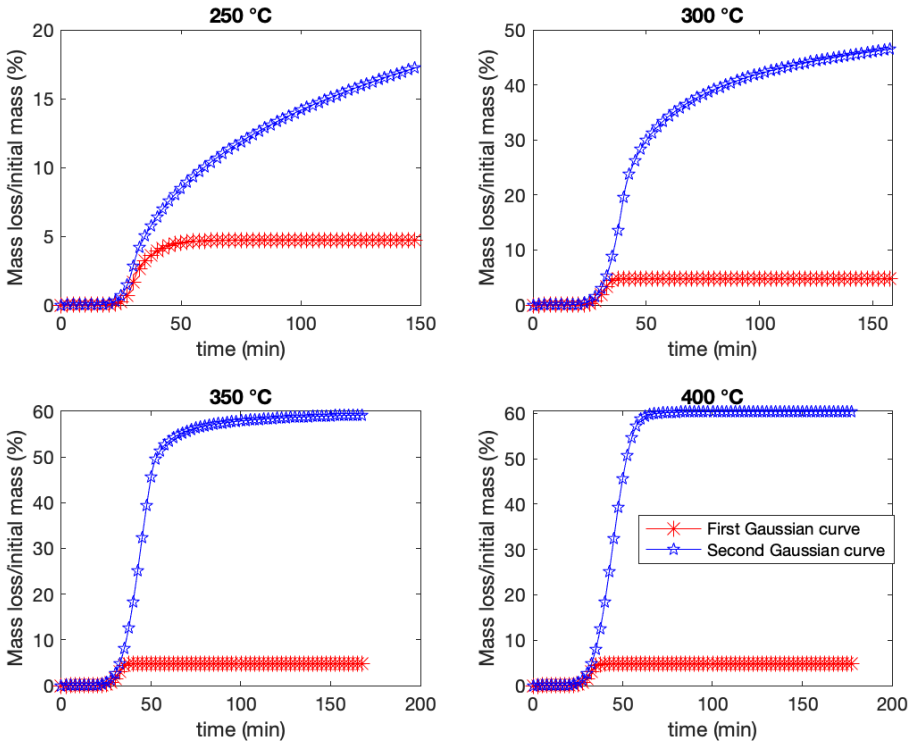

(a)

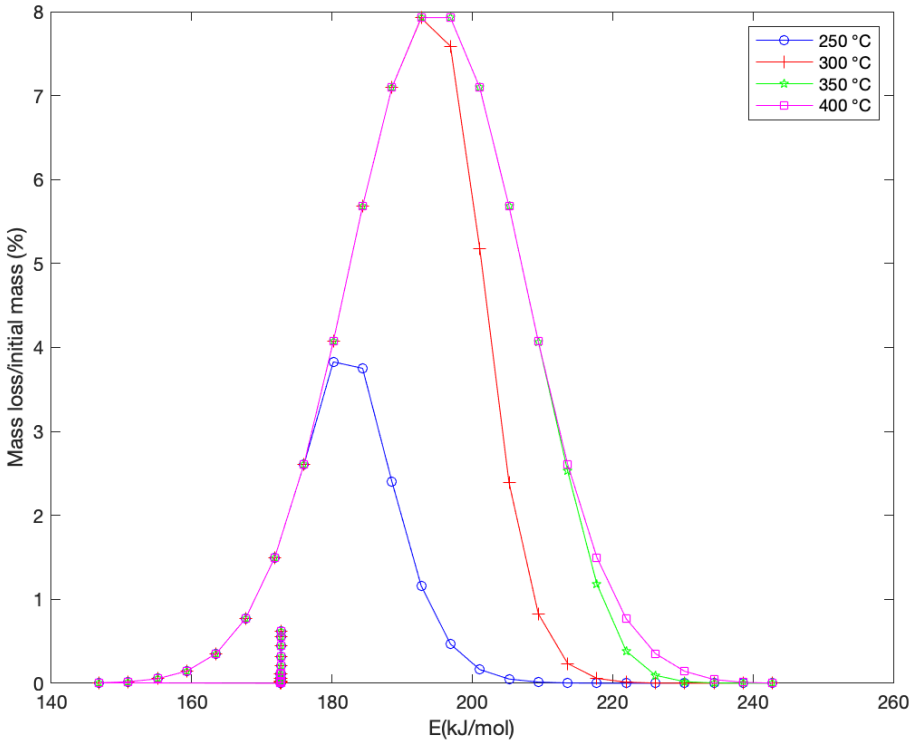

(b)

Figure 4.4: (a) Volatile fractions of the model, for the two Gaussian curve. (b) Volatiles emitted as a function of activation energy, for the isotherms.

nents of the coconut endocarp decompose over different temperature ranges.

The total volatile emitted by each isotherm and for each activation energy are shown in Fig. 4.4b. It is clear that at lower temperatures, the curves are shifted towards minor energies, and the opposite occurs for higher temperatures. Only the smallest energy values are affected by the decomposition. At higher temperature levels, decomposition gradually affects larger energy values.

The activation energies of the decomposition of the first pseudo-component were found to be $172.7 \pm 6.7\text{e}{-3}\ kJ \cdot mol^{-1}$ and for the second pseudo-component was found to be $194.8 \pm 12,52\ kJ \cdot mol^{-1}$, which are very close to that reported for xylan and cellulose pyrolysis at a heating rate of 5 $Kmin^{-1}$ by Cai et al. (2013) [254].

Three Gaussian DAEM distributions

Fig. 4.5 shows the curve adjustment considering three Gaussian distributions, discretized in 72 fractions.

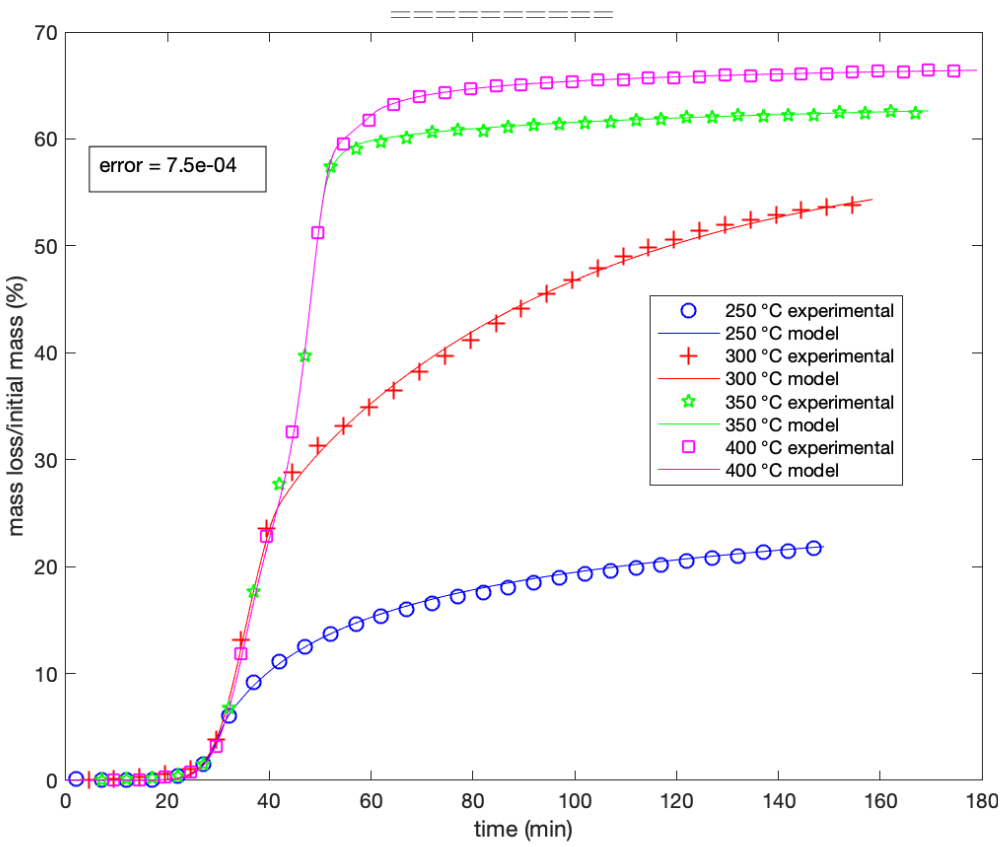

Figure 4.5: (a) Curve adjustment considering three Gaussian DAEM distributions.

Therefore, the lignocellulose biomass can be considered as a sum of several pseudocomponents without interaction between them. Thus the pyrolysis of each pseudocomponent is represented by a single distribution of parallel first-order Gaussian reactions. The first, second and third pseudo-components represent the fractions of hemicellulose, cellulose and lignin, respectively.

Figure 4.6 shows the volatiles of each Gaussian curve, for each isotherm.

The first Gaussian curve has a greater influence at 250 °C, which is consistent with hemicellulose decomposition, known to be the first component to degraded. In the same way, the second Gaussian curve has a greater influence at 300 °C. Considering the isothermal treatment during 2 h at 300 °C, the cellulose decomposition is expected. For 350 °C and 400 °C, the first and second distribution are not more acting from 40 min and 50 min of treatment respectively (40 min is the time it takes to reach 350 °C under the dynamic treatment). After this time, the temperature level is enough for the fraction of biomass related to hemicellulose and cellulose to be already volatilized.

Finally, one observes how the third Gaussian curve begins to have more influence on the volatility distribution as the final treatment temperature increases. The third Gaussian curve should represents the lignin decomposition, which occurs with lower decomposition rate that cellulose and over a wide temperature range (250-500 °C) [211, 212].

Table 4.5 shows the parameters obtained and Fig. 4.6b the total volatile emitted by each isotherm and for each activation energy. The activation energy distribution peaks for the three pseudo-components were centered at 178.6, 198.9 and 221.4 $kJ \cdot mol^{-1}$. The standard deviations of the activation energies were 5.48, 0.16e−3, and 18.1 $kJ \cdot mol^{-1}$ for the hemicellulose, cellulose and lignin fractions respectively.

These values are in agreement with with those reported for other lignocellulose biomass [255, 254] and indicates that the activation energy distribution for lignin has the widest distribution.

On the contrary, the distribution associated to cellulose is very narrow and indeed degenerated into one single first-order reaction. This is consistent with the sudden degradation of cellulose, once melt, at around 300 °C. Finally, the proportion of each pseudocomponents (respectively 0.33, 0.48 and 0.18) are also consistent with the composition of lignocellulosic materials.

By comparing DAEM models with 3-step model, a relatively large difference between the values of the parameters is observed (Table 4.3 and 4.5). The DAEM uses constant pre-exponential factor for all reactions, then there is a compensation effect between E_i and A. In this way, the values of the activation energies are forced to adjust to the frequency factor.

An appreciable improvement is observed regarding the two and three Gaussian distribution model. The three Gaussian distribution model presented minimal error, hence the best fit.

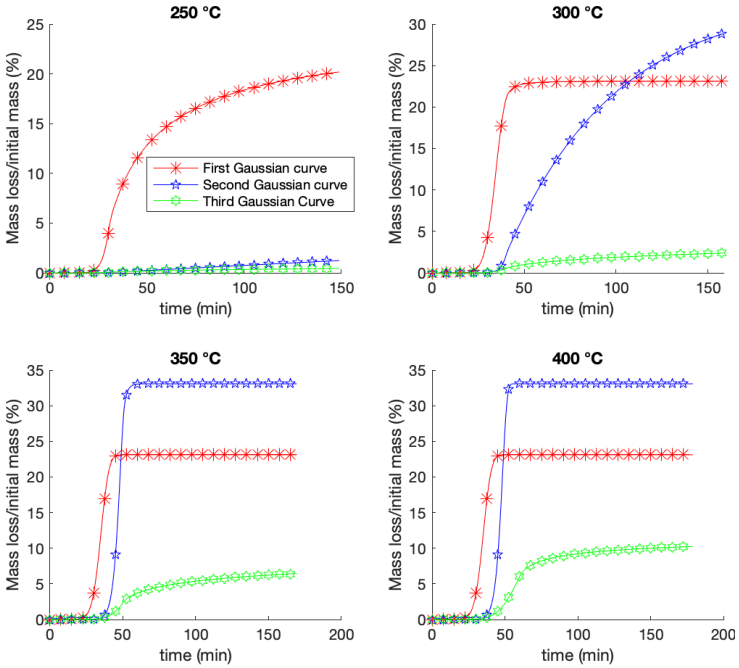

(a)

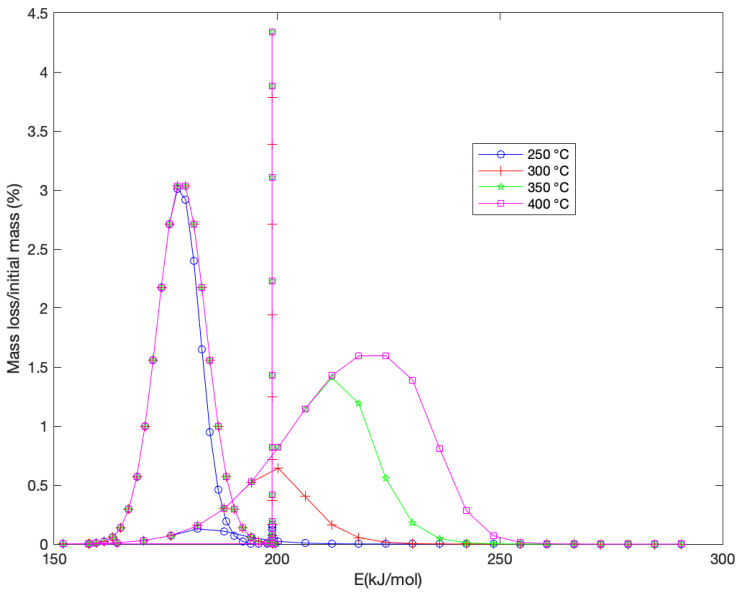

(b)

Figure 4.6: (a) Volatile fractions of the model, for the three Gaussian curve. (b) Volatiles emitted as a function of activation energy, for the isotherms.

Table 4.5: Kinetic parameters estimated for the DAEM.

Kinetic parameters	**Two Gaussian DAEM**	**Three Gaussian DAEM**
E_{01} $(kJ \cdot mol^{-1})$	172.7	178.6
E_{02} $(kJ \cdot mol^{-1})$	194.8	198.9
E_{03} $(kJ \cdot mol^{-1})$		221.4
σ_1 $(kJ \cdot mol^{-1})$	6.7e−3	5.48
σ_2 $(kJ \cdot mol^{-1})$	12.52	0.16e−3
σ_3 $(kJ \cdot mol^{-1})$		18.1
A (s^{-1})	3.750e+14	3.750e+14
α_1	0.0726	0.3382
α_2	0.9274	0.4839
α_3		0.1779
error	0.966	7.5e−4

After the parameter identification on the learning database, we have tested the robustness of the 3-step and three Gaussian distribution models (Fig. 4.7) using a validation test, which consists in thermal decomposition program with a stepped rise in temperature from 100 to 450 °C, with isotherms of 2 hours at the same final temperatures used in this work.

The 3-step model presents a very poor prediction ability for this test. On the contrary, it is observed that three Gaussian distribution model fits well the data for the two curves at 5 K/min and 20 K/min. Therefore, in addition to the very good individual adjustment of each curve of the DAEM, it has the ability to simulate the kinetic for different heating rates.

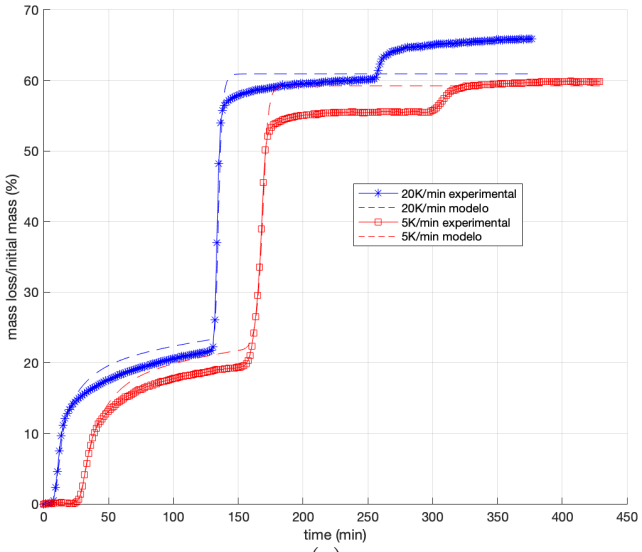

(a)

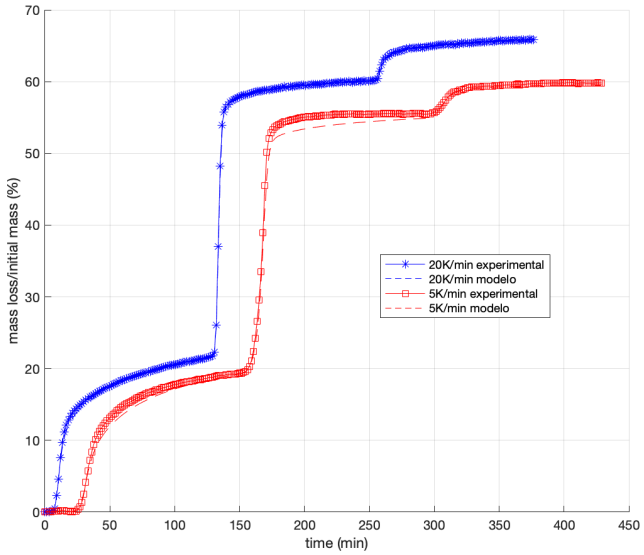

(b)

Figure 4.7: (a) Application of a stepped thermal program to 3-step model. (b) Application of a stepped thermal program to three Gaussian DAEM.

4.4 Conclusion

The pyrolysis of cococunt endocarp was studied by thermogravimetry with an isothermal program. Three-step and distributed activation energy (DAE) models, assuming a first order reaction model fitting, were used to estimated the kinetic parameters of isothermal pyrolysis with 2h of residence times of coconut endocarp —*Acrocomia aculeata*—. It was taken into account simultaneously different level of temperatures (250, 300, 350, 400 °C). The results showed that three-step kinetics was a poor representation of the decomposition behavior. However, reasonable approximate simulations were obtained for thermal degradation at 250 °C, which is assumed to represent the formation of a solid with a reduced degree of polymerization in a first stage.

The kinetic parameters identified using the three Gaussian distribution model, are able to predict the measured mass loss with good accuracy even for the highest temperature throughout the entire experimental time. The activation energies of the decomposition of the first, second and third pseudo-components, related to the primary pyrolysis of hemicellulose, cellulose and lignin respectively, were found to be $178.6 \pm 5.48\ kJ \cdot mol^{-1}$, $198.9 \pm 0.16\text{e}{-3}\ kJ \cdot mol^{-1}$, and $221.4 \pm 18.1\ kJ \cdot mol^{-1}$ respectively. Also, using a stepped rise program, the three Gaussian DAEM has a greater ability than the 3-step model to simulate the kinetic for different heating rates.

In a future work, we will compare this results with those obtained using an asymmetric distribution, such as gamma distribution, and under different thermal program.

Chapter 5

Slow pyrolysis and gasification of coconut endocarp using H_2O

This chapter presents the gasification approach employed to obtain activated carbon of coconut endocarp. The different pyrolysis conditions used to obtain the char samples are presented, followed by the gasification conditions. The characteristics of the thermogravimetric curves are analyzed as well as the corresponding conversion rate. Then, the BET surface area and porosity properties are presented. Finally, the pore size distribution are given and a short explanation of the mesoporosity development and some applications for the activated carbons are presented.

5.1 Introduction

Activated carbon is one of the most widely used adsorbent for water purification and for many other advanced applications, such as catalyst supports, medicine, electrode materials, air filters and gas storage [147]. Therefore, the world demand for activated carbon can be expected to dramatically increase as the urbanization and industrialization increase, what it entails an environmental contamination and consequently, the cost of activated carbon will be further increased [256].

In this context, agroindustrial wastes, such as coconut endocarp, is an interesting feedstock to produce cheap and efficient activated carbons from low-cost and renewable sources and because during the gasification process synthesis gas (H_2 + CO) are produced, which at the same time have many important applications.

However, during the gasification process are produced also, bottom ash (primarily minerals and metals with minimal carbon) and char as unavoidable by-products. From Rong et al. study [257], they could create potential risks to human health and

environment as they may contain various inorganic components such as alkali and alkaline earth metals (such as K, Ca, Mg and Na) and trace amounts of heavy metals. Therefore, the activated carbon produced from them, could provide an environmental friendly and economical way to re-utilize the solid residues from woody biomass gasification .

When steam reacts with the carbon in char, produces normally CO and H_2. Under certain conditions, the steam and carbon reaction can also produce CH_4 and CO_2. The followings are typical char in steam gasification reaction [90].

- Water-Gas: $C + H_2O \rightarrow H_2 + CO$
- Water-Gas Shift: $CO + H_2O \rightarrow H_2 + CO_2$
- Hydrogasification: $C + 2H_2 \rightarrow CH_4$

The first one, an endothermic reaction is perhaps the most important gasification reaction. However, according to Barrio et al. (2001), the presence of hydrogen in the gases products has a strong inhibiting effect on the char gasification rate in steam, that could be overcome by continuous removal of hydrogen from the reaction site [258].

Water-Gas Shift reaction is a gas phase reaction slightly exothermic, that takes place between steam and an intermediate product of the gasification reaction. Probstein and Hicks (2006, p. 63) showed that this reaction has higher yield of H_2 at a lower temperature and optimum yield is obtained at about 225 °C [259].

Hydrogasification reaction involves the gasification of char in a hydrogen environment, which leads to the production of methane. The rate of this reaction is much slower than that of other reactions, and as such, it does not play any important role in conventional gasification [90].

When a biomass particle is gasified, it dries first, then pyrolysis is an important intermediate stage to produce a volatile and char as the main solid residue of the biomass. Usually, pyrolysis is carried out in an inert atmosphere. However, oxygenated gas like steam (H_2O) can be used during pyrolysis, called steam pyrolysis, or as gasifying agents depending on the thermal conditions [260; 261; 262].

Thermal behavior of the steam pyrolysis of cellulose, xylan and lignin and its mixtures has shown significant changes in char porosity according cellulose or lignin proportion [262]. Char produced by cellulose steam pyrolysis at 600 °C, has shown similar surface area values that those from chemical alkaline activation and has exceed the BET surface area that those obtained by physical activation in nitrogen atmospheres at 700 °C [263].

Also, the bio-oil yield and composition have showed improvements under steam pyrolysis conditions of different lignocellusic biomass. High bio-oil yield with H/C

ratios between light and heavy petroleum products with characteristics more paraffinic that those obtained under static and nitrogen atmospheres were found [264; 265].

Researches have concluded that the presence of steam has a strong effect on the yield and properties of pyrolysis products. Slow steam pyrolysis/activation of various agricultural residues biomass in a temperature range of 700-800 °C and for 1 or 2 h were studied. The yield of liquid products has increased. In general, the steam produces solid residues with high surface area and good adsorption capacities [266].

In Chapter 3, coconut pyrolysis experiments were previously carried out using nitrogen (N_2) as the reaction atmosphere and its physical and chemical char properties were evaluated. From these results, the char obtained at 550 °C and 2 h of treatment should be microporous and should have an aromatic structure with about 85.7 % of carbon content and about 216 m^2/g of surface area. These are promising values if we are considering them for the production of activated carbon or for energy production through gasification (hydrogen-rich syngas).

The aim of the present work is to study the surface area and porosity characteristics of the activated carbon obtained from coconut endocarp and compare it to the expected values.

5.2 Experiments

We propose slow pyrolysis/gasification of coconut endocarp using water vapor (WV) or nitrogen (N_2) during pyrolysis, and exclusively WV as gasifying agent, as is explained in section 5.2.1. The solid products from both slow pyrolysis and gasification, were characterized.

This approach could be then used to propose a gasification reactor that works exclusively under steam slow pyrolysis/gasification conditions, in view of taking advantage at the same time of the liquid products of pyrolysis as well as the solid produced by the gasification process.

5.2.1 Sample preparation and gasification conditions

The raw materials for the experiments were native coconut endocarp and char obtained after 2h of isothermal pyrolysis at 550 °C (550 °C-Char).

Coconut endocarp particles, between 0.2 and 0.63 mm selected from our previous work Duarte et al. (2016) [6], were obtained using a grinder (IKA M20 Universal mill) and sieved subsequently.

The ash content, elemental and surface analyses for coconut endocarp and 550 °C-Char samples are showed in Table 5.1 (some data were extracted from Duarte et al. (2016) [6]).

Table 5.1: Elemental composition and physical properties for untreated and char samples [6].

Analysis	Coconut endocarp native	550 °C-Char, 2h
Ash %	0.6	5.1
Elemental analysis %		
C	51.1	85.7
H	5.53	2.55
O	42.6	6.08
N	0.37	0.59
S	ND	ND
Surface area BET (m^2/g)	0.28	216
Total pores volume (cc/g) 10^{-3}	0.603	89.1
Micropore volume (cc/g) 10^{-3}	0.014	84.2

The experiments were carried out in a NETZSCH STA 449 F3 Jupiter thermal analyzer combined with an ASTEAM DV2 water vapor generator (Figure 5.1). The evaporator unit is integrated with a water dosing unit, and an additional gas feeding. The gas flow fed was 20 mL/min that was mixed with the steam, thus the outlet of the evaporator consists of one tube for the steam/purge gas mixture.

Initially, about 12 ± 2 mg of sample was placed in an alumina crucible and heated at 5 °C min^{-1}. The samples were heated under nitrogen flow of 50 mL min^{-1} (STP) from ambient temperature to 100 °C, and dried for 30 min.

Then, dried samples are heated with a heating rate of 5 °C/min to a final temperature of 800 °C (dynamic treatment), and kept 2 h at this temperature to completed the gasification (isothermal treatment).

The samples of coconut endocarp (sample 2) and 550 °C-Char (Sample 3) are pyrolysed and activated in one-step thermochemical treatment (dynamic and isothermal treatments) in presence of steam with a flow rate of 3 g h^{-1} of WV. For comparison, sample 1 (coconut endocarp) is treated also in inert atmosphere of nitrogen of 50 $mLmin^{-1}$ during the dynamic treatment (pyrolysis), according to the Table 5.2.

Table 5.2: Experimental conditions.

Samples	Pyrolysis (dynamic treatment) (atmosphere/flow rate)	Gasification (isothermal treatment) (atmosphere/flow rate)
Coconut endocarp ($Sample_1$)	Nitrogen / $50mLmin^{-1}$	WV[1] / $3gh^{-1}$
Coconut endocarp ($Sample_2$)	WV / $3gh^{-1}$	WV / $3gh^{-1}$
550 °C-Char, 2h[2] ($Sample_3$)	WV / $3gh^{-1}$	WV / $3gh^{-1}$

[1] Water vapor.
[2] Obtained by pyrolysis at 550 °C and 2 h.

The samples were characterized at initial time of gasification "t_0" (end of dynamic treatment), at half-life time "$t_{0.5}$" indicating the time needed from the start of isothermal treatment for 50 % conversion of carbon in chars [267], which is used as a reactivity index to characterize the gasification reactivity of chars for quantitative comparisons, and at the end of gasification "t_f" (end of 2 h of isothermal treatment)

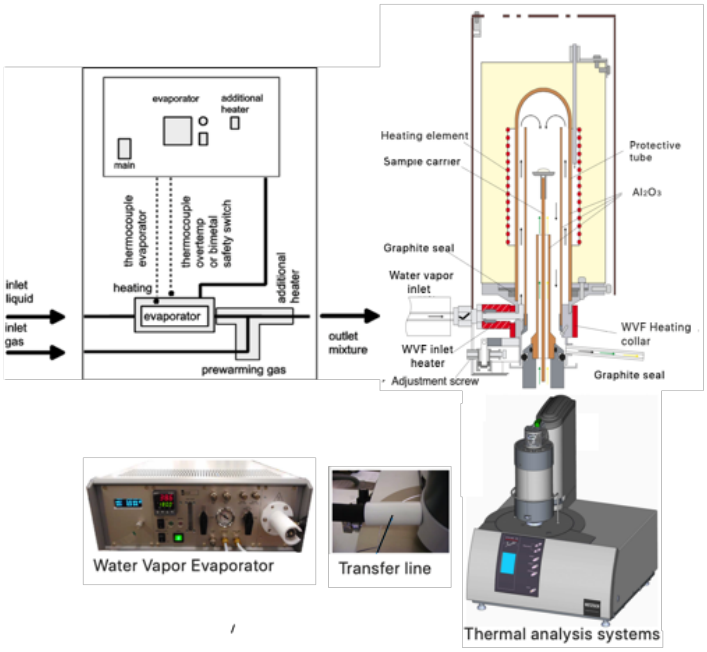

Figure 5.1: Scheme of the components of the WV generator (left) combined with the system for thermal analyzer with a WV Furnace (right).

[268]. Represented as conversion grade of, "X_0", "$X_{0.5}$" and "X_f" respectively.

Where "X" is defined as a conversion level of the gasification process, given by:

$$X = \frac{m_0 - m_t}{m_0 - m_{ash}}, \tag{5.1}$$

where m_0 is the initial mass at the moment when the gasification starts (at the beginning of the isothermal treatment), m_t is the mass of the sample at time t (during the isothermal treatment), and m_{ash} is is the remaining mass corresponding to the ash content of the sample.

5.2.2 Surface area BET analysis and porosity characteristics

The surface area evolution of the gasified samples was evaluated at X_0, $X_{0.5}$ and X_f by the adsorption of nitrogen at 77 K in the Micromeritics 3 Flex surface characterization analyzer.

Prior to analysis, the samples were outgassed at 250 °C for at least 3 h until achieving a residual pressure of $10^{-4} mmHg$. BET surface area, from the isotherms,

was calculated using the Brunauer-Emmett-Teller (BET) equation. The relative pressure P/P_0 range for adsorption isotherm was 10^{-4} to 1. The total mass of the samples used was enough to achieve a good isotherm plot without mathematical smoothing. The pore size distribution was calculated using the Density Functional Theory (DFT) and the total pore volumes were determined from a single adsorption point at a relative pressure P/P_0 0.95. The mesopore volume was obtained by subtracting the micro-pore volume from the total pore volume. The micropore volume was estimated using the t-plot. The experiments were performed in triplicate.

5.3 Results and Discussion

The thermogravimetric curves (TG) and char conversion were used to investigate the gasification rate of the samples. Besides the activated carbon properties produced from coconut endocarp chars were evaluated.

5.3.1 TG curves of slow pyrolysis/gasification of the samples

Slow pyrolysis/gasification TG curves are showed in Fig. 5.2. For samples 1 and 2, a deviation of about 5% for three tests was observed under our conditions. The repeatability is acceptable considering the heterogeneity of the coconut endocarp and the distribution of the particles size.

The TG curves of the coconut native, treated with N_2 and water vapor (WV) during the pyrolysis (dynamic treatment), samples 1 and 2 respectively, indicates similar characteristics. However from 350 °C, there is a higher decomposition rate for the sample treated with WV which conducts to a subsequently higher mass loss. This lower yield of solid residue under a flow of steam is related to the ability of the water vapour to penetrate the solid material and to help desorption, distillation, hydrolysis and efficient removal of the volatile products from it [266]. Which probably result in the formation of a solid product with higher surface area at the end of the pyrolysis (isothermal treatment) than the obtained using N_2 (sample 1), as it was reported by Mehandjiev et al. (1997) [269] and Nickolov and Mehandjiev (1995) [270].

The same happens for sample 3 (char obtained at 550 °C and 2 h). TG curve shows two behaviors when treated with WV on dynamic treatment, between 600-800 °C, there is a mass loss of about 5%, which is explained by the reactivity of the water vapour at these high temperatures [266], which reacts with the pyrolysis products such as tar inside the porous structure of this sample and from the isothermal treatment at 800 °C, gasification reactions start with at high conversion rate. At 800 °C, a change in the slope, allow us to distinguish clearly that the WV gasification begin in all cases.

The residual mass were $fml_1 = 3.4\%$, $fml_2 = 2.94\%$ and $fml_3 = 0.95\%$ for samples 1, 2 and 3 respectively. These values infers that the complete gasification of them occurs after 2 h of treatment at 800 °C.

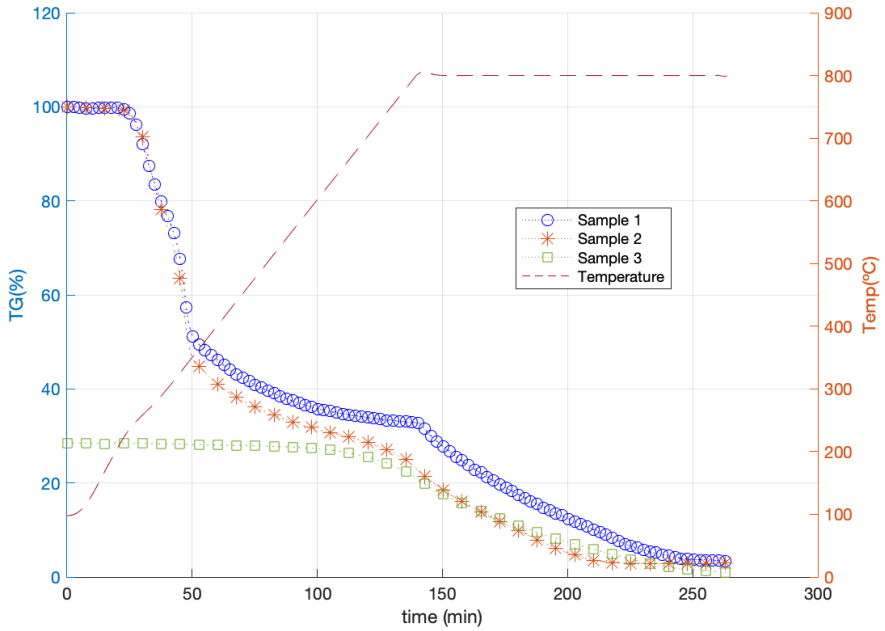

(a)

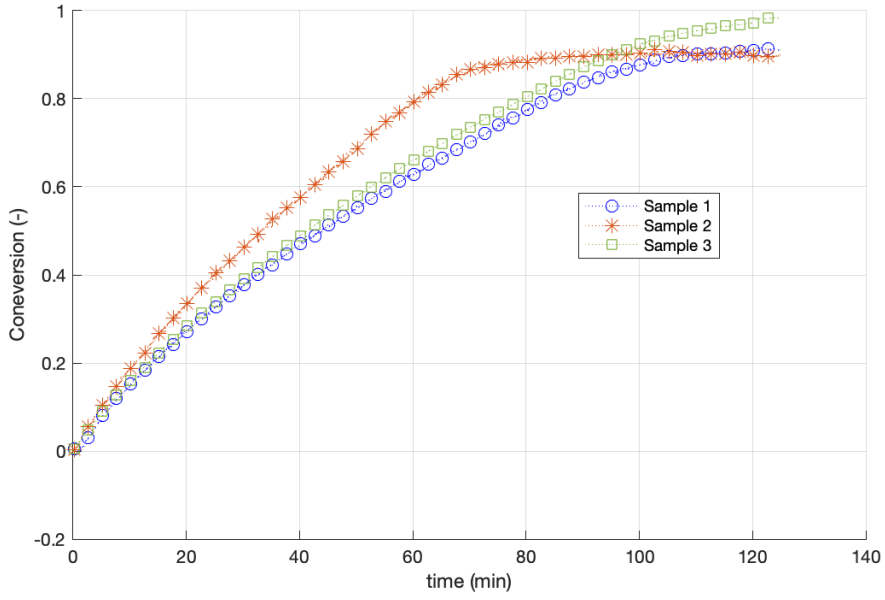

(b)

Figure 5.2: (a) Comparison between TG curves and (b) Char conversion of coconut endocarp observed in various atmospheres (N_2 and WV). The red dashed line in (a) indicate the temperature evolution as function of time.

In Fig. 5.2b, sample 2 has higher conversion rate and it suddenly stabilizes at about 90 % of conversion level. Conversion rate of sample 1 and 3 are very close to each other and its reactivity continuously increases during the conversion, with an almost constant slope during nearly 80% of conversion level. This straight shape is characteristic of biomass chars due to continuous increase in the surface area [271]. As the char conversion proceeds, the pore enlargement increases the contribution of micro-pores; consequently the effective surface area will increase. The increase in the effective surface area leads to an increased reactivity of char during the entire conversion process [272].

5.3.2 Surface area BET analysis and porosity characteristics

The specific surface area and porosity characteristics of the samples at various levels of conversion, using BET technique are showed in Table 5.3.

Table 5.3: Gasified samples structural characteristics.

Samples	$t_{0.5}$ (min)	Conversion	S_{BET} (m^2/g)	V_{total} (cc/g) $x10^{-3}$	V_{micro} (cc/g) $x10^{-3}$	V_{meso}/V_{total} (%)	d (nm)
$Sample_1$	45	X_0	306.5	120.7	120.6	0.08	1.57
		$X_{0.5}$	717.4	326.6	241.6	26.0	1.82
		$X_f = 0.91$	1261.8	748.2	311.2	58.0	2.66
$Sample_2$	35	X_0	689.1	272.9	257.3	5,7	1.58
		$X_{0.5}$	799.31	379.6	255.9	32.6	1.90
		$X_f = 0,89$	887.0	569.7	183.3	67.8	2.6
$Sample_3$	43	X_0	736.3	315.7	262.3	16,9	1.72
		$X_{0.5}$	763.3	368.0	240.0	34.8	1.93
		$X_f = 0,98$	1134.6	659.2	302.0	54,2	2.32

At the end of the dynamic treatment (pyrolysis), i.e. at the beginning of the gasification, where was defined that char conversion is zero (X_0), the surface obtained are very similar for samples 2 and 3 treated with WV during the pyrolysis (dynamic treatment), regardless of whether the starting sample is coconut endocarp or char respectively. At X_0, in all cases, the BET surface area is lower for native coconut endocarp treated with N_2 (sample 1) during pyrolysis. This was expected given the high reactivity of the water vapor as explained in the last subsection 5.3.1.

The advantage of using steam/vapor in pyrolysis is described in favor of producing solid residues with high surface area and good adsorption capacities. However, despite this being true for the pyrolysis process, as described in the previous paragraph, it is observed at the end of gasification treatment (X_f), that samples 1 and 3 have superior BET surface areas than native coconut endocarp (sample 2) treated entirely with water vapor during pyrolysis and gasification.

Several factors such as non-uniform distribution of raw material particle size, char porosity, micropore, mesopore and macropore development can affect the activation rate and produce the collapse of the solid linkage between the adjoining pores, which decreases the surface area available for the reaction. Although the surface area

of the carbonaceous solid can be high at the beginning of the process (X_0), the gasification rate can be different as result of these factors, giving different final properties in the activated carbon [273, 272].

As we have seen, the surface area increases to similar values at $X_{0.5}$, for all samples (1, 2 and 3). However, at X_f, the sample 2 show lower BET surface area than samples 1 and 3, which can be explained because a reduction in the conversion rate after 65 min of gasification (isothermal treatment). This reduction can be due a decrease of the surface area available for the reaction. Besides, there is a reduction of the micropore development that is evidenced by the consequent reduction of the micropore volume as the reaction progress (V_{micro}).

Otherwise, the higher surface areas of the samples 1 and 3 at X_f, are consequence of both, as a result of the mesoporosity development (the percentage of mesopore to total pore volume, V_{me}/V_{tot}), and a progressive increment in the microporosity V_{micro}. Similar to that reported by Hu et al. [274] there is an increase in the total pore volume which is accompanied by an increase in mesoporosity for all samples, from X_0 to X_f. Besides, the average pore diameter of the samples (last column of Table 5.3) increased as the conversion progressing (from X_0 to X_f). In all cases, it was greater than 2 nm for X_f indicating the development of mesoporosity.

During the char conversion, different pores may evolve with different rates and their accessibility to the reactants may change during the conversion [272]. The pore size distribution of the samples at X_0 and X_f are showed in Fig. 5.3.

For sample 1, it is evident the creation of new micropores and also an expansion of these pores along to the existing ones, thereby both contributions cause the development of micro and mesoporosity. This is consistent with the increase in its V_{micro} and its large increase in the BET surface area as the gasification reaction progresses.

For sample 2, the increase of total pore volume (V_{total}) along to the decrease in micropore volume (V_{micro}), suggests an increase in mesopores at the expense of micropores. As a result, for this sample, the mesoporosity changes enormously from 5.7 % to 68 %.

Finally in sample 3, it is possible to observe clearly the widening of the micropores, which causes at the same time the increase of the micropores volume and as results of this, the emergence of mesopores, which increases the total volume adsorbed (Table 5.3).

These results will support the design of a multipurpose gasifier, to obtain activated carbon and to collect syn-gas during the process, within the framework of the "14-INV-087" Paraguayan project [0]. Based on the results presented here and the complementary analysis to be made of the composition of the gases, a model for the gasification of char will be proposed.

[0] https://datos.conacyt.gov.py/proyectos/nid/126

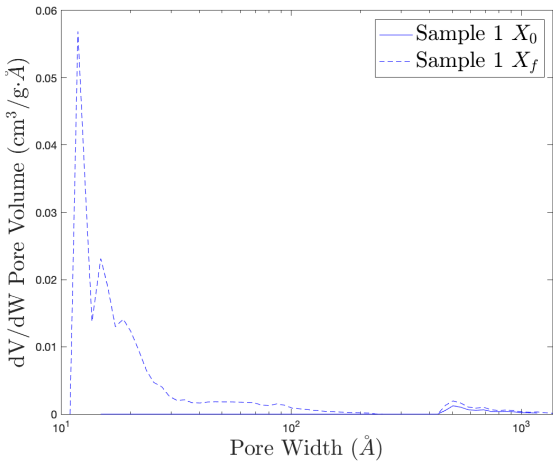

(a)

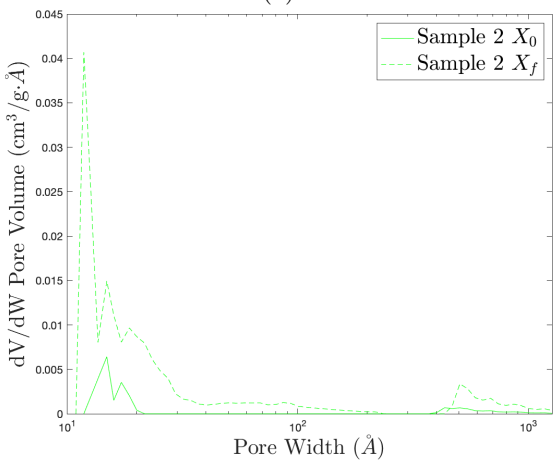

(b)

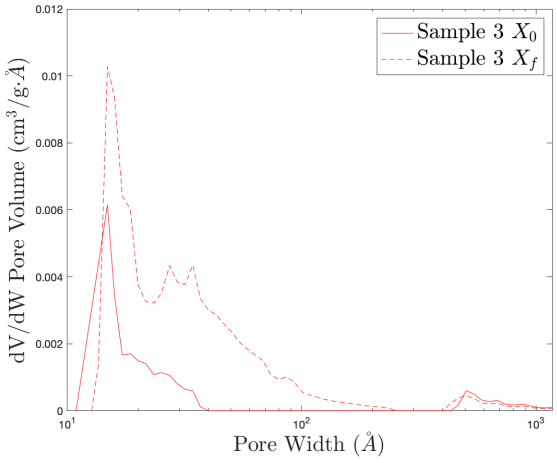

(c)

Figure 5.3: Pore size distribution for (a) sample 1, (b) sample 2 and (c) sample 3, for a conversion at t_0 and t_f.

5.4 Conclusion

Slow pyrolysis was performed in two atmospheres (N_2 and WV) on native coconut endocarp and on char under WV. After the pyrolysis (dynamic treatment) the samples were gasified by isothermal treatment at 800 °C using WV. The solid products were analyzed using BET technique.

Based on the TG curves and BET analysis, there are differences in the final mass loss and porosities characteristics according to the atmospheres employed during the slow pyrolysis. At the end of pyrolysis on native coconut endocarp (dynamic treatment until 800 °C), sample 1 (treated with N_2) has a lower mass loss and BET surface area, compared to sample 2 (treated with WV). These results agree with those of Minkova et al. (2001) where the steam produces solid residues with high surface area. For the char (sample 3), the surface area increase from 210 to 736 m^2/g (at X_0) during the dynamic treatment under WV .

After the dynamic treatment, gasification start at 800 °C (2 h of isothermal treatment) with at higher conversion rate for sample 2. However, although sample 2 has presented at X_0 higher surface area than sample 1, at the final time of treatment (X_f) sample 2 shows lower BET surface area, such as consequences of a decrease in the conversion rate after 65min of gasification and a progressive decrease of the microporosity, showing that the evolution of porous structures is very important and depends on several factors and not only to the surface area of carbonized at the beginning of the process.

Surface area requirements of activated carbon depend on its applications (municipal drinking water, food and beverage processing, odor removal, industrial pollution control, etc.). Activated carbon is produced specifically so as to achieve a very big internal surface (between $500 - 1500 m^2/g$). However, it should be noted that the surface area obtained for all samples 1, 2 and 3 at $X_{0.5}$ are higher than 700 m^2/g and even for sample 2 reaches up to 880 m^2/g, which is enough for most applications.

Chapter 6

Numerical Combustion Studies of Pyrolysis Bio-oil from Torrefied coconut endocarp

Bio-oil is a complex real fuel, considered as a carbon-neutral alternative to hydrocarbons in the transport sector, which is composed of hundreds of compounds, mostly oxygenated. These characteristics make it totally different from petroleum fuels affecting the combustion process. Pyrolysis oil has high acidity, low thermal stability, low calorific value, high water content, high viscosity and poor lubrication characteristics. Therefore, its use in transportation is limited. Blends of bio-oil/diesel/alcohols are viable short-term alternatives to utilize an important fraction of these oils. In the present work, pyrolysis was performed on torrefied coconut endocarp and the collected bio-oil was analyzed using gas chromatography/mass spectrometry (GC/MS). Based on the GC/MS analysis, three different blends of toluene, ethanol and acetic acid representative of the real fuel chemistry were proposed as the surrogates to carry out numerical combustion studies. The objective of this work is to develop and validate a new chemical reaction model for the combustion of toluene/ethanol/acetic-acid blends by carefully combining two recent chemical models from the literature. The first one is the model due to Huang et al (2017) for the combustion of toluene, and the second one is due to Christensen et al (2016) for the combustion of ethanol/acetic-acid. The combined model consists of 180 *species and* 1495 *reactions. In order to validate the proposed model, the work focuses on numerical studies of the combustion of toluene/ethanol/acetic-acid blends using 0-D constant-volume auto-ignition as well as 1-D freely-propagating gaseous premixed flame configurations. Then, as Huang et al original model was developed and validated for diesel/n-butanol blends, auto-ignition delays and laminar flame speed simulations of bio-oil/diesel/n-butanol are presented.*

6.1 Introduction

Chemical and physical properties of bio-oils are completely different from petroleum fuels affecting the combustion process [141]. Physical properties of bio-oils from coconut endocarp -*Acrocomia aculeata*- have been analyzed in a previous work [6], showing water content higher than 50 wt%, presence of suspended solids, relative density of about 1.07, viscosity of about 1.55 cSt, pH $\approx$ 2.4 and a higher heating value (HHV) of about 13 MJ/kg. The presence of water causes difficulties in ignition and increases the ignition delay time but for spray combustion applications it will expect enhances in the atomization properties [141].

Torrefaction is a potential upgrading method to improve the quality of bio-oil. It has showing that produces pyrolytic bio-oil with lower oxygen-to-carbon ratios, different compositions (becomes more concentrated in pyrolytic lignin) and less water content compared to those from the original untreated biomass [275]. We found in Chapter 3.4 an improvement in hydrophobicity of torrefied coconut endocarp, a decrease in the oxygen content to 38.6% from 42.6% and an increase in the carbon content from 51.1% to 56.9%, after torrefaction for 120 min at 250 °C [238]. In fact, at low temperatures (between 200-250 °C), both oxygen and carbon are released (in the form of H_2O, CO and CO_2 molecules), but the oxygen is released in greater proportion, therefore the carbon relative percentage (in mass) increases. Also the heating value and pH of the bio-oil was improved [172]. Even with these improvements, this is a low-quality fuel compared to conventional fossil fuels but it could be manageable in combustion processes and should generate lower pollutants emissions.

In this work, torrefied coconut endocarp was used to produce pyrolysis bio-oil for combustion application. The chemical composition of the collected bio-oils were analyzed by GC/MS to propose a surrogate in function of its major components.

The purpose of using surrogates is to simplify the combustion mechanism by using a single fuel molecule or a blend of relatively small molecules to represent the real fuel. Numerically, the use of surrogate fuels reduces significantly the number of possible chemical reactions in the kinetic scheme, while still representing the main properties of the real fuel.

However, the use of pyrolysis oil as a transportation fuel is limited due to its high acidity, low thermal stability, low calorific value, high water content, high viscosity and poor lubrication characteristics [276; 277]. Therefore, blends are a viable short-term alternative to utilize an important fraction of these oils [196]. In this sense, phase behaviors and fuel properties of bio-oil-diesel-alcohol blends were performed by Weerachanchai et al. [197]. The objective was to improve certain characteristics of bio-oil derived from palm kernel pyrolysis by blending it with diesel fuel and alcohols (ethanol or butanol). In addition, a review of blends of pyrolysis oil, petroleum diesel, and other bio-based (biodiesel) fuels was conducted by Krutof and Hawboldt [278]. In this work it was pointed out that blends allow the utilization of low-cost large-scale mass production diesel engines with only minor modifications as the dual injection system is not necessary. This is especially true for blends with low bio crude oil and high petroleum diesel content. Furthermore, the combustion of bio-oil/ethanol

blends at elevated pressure was performed by Nguyen and Honnery[279]. Experiments were conducted in a constant volume vessel operating at a pressure of 25 bar and temperature 1100 K. Bio-oil produced via the fast pyrolysis of a spruce feedstock was blended to ethanol to form three stable blends containing 10%, 20% and 40% bio-oil by weight. Results show that for similar injections of fuel energy, use of up to 20% bio-oil in ethanol has limited impact on the performance of ethanol while 40% bio-oil in ethanol produced instability in the pressure trace near the end of the combustion process.

As it was presented, bio-oil combustion has been the focus of intense research quite recently. However, there is little information concerning bio-oil chemical kinetics modeling. The present work concerns numerical studies of the combustion of bio-oil surrogates using toluene/ethanol/acetic-acid blends in a 0-D constant-volume auto-ignition and 1-D freely-propagating gaseous premixed flame configurations. The objective is to develop and validate a new chemical scheme for the combustion of toluene/ethanol/acetic-acid blends while guaranteeing a correct reproduction of the principal features of the original pure fuels combustion (such as ignition delay and laminar flame speed). This is done by carefully combining two chemical schemes: one for the combustion of toluene [13] and the other for ethanol/acetic-acid blends [12]. Numerical simulations were performed using the REGATH package developed at EM2C laboratory [190; 198; 191; 280; 281], that takes into account the detailed chemical kinetics and multi-component transport properties.

During the merging procedure, reactions present in both chemical schemes were found, and as it will be seen in Sec. 6.5, auto-ignition delays and laminar flame speeds of toluene, ethanol and acetic-acid are sensitive to common reactions Arrhenius constants. Therefore, a careful analysis of these parameters will be performed in order to obtain reasonable results for the pure fuels separately.

The new combined model is validated by comparing auto-ignition delays and laminar flame speeds of the pure fuels obtained by both the combined model and the original models, as well as available experimental data.

6.2 Bio-oil obtainment and chemical analysis

6.2.1 Raw material

The coconut endocarp —*A. aculeata*— fruit, was used in this study. It was provided as agro industrial waste by Cavallaro Company [282]. Prior to the experiments, the coconut was cleaned with water and dried in an oven at 110 °C.

6.2.2 Torrefaction and pyrolysis experiments

Torrefaction and pyrolysis experiments were performed using a tubular fixed-bed reactor as described in section 2.3.1 and shown in Fig. 2.8. Nitrogen was used as the carrier gas at a flow rate of 2 L/min and the heating rate media was 18 °C/min for both processes.

For torrefaction, 65 g of sample were placed in the reactor, then the furnace heating rate (18 °C/min) was programmed to the target temperature of 210 °C, where it was maintained for 2 h. The cooling time of the samples at the end of the experiment was approximately 2 h. Then, a 0.2-0.63 mm diameter powder was obtained using a grinder (IKA M20 Universal mill).

The pyrolysis experiments of dried, grinded and torrefied coconut endocarp were performed using 70 g of sample. The temperature was increased to a final value of 500 °C and it was controlled during 40 min. After each experiment, the bio-oil was collected at the outlet of the condenser and stored in a refrigerated amber glass bottle, under inert atmosphere (using N_2 gas) for one day until the bio-oil analysis. The liquid product yield was 32 %wt (Fig. 6.1).

Figure 6.1: Bio-oil collected from coconut endocarp pyrolysis

6.2.3 Bio-oil composition analysis

Fractionation by liquid-liquid extraction (LLE) based on the water addition [283; 284; 285] was applied as follows. After adding distilled water into the pyrolysis bio-oil (2.5:1 v/v), the sample was divided into water-solubles and water-insolubles fractions (pyrolytic lignin). The powder-like water-insoluble fraction was removed by filtration ($<$ 0.1 mm), whereas the water-soluble fractions were further extracted with ethyl acetate (1:1.25 v/v) and subjected to sonication (25 °C, 30 min). Two phases were formed and the ethyl acetate phase was analyzed by GC/MS as the remaining aqueous phase were further extracted with diethylether (1:1.25 v/v) immediately after separation and subjected to stirring (850 rpm, 30 min). The diethylether soluble fractions were analyzed by GC/MS. In the ether soluble fraction, aldehydes, ketones, and lignin monomers can be detected. The ether-insoluble consists of sugars and C $<$ 10 aliphatic hydroxy acids.

The water-soluble fractions were analyzed for volatile acids and alcohols identification by GC/MS. In each fraction, major bio-oil compounds were determined using a gas chromatograph/mass spectrometer (Shimadzu QP 2010 plus). The GC column used was a Restek Rtx-5ms (30 m x 0.25 mm i.d. x 0.25 μm d_f). The oven was programed initially at 60 °C for 5 min, and then increased at 3 °C/min to 220 °C and then it was kept constant for 10 min. Helium was used as carrier gas. The injector temperature was 250 °C. The injection was in Split mode, with a ratio of 20:1. The MS detector was set in full scan mode with a range from 35 to 400 amu. Standard electron impact (EI) ionization at 70 eV was employed. The detector temperature was 220 °C and the ion source temperature was 250 °C.

6.2.3.1 Bio-oil characterization: chemical analysis

The analysis of the pyrolysis of coconut endocarp bio-oil was performed within 48 h after being produced, in order to avoid aging reactions [6]. The chromatograms of the different fractions of coconut endocarp pyrolysis oil are shown in Fig. 6.2.

The ethyl acetate and diethylether soluble fractions contained low molecular mass degradation products of lignin. (Figs. 6.2 (a) and (b)). Their composition gave information on the raw material used and on the degree of thermal decomposition of the material.

GC/MS analysis results of bio-oil are listed in Tab. 6.1. The peak area % was calculated considering that retention times for all analysis were the same.

The sum of minority and unidentified species peak areas (related to the concentrations) are consistent for this type of fuels [185, 171]. Minority species are defined as those with an individual peak area smaller than 0.35, which is the smallest peak area presented in the Table 6.1. The list of minority species is presented in Table 6.2 and they were taken into account for the estimation of bio-oil equivalent formula.

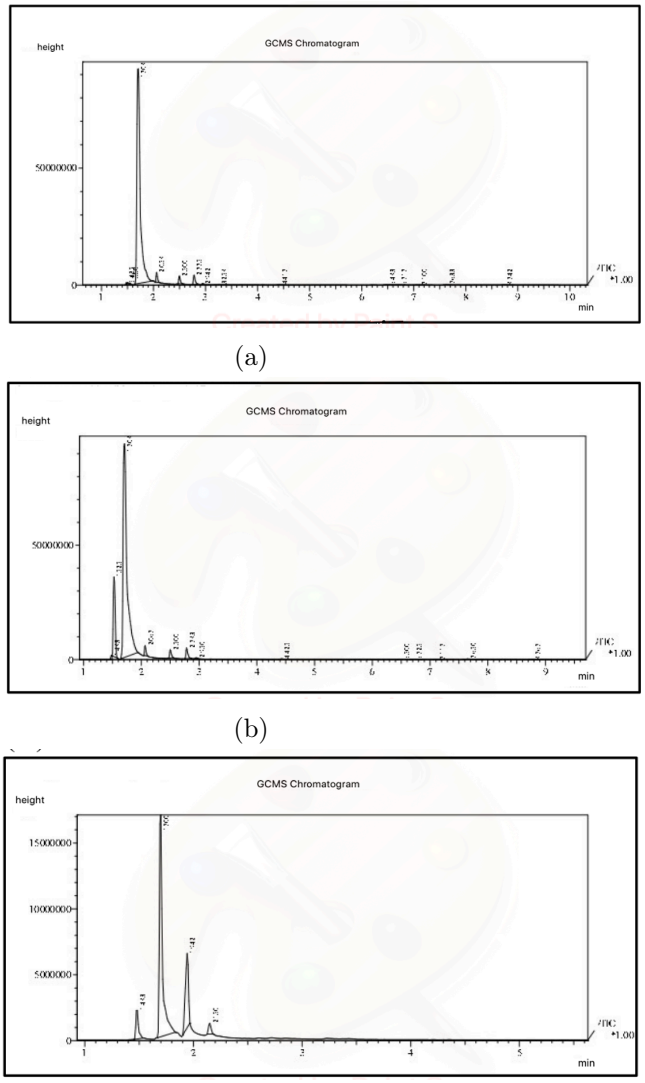

Figure 6.2: Total ion chromatograms (TIC) of coconut endocarp pyrolysis oil: (a) ethyl acetate fraction (b) diethylether fraction and (c) water fraction of the oil.

Table 6.1: GC/MS analysis results of Bio-oil.

No.	Group	Compounds	Peak area/%	Mole fraction	Atoms per molecule		
					C	H	O
1	Alcohols	Ethanol	5.6	0.119	2	6	1
2	Carboxylic Acids	Acetic acid	7.2	0.118	2	4	2
3	Aromatic Compounds	Toluene	11	0.117	7	8	0
4	Nonaromatic Ketones	1-Hydroxy-2-propanone	0.87	0.011	3	6	2
5	Aromatic Compounds (Nonoxygenated)	1,4-Dimethylbenzene	1.5	0.014	8	10	0
6	Aromatic Compounds (Nonoxygenated)	1-Ethyl-2-methylbenzene	0.35	0.003	9	12	0
7	Aromatic Compounds (Nonoxygenated)	1-Ethyl-3-methylbenzene	1.9	0.016	9	12	0
8	Aromatic Compounds (Nonoxygenated)	1,2,3-Trimethylbenzene	0.78	0.006	9	12	0
9	Aromatic Compounds (Nonoxygenated)	1,3,5-Trimethylbenzene	2.9	0.024	9	12	0
10	Aromatic Compounds (Nonoxygenated)	1,2,4-Trimethylbenzene	0.41	0.003	9	12	0
11		Sum of minority species	56.46	0.567	5.29	8.34	1.59
12		Sum of unidentified species	11.03				
	Equivalent formula				4.91	7.70	1.28

Table 6.2: Chemical composition of bio-oil: Minority species

Ethyl acetate Fraction	Ethyl ether fraction	Aqueous fraction
4-methoxyphenol	Pentanoic acid	Acetaldehyde
2-methoxyphenol	3-hydroxybutyric acid	2-butanone
4-methyl-2-methoxyphenol	2-butanone	cis-2-penten-1-ol
1,2-benzenediol	Cyclobutane	3,3-dimethylacrylic acid
2,6-dimethoxyphenol	3,3-dimethyloxetane	Trimethylene oxide
3-hydroxy-4-methoxybenzoic acid	2,2-dimethylpropane	
5-hexen-2-ol	Maleic acid	
3,3-dimethyloxetane	Propanoic anhydride	
Propanoic acid	Trimethylene oxide	
4-hydroxy-2-butanone	Pyruvic acid	
2,3-dihydro-1,4-dioxane	2-methylpropanoic anhydride	
Butoxybenzyl ether	o-Xylene	
(2-methylbutyl) benzene	2-furoic acid	
3-methoxy-1-heptene	2-butoxyethanol	
1,2-ethanediol monoformate	Propylbenzene	
2,5-dimethylfuran		
4-ethyl-2,2,6,6-tetramethylheptane		
1,3-dioxolan-2-one		
1- (2-furanyl) -1-pentanone		
1- (2-furanyl) -1-hexanone		
Furane		
2-Cyclohexen-1-one		
Methylmaleic anhydride		
1-cyclopropyl-1-propanone		
1,4-dioxan-2,6-dione		
5-methyl-2-furancarboxaldehyde		
2-methoxyacetic acid		
2-heptyl-1,3-dioxolane		

From this Table, one can see that the studied bio-oil is mainly composed of toluene, acetic acid and ethanol. Bio-oil equivalent formula has been estimated using each component mole fraction: $C_{4.91}H_{7.70}O_{1.28}$, whereas H/C and O/C ratios were estimated consequently to 1.57 and 0.26, respectively.

Acetic acid is typically formed from hemicelluloses and pyrolysis [286], whereas ethanol mainly comes from thermal cracking of cellulose [182] and hydroxyacetone (acetol) is a product of reactions that are competitive to levoglucosan formation. Also, as levoglucosan was not detected in the liquid pyrolysis, dehydration steps are expected in the reaction mechanisms [287]. The high yield of aromatic hydrocarbons (toluene, benzenes, etc.) can be attributed to an extent of thermal reactions of olefins and diolefins (Diels–Alder cyclization) and also the increase of the pyrolysis temperature, increases cracking severity.

As these results are approximative, it is necessary to make a correction considering environmental variances. For that purpose, peak retention times and peak area ratios should be calculated relative to an internal standard.

The pyrolysis condition (500 °C, 18 °C/min and 40 min residence time) seems to favor the Diels–Alder cyclization, producing more aromatic compounds (no oxygenated), which could have a positive impact on the combustion parameters due to the high oxygen removal.

6.2.4 Bio-oil surrogates chosen

In the present work, the objective is to carry out bio-oil combustion studies. However, as it was presented in the previous section, bio-oil composition is quite complex. Therefore, we must choose a surrogate representative of the coconut endocarp bio-oil in order to perform combustion simulations. Taking into account bio-oil chemical composition (see Tab. 6.1), it was found that the most simple bio-oil surrogate can be composed of the three major compounds: toluene, acetic acid and ethanol. Furthermore, different surrogates (I, II and III) consisting of blends of toluene, acetic acid and ethanol having equivalent formulas and ratios H/C and O/C very close to those of bio-oil are considered, as it can be seen in Table 6.3. These surrogates would represent bio-oil chemistry in order to analyze the influence of these molecules mole fractions on bio-oil combustion properties. In our knowledge, these are the first surrogates proposed to represent pyrolysis coconut endocarp bio-oil combustion. In addition, it must be pointed out that for different bio-oils compositions, other percentages of toluene, ethanol and acetic acid could be chosen in order to match the desired bio-oil composition.

Table 6.3: Chemical composition of bio-oil surrogates (vol)

	Surr I	Surr II	Surr III
Ethanol	0.4	0.3	0.2
Ac. acid	0.2	0.3	0.4
Toluene	0.4	0.4	0.4
Formula	$C_4H_{6.4}O_{0.8}$	$C_4H_{6.2}O_{0.9}$	$C_4H_6O_1$
H/C	1.6	1.55	1.5
O/C	0.2	0.225	0.25

6.3 Toluene, acetic acid and ethanol chemical models and experimental data

6.3.1 Toluene chemical kinetics and experimental data

Aromatic species represent a significant fraction (about one third by weight) of both diesel and gasoline fuels. Much of the aromatics in diesel and gasoline are alkyl-benzene species. Toluene, the lightest of the alkyl-benzenes, has been the subject of extensive literature investigations [288].

In this sense, the chemical kinetics of toluene combustion has been extensively studied . For instance, a kinetic model for the oxidation of toluene near 1200 K was performed by Emdee et al. [289]. Also, a detailed kinetic modelling of toluene combustion was presented by Lindstedt and Maurice [290], and validated using counterflow diffusion flames, plug flow reactors, shock tubes and premixed flames. The

reaction mechanism features 743 elementary reactions and 141 species and represents an attempt to develop a chemical kinetic mechanism applicable to intermediate and high temperature oxidation. Furthermore, experimental and detailed chemical kinetic modeling of the oxidation, ignition and combustion of toluene was done by [291]. New experimental results were obtained over the high temperature range 1000-1375 K, and variable equivalence ratio. These experiments were modeled using a detailed kinetic reaction mechanism (120 species and 920 reactions, most of them reversible). Later, a comprehensive detailed chemical kinetic modeling study of toluene oxidation containing 329 species and 1888 reversible reactions was developed by Metcalfe et al. [292], and validated over a wide range of experimental conditions, including flow reactor, shock tube, jet-stirred reactor. Also, an optimized chemical mechanism for combustion of n-heptane/iso-octane/toluene blends (a gasoline surrogate) fuels was done by Cai and Pitsch [293]. The resulting mechanism retains a compact size and was successfully validated against experimental measurements. Finally, the development and validation of a new reduced diesel-n-butanol blends (reduced n-heptane-toluene-n-butanol-polycyclic aromatic hydrocarbon (PAH)) mechanism for engine applications was performed by Huang et al. [13]. The model includes 101 species and 531 reactions and it has been widely validated with ignition delays, laminar flame speeds, species concentrations in premixed flame and counterflow flame, and homogeneous charge compression ignition (HCCI) engine combustion.

A non-exhaustive list of available chemical schemes for toluene, with the corresponding number of species and reactions, as well as validation domains and configurations, is presented in Tab. 6.4.

For more information, an extensive review was recently published by Zhen et al. [302], including toluene chemical reaction mechanisms.

In the present work, a chemical scheme for the simulation of combustion of toluene/ethanol/acetic-acid blends is needed. The scheme due to Huang et al. [13] has been chosen to combine it to a ethanol/acetic-acid scheme, because it has been extensively validated in different configurations and operating conditions, and also because it has been developed for diesel/n-butanol blends. In fact, as explained before, blends of bio-oil/diesel/alcohols are a viable short-term alternative to utilize an important fraction of these oils, and therefore as it will be seen in Sec. 6.5.3 and 6.5.4, once the developed bio-oil surrogate model has been validated, simulations of the combustion of bio-oil/diesel/n-butanol will be performed.

As mentioned in Sec. 6.1, validations of our combined mechanism include both auto-ignition delays and laminar flame speeds of individual components. As we will see in Sec. 6.5, the prediction of toluene auto-ignition delays are little impacted by the combination procedure, however larger discrepancies between the combined model toluene laminar flame speeds and those of Huang et al. [13] model are observed. Therefore, experimental data for toluene laminar flame speed are of specific interest here. In this sense, the heat flux method was used by Dirrenberger et al. [24] to determine laminar burning velocities for gasoline surrogates, as well as pure n-heptane, toluene, iso-octane and ethanol, at 298 K, 358 K, 398 K and 1 bar. In the present work, the measurements from their experimental data at 1 bar and 298 K will be used

Table 6.4: Non-exhaustive list of available chemical schemes for toluene, ethanol and acetic acid. ST: shock tubes, PSR: perfectly stirred reactor, LFS: laminar flame speed, , FR: flow reactors, TR: turbulent reactor, JSR: jet-stirred reactor, LPF: laminar premixed flames, HCCI: homogeneous charge compression ignition, CFF: counterflow flame, EA: engine application.

Reference	Number of species and reactions	Validation domain	Mechanism validation	Toluene	Ethanol	Acetic acid
Sivaramakrishnan et al., (2006) [294]	87 species 262 reactions	1200-1900 K 27-45 bar	ST	x		
Dagaut et al., (2002) [291]	120 species 920 reactions	1000-1375 K 1 bar ϕ = 0.5-1.5	PSR, LFS	x		
Colket et al., (1994) [295]	98 species 529 reactions	1200-1850 K 10.0 bar	ST	x		
Emdee et al., (1992) [296]	130 reactions	1100-1190 K 1 bar ϕ = 0.65-1.38	FR	x		
Lindstedt et al., (1996)[290]	141 species 743 reactions	1515-2100 K 0.3-7.01 bar ϕ = 0.63-1.4	TR	x		
Metcalfe et al., (2011) [292]	329 species 1888 reactions	800-1500 K 1-550 bar ϕ = 0.3-5.0	ST, FR JSR, LFS	x		
Huang et al., (2017) [13]	120 species 531 reactions	K 0.04-80 bar ϕ = 0.5-1.5	ST, LFS, LPF, HCCI, CFF, EA	x		
Cai et al., (2015) [293]	335 species 1610 reactions	300-1250 K 1-40 bar ϕ = 0.5-2.0	ST, LFS, JSR	x	x	
Leplat et al., (2012) [297]	43 species 270 reactions	400 K 0.05 bar ϕ = 0.77, 0.9, 1.05	LPF			x
Christensen et al., (2016) [12]	100 species 1140 reactions	338-358 K 0.05, 1 bar ϕ = 0.7-1.3	LFS, LPF		x	x
Marinov et al., (1999) [298]	57 species 387 reactions	1000-1700 K 1-4.5 bar ϕ = 0.5-2.0	ST, JSR FR, CFF		x	
Saxena et al., (2007) [299]	36 species 192 reactions	$\leq$ 1000 K $\leq$ 100 bar ϕ =$\leq$ 3.0	CFF, ST		x	
Cancino et al., (2010) [300]	136 species 1349 reactions	650-1220 K 30-50 bar ϕ = 0.3-1.0	ST		x	
Leplat et al., (2011) [301]	36 species 252 reactions	890-1250 K 1 bar ϕ = 0.25-2.0	LPF, JSR ST		x	
Present work	180 species 1495 reactions	300-2000 K 1-100 bar ϕ = 0.5-1.5	ST LFS	x	x	x

for validations for toluene.

6.3.2 Acetic-acid and ethanol chemical kinetics and experimental data

Concerning acetic-acid, two chemical schemes were recently developed and are available in the literature [297; 12] (see Tab. 6.4). Experimental mole fraction profiles of chemical species have been measured by Leplat et al. [297], in three acetic-acid/O_2/Ar flat premixed flames burning at low pressure (50 mbar) and with equivalence ratios equal to 0.77, 0.9 and 1.05. In order to simulate the experimental results, a sub-mechanism consisting of 36 species and 252 reactions, concerning the combustion of CH_3COOH and CH_2CO has been built and added to a global mechanism recently proposed. This ensures a reasonably good modeling for the structures of acetic acid flames. Moreover, laminar burning velocities of acetic-acid/ air flames at 1 bar and initial gas temperatures of 338 K, 348 K, and 358 K were determined by Christensen and Konnov [12], using the heat flux method. Seventy reactions pertinent to acetic acid and ketone have been reviewed and detailed reaction mechanism for acetic acid combustion was developed. The model consisting of 100 species and 1140 reactions over-predicts measured burning velocities by about 3 cm/s. An ethanol model is also incorporated into the proposed mechanism. This facilitates the prediction of acetic-acid/ethanol blend combustion. The mechanism was also tested comparing with flame structure of the low-pressure flame of acetic acid [297] with overall good agreement. It was found that the calculated burning velocities are insensitive to the reactions of acetic acid and mostly governed by C_1 chemistry typical for all hydrocarbons and by reactions of ketone.

In the present work, we choose the kinetic model of acetic acid due to Christensen and Konnov [12] to combine it with the toluene kinetic model of Huang et al. [13], as it was especially developed for laminar burning velocities.

Concerning ethanol, several chemical schemes are available in the literature [298; 299; 300; 301 (see Tab. 6.4)] for a list of these chemical models with the corresponding number of species and reactions, as well as their validation domains and configurations). However, the chemical model of Christensen and Konnov [12] has been chosen because it has been extensively validated in different configurations and operating conditions, and also because it includes an ethanol sub-model.

As for toluene, the prediction of acetic acid and ethanol auto-ignition delays are little impacted by the combination procedure, however larger discrepancies between the combined model acetic acid and ethanol laminar flame speeds and those of Christensen and Konnov [12] are observed. Therefore, experimental data for acetic acid and ethanol laminar flame speed are of specific interest here. For acetic acid, the measurements from the experimental works of Christensen and Konnov [12] at 1 bar and 338 K will be used for validations.

Concerning ethanol experimental data, we have focused on the recent works of Konnov et al. [25, vanLipzig et al. 26] and Dirrenberger et al. [24]. Konnov et al. [25]

have performed measurements of the adiabatic burning velocity of ethanol-air flames in the range of initial mixture temperatures from 298 to 358 K. The experimental results were in a good agreement with the recent literature data obtained in constant volume reactors. Moreover, vanLipzig et al. [26] have realized measurements of the adiabatic laminar burning velocities of n-heptane, iso-octane, ethanol and their binary and tertiary mixtures. Initial temperatures of the gas mixtures with air were 298 and 338 K. Therefore concerning ethanol experimental data, the works of Konnov et al. [25], vanLipzig et al. [26] and Dirrenberger et al. [24] at 1 bar and 298 K have been chosen to validate the developed combined chemical scheme.

6.4 Kinetic modeling

The objective here is to develop a detailed reaction mechanism for the combustion of toluene/ethanol/acetic-acid/air mixtures.

The mechanism due to Huang et al. [13], consisting of 120 species and 531 reactions, has been chosen to represent toluene chemistry. On the other hand, the mechanism due to Christensen and Konnov [12], with 100 species and 1140 reactions, has been chosen to represent ethanol/acetic-acid chemistry. Now, to simulate toluene/ethanol/acetic-acid/air flames, the two chemical mechanisms will be merged, species representing these fuels must indeed be present in a single reaction scheme.

As a starting base mechanism, the scheme proposed in the present work will be designed from the original oxidation framework of Huang et al. [13]. Then additional species and corresponding reactions which are present in the kinetic scheme of Christensen and Konnov [12] should be carefully included in Huang's mechanism. There are 40 common species in both chemical schemes (see Tab. 6.5). Therefore, the new combined scheme will consist of 180 species; 120 from Huang's mechanism, and 60 from Christensen's. In addition, there are 181 common elementary reactions in both mechanisms, most of them with different reaction constants. As it will be seen in Sec. 6.5, auto-ignition delays and laminar flame speeds of toluene, ethanol and acetic-acid are sensitive to common reactions Arrhenius constants. Therefore, a careful analysis of these parameters will be performed in order to obtain reasonable results for the pure fuels separately.

Table 6.5: Forty common species.

Common species
H_2, H_2O, HO_2, H_2O_2
CO, CO_2, HCO, CH, CH_2, CH_3, CH_4
CH_2O, CH_3O, CH_2OH, CH_3OH, CH_3O_2, CH_3O_2H
C_2H, C_2H_2, C_2H_3, C_2H_4, C_2H_5, C_2H_6
$HCCO$, CH_2CO, CH_3CO, C_3H_2, C_3H_3,
C_3H_5, C_3H_6, nC_3H_7, C_2H_3CO, CH_3COCH_3
O, H, O_2, OH
N_2, Ar, iC_3H_7

In order to identify the sensitive reactions for the estimation of the pure fuels auto-ignition delay and flame speed, 5 reactions packages were made as presented in Tab. 6.11. These 5 packages were chosen taking into account similar structures of species and reactions groups. These packages along with the Arrhenius reaction constants of Huang et al. [13] and Christensen and Konnov [12] are given in Tabs. 6.6 to 6.10.

It should be noted that some common species from Tab. 6.5, such as O, H, O_2 and OH, are present in more than one package. In addition, although N_2, Ar and iC_3H_7 are common in both detailed schemes, they do not belong to any of the 5 above packages.

Now, in Tabs. 6.6 to 6.10, in order to easily identify the common reactions with identical forward constants in both chemical schemes, we have highlighted them in bold. As one can see, the number of these reactions is not very important. In fact, in Package I, 12 out of 18 reactions have different forward constants; in Package II, 25 out of 36 reactions; in Package III, 39 out of 49 reactions; in Package IV, 34 out of 43 reactions; and finally in Package V, 25 out of 35 reactions have different forward constants, justifying the analysis of common reactions pathways.

Then, several combinations of chemical schemes were examined containing 180 species and 1495 reactions, with 181 common reactions as presented in Tab. 6.11. Concerning reaction constants, different possible combinations A-L are considered as presented in Tab. 6.12, where "h" signifies that common reactions constants are taken from Huang et al. [13], while "C" signifies that common reactions constants are taken from Christensen and Konnov [12].

For each of these combined models (A to L), thermodynamic and transport properties of 40 common species were taken from Huang et al. [13], since they gave better results for both auto-ignition delays and flame speeds than those obtained with models with data for the common species taken from Christensen and Konnov [12].

6.5 Results and Discussion

The chemical kinetics modeling for toluene/ethanol/acetic-acid blends oxidation in 0-D constant-volume auto-ignition and 1-D freely-propagating flame was performed with detailed thermochemical and transport properties, using the REGATH package [190; 198; 191; 280; 281] developed at EM2C laboratory. The inputs to each simulation include a chemical kinetic reaction mechanism, a dataset of thermochemical properties and a dataset of transport properties.

Table 6.6: Package 1 (Species H_2, H_20, HO_2, H_2O_2). Reaction rate coefficients given in the form $k = AT^n exp(-E/RT)$. Units are mol cm cal s. Highlighted reactions correspond to those with similar Arrhenius constants for both models. Superscript ^{rev} in [12] corresponds to the reverse reactions constants, as for these reactions, the reactives in [13] correspond to the products in [12], and vice versa.

	Huang et al. [13]			Christensen and Konnov [12]		
Reactions	A	n	E	A	n	E
$H_2 + M = 2H + M$	4.577E19	-1.4	1.044E5	7.000E+17^{rev}	-1.0000^{rev}	0.00^{rev}
$2O + M = O_2 + M$	6.165E15	-0.5	0.0E0	1.000E+17	-1.0000	0.00
$O + H + M = OH + M$	4.714E18	-1.0	0.0E0	6.750E+18	-1.0000	0.00
$H + OH + M = H_2O + M$	3.5E22	-2.0	0.0E0	6.060E+27^{rev}	-3.3120^{rev}	120769.99^{rev}
$\mathbf{H + O_2(+M) = HO_2(+M)}$	4.65E12	0.44	0.0E0	4.660E+12	0.4400	0.00
$\mathbf{H_2O_2(+M) = 2OH(+M)}$	2.0E12	0.9	4.875E4	2.000E+12	0.9000	48749.99
$\mathbf{O + H_2 = H + OH}$	5.08E4	2.67	6.292E3	5.080E+04	2.6700	6292.00
$\mathbf{H + O_2 = O + OH}$	1.04E14	0.0	1.529E4	1.040E+14	0.0000	15286.00
$OH + H_2 = H + H_2O$	4.38E13	0.0	6.99E3	2.140E+08	1.5200	3450.00
$O + H_2O = 2OH$	2.97E6	2.02	1.34E4	3.340E+04^{rev}	2.4200^{rev}	-1930.00^{rev}
$HO_2 + O = OH + O_2$	3.25E13	0.0	0.0E0	2.850E+10	1.0000	-723.90
$\mathbf{HO_2 + H = 2OH}$	7.079E13	0.0	2.95E2	7.080E+13	0.0000	300.00
$H_2 + O_2 = H + HO_2$	5.176E5	2.433	5.35E4	7.400E+05	2.4300	53499.99
$HO_2 + OH = H_2O + O_2$	2.456E13	0.0	-4.97E2	7.000E+12	0.0000	-1093.00
$HO_2 + OH = H_2O + O_2$	2.456E13	0.0	-4.97E2	4.500E+14	0.0000	10930.00
$H_2O_2 + H = H_2 + HO_2$	2.15E10	1.0	6.0E3	5.020E+06	2.0700	4300.00
$H_2O_2 + H = H_2O + OH$	2.41E13	0.0	3.97E3	2.030E+07	2.0200	2620.00
$\mathbf{H_2O_2 + O = OH + HO_2}$	9.55E6	2.0	3.97E3	9.550E+06	2.0000	3970.00

Table 6.7: Package 2 (Species CO, CO_2, HCO, CH, CH_2, CH_3, CH_4). Reaction rate coefficients given in the form $k = AT^n exp(-E/RT)$. Units are mol cm cal s. Highlighted reactions correspond to those with similar Arrhenius constants for both models. Superscript ^{rev} in [12] corresponds to the reverse reactions constants, as for these reactions, the reactives in [13] correspond to the products in [12], and vice versa.

	Huang et al. [13]			Christensen and Konnov [12]		
Reactions	A	n	E	A	n	E
$CH + O = CO + H$	5.7E13	0.0	0.0E0	4.000E+13	0.0000	0.00
$\mathbf{CH + OH = HCO + H}$	3.0E13	0.0	0.0E0	3.000E+13	0.0000	0.00
$CH_2 + H = CH + H_2$	1.0E18	-1.56	0.0E0	$1.750E{+}14^{rev}$	0.0000^{rev}	3320.00^{rev}
$CH + H_2O = H + CH_2O$	1.713E13	0.0	-7.55E2	1.770E+16	-1.2200	24.00
$CH + O_2 = HCO + O$	3.3E13	0.0	0.0E0	4.800E+12	0.0000	0.00
$CH_2 + O => CO + 2H$	5.0E13	0.0	0.0E0	1.000E+14	0.0000	536.00
$CH_2 + OH = CH + H_2O$	1.13E7	2.0	3.0E3	8.630E+05	2.0190	6776.00
$CH_2 + O_2 = HCO + OH$	1.06E13	0.0	1.5E3	1.650E+12	0.0000	1737.00
$CH_2 + O_2 => CO_2 + 2H$	2.64E12	0.0	1.5E3	8.250E+11	0.0000	1737.00
$CH_3 + O = CH_2O + H$	5.54E13	0.05	-1.36E2	4.432E+13	0.0500	-136.00
$CH_3 + O_2 = CH_3O + O$	7.546E12	0.0	2.832E4	2.110E+13	0.0000	32471.00
$CH_3 + O_2 = CH_2O + OH$	2.641E0	3.283	8.105E3	6.390E+11	0.0000	13515.00
$\mathbf{CH_3 + O_2(+M) = CH_3O_2(+M)}$	7.812E9	0.9	0.0E0	7.810E+09	0.9000	0.00
$\mathbf{CH_3 + HO_2 = CH_3O + OH}$	1.0E12	0.269	-6.875E2	1.000E+12	0.2688	-688.00
$\mathbf{CH_3 + HO_2 = CH_4 + O_2}$	1.16E5	2.23	-3.022E3	1.190E+05	2.2280	-3023.00
$2CH_3 = H + C_2H_5$	2.109E5	2.297	1.215E4	5.400E+13	0.0000	16055.00
$2CH_3(+M) = C_2H_6(+M)$	2.277E15	-0.69	1.749E2	3.610E+13	0.0000	0.00
$CH_3 + H(+M) = CH_4(+M)$	1.27E16	-0.63	3.83E2	2.890E+13	0.1930	-10.00
$\mathbf{CH_4 + H = CH_3 + H_2}$	6.14E5	2.5	9.587E3	6.140E+05	2.5000	9590.00
$CH_4 + O = CH_3 + OH$	1.02E9	1.5	8.6E3	4.400E+05	2.5000	6577.00
$CH_4 + OH = CH_3 + H_2O$	5.83E4	2.6	2.19E3	1.000E+06	2.1800	2462.00
$CH_4 + HO_2 = CH_3 + H_2O_2$	1.695E1	3.74	2.101E4	1.130E+01	3.7400	21000.00
$CO + O(+M) = CO_2(+M)$	1.362E10	0.0	2.384E3	1.060E+13	-0.3080	6943.00
$CO + OH = CO_2 + H$	7.015E4	2.053	-3.557E2	2.230E+05	1.9000	-1160.00
$CO + O_2 = CO_2 + O$	1.119E12	0.0	4.77E4	5.060E+13	0.0000	63189.99
$\mathbf{CO + HO_2 = CO_2 + OH}$	1.57E5	2.18	1.794E4	1.570E+05	2.1800	17940.00
$HCO + M = H + CO + M$	5.7E11	0.66	1.487E4	4.750E+11	0.6600	14870.00
$HCO + H = CO + H_2$	7.34E13	0.0	0.0E0	1.200E+14	0.0000	0.00
$\mathbf{HCO + O = CO + OH}$	3.02E13	0.0	0.0E0	3.000E+13	0.0000	0.00
$\mathbf{HCO + O = CO_2 + H}$	3.0E13	0.0	0.0E0	3.000E+13	0.0000	0.00
$HCO + OH = CO + H_2O$	1.02E14	0.0	0.0E0	1.100E+14	0.0000	0.00
$HCO + O_2 = CO + HO_2$	7.58E12	0.0	4.1E2	6.920E+06	1.9000	-1370.00
$\mathbf{HCO + HO_2 => CO_2 + H + OH}$	3.0E13	0.0	0.0E0	3.000E+13	0.0000	0.00
$HCO + CH_3 = CH_4 + CO$	2.65E13	0.0	0.0E0	1.849E+20	-2.3000	4781.00
$\mathbf{2HCO = CH_2O + CO}$	1.8E13	0.0	0.0E0	1.800E+13	0.0000	0.00
$\mathbf{2HCO => H_2 + 2CO}$	3.0E12	0.0	0.0E0	3.000E+12	0.0000	0.00

Table 6.8: Package 3 (Species CH_2O, CH_3O, CH_2OH, CH_3OH, CH_3O_2, CH_3O_2H). Reaction rate coefficients given in the form $k = AT^n exp(-E/RT)$. Units are mol cm cal s. Highlighted reactions correspond to those with similar Arrhenius constants for both models. Superscript ^{rev} in [12] corresponds to the reverse reactions constants, as for these reactions, the reactives in [13] correspond to the products in [12], and vice versa.

	Huang et al. [13]			Christensen and Konnov [12]		
Reactions	A	n	E	A	n	E
$HCO + H(+M) = CH_2O(+M)$	1.09E12	0.48	-2.6E2	1.260E+36^{rev}	-5.5000^{rev}	93993.99^{rev}
$CO + H_2(+M) = CH_2O(+M)$	4.3E7	1.5	7.96E4	4.400E+38^{rev}	-6.1000^{rev}	93993.99^{rev}
$CH_2O + H = HCO + H_2$	5.74E7	1.9	2.74E3	5.860E+03	3.1300	1514.00
$CH_2O + O = HCO + OH$	6.26E9	1.15	2.26E3	4.160E+11	0.5700	2762.00
$CH_2O + OH = HCO + H_2O$	7.82E7	1.63	-1.055E3	2.390E+07	1.8300	-1117.00
$CH_2O + O_2 = HCO + HO_2$	8.07E15	0.0	5.342E4	2.440E+05	2.5000	36465.00
$CH_2O + HO_2 = HCO + H_2O_2$	1.88E4	2.7	1.152E4	4.100E+04	2.5000	10210.00
$CH + CH_2O = H + CH_2CO$	9.46E13	0.0	-5.15E2	1.460E+16	-0.8000	-81.80
$CH_2O + CH_3 = HCO + CH_4$	3.83E1	3.36	4.312E3	3.190E+01	3.3600	4312.00
$CH_3O(+M) = CH_2O + H(+M)$	6.8E13	0.0	2.617E4 3+6	1.130E+10	1.2100	24085.00
$CH_3O + H = CH_2O + H_2$	2.0E13	0.0	0.0E0	3.780E+13	0.0000	596.00
$CH_3O + O_2 = CH_2O + HO_2$	4.38E-19	9.5	-5.501E3	2.290E+03	2.4000	413.00
$CH_3O + CH_3 = CH_2O + CH_4$	1.2E13	0.0	0.0E0	2.410E+13	0.0000	0.00
$CH_2O + CH_3O = CH_3OH + HCO$	6.62E11	0.0	2.294E3	6.600E+11	0.0000	2300.00
$2CH_3O = CH_3OH + CH_2O$	6.03E13	0.0	0.0E0	7.800E+12	0.0000	0.00
$CH_2O + H(+M) = CH_2OH(+M)$	5.4E11	0.454	3.6E3	7.370E+10^{rev}	0.8110^{rev}	39585.00^{rev}
$CH_2OH + H = CH_2O + H_2$	6.0E12	0.0	0.0E0	3.000E+13	0.0000	0.00
$O + CH_2OH = OH + CH_2O$	4.2E13	0.0	0.0E0	6.560E+12	0.0000	-693.00
$OH + CH_2OH = H_2O + CH_2O$	2.4E13	0.0	0.0E0	2.400E+13	0.0000	0.00
$CH_2OH + HO_2 = CH_2O + H_2O_2$	1.2E13	0.0	0.0E0	6.300E+11	0.2800	-813.00
$CH_2OH + HO_2 = CH_2O + H_2O_2$	1.2E13	0.0	0.0E0	6.800E+11	0.2100	-454.00
$CH_2OH + HCO = 2CH_2O$	1.8E14	0.0	0.0E0	1.500E+13	0.0000	0.00
$CH_3OH + HCO = CH_2OH + CH_2O$	9.63E3	2.9	1.311E4	5.480E+03^{rev}	2.8100^{rev}	5862.00^{rev}
$CH_2OH + CH_3O = CH_2O + CH_3OH$	2.4E13	0.0	0.0E0	2.400E+13	0.0000	0.00
$2CH_2OH = CH_2O + CH_3OH$	3.0E12	0.0	0.0E0	9.000E+12	0.0000	0.00
$CH_3OH(+M) = CH_3 + OH(+M)$	2.084E18	-0.615	9.254E4	2.080E+18	-0.6148	92549.99
$CH_3OH(+M) = CH_2OH + H(+M)$	7.896E-3	5.038	8.447E4	7.900E-03	5.0380	84475.99
$CH_3OH + H = CH_2OH + H_2$	3.07E5	2.55	5.44E3	3.040E+14	-0.1690	7796.00
$CH_3OH + H = CH_3O + H_2$	1.99E5	2.56	1.03E4	7.470E+14	-0.4010	12774.00
$CH_3OH + O = CH_2OH + OH$	3.88E5	2.5	3.08E3	5.300E+04	2.6100	1870.00
$CH_3OH + OH = CH_2OH + H_2O$	3.08E4	2.65	-8.067E2	5.140E+04	2.6200	-682.00
$CH_3OH + OH = CH_3O + H_2O$	1.5E2	3.03	-7.63E2	5.710E+03	2.6200	-682.00
$CH_3OH + O_2 = CH_2OH + HO_2$	2.05E13	0.0	4.49E4	3.580E+05	2.2700	42764.00
$CH_3OH + HO_2 = CH_2OH + H_2O_2$	1.08E4	2.55	1.053E4	3.500E-04	4.8500	10134.00
$CH_3OH + CH_3 = CH_2OH + CH_4$	3.19E1	3.17	7.172E3	7.100E+00	3.4800	7055.00
$CH_3 + CH_3OH = CH_4 + CH_3O$	1.44E1	3.1	6.935E3	4.290E+02	2.6400	7101.00
$CH_3O + CH_3OH = CH_2OH + CH_3OH$	3.0E11	0.0	4.074E3	3.000E+11	0.0000	4070.00
$CH + CO_2 = HCO + CO$	1.7E12	0.0	6.85E2	6.360E+07	1.5100	-715.00
$CH_3O_2 + H = CH_3O + OH$	9.6E13	0.0	0.0E0	9.600E+13	0.0000	0.00
$CH_3O_2 + O = CH_3O + O_2$	3.6E13	0.0	0.0E0	2.600E+13	0.0000	0.00
$CH_3O_2 + OH = CH_3OH + O_2$	6.0E13	0.0	0.0E0	6.000E+13	0.0000	0.00
$CH_3O_2 + HO_2 = CH_3O_2H + O_2$	2.47E11	0.0	-1.57E3	2.530E+11	0.0000	-1490.00
$CH_3O_2 + CH_3 = 2CH_3O$	5.08E12	0.0	-1.411E3	5.000E+12	0.0000	-1410.00
$CH_4 + CH_3O_2 = CH_3 + CH_3O_2H$	9.6E-1	3.77	1.781E4	1.210E+01	3.7500	21200.00
$CH_3O_2 + CH_2O = CH_3O_2H + HCO$	1.99E12	0.0	1.166E4	2.000E+12	0.0000	11660.00
$CH_3OH + CH_3O_2 = CH_2OH + CH_3O_2H$	1.81E12	0.0	1.371E4	1.810E+11	0.0000	13700.00
$2CH_3O_2 => CH_2O + CH_3OH + O_2$	3.11E14	-1.61	-1.051E3	2.240E+15	-1.8700	-541.00
$2CH_3O_2 => O_2 + 2CH_3O$	1.4E16	-1.61	1.86E3	5.870E+16	-1.8700	1700.00
$H_2 + CH_3O_2 = H + CH_3O_2H$	1.5E14	0.0	2.603E4	8.790E+10^{rev}	0.0000^{rev}	1860.00^{rev}

Table 6.9: Package 4 (Species C_2H, C_2H_2, C_2H_3, C_2H_4, C_2H_5, C_2H_6). Reaction rate coefficients given in the form $k = AT^n exp(-E/RT)$. Units are mol cm cal s. Highlighted reactions correspond to those with similar Arrhenius constants for both models. Superscript ^{rev} in [12] corresponds to the reverse reactions constants, as for these reactions, the reactives in [13] correspond to the products in [12], and vice versa.

	Huang et al. [13]			Christensen and Konnov [12]		
Reactions	A	n	E	A	n	E
$H_2 + C_2H <=> C_2H_2 + H$	0.1080E+14	0.0000	0.2165E+04	2.100E+06	2.3200	880.00
$\mathbf{C_2H + OH <=> CH_2 + CO}$	0.1810E+14	0.0000	0.0000E+00	1.800E+13	0.0000	0.00
$C_2H_2 + O = CH_2 + CO$	7.395E8	1.28	2.472E3	2.350E+08	1.4000	2200.00
$C_2H_2 + O = HCCO + H$	2.958E9	1.28	2.472E3	9.400E+08	1.4000	2200.00
$C_2H_2 + OH = CH_3 + CO$	1.00E7	1.432	4.315E3	1.280E+09	0.7300	2579.00
$C_2H_2 + OH <=> C_2H + H_2O$	0.6000E+14	0.0000	0.1292E+05	2.630E+06	2.1400	17060.00
$C_2H_2 + OH = CH_2CO + H$	1.50E5	2.132	4.048E3	7.530E+06	1.5500	2106.00
$\mathbf{C_2H_2 + CH_2 <=> C_3H_3 + H}$	0.1200E+14	0.0000	0.6577E+04	1.200E+13	0.0000	6620.00
$C_2H_2 + H(+M) = C_2H_3(+M)$	1.71E10	1.266	2.709E3	3.860E+08^{rev}	1.6200^{rev}	37060.00^{rev}
$\mathbf{C_2H_3 + H(+M) = C_2H_4(+M)}$	6.08E12	0.27	2.8E2	6.080E+12	0.2700	280.00
$C_2H_3 + H = C_2H_2 + H_2$	9.0E13	0.0	0.0E0	4.200E+13	0.0000	0.00
$\mathbf{C_2H_3 + OH = C_2H_2 + H_2O}$	3.011E13	0.0	0.0E0	3.000E+13	0.0000	0.00
$C_2H_3 + O_2 <=> C_2H_2 + HO_2$	0.1120E+15	-0.8330	0.2541E+04	5.190E+15	-1.2600	3310.00
$C_2H_3 + O_2 <=> C_2H_2 + HO_2$	0.1120E+15	-0.8330	0.2541E+04	2.120E-06	6.0000	9484.00
$C_2H_3 + O_2 = CH_2O + HCO$	1.7E29	-5.312	6.503E3	4.150E+12	0.0000	-240.00
$\mathbf{CH_3 + C_2H_3 = C_3H_5 + H}$	1.5E24	-2.83	1.861855E4	1.500E+24	-2.8300	18618.00
$\mathbf{C_2H_3 + CH_2O <=> C_2H_4 + HCO}$	0.5420E+04	2.8100	0.5824E+04	5.420E+03	2.8100	5862.00
$C_2H_4 + CH_3O = C_2H_3 + CH_3OH$	1.2E11	0.0	6.75E3	1.440E+01^{rev}	3.1000^{rev}	6940.00^{rev}
$C_2H + C_2H_3 <=> 2C_2H_2$	0.1900E+14	0.0000	0.0000E+00	3.000E+13	0.0000	0.00
$2C_2H_3 = C_2H_2 + C_2H_4$	9.6E11	0.0	0.0E0	1.450E+13	0.0000	0.00
$C_2H_4 + H = C_2H_3 + H_2$	5.07E7	1.93	1.295E4	2.340E+02	3.6200	11270.00
$C_2H_4 + O = CH_3 + HCO$	7.453E6	1.88	1.83E2	8.100E+06	1.8800	180.00
$C_2H_4 + OH = CH_2O + CH_3$	5.00E+11	0.0	960.	1.780E+05	1.6800	2061.00
$C_2H_4 + OH = C_2H_3 + H_2O$	2.23E4	2.745	2.216E3	1.310E-01	4.2000	-860.00
$\mathbf{C_2H_4 + O_2 = C_2H_3 + HO_2}$	4.22E13	0.0	5.762E4	4.220E+13	0.0000	57629.99
$C_2H_3 + H_2O_2 <=> C_2H_4 + HO_2$	0.1210E+11	0.0000	-.5901E+03	4.800E+04^{rev}	2.5000^{rev}	27620.00^{rev}
$C_2H_4 + CH_3 = C_2H_3 + CH_4$	6.62E0	3.7	9.5E3	6.000E+07	1.5600	16630.00
$C_2H_4 + CH_3O_2 = C_2H_3 + CH_3O_2H$	8.59E0	3.754	2.713E4	1.000E+13	0.0000	25000.00
$\mathbf{2C_2H_4 = C_2H_5 + C_2H_3}$	4.82E14	0.0	7.153E4	4.820E+14	0.0000	71539.99
$C_2H_4 + H(+M) = C_2H_5(+M)$	9.569E8	1.463	1.355E3	1.110E+10^{rev}	1.0370^{rev}	36767.00^{rev}
$C_2H_5 + H = C_2H_4 + H_2$	2.0E12	0.0	0.0E0	1.700E+12	0.0000	0.00
$C_2H_5 + O_2 = C_2H_4 + HO_2$	7.561E14	-1.01	4.749E3	2.560E+19	-2.7700	1980.00
$CH_3 + C_2H_5 = CH_4 + C_2H_4$	1.18E4	2.45	-2.921E3	9.000E+11	0.0000	0.00
$C_2H_6 + CH_3O = C_2H_5 + CH_3OH$	2.41E11	0.0	7.09E3	1.440E+01^{rev}	3.1000^{rev}	8942.00^{rev}
$C_2H_5 + H(+M) = C_2H_6(+M)$	5.21E17	-0.99	1.58E3	8.850E+20^{rev}	-1.2280^{rev}	102209.99^{rev}
$C_2H_6 + H = C_2H_5 + H_2$	1.15E8	1.9	7.53E3	1.400E+09	1.5000	7400.00
$\mathbf{C_2H_6 + O = C_2H_5 + OH}$	3.55E6	2.4	5.83E3	3.550E+06	2.4000	5830.00
$C_2H_6 + OH = C_2H_5 + H_2O$	1.48E7	1.9	9.5E2	7.200E+06	2.0000	870.00
$C_2H_6 + O_2 = C_2H_5 + HO_2$	6.03E13	0.0	5.187E4	7.260E+05	2.5000	49159.99
$C_2H_6 + HO_2 = C_2H_5 + H_2O_2$	3.46E1	3.61	1.692E4	7.080E+04	2.5000	16850.00
$C_2H_6 + CH_3 = C_2H_5 + CH_4$	5.48E-1	4.0	8.28E3	5.600E+10	0.0000	9420.00
$C_2H_6 + CH_3 = C_2H_5 + CH_4$	5.48E-1	4.0	8.28E3	8.400E+14	0.0000	22250.00
$C_2H_6 + CH_3O_2 = C_2H_5 + CH_3O_2H$	1.94E1	3.64	1.71E4	2.950E+11	0.0000	14940.00

Table 6.10: Package 5 (Species $HCCO$, CH_2CO, CH_3CO, C_3H_2, C_3H_3, C_3H_5, C_3H_6, NC_3H_7, C_2H_3CO, CH_3COCH_3). Reaction rate coefficients given in the form $k = AT^n exp(-E/RT)$. Units are mol cm cal s. Highlighted reactions correspond to those with similar Arrhenius constants for both models. Superscript ^{rev} in [12] corresponds to the reverse reactions constants, as for these reactions, the reactives in [13] correspond to the products in [12], and vice versa.

	Huang et al. [13]			Christensen and Konnov [12]		
Reactions	A	n	E	A	n	E
$HCCO + O => H + 2CO$	8.0E13	0.0	0.0E0	1.000E+14	0.0000	0.00
$\mathbf{HCCO + O_2 => CO_2 + CO + H}$	4.78E12	-0.142	1.15E3	4.760E+12	-0.1420	1150.00
$\mathbf{HCCO + O_2 => OH + 2CO}$	1.91E11	-0.02	1.02E3	1.900E+11	-0.0200	1023.00
$\mathbf{CH + HCCO = CO + C_2H_2}$	5.0E13	0.0	0.0E0	5.000E+13	0.0000	0.00
$CH_2 + CO(+M) = CH_2CO(+M)$	8.1E11	0.0	0.0E0	3.000E+14	0.0000	70999.99
$CH_2CO + H = CH_3 + CO$	7.704E13	-0.171	4.183E3	7.770E+08	1.4500	2780.00
$CH_2CO + H = HCCO + H_2$	1.401E15	-0.171	8.783E3	1.000E+14	0.0000	12300.00
$CH_2CO + O = HCCO + OH$	1.0E13	0.0	8.0E3	1.870E+14	0.0000	16690.00
$CH_2CO + O = CH_2 + CO_2$	1.75E12	0.0	1.35E3	1.080E+12	0.0000	1350.00
$CH_2CO + OH = CH_2OH + CO$	2.0E12	0.0	-1.01E3	2.640E+12	0.0000	-550.00
$CH_2CO + OH = HCCO + H_2O$	1.0E13	0.0	2.0E3	1.780E+13	0.0000	5840.00
$CH_2CO + CH_3 = C_2H_5 + CO$	4.769E4	2.312	9.468E3	2.400E+12	0.0000	8000.00
$CH_3CO + H = CH_2CO + H_2$	2.0E13	0.0	0.0E0	1.150E+13	0.0000	0.00
$\mathbf{CH_3CO + H <=> CH_3 + HCO}$	0.2100E+14	0.0000	0.0000E+00	2.150E+13	0.0000	0.00
$CH_3CO + O = CH_2CO + OH$	2.0E13	0.0	0.0E0	5.250E+13	0.0000	0.00
$CH_3CO + OH <=> CH_2CO + H_2O$	0.1200E+14	0.0000	0.0000E+00	2.800E+13	0.0000	0.00
$CH_3CO + CH_3 = CH_2CO + CH_4$	5.0E13	0.0	0.0E0	6.100E+12	0.0000	0.00
$CH_3COCH_3 = CH_3CO + CH_3$	5.113E30	-4.194	8.978E4	4.040E+15	-0.8000	0.00
$C_3H_2 + O <=> C_2H + H + CO$	0.6800E+14	0.0000	0.0000E+00	3.000E+13	0.0000	0.00
$C_3H_3 + O <=> C_2H_2 + CO + H$	0.1390E+15	0.0000	0.0000E+00	7.000E+13	0.0000	0.00
$C_3H_3 + O <=> CH_2O + C_2H$	0.1400E+15	0.0000	0.0000E+00	2.000E+13	0.0000	0.00
$C_3H_3 + OH <=> HCO + C_2H_3$	0.4000E+14	0.0000	0.0000E+00	1.330E+13	0.0000	0.00
$\mathbf{C_3H_3 + O_2 = CH_2CO + HCO}$	3.0E10	0.0	2.86807E3	3.010E+10	0.0000	2870.00
$\mathbf{C_3H_3 + HO_2 = OH + CO + C_2H_3}$	8.0E11	0.0	0.0E0	8.000E+11	0.0000	0.00
$\mathbf{C_3H_5 + H(+M) = C_3H_6(+M)}$	2.0E14	0.0	0.0E0	2.000E+14	0.0000	0.00
$C_3H_6 + H = C_3H_5 + H_2$	1.7E5	2.5	2.49283E3	6.457E+12	0.0000	4445.00
$C_3H_6 + H = C_2H_4 + CH_3$	1.6E22	-2.39	1.118547E4	2.600E+08	1.5000	2000.00
$C_3H_6 + O = C_2H_5 + HCO$	3.5E7	1.65	-9.7275E2	6.833E+06	1.5700	-628.00
$\mathbf{C_3H_6 + OH = C_3H_5 + H_2O}$	3.1E6	2.0	-2.9828E2	3.120E+06	2.0000	-300.00
$C_3H_5 + HO_2 = C_3H_6 + O_2$	2.66E12	0.0	0.0E0	1.080E+04	2.5000	35730.00
$NC_3H7 = CH_3 + C_2H_4$	2.284E14	-0.55	2.84E4	1.260E+13	0.0000	30404.00
$\mathbf{NC_3H7 + H = C_2H_5 + CH_3}$	3.7E24	-2.92	1.25E4	3.700E+24	-2.9200	12505.00
$\mathbf{NC_3H7 + OH = C_3H_6 + H_2O}$	2.4E13	0.0	0.0E0	2.400E+13	0.0000	0.00
$NC_3H7 + O_2 = C_3H_6 + HO_2$	1.71E42	-9.211	1.979E4	1.000E+12	0.0000	5000.00
$C_2H_3CO = C_2H_3 + CO$	1.37E21	-2.179	3.941E4	2.000E+13	0.0000	28700.00

Table 6.11: Reaction packages, see Tabs. 6.6 to 6.10 for reactions.

Package	Number of reactions	Number of species	Species concerned by reactions
I	18	4	H_2, H_2O, HO_2, H_2O_2
II	36	7	CO, CO_2, HCO, CH, CH_2, CH_3, CH_4
III	49	6	CH_2O, CH_3O, CH_2OH, CH_3OH, CH_3O_2, CH_3O_2H
IV	43	6	C_2H, C_2H_2, C_2H_3, C_2H_4, C_2H_5, C_2H_6
V	35	10	$HCCO$, CH_2CO, CH_3CO, C_3H_2, C_3H_3, C_3H_5, C_3H_6, nC_3H_7, C_2H_3CO, CH_3COCH_3

Table 6.12: Combined models h: Common reactions constants from Huang et al. [13], C: Common reactions constants from Christensen and Konnov [12]

	Package				
Model	I	II	III	IV	V
A	h	h	h	h	h
B	C	h	h	h	h
C	h	C	h	h	h
D	h	h	C	h	h
E	h	h	h	C	h
F	h	h	h	h	C
G	C	C	C	C	C
H	h	C	C	C	C
I	C	h	C	C	C
J	C	C	h	C	C
K	C	C	C	h	C
L	C	C	C	C	h

6.5.1 Chemical mechanism validations

6.5.1.1 Auto-ignition delay Simulations, comparison to the original schemes

Auto-ignition delays estimated as a function of initial temperature ($1000/T_0 = 0.5$ to 1.42) for different equivalence ratios ($\phi = 0.5, 1.0$ and 1.5) and pressures (1, 10 and 100 bar) are presented for toluene/air in Figs. 6.3-6.4, ethanol/air in Figs. 6.5-6.6 and acetic-acid/air in Figs. 6.7-6.8.

Results are presented for models A through L. In Figs. 6.3-6.4, results are compared to those obtained using the original scheme of Huang et al. [13], while in Figs. 6.5-6.8 they are compared to those obtained using the original scheme of Christensen and Konnov [12]. These results show that the merging procedure has insignificant impact on the ignition delay of toluene/air, ethanol/air and acetic-acid/air mixtures, as all developed A-L combined mechanisms reproduce very well the ignition delays calculated using the original models.

6.5.1.2 Laminar Flame Speed Simulations, comparison to the original schemes and experimental data

We have observed that the combined models give very good results concerning auto-ignition delays in comparison to those of the original models. However, as we will see below, some differences were observed in laminar flame speed results. Therefore, in order to make a comprehensive validation of the combined model, we have focused on toluene, ethanol and acetic-acid experimental data related to flame speeds.

Pure toluene/air, ethanol/air and acetic-acid/air flame speeds estimated at 1 bar as a function of equivalence ratio using new combined Schemes A-L are presented in Figs. 6.9 and 6.10.

Results obtained using the original scheme due to Huang et al. [13] as well as experimental data from Dirrenberger et al. [24] are used to validate results obtained using the combined scheme for toluene/air (Figs. (a)). Results for ethanol (Figs. (b)) are compared to those obtained using the original scheme due to Christensen and Konnov [12] and to experimental data from Konnov [25], van Lipzig et al. [26] and Dirrenberger et al. [24]. Finally, results for acetic-acid (Figs. (c)) are compared to those obtained using the original scheme due to Christensen and Konnov [12] and to experimental data from Christensen and Konnov [12].

One can see that for toluene (Figs. 6.9(a) and 6.10(a)), the predictions of the original Huang et al. [13] model flame speeds are very good by most of combined models, and they are all very close to the experimental results of Dirrenberger [24]. However, for ethanol (Figs. 6.9(b) and 6.10(b)) and acetic-acid (Figs. 6.9(c) and 6.10(c)), larger discrepancies are observed between the results of the original Chris-

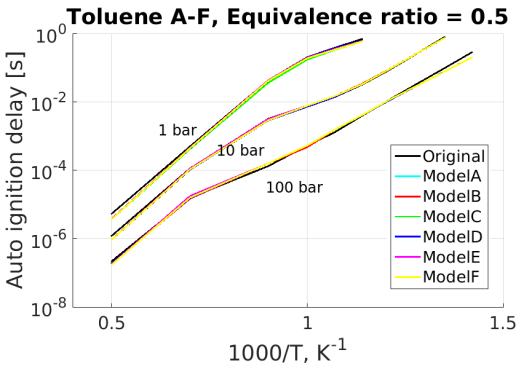

(a) Equivalence ratio=0.5

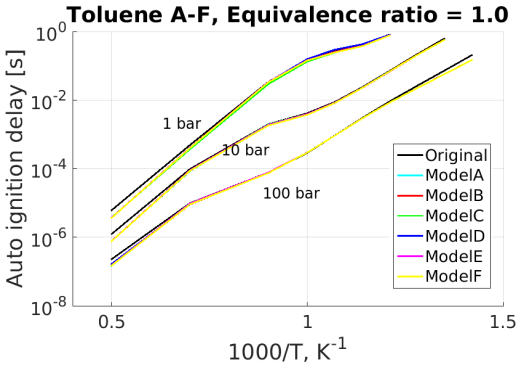

(b) Equivalence ratio=1.0

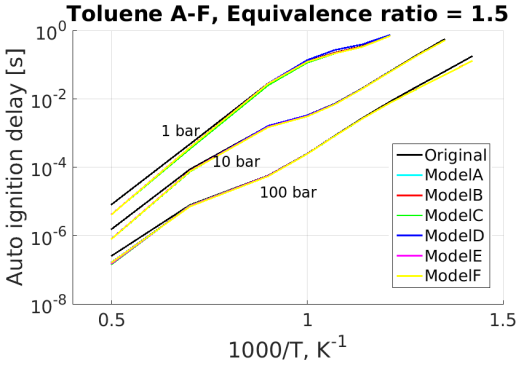

(c) Equivalence ratio=1.5

Figure 6.3: Toluene/air auto-ignition delay as a function and temperature, for different pressures and equivalence ratios, using the original scheme of [13] and the new combined Schemes $A - F$.

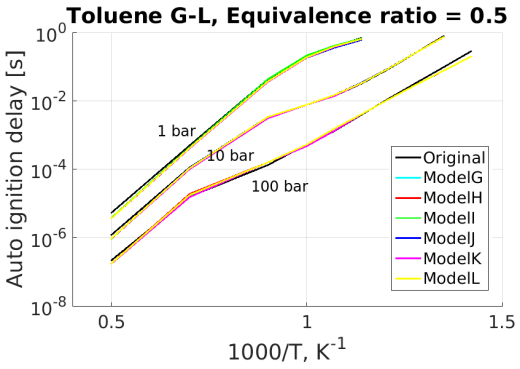

(a) Equivalence ratio=0.5

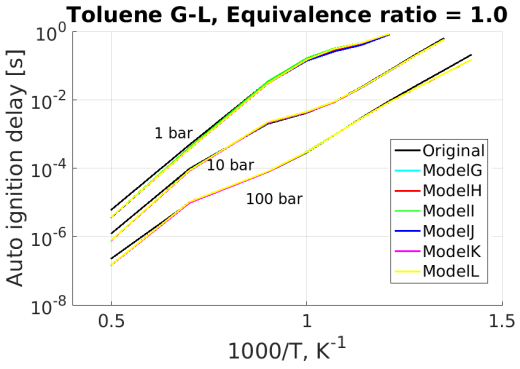

(b) Equivalence ratio=1.0

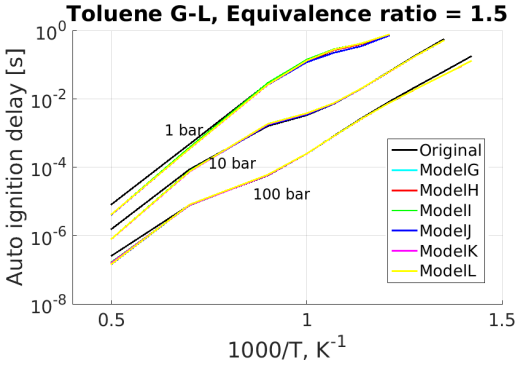

(c) Equivalence ratio=1.5

Figure 6.4: Toluene/air auto-ignition delay as a function and temperature, for different pressures and equivalence ratios, using the original scheme of Huang et al. [13] and the new combined Schemes $G - L$.

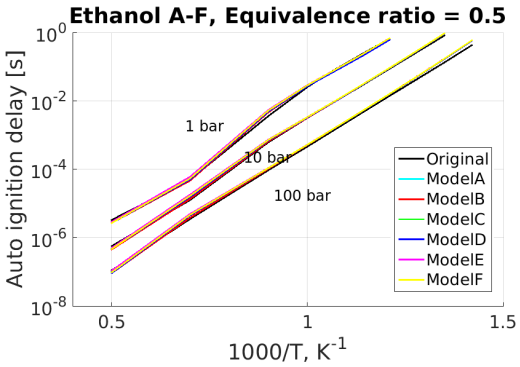

(a) Equivalence ratio=0.5

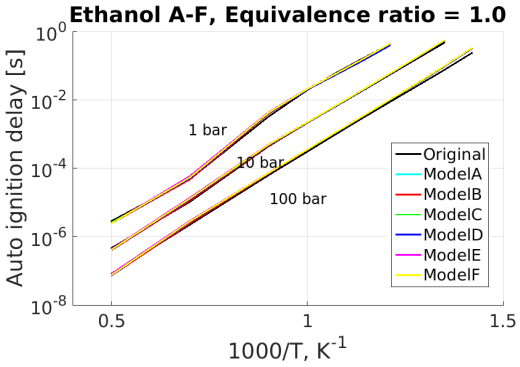

(b) Equivalence ratio=1.0

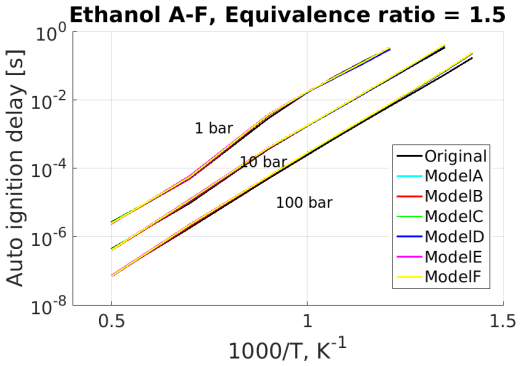

(c) Equivalence ratio=1.5

Figure 6.5: Ethanol/air auto-ignition delay as a function and temperature, for different pressures and equivalence ratios, using the original scheme of Christensen and Konnov [12] and the new combined Schemes $A - F$.

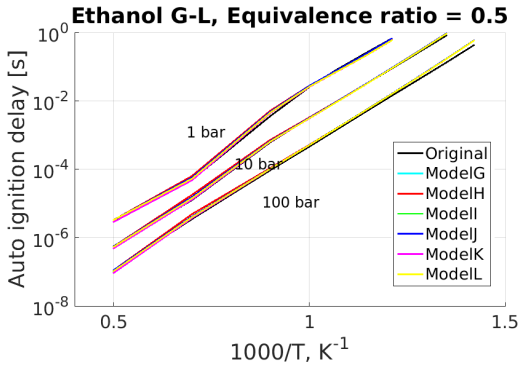

(a) Equivalence ratio=0.5

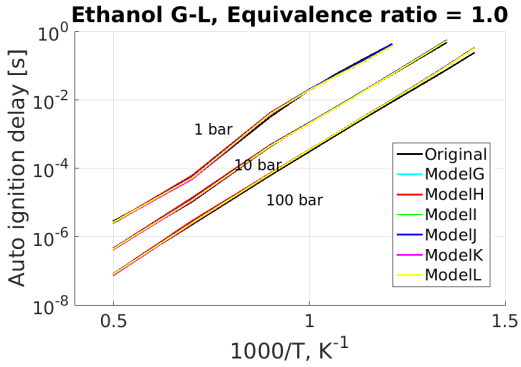

(b) Equivalence ratio=1.0

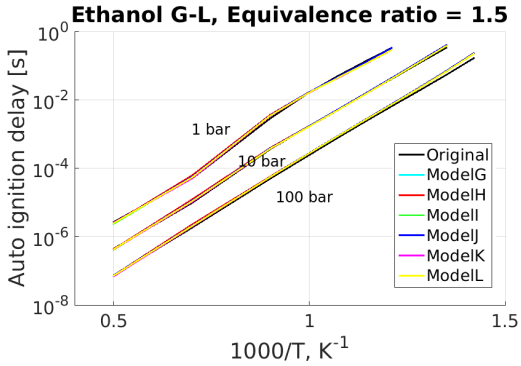

(c) Equivalence ratio=1.5

Figure 6.6: Ethanol/air auto-ignition delay as a function and temperature, for different pressures and equivalence ratios, using the original scheme of Christensen and Konnov [12] and the new combined Schemes $G - L$.

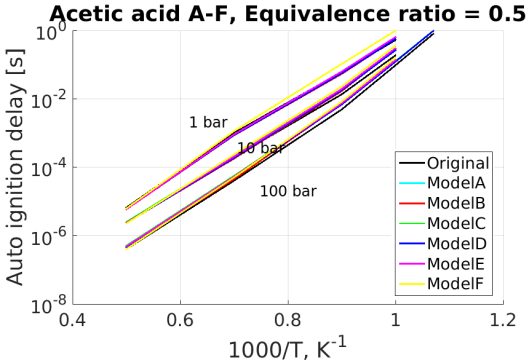

(a) Equivalence ratio=0.5

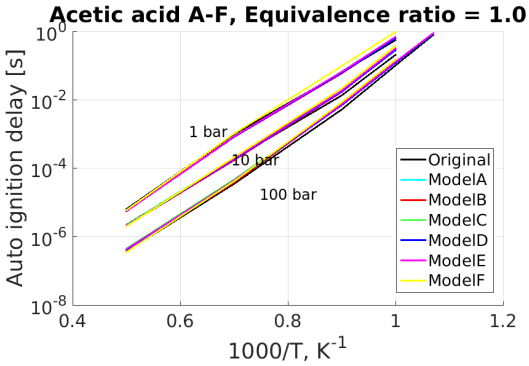

(b) Equivalence ratio=1.0

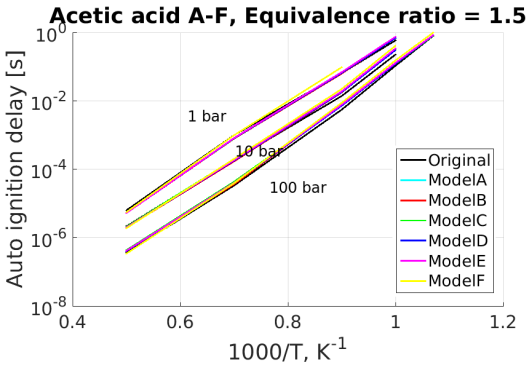

(c) Equivalence ratio=1.5

Figure 6.7: Acetic acid/air auto-ignition delay as a function and temperature, for different pressures and equivalence ratios, using the original scheme of Christensen and Konnov [12] and the new combined Schemes $A - F$.

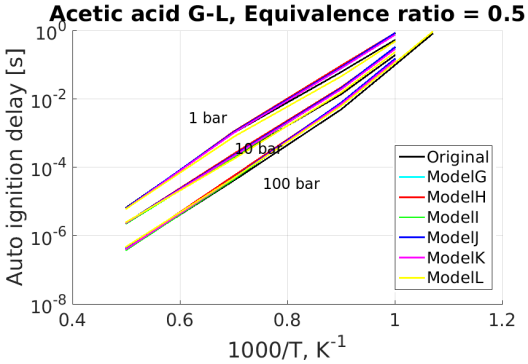

(a) Equivalence ratio=0.5

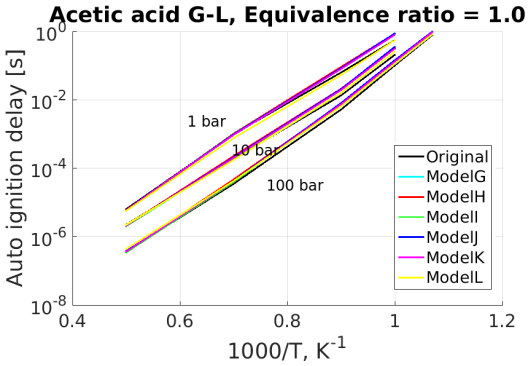

(b) Equivalence ratio=1.0

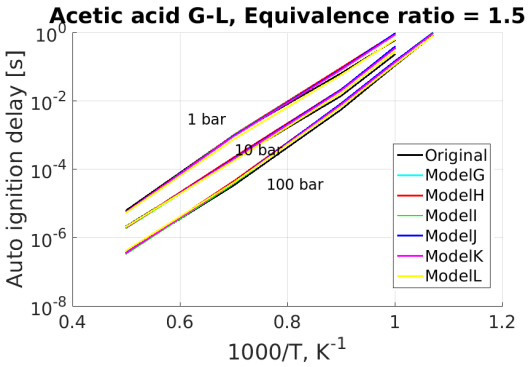

(c) Equivalence ratio=1.5

Figure 6.8: Acetic acid/air auto-ignition delay as a function and temperature, for different pressures and equivalence ratios, using the original scheme of Christensen and Konnov [12] and the new combined Schemes $G - L$.

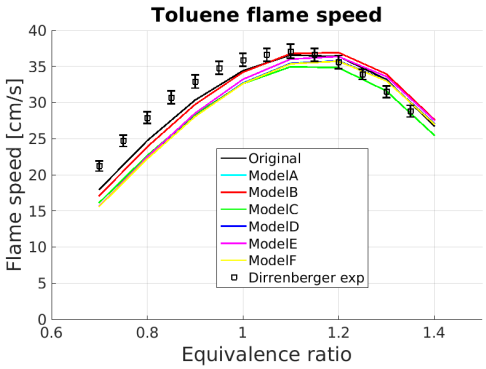

(a) Toluene/air

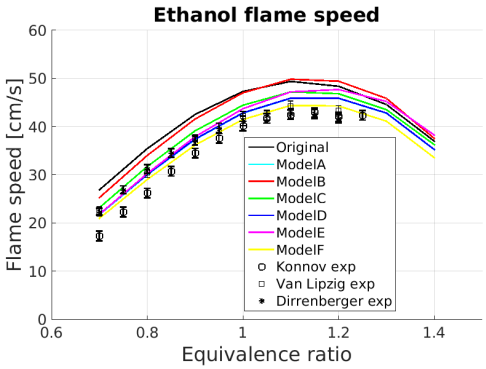

(b) Ethanol/air

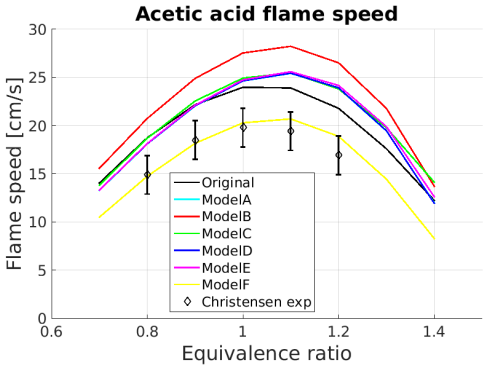

(c) Acetic acid/air

Figure 6.9: (a) Toluene/air, (b) Ethanol/air and (c) Acetic acid/air laminar flame speeds as a function of equivalence ratio at 1 bar, using new combined Schemes $A - F$. The original schemes are due to [13] (a) and [12] ((b) and (c)). Results of (a) are compared to experimental data due to [24] at $T = 298$ K; whereas those of (b) are compared to experimental data due to [25, 26 and 24] at $T = 300$ K; and those of (c) are compared to experimental data due to [12] at $T = 338$ K.

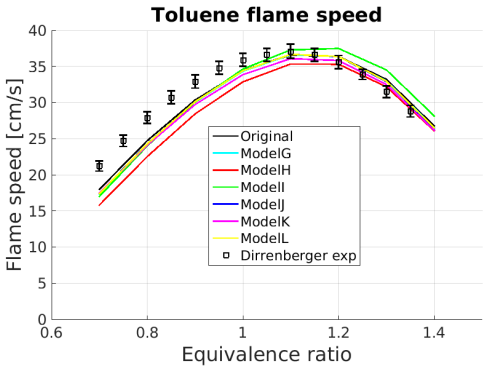

(a) Toluene/air

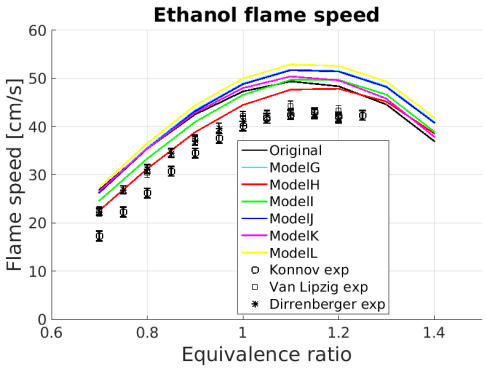

(b) Ethanol/air

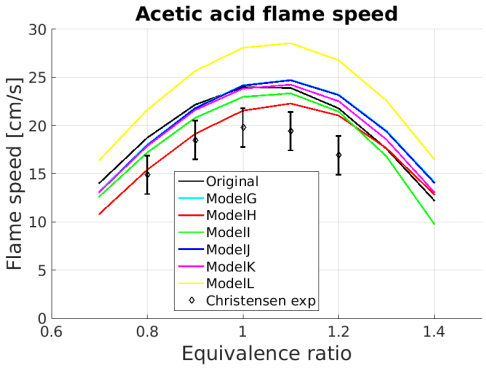

(c) Acetic acid/air

Figure 6.10: (a) Toluene/air, (b) Ethanol/air and (c) Acetic acid/air laminar flame speeds as a function of equivalence ratio at 1 bar, using new combined Schemes $G - L$. The original schemes are due to [13] (a) and [12] ((b) and (c)). Results of (a) are compared to experimental data due to [24] at $T = 298$ K; whereas those of (b) are compared to experimental data due to [25, 26 and 24] at $T = 300$ K; and those of (c) are compared to experimental data due to [12] at $T = 338$ K.

tensen and Konnov [12] model and the combined models. This can be explained by the fact that laminar flame speeds are sensitive to the small hydrocarbon chemistry part of the model: the small hydrocarbon chemistry in the ethanol and acetic-acid model was modified with that of the toluene model during the merging process. Moreover, concerning the experimental results of Konnov et al. [25], van Lipzig et al. [26] and Dirrenberger et al. [24] (ethanol) and Christensen and Konnov [12] (acetic-acid), the original model of Christensen and Konnov [12] sligthly overestimates both experimental data, however as it can be seen several developed combined models are closer to both ethanol and acetic-acid experimental results.

For instance, models C, D and especially F give a very good prediction of ethanol experimental data, whereas once again model F gives an excellent prediction of acetic acid experimental results. Although it is possible that the E model fits better than the C model in proportions less than 1.1, the difference is minimal and we consider those that give better results in general (in the entire equivalence ratio of the analysis).

In the present work, we will focus on the validation of the developed combined models with respect to the original schemes of Huang et al. [13] and Christensen and Konnov [12], therefore in order to quantify how much close are the combined schemes flame speed results to the original scheme results, we have estimated standard deviations of all results relatively to the original schemes, in Tab. 6.13.

Table 6.13: Standard deviation of laminar flame speed obtained using schemes A through L, with respect to the original schemes of Huang et al. [13] (toluene) and Christensen and konnov [12] (ethanol and acetic acid).

Models	Toluene	Ethanol	Acetic acid
A	1.60	4.01	**1.20**
B	0.67	**1.05**	3.30
C	1.73	2.65	1.41
D	1.64	3.94	1.22
E	1.43	3.43	1.38
F	1.67	5.19	3.58
G	**0.33**	2.51	**1.20**
H	1.57	2.81	2.23
I	0.94	**1.66**	1.33
J	**0.32**	2.40	**1.16**
K	**0.59**	**0.83**	**0.73**
L	**0.31**	3.35	4.08

In this Table, one can see that for toluene, ethanol and acetic acid, models G-L, i.e. most packages of common reactions from Christensen and Konnov [12] (see Tab. 6.12), give slightly better results than models A-F, i.e. most packages of common reactions from Huang et al. [13]. Also, this table shows that globally the prediction of toluene flame speeds are better estimated than those of ethanol and acetic acid with respect to the original scheme of Huang et al. [13] or Christensen and Konnov [12]

respectively. In conclusion, from Figs. 6.9 and 6.10 and Tab. 6.13 it can be seen that toluene, ethanol and acetic acid flame speeds were impacted by the combination procedure, and that they are very sensitive to the common reactions Arrhenius constants, and therefore justifying the analysis of packages I-V (Tab. 6.11).

On the first column of Tab. 6.13 corresponding to toluene, we note that the standard deviation of the results obtained using model L is the smallest, followed very closely by those of scheme J, G and K (in bold). In addition, on the second column corresponding to ethanol, we note that the standard deviation of the results obtained using model K is the smallest, followed by those of scheme B and I (in bold). Finally, on the third column corresponding to acetic acid, we note that the standard deviation of the results obtained using model K is once again the smallest, followed by those of scheme J, A and G (in bold). Therefore, taking into account flame speed standard deviations for all 3 fuels, scheme K is considered as the best (3 fuels standard deviation values in bold), and consequently closest to the original schemes flame speeds.

Now, by comparing the results of Figs. 6.3-6.8 and 6.9-6.10 we attempt to choose one single model giving good results for both auto-ignition delay and flame speed parameters. As explained before, considering auto-ignition delay standard deviations, all combined schemes reproduce very well the auto-ignition delays obtained by the original schemes, whereas concerning laminar flame speeds scheme K (Package I-III and V from Christensen and Konnov [12] and Package IV from Huang et al. [13], see Tab. 6.11) is considered as the best, showing that the reactions pathways of the package IV of species C_2H, C_2H_2, C_2H_3, C_2H_4, C_2H_5 and C_2H_6 are very important in the estimation of these fuels flame speeds. Therefore, the developed combined model K has been chosen to carry out the simulations of bio-oil surrogates.

6.5.2 Bio-oil surrogates simulations

6.5.2.1 Auto-ignition delay simulations

Using combined model K, auto-ignition delays for bio-oil surrogates/air estimated as a function of temperature ($1000/T_0 = 0.5$ to 1.42) for different equivalence ratios ($\phi = 0.5, 1.0$ and 1.5) and pressures (1, 10 and 100 bar) are presented in Fig. 6.11.

As described in Sec. 6.2.4, three different mixtures of toluene, ethanol and acetic acid (Surrogates I, II and III) have been chosen as bio-oil surrogates (see Tab. 6.3). In this figure, toluene auto-ignition delay results were taken as a reference, as toluene is the major component in the surrogates.

In this figure, it can be seen that bio-oil surrogates auto-ignition delays are very close to each other and to those of toluene for $\phi = 0.5 - 1.5$ and pressures 1-100 bar, from a temperature of 1250 K ($1000/T_0 = 0.8$) to 2000 K ($1000/T_0 = 0.5$), and then larger differences are observed between these fuels results for temperatures between 700 K ($1000/T_0 = 1.42$) and 1250 K, as bio-oil surrogates delays are lower than the corresponding values found for toluene.

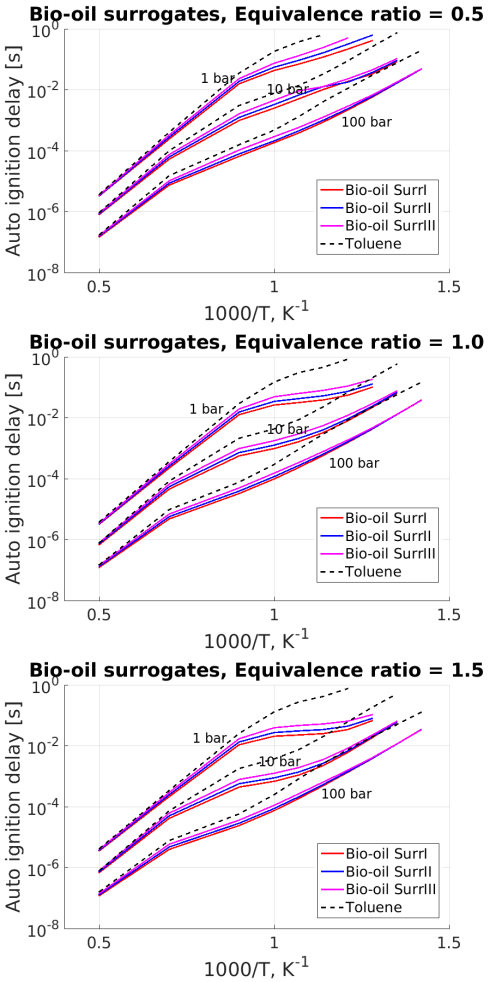

Figure 6.11: Bio-oil surrogates/air and toluene/air auto-ignition delay as a function and temperature, for different pressures and equivalence ratios, using the new combined Scheme K.

Furthermore, in this last range, delays of bio-oil surrI (0.4 % ethanol, 0.2 % acetic-acid and 0.4 % toluene (vol)) are lower than those of SurrII (0.3 % ethanol, 0.3 % acetic-acid and 0.4 % toluene) and they are both lower than those of SurrIII (0.2 % ethanol, 0.4 % acetic-acid and 0.4 % toluene), showing that as ethanol mole fraction increases (and acetic-acid's decreases) in the surrogate, auto-ignition delays of the mixture decreases.

In order to properly explain the reasons for larger discrepancies when the temperature is below 1250 K, it is necessary to carry out a sensitivity study. The study consists of evaluating which reactions are influential in the estimation of a certain fundamental parameter of combustion, in our case on the laminar flame speed and the auto-ignition delay.

These parameters depend on the initial conditions of the mixtures: temperature, pressure, F/A (through richness). Then, through REGATH, Cantera, CHEMKIN, or another tool available in various combustion codes, the kinetic model studied is analyzed for the initial conditions (T, P and ϕ).

In this way it is possible to quickly identify the differences between influencing reactions in different models for the same surrogate, or for different surrogates using a single model.

However, this analysis was not carried out, since there are no experimental results available for a fuel similar to bio-oil and therefore it will not be possible to have real estimates of the deviations of the simulations with respect to the experimental results.

6.5.2.2 Laminar Flame Speed Simulations

Using combined Scheme K, flame speeds for bio-oil surrogates I, II and III estimated at 1 bar as a function of equivalence ratio are presented in Fig. 6.12.

Toluene flame speed results were taken again as a reference. In addition, toluene/air experimental data at $T_0 = 298$ K from Dirrenberger et al. [24] are also presented.

In this figure, it can be seen that bio-oil surrogates flame speeds are very close to those of toluene for $\phi = 0.7 - 1.1$, and then a slight difference can be observed in the very rich range of $\phi = 1.2 - 1.4$. Moreover, flame speeds of bio-oil SurrI (0.4 % ethanol, 0.2 % acetic-acid and 0.4 % toluene) are higher than those of SurrII (0.3 % ethanol, 0.3 % acetic-acid and 0.4 % toluene) and they are both higher than those of SurrIII (0.2 % ethanol, 0.4 % acetic-acid and 0.4 % toluene), showing that as ethanol mole fraction increases (and acetic-acid's decreases) in the surrogate, the flame speed of the mixture increases.

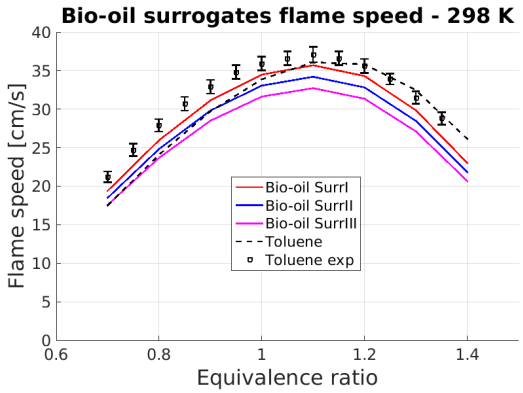

Figure 6.12: Bio-oil surrogates/air laminar flame speeds as a function of equivalence ratio at 1 bar, using new combined Scheme K. Results are compared to experimental data due to Dirrenberger et al. [24] at $T = 298$ K.

6.5.3 Bio-oil/diesel simulations

Concerning diesel simulations, the chemical kinetics model of Huang et al. [13] was developed for diesel (n-heptane/toluene)/n-butanol mixtures. Several blends of n-heptane/toluene were proposed as diesel surrogates in the literature [303; 304; 305]. For instance, [305] have shown that the ignition delay and smoke emission of TRF20 (80% n-heptane/20% toluene in volume) were closer to that of diesel fuel as compared with the pure n-heptane and TRF30 (70% n-heptane/30% toluene in volume) fuel. Therefore, in the present work TRF20 (80% n-heptane/20% toluene in volume) have been chosen as a diesel surrogate.

Unfortunately, for comparison purposes, no experimental data concerning auto-ignition delays and laminar flame speeds was found for bio-oil/diesel blends in the literature. Therefore, as blending effects, especially for ignition, are not trivial, we will focus on the results of pure bio-oil and pure diesel.

6.5.3.1 Auto-ignition delay simulations

Using combined model K, auto-ignition delays for pure bio-oil and pure diesel estimated as a function of temperature ($1000/T_0 = 0.5$ to 1.42) for different equivalence ratios ($\phi = 0.5, 1.0$ and 1.5) and pressures (1, 10 and 100 bar) are presented in Fig. 6.13.

In this figure, it was verified that the merging procedure has little impact on pure diesel auto-ignition delay results, as Model K results are close to those of Huang et al. [13] model.

It can also be seen that diesel auto-ignition delays for 10 and 100 bar pressure

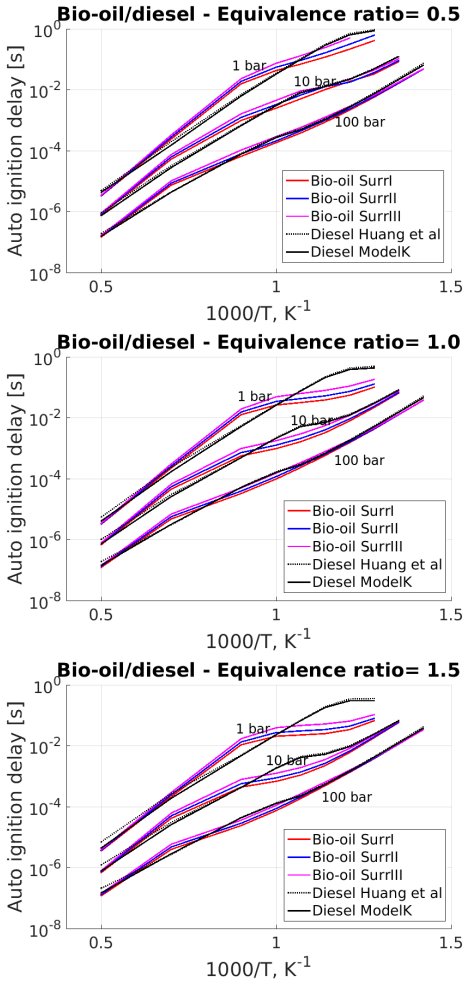

Figure 6.13: Pure bio-oil and pure diesel auto-ignition delay as a function and temperature, for different pressures and equivalence ratios, using the original scheme of [13] (diesel) and the new combined Scheme K.

are close to those of bio-oil surrogates, for $\phi = 0.5 - 1.5$ and temperatures from 704 K ($1000/T_0 = 1.42$) to 2000 K ($1000/T_0 = 0.5$). Moreover, for 1 bar pressure, diesel auto-ignition delays are close to those of bio-oil surrogates in the temperature range from 1428 K ($1000/T_0 = 0.7$) to 2000 K ($1000/T_0 = 0.5$), and then larger differences are found in the temperature range from 704 K ($1000/T_0 = 1.42$) and 1428 K ($1000/T_0 = 0.7$). Again to explain the reasons for the large discrepancies, it is necessary to carry out a sensitivity study as was described in subsection 6.5.2.1.

6.5.3.2 Laminar Flame Speed Simulations

Using combined Scheme K, flame speeds for bio-oil and diesel estimated at 1 bar and 470 K as a function of equivalence ratio are presented in Fig. 6.14.

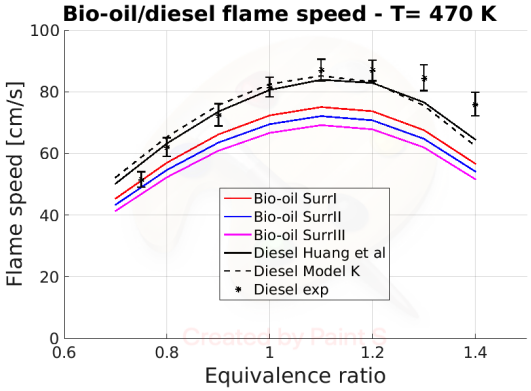

Figure 6.14: Bio-oil/diesel laminar flame speeds as a function of equivalence ratio at 1 bar, using new combined Scheme K. Results are compared to experimental data due to Chong and Hochgreb [27] at $T = 470$ K.

Concerning diesel flame speed experimental data, Chong and Hochgreb [27] performed simulations to obtain laminar flame speeds of practical fuels including Jet-A1, diesel, palm methyl esters (PME) and blends of PME with diesel and Jet-A1 fuels using a jet-wall stagnation premixed flame configuration and particle imaging velocimetry (PIV) technique. The experiments were performed over a range of equivalence ratios at elevated temperature of 470 K and atmospheric pressure, and these results are presented in Fig. 6.14.

In this figure, it is also shown that the merging procedure has little impact on pure diesel flame speed results, as Model K results are close to those of Huang et al. [13] model, and they both well predict the experimental results of Chong and Hochgreb [27], especially in the range of $\phi = 0.7 - 1.2$. It can also be seen that diesel flame speed curves are systematically higher than those of bio-oil surrogates I, II and III, for all equivalence ratios. Moreover, concerning Surrogates I, II and III at 470 K, once again, as ethanol mole fraction increases (and acetic-acid's decreases) in the surrogate, the flame speed of the mixture also increases.

6.5.4 Bio-oil/n-butanol simulations

Concerning n-butanol simulations, as Huang et al. [13] model was developed for diesel/n-butanol mixtures, and n-butanol does not need a surrogate, simulations were carried out simply using C_4H_9OH molecule in Model K. Unfortunately, once again no experimental data concerning auto-ignition delays and laminar flame speeds was found for bio-oil/n-butanol blends in the literature. Therefore, as for diesel, we will focus on the results of pure bio-oil and pure n-butanol.

6.5.4.1 Auto-ignition delay simulations

Using combined model K, auto-ignition delays for pure bio-oil and pure n-butanol estimated as a function of temperature ($1000/T_0 = 0.5$ to 1.42) for different equivalence ratios ($\phi = 0.5, 1.0$ and 1.5) and pressures (1, 10 and 100 bar) are presented in Fig. 6.15 .

Once again, it is shown that the merging procedure has little impact on pure n-butanol auto-ignition delay results, as Model K results are close to those of Huang et al. [13] model. In this figure, it can also be seen that n-butanol auto-ignition delays curves are very different to those of pure bio-oil surrogates, for all studied ranges of equivalence ratio, pressure and temperature.

6.5.4.2 Laminar Flame Speed Simulations

Using new combined Scheme K, flame speeds for bio-oil and n-butanol estimated at 1 bar and 343 K as a function of equivalence ratio are presented in Fig. 6.16.

Concerning n-butanol flame speed experimental data, Huang et al. [13] model was validated using the experimental data of Veloo and Egolfopoulos [28]. In this work, the experiments were performed in the counterflow configuration under atmospheric pressure, unburned mixture temperature of 343 K, and for a wide range of equivalence ratios, and these results are presented in Fig. 6.16. It is also shown that the merging procedure has little impact on pure n-butanol flame speed results, as Model K results are close to those of Huang et al. [13] model, and they both well predict the experimental results of [28], especially in the range of $\phi = 0.7 - 1.1$.

From figures 6.12, 6.14 and 6.16, it can also be seen that, as for diesel, n-butanol flame speed curves are systematically higher than those of bio-oil surrogates I, II and III, for all equivalence ratios. Moreover, concerning Surr I, II and III at 343 K, again, as ethanol mole fraction increases in the surrogate, the flame speed of the mixture also increases.

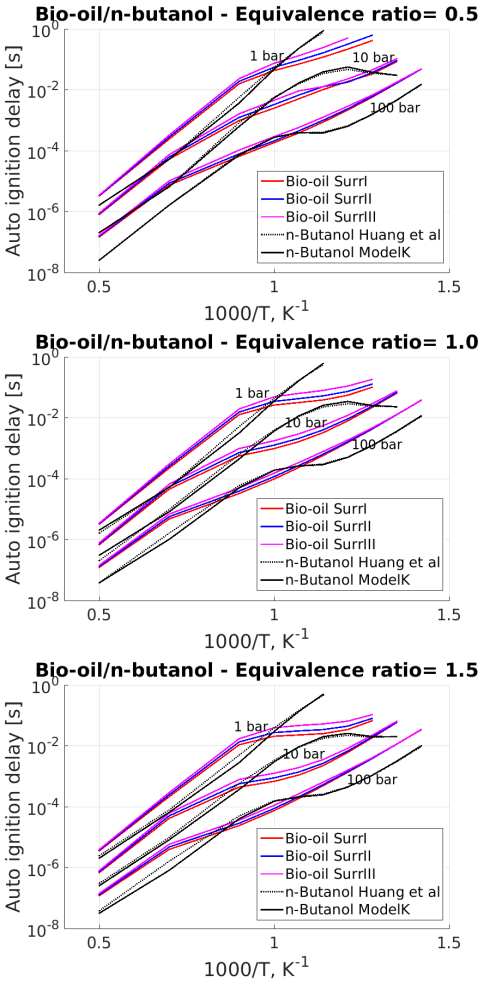

Figure 6.15: Pure bio-oil and pure n-butanol auto-ignition delay as a function and temperature, for different pressures and equivalence ratios, using the original scheme of [13] (n-butanol) and the new combined Scheme K.

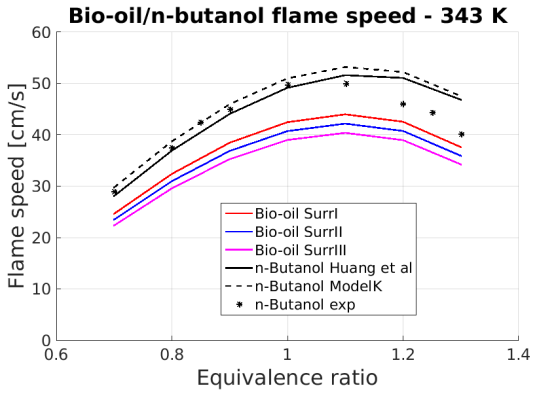

Figure 6.16: Bio-oil/n-butanol laminar flame speeds as a function of equivalence ratio at 1 bar, using new combined Scheme K. Results are compared to experimental data due to Veloo and Egolfopoulos [28] at $T = 343$ K.

6.6 Conclusion

Pyrolysis was performed on torrefied coconut endocarp and the collected bio-oil was analyzed using gas chromatography/mass spectrometry (GC/MS). Based on the GC/MS analysis, three different blends of toluene, ethanol and acetic acid representative of the real fuel chemistry were proposed as the surrogates to carry out numerical combustion studies in 0-D constant-volume auto-ignition and 1-D freely-propagating gaseous premixed flames configurations.

A new chemical scheme was developed and validated by carefully combining the schemes proposed by Huang et al. [13] (toluene) and Christensen and Konnov [12] (acetic acid/ethanol). Combining the chemical schemes consists in identifying and analyzing the common reactions with different reaction constants (which are 181) in both chemical schemes, in order to obtain reasonable results for the pure fuels separately. In order to identify the sensitive reactions for the estimation of the pure fuels auto-ignition delays and flame speeds, 5 reaction packages containing particular species were created. Then, 12 combined chemical schemes (180 species and 1495 elementary reactions) called A to L were developed using these packages.

We have first simulated pure toluene/air, ethanol/air and acetic acid/air auto-ignition delays estimated for different values of equivalence ratio, pressure and temperature. It was shown that the prediction of auto-ignition delays of all three fuels to be barely impacted by the scheme combination procedure.

In addition, we have used the kinetic schemes proposed by Huang et al. [13] and Christensen and Konnov [12], as well as the combined schemes A through L, to simulate 1-D freely-propagating pure toluene, ethanol and acetic acid premixed flames. Larger discrepancies between the combined chemical model and those of Huang et al. [13] and Christensen and Konnov [12] are observed, which means flame speeds of all three

fuels surrogates are very sensitive to the common reactions in both mechanisms, and in particular to some reactions packages. Therefore, experimental data for toluene/air, ethanol/air and acetic acid/air laminar flame speed were used to validate the combined scheme.

In conclusion, scheme K, including Packages I-III and V from Christensen and Konnov [12] and Package IV from Huang et al. [13] was considered as the "best" model, showing that the reactions pathways of the package IV of species C_2H, C_2H_2, C_2H_3, C_2H_4, C_2H_5 and C_2H_6 are very important in the flame speeds estimation for these fuels.

Furthermore, different surrogates consisting of blends of toluene, acetic acid and ethanol have equivalent formulas and ratios H/C and O/C very close to those of bio-oil, thus these were the surrogates chosen to represent bio-oil chemistry, and to analyze the influence of these molecules mole fractions on bio-oil combustion properties.

Moreover, as the use of pyrolysis oil as a transportation fuel is limited due to its high acidity, low thermal stability, low calorific value, high water content, high viscosity and poor lubrication characteristics, blends of bio-oil/diesel/alcohols are a viable short-term alternative to utilize an important fraction of these oils. Therefore, auto-ignition delays and flame speeds of bio-oil/diesel and bio-oil/n-butanol were calculated and presented using the new combined developed scheme K.

Summary and perspectives

The aim of this work was to investigate the chemical and structural alterations of coconut endocarp —*Acrocomia aculeata*— during its isothermal pyrolysis and to proposes a surrogate to study the combustion of its bio-oil, and to validate numerically a chemical kinetic mechanism for its oxidation. This work was carried out by using experimental techniques and numerical approaches.

In Chapter 1 we did a review of the main concepts addressed in this work. First, the current situation of our energy future and the trend towards a bio-based economy and concerning biomass as sustainable resource, a non-exhaustive review about its compositions and the main thermochemical process to turn it into biofuels, were presented. Then, the background of the current situation to consider *Acrocomia aculeata* as an alternative oil crop was introduced, along with the state of the art of coconut endocarp as feedstocks available for producing biofuels. In addition, important combustion characteristics and also how modelling the combustion chemistry, were analyzed. Finally, physico-chemical properties of bio-oil were given and standards established to considered this product into the market.

The experimental approaches and facilities to carry out this study were presented in Chapter 2. Our work has two main approaches, experimental to evaluate the physical, chemical and structural changes of the coconut endocarp during its thermal degradation and a numerical one, to propose a chemical kinetic mechanism for the oxidation of a valid surrogate proposed for coconut endocarp bio-oil. First, we explain the main properties of our study system, fine coconut endocarp particles, which will be decomposed thermally. In this sense, thermogravimetric analysis was the most suitable technique to carry out the pyrolysis, since its controlled temperature program in a controlled atmosphere. In addition, the analysis techniques used to study the physical, structural and chemical changes in our feedstocks, were presented. In the second part, we have builded a fixed bed reactor, in order to obtain the necessary quantities of the liquid product. Then, we presents how we carry out the chemical analysis of the bio-oil, based in the gas chromatography (GC-MS) technique. In adition, we discussed the choice of a surrogate fuel to represent coconut endocarp bio-oil fuel and finally, the developing and validating of the chemical kinetic mechanism numerically, where the chemically reacting flow equations governing the phenomenon were presented.

In the follow chapters 3 to 6, the results of each of part of this work were pre-

sented. The experimental data provided by this work in Chapter 3 includes: elemental analysis, surface area and pore size analyses, ESEM and SEM/FEG observation and dynamic vapor sorption determination, for the solid products of the isothermal pyrolysis at different final temperatures. This data was used to obtain expressions for O/C and H/C ratios as a function of the mass loss that can be used for prediction purposes. Our results provide sufficient evidence for the long-term application of this feedstock and its chars as solid biofuel or raw material in the gasification process.

Chapter 4 and 5, presents results of complementary studies developed in the context of this thesis:

In Chapter 4, based on the set of experimental data obtained in chapter 3, kinetic models suitable in the literature have been evaluated. Inverse method as described for [240], has been used to determine the kinetic parameters for multi-step series reaction mechanisms and for two and three parallel first-order Gaussian DAEM reactions. In addition, the models are valid in temperature range between 250 and 400 °C, considering that it has takes into account simultaneously the four temperature levels for all samples.

In Chapter 5, gasification process using two atmospheres (nitrogen gas and water vapor) for the slow pyrolysis step, was evaluated in regards to the conversion rate of the process and the porosity characteristics of the activated carbon obtained. In general, during the slow-pyrolysis, the water vapor produce char with higher surface area. However, although the surface area of the chars at the beginning of the gasification process is important, the evolution of the porous structure during the gasification process is which will determine the final adsorption characteristics of the activated carbon obtained.

The numerical approach and the results from the bio-oil combustion simulations was presented in Chapter 6. First, three different blends of toluene, ethanol and acetic acid representative of the real fuel chemistry were proposed as the surrogates to carry out numerical combustion studies. Then, a new chemical scheme was developed and validated by carefully combining the schemes proposed by Huang et al. (toluene) and Christensen and Konnov (acetic acid/ethanol). The combined model consists of 180 species and 1495 elementary reactions. Experimental data for toluene/air, ethanol/air and acetic acid/air laminar flame speed were used to validate the combined scheme. Then, auto-ignition delays and laminar flame speed simulations of bio-oil/diesel/n-butanol are presented.

Concerning future work and perspectives, for optimal design of pyrolysis reactors, additional experimental of thermal analysis combined with evolved gas analysis are needed. In this context, thermogravimetry (TG) coupled with Fourier transform infrared (FTIR) spectroscopy (TG/FTIR) or coupled with mass spectrometry (TG/MS) can be used to understanding better the chemical kinetic mechanic of coconut endocarp pyrolysis and improves the numerical studies.

Respect the combustion of coconut endocarp bio-oil, experimental studies in a counterflow burner using a spray premixed bio-oil as fuel with different atomization systems are required to validate the new chemical scheme proposed for bio-oil flames.

Furthermore, different measurement techniques as Planar Laser Induced Fluorescence (PLIF), Emission Spectroscopy, Laser Doppler Velocimetry, can be used to characterize chemically the bio-oil fuel.

In addition, a gas composition analysis can be done in a countercurrent configuration, either in diffusion or premix, to compare the experimental and numerical profiles and thus validate the formation of different combustion intermediary species, since the model can predict hundreds of species. In these flames, a parametric study can be made, depending on the richness and speed of injection, to study the flame structure by visualizing the excited radicals CH*, C2* and OH*, using an intensified chamber. Numerically, it is also possible to add CH*, C2* and OH* excited radical reactions to the kinetic model in order to make a comparison between the experimental and numerical results to validate the Arrhenius constants of the added reactions.

Experimental installations are planned to be set up by the authors to make a comprehensive validation of the proposed kinetic model by measuring auto-ignition delays and laminar flame speeds of bio-oil/diesel blends and bio-oil/n-butanol blends.

Appendixes

Appendixes

Résumé en Français

Introduction

Le monde s'oriente vers une bioéconomie, où l'introduction progressive mais durable des biocarburants et des bioproduits sur le marché mondial est recherchée. Il y a un remplacement progressif des combustibles fossiles et des produits pétroliers, par exemple, en utilisant des mélanges avec de biocombustibles liquides à des fins de transport et autres énergétiques.

La biomasse joue un rôle de plus en plus important dans cette transition vers une bioéconomie. En effet, c'est la principale source de matière première renouvelable pour la production de ces produits. On s'attend à ce que le concept de bioéconomie affecte progressivement toutes les industries, où un changement continu vers des matières premières bio-renouvelables plus complexes comme les résidus agricoles se produira.

L'endocarpe de noix de coco —*Acrocomia Aculeata*— a l'avantage d'être une matière première de deuxième génération. Ces déchets agro-industriels sont générés en grande quantité, environ 7 tonnes par ha/an lors de la production d'huiles d'amande et de pulpe à partir du fruit d'Acrocomia aculeata. Les rendements élevés en huile (environ 4-6 tonnes d'huile / ha) et les propriétés de l'huile similaires à l'huile de palme (Elaeis guineensis), qui détient les 35% du marché des huiles végétales, ont attiré l'attention des chercheurs. De plus, l'huile de pulpe du fruit, elle peut être utilisée pour la production de biodiesel et des applications cosmétiques (la pulpe de fruits présente une teneur en matières grasses d'environ 25,1 à 32,1%) et l'huile d'amande pour cosmétique comme huile comestible (avec une teneur moyenne en matières grasses d'environ 59,3 à 68,9%).

Au cours des dernières décennies, plusieurs études ont été menées avec des objectifs différents concernant l'*Acrocomia aculeata* ou "coco". La plupart de ces travaux se sont concentrés sur les performances et la qualité des huiles extraites de leur pulpe et de leurs amandes. D'autres recherches portent sur les propriétés comme combustibles des sous-produits générés lors de la transformation de leurs fruits. En ce qui concerne la production de biocarburants, les recherches se sont concentrées sur la production

de biodiesel et ses propriétés à partir de l'huile de pulpe.

Cependant, il y a un manque de recherche scientifique liée à l'évaluation des sous-produits de la transformation des fruits d'Acrocomia aculeata, en particulier "l'endocarpe de noix de coco". Des recherches scientifiques plus importantes sont nécessaires pour évaluer la diversité des produits finaux potentiels pour une bioraffinerie. En ce sens, il existe une lacune dans la littérature liée à l'évolution des propriétés chimiques et structurelles de l'endocarpe de noix de coco lors de sa pyrolyse isotherme. En particulier, les propriétés du charbon indiqueront les utilisations les plus appropriées de ce matériau (c'est-à-dire comme combustible solide, matière première pour le processus de gazéification, ou autres applications).

De plus, les paramètres cinétiques du processus de pyrolyse de l'endocarpe de noix de coco n'ont pas encore été déterminés. Le processus de pyrolyse peut être effectué dans le but principal d'obtention du bio-huile. Les propriétés physiques des bio-huiles de l'endocarpe de noix de coco ont été analysées dans nos travaux antérieurs. Cependant, sa composition chimique et son mécanisme de cinétique chimique de combustion n'ont pas encore été analysés. Enfin, le charbon actif généré à partir de l'endocarpe de noix de coco a montré une très grande surface, et 'a notre connaissance, c'est la première fois que la vapeur d'eau est utilisée simultanément comme agent de pyrolyse et de gazéification pour cette matière première.

Les objectifs de ce projet doctoral sont d'évaluer l'évolution des propriétés chimiques et structurelles de l'endocarpe de noix de coco —*Acrocomia aculeata*— au cours de sa pyrolyse isotherme, de déterminer les paramètres cinétiques du processus de pyrolyse, en utilisant au moins cinq températures simultanément, d'évaluer la surface et la porosité des charbons actifs obtenus dans différentes conditions de pyrolyse/gazéification lente, de déterminer la composition chimique du bio-huile produite à partir d'endocarpe de noix de coco torréfié, et enfin de proposer une mécanique cinétique chimique pour la combustion du bio-huile à partir d'un substitut choisi dans sa composition chimique.

Pour atteindre les objectifs de ce travail, une combinaison d'approches expérimentales et numériques a été utilisée pour étudier le comportement thermochimique de l'endocarpe de noix de coco et de ses produits dans différentes conditions.

Questions de recherche

En résumé, l'objectif principal de cette thèse était d'évaluer trois produits d'endocarpe de noix de coco (c'est-à-dire char, bio-huile et charbon actif) pour proposer des utilisations alternatives pour cette matière première. Ceci peut être synthétisé comme une tentative de répondre aux suivantes questions de recherche:

- Comment la pyrolyse isotherme affecte-t-elle la composition du charbon et ses propriétés structurelles?

- Quels sont les paramètres cinétiques pour simuler la pyrolyse isotherme de l'endocarpe de coco?

- Quelles sont les caractéristiques de surface et de porosité du charbon actif issue de l'endocarpe de noix de coco obtenu par pyrolyse/gazéification à la vapeur?

- Quelle est la composition chimique du bio-huile d'endocarpe de coco?

- Quels sont les substituts du mécanisme de cinétique chimique de combustion du bio-huilenn?

- Comment deux paramètres de combustion principaux "Temps de retard d'allumage (IDT) et Vitesse de Flamme Laminaire (LFS)" changent, en fonction de la température, de la pression et du rapport d'équivalence pour le bio-huile?

Méthodologie

Pour répondre à ces questions et atteindre les objectifs, nous avons utilisé l'approche expérimentales et numériques suivante:

Une expérience de pyrolyse à micro-échelle, utilisant une thermo-balance pour produire les chars et différentes techniques analytiques pour évaluer ses propriétés comme l'analyse élémentaire (EA), la surface spécifique BET, l'observation en microscopie électronique (ESEM, SEM/FEG), et les mesures de sorption de vapeur d'eau (DVS).

Ensuite, les paramètres cinétiques de pyrolyse ont été déterminés à l'aide du principe de la méthode inverse et deux modèles cinétiques: le modèle en 3 étapes et le modèle d'énergie d'activation distribuée (DAEM).

En outre, nous menons une expérience de pyrolyse à l'échelle du réacteur pour produire du bio-huile. Cette bio-huile a été chimiquement caractérisée par chromatographie en phase gazeuse-spectrométrie de masse (GC-MS) pour proposer un substitut et un mécanisme de cinétique chimique pour nous permettre de réaliser la simulation de combustion de bio-huile.

Enfin, pour produire du charbon actif, nous avons couplé un générateur de vapeur d'eau à une thermobalance. Ensuite, la surface spécifique du produit final et sa porosité ont été analysées et comparées à ceux du charbons actifs commerciaux typiques.

Cette thèse a été réalisée en collaboration entre le Laboratoire de Génie des

Procédés et Matériaux (LGPM, CentraleSupélec-Université Paris Saclay, France) et Laboratorio de Mecánica y Energía (LME, FIUNA - Facultad de Ingeniería de la Universidad Nacional de Asunción, Paraguay).

Ce manuscrit est écrit sous forme d'articles. Deux publications constituent donc les chapitres 3 et 6, avec des informations supplémentaires non publiées incluses dans les chapitres 4 et 5. Le contenu des publications a été légèrement modifié par rapport aux versions publiées, selon le format général du manuscrit et principalement dans les sections Introduction, Matériel et Méthodes des divers articles, afin d'éviter des informations redondantes pour le lecteur.

Principaux résultats et conclusions

La perte de masse résulte de nombreuses réactions compétitives et ces courbes thermogravimétriques nous donnent un aperçu des mécanismes de réaction pour la pyrolyse de l'endocarpe de noix de coco.

Les données expérimentales fournies par ce travail lors de la pyrolyse isotherme de l'endocarpe de noix de coco ont été utilisées pour obtenir des expressions de ratios O/C et H/C en fonction de la perte de masse utilisable à des fins de prédiction.

De par sa structure microporeuse, sa surface et sa teneur en carbone, le charbon à 500 °C et le charbon à 550 °C sont proposés comme matière première pour la production de charbon actif ou de gaz de synthèse à partir du processus de gazéification, en raison de son transfert de gaz plus uniforme attendu, qui devrait maintenir la réactivité de gazéification avec le temps écoulé.

Enfin, les résultats montrent clairement que l'endocarpe de noix de coco subit des changements chimiques en conséquence de la décomposition primaire, mais pas de changements majeurs dans la structure poreuse jusqu'à 450 °C.

Nos résultats fournissent des preuves suffisantes pour l'application à long terme de ce chars comme biocarburant solide ou matière première dans le processus de gazéification.

Les modèles cinétiques de pyrolyse appropriés dans la littérature ont été évalués. La méthode inverse telle que décrite par Cavagnol et al. 2013 [240], a été utilisée pour déterminer les paramètres cinétiques pour les mécanismes de réaction en série à plusieurs étapes et pour deux et trois réactions DAEM (Modèle d'énergie d'activation distribuée) Gaussiennes de premier ordre parallèles. De plus, les modèles sont valables dans une plage de température comprise entre 250 et 450 °C, étant donné qu'il a pris en compte simultanément cinq niveaux de température pour tous les échantillons.

Les pics de distribution d'énergie d'activation pour les trois pseudo-composants étaient centrés à 178.6, 198.9 et 221.4 $kJ \cdot mol^{-1}$. Les écarts-types des énergies d'activation étaient de 5.48, 0.16e−3 et 18.1 $kJ \cdot mol^{-1}$ pour les fractions hémicellulose, cellulose et lignine respectivement.

Ces valeurs sont en accord avec celles rapportées pour d'autres biomasses de lignocellulose et indiquent que la distribution d'énergie d'activation pour la lignine a la distribution la plus large.

Au contraire, la distribution associée à la cellulose est très étroite et en fait dégénérée en une seule réaction de premier ordre. Ceci est cohérent avec la dégradation soudaine de la cellulose, une fois fondue, à environ 300 °C. Enfin, la proportion de chacun des pseudo-composants (respectivement 0.33, 0.48 et 0.18) est également cohérente avec la composition des matériaux lignocellulosiques.

Le modèle en 3 étapes présente une très faible capacité de prédiction. Au contraire, on observe que le modèle de distribution à trois Gaussiennes correspond bien aux données des deux courbes à 5 K/min et 20 K/min. Par conséquent, en plus du très bon réglage individuel de chaque courbe du DAEM, il a la possibilité de simuler la cinétique pour différentes vitesses de chauffage.

Ensuite, le procédé de gazéification utilisant deux atmosphères (azote gazeux et vapeur d'eau) pour l'étape de pyrolyse lente, a été évalué au regard du taux de conversion du procédé et des caractéristiques de porosité du charbon actif obtenu. En général, lors de la pyrolyse lente, la vapeur d'eau produit du charbon de plus grande surface, mais bien que la surface des chars au début du processus de gazéification soit importante, l'évolution de la structure poreuse pendant le processus de gazéification est ce qui déterminera les caractéristiques d'adsorption finales du charbon actif obtenu.

Les besoins en superficie du charbon actif dépendent de ses applications (filtrage d'eau potable municipale, transformation des aliments et boissons, élimination des odeurs, dépollution industrielle, etc.). Le charbon actif est produit spécifiquement de manière à atteindre une très grande surface interne (entre 500 et 1500 m^2/g). Cependant, il est à noter que la surface obtenue pour tous les échantillons 1, 2 et 3 à $X = 0.5$ est supérieure à 700 m^2/g et même pour l'échantillon 2 atteint jusqu'à 880 m^2/g, ce qui est suffisant pour la plupart des applications.

Les résultats des simulations de la combustion du bio-huile sont les suivants.

Premièrement, trois mélanges différents de toluène, d'éthanol et d'acide acétique représentatifs de la chimie réelle du carburant ont été proposés comme substituts pour réaliser des études numériques de combustion.

Ensuite, un nouveau schéma chimique a été développé et validé en combinant soigneusement les schémas proposés par Huang et al. (2016) (toluène) [13] et Christensen et Konnov (2017) (acide acétique/éthanol) [12]. Le modéle combiné comprend 180 espèces et 1495 réactions élémentaires. Nous avons d'abord simulé les retards d'auto-allumage toluène/air pur, éthanol/air et acide acétique/air estimés pour différentes valeurs de rapport d'équivalence, de pression et de température.

Il a été démontré que la prévision des retards d'auto-allumage des trois carburants serait à peine affectée par la procédure de combinaison des schémas. De plus, nous avons utilisé les schémas cinétiques proposés par Huang et al. (2017) et Christensen et Konnov (2016), ainsi que les schémas combinés A à L, pour simuler

des flammes prémélangées de toluène pur, d'éthanol et d'acide acétique à propagation libre 1-D. Des écarts plus importants entre le modèle chimique combiné et ceux de Huang et al. (2016) et Christensen et Konnov (2017) sont observés, ce qui signifie que les vitesses de flamme des trois carburants substituts sont très sensibles aux réactions communes dans les deux mécanismes, et en particulier à certains ensembles de réactions. Par conséquent, des données expérimentales sur la vitesse de flamme laminaire toluène/air, éthanol/air et acide acétique/air ont été utilisées pour valider le schéma combiné.

En conclusion, le schéma K, comprenant les packages I-III et V de Christensen et Konnov (2017) et le package IV de Huang et al. (2016) a été considéré comme le "meilleur" modéle, montrant que les voies de réaction du package IV des espèces C_2H, C_2H_2, C_2H_3, C_2H_4, C_2H_5 et C_2H_6 sont très importantes dans l'estimation des vitesses de flamme pour ces combustibles.

De plus, différents substituts constitués de mélanges de toluène, d'acide acétique et d'éthanol ont des formules et des rapports équivalents H/C et O/C très proches de ceux des bio-huiles, ce sont donc les substituts choisis pour représenter la chimie des bio-huiles, et pour analyser le influence de ces molécules des fractions molaires sur les propriétés de combustion des bio-huiles.

Enfin, comme l'utilisation de l'huile de pyrolyse comme carburant pour le transport est limitée en raison de sa forte acidité, sa faible stabilité thermique, son faible pouvoir calorifique, sa teneur élevée en eau, sa viscosité élevée et ses mauvaises caractéristiques de lubrification, les mélanges de bio-huile/diesel/alcools sont une alternative viable à court terme pour utiliser une fraction importante de ces huiles. Par conséquent, les délais d'auto-inflammation et les vitesses de flamme du bio-huile/diesel et du bio-huile/n-butanol ont été calculés et présentés en utilisant le nouveau schéma développé combiné K.

Perspectives

Concernant les travaux futurs et les perspectives, pour une conception optimale des réacteurs de pyrolyse, une expérience supplémentaire d'analyse thermique combinée à une analyse des gaz dégagés est nécessaire.

Dans ce contexte, la thermogravimétrie (TG) couplée à la spectroscopie infrarouge à transformée de Fourier (FTIR) (TG / FTIR) ou couplée à la spectrométrie de masse (TG/MS) permet de mieux comprendre la mécanique cinétique chimique de la pyrolyse des endocarpes de noix de coco et améliore la études.

De plus, il est nécessaire de comparer les résultats cinétiques avec ceux obtenus en utilisant une distribution asymétrique et sous différents programmes thermiques et de réaliser une modélisation multi-échelle de pyrolyse de biomasse lignocellulosique

Respecter la combustion du bio-huile d'endocarpe de noix de coco, des études expérimentales dans un brûleur à contre-courant utilisant une bio-huile pré-mélangée

en spray comme carburant avec différents systèmes d'atomisation sont nécessaires pour valider le nouveau schéma chimique proposé pour les flammes de bio-huile. En outre, différentes techniques de mesure comme la fluorescence planaire induite par laser (PLIF), la spectroscopie par émission, la vélocimétrie laser Doppler, peuvent être utilisées pour caractériser chimiquement le carburant bio-huile.

Pour terminer, il sera très utile d'effectuer des analyses numériques et expérimentales de mélanges de bio-huile/biodiesel et d'autres carburants/biocarburants.

References

[1] A. da Silva César, F. de Azedias Almeida, R. P. de Souza, G. C. Silva, A. Atabani, The prospects of using acrocomia aculeata (macaúba) a non-edible biodiesel feedstock in brazil, Renewable and Sustainable Energy Reviews 49 (2015) 1213–1220. p. v, 2, 21, 22

[2] D. M. Mason, K. N. Gandhi, Formulas for calculating the calorific value of coal and coal chars: Development, tests, and uses, Fuel Processing Technology 7 (1) (1983) 11–22. p. v, 22

[3] D. Özçimen, F. Karaosmanoğlu, Production and characterization of bio-oil and biochar from rapeseed cake, Renewable energy 29 (5) (2004) 779–787. p. v, 26, 27, 29

[4] S. Xiu, A. Shahbazi, V. Shirley, D. Cheng, Hydrothermal pyrolysis of swine manure to bio-oil: effects of operating parameters on products yield and characterization of bio-oil, Journal of analytical and applied pyrolysis 88 (1) (2010) 73–79. p. v, 27

[5] Z. Hu, Y. Zheng, F. Yan, B. Xiao, S. Liu, Bio-oil production through pyrolysis of blue-green algae blooms (bgab): product distribution and bio-oil characterization, Energy 52 (2013) 119–125. p. v, 26, 27

[6] S. J. Duarte, J. Lin, D. Alviso, J. C. Rolón, Effect of Temperature and Particle Size on the Yield of Bio-oil, Produced from Conventional Coconut Core Pyrolysis, International Journal of Chemical Engineering and Applications 7 (2) (2016) 102–108. p. v, 2, 23, 26, 27, 42, 46, 55, 65, 66, 86, 107, 108, 118, 121

[7] B. Jenkins, L. Baxter, T. Miles Jr, T. Miles, Combustion properties of biomass, Fuel processing technology 54 (1-3) (1998) 17–46. p. v, 29

[8] K. Gupta, A. Rehman, R. Sarviya, Bio-fuels for the gas turbine: A review, Renewable and Sustainable Energy Reviews 14 (9) (2010) 2946–2955. p. v, 35, 36

[9] D. Chiaramonti, A. Oasmaa, Y. Solantausta, Power generation using fast pyrolysis liquids from biomass, Renewable and sustainable energy reviews 11 (6) (2007) 1056–1086. p. v, 35, 36, 39, 55

[10] A. Oasmaa, D. C. Elliott, S. Müller, Quality control in fast pyrolysis bio-oil production and use, Environmental Progress & Sustainable Energy: An Official Publication of the American Institute of Chemical Engineers 28 (3) (2009) 404–409. p. v, 37

[11] A. Oasmaa, A. Källi, C. Lindfors, D. C. Elliott, D. Springer, C. Peacocke, D. Chiaramonti, Guidelines igueredor transportation, handling, and use of fast pyrolysis bio-oil. 1. flammability and toxicity, Energy & Fuels 26 (6) (2012) 3864–3873. p. v, 37

[12] M. Christensen, A. A. Konnov, Laminar burning velocity of acetic acid + air flames, Combustion and Flame 170 (2016) 12 – 29. doi:https://doi.org/10.1016/j.combustflame.2016.05.007. p. vi, vii, xi, xii, 119, 127, 128, 129, 130, 131, 132, 133, 134, 135, 136, 137, 139, 140, 141, 142, 143, 151, 152, 163

[13] H. Huang, J. Zhu, Z. Zhu, H. Wei, D. Lv, P. Zhang, H. Sun, Development and validation of a new reduced diesel-n-butanol blends mechanism for engine applications, Energy Conversion and Management 149 (2017) 553 – 563. doi:https://doi.org/10.1016/j.enconman.2017.07.056. p. vi, vii, xi, xii, xiii, 119, 126, 127, 128, 129, 130, 131, 132, 133, 134, 135, 136, 137, 138, 141, 142, 143, 146, 147, 148, 149, 150, 151, 152, 163

[14] L. Capuano, International energy outlook 2018 (ieo2018), US Energy Information Administration (EIA): Washington, DC, USA 2018 (2018) 21. p. ix, 6

[15] E. M. Rubin, Genomics of cellulosic biofuels, Nature 454 (7206) (2008) 841. p. ix, 6, 7

[16] J. Rencoret, H. Kim, A. B. Evaristo, A. Gutiérrez, J. Ralph, J. C. del Río, Variability in lignin composition and structure in cell walls of different parts of macaúba (acrocomia aculeata) palm fruit, Journal of agricultural and food chemistry 66 (1) (2017) 138–153. p. ix, 8, 9, 46, 47

[17] B. Balagurumurthy, R. Singh, P. Ohri, A. Prakash, T. Bhaskar, Thermochemical biorefinery, in: Recent Advances in Thermo-Chemical Conversion of Biomass, Elsevier, 2015, pp. 157–174. p. ix, 7, 10, 11, 21

[18] I. Gauto, R. E. Spichiger, F. W. Stauffer, Diversity, distribution and conservation status assessment of paraguayan palms (arecaceae), Biodiversity and Conservation 20 (12) (2011) 2705. doi:10.1007/s10531-011-0100-6. URL https://doi.org/10.1007/s10531-011-0100-6 p. ix, x, 2, 14, 15, 16, 56, 86

[19] G. W. Huber, S. Iborra, A. Corma, Synthesis of transportation fuels from biomass: chemistry, catalysts, and engineering, Chemical reviews 106 (9) (2006) 4044–4098. p. x, 25

[20] D. Stokes, Principles and practice of variable pressure/environmental scanning electron microscopy (VP-ESEM), John Wiley & Sons, 2008. p. x, 51

[21] P. McKendry, Energy production from biomass (part 2): conversion technologies, Bioresource technology 83 (1) (2002) 47–54. p. x, 52, 75

[22] M. Naderi, Surface area: Brunauer–emmett–teller (bet), in: Progress in filtration and separation, Elsevier, 2015, pp. 585–608. p. x, 52, 53

[23] C. A. S. Hill, A. J. Norton, G. Newman, The water vapour sorption properties of sitka spruce determined using a dynamic vapour sorption apparatus, Wood Science and Technology 44 (3) (2010) 497–514. doi:10.1007/s00226-010-0305-y.

URL http://dx.doi.org/10.1007/s00226-010-0305-y p. x, 28, 53, 54, 69

[24] P. Dirrenberger, P. Glaude, R. Bounaceur, H. L. Gall, A. P. da Cruz, A. Konnov, F. Battin-Leclerc, Laminar burning velocity of gasolines with addition of ethanol, Fuel 115 (2014) 162 – 169. doi:http://dx.doi.org/10.1016/j.fuel.2013.07.015. p. xii, 126, 128, 129, 137, 141, 142, 145, 146

[25] A. Konnov, R. Meuwissen, L. de Goey, The temperature dependence of the laminar burning velocity of ethanol flames, Proceedings of the Combustion Institute 33 (1) (2011) 1011 – 1019. p. xii, 128, 129, 137, 141, 142

[26] J. van Lipzig, E. Nilsson, L. de Goey, A. Konnov, Laminar burning velocities of n-heptane, iso-octane, ethanol and their binary and tertiary mixtures, Fuel 90 (8) (2011) 2773 – 2781. p. xii, 128, 129, 137, 141, 142

[27] C. T. Chong, S. Hochgreb, Measurements of laminar flame speeds of liquid fuels: Jet-a1, diesel, palm methyl esters and blends using particle imaging velocimetry (piv), Proceedings of the Combustion Institute 33 (1) (2011) 979 – 986. doi:http://dx.doi.org/10.1016/j.proci.2010.05.106. p. xii, 148

[28] P. S. Veloo, F. N. Egolfopoulos, Flame propagation of butanol isomers/air mixtures, Proceedings of the Combustion Institute 33 (1) (2011) 987 – 993. doi:https://doi.org/10.1016/j.proci.2010.06.163. p. xiii, 149, 151

[29] U. E. I. Administration, International Energy Outlook 2018 (IEO 2018), Available from:,https://www.eia.gov/, 2018. p. 1, 5, 12

[30] A. Demirbas, Biofuels securing the planet's future energy needs, Energy conversion and management 50 (9) (2009) 2239–2249. p. 1, 6

[31] E. Bohn, Tablero de comando para la promoción de los biocombustibles en paraguay, Tech. rep., Naciones Unidas Comisión Económica para América Latina y el Caribe (CEPAL) (2009). p. 1, 21, 66

[32] L. Pimentel, S. Motoike, E. Costa, C. Manfio, C. Bruckner, Estimativa de custo de produção e viabilidade econômica do cultivo da palmeira macaúba (acrocomia aculeata) para produção de óleo vegetal, 61Congresso Brasileiro de Plantas Oleaginosas, Gorduras e Biodiesel. p. 1, 14

[33] L. Pimentel, C. Manfio, S. Motoike, J. Paes, C. Bruckner, Coeficientes técnicos e custos de produção do cultivo da macaúba, Informe Agropecuário 32 (265) (2011) 61–69. p. 1, 14

[34] A. Rival, P. Levang, Palms of controversies: Oil palm and development challenges, CIFOR, 2014. p. 1, 2, 14

[35] D. Haupenthal, C. Sorol, A. A. Schneider, Caracterización de frutos de mbokaja—Acrocomia aculeata— de la zona centro-sur del departamento de Itapúa, Paraguay, Congreso Nacional de Ciencias Agrarias. Seminario Nacional de Energías Renovables (2a, 3a : 2012 marz. 21-23; San Lorenzo, Paraguay). 1 (2012) 236 – 239.
URL http://www.agr.una.py/descargas/tapas/LibroIICNCA2012.pdf p. 1, 14

[36] C. E. Manfio, S. Y. Motoike, M. D. V. Resende, C. E. M. dos Santos, A. Y. Sato, Avaliação de progênies de macaúba na fase juvenil e estimativas de parâmetros genéticos e diversidade genética, 2012. p. 1, 2

[37] G. Ciconini, S. Favaro, R. Roscoe, C. Miranda, C. Tapeti, M. Miyahira, L. Bearari, F. Galvani, A. Borsato, L. Colnago, M. Naka, Biometry and oil contents of Acrocomia aculeata fruits from the Cerrados and Pantanal biomes in Mato Grosso do Sul, Brazil, Industrial Crops and Products 45 (2013) 208 – 214. doi:http://dx.doi.org/10.1016/j.indcrop.2012.12.008.
URL http://www.sciencedirect.com/science/article/pii/S0926669012006425 p. 1, 2, 14, 86

[38] S. G. Montoya, S. Y. Motoike, K. N. Kuki, A. D. Couto, Fruit development, growth, and stored reserves in macauba palm (Acrocomia aculeata), an alternative bioenergy crop, Planta 244 (4) (2016) 927–938. p. 2, 14

[39] J. Poetsch, D. Haupenthal, I. Lewandowski, D. Oberlander, T. Hilger, Acrocomia aculeataa sustainable oil crop, Rural 21 (2012) 41 – 44. p. 2, 14, 15, 86

[40] A. B. Evaristo, J. A. S. Grossi, A. d. C. O. Carneiro, L. D. Pimentel, S. Y. Motoike, K. N. Kuki, Actual and putative potentials of macauba palm as feedstock for solid biofuel production from residues, Biomass and Bioenergy 85 (2016) 18–24. doi:10.1016/j.biombioe.2015.11.024.
URL http://dx.doi.org/10.1016/j.biombioe.2015.11.024 p. 2, 14, 46, 65, 74, 86

[41] S. B. Reis, M. O. Mercadante-Simões, L. M. Ribeiro, Pericarp development in the macaw palm acrocomia aculeata (arecaceae), Rodriguésia 63 (3) (2012) 541–549. doi:10.1590/s2175-78602012000300005.
URL http://dx.doi.org/10.1590/s2175-78602012000300005 p. 2, 14, 78, 80, 86

[42] M. Plath, C. Moser, R. Bailis, P. Brandt, H. Hirsch, A.-M. Klein, D. Walmsley, H. von Wehrden, A novel bioenergy feedstock in latin america? cultivation potential of acrocomia aculeata under current and future climate conditions, Biomass and Bioenergy 91 (2016) 186–195. p. 2, 14, 86

[43] R. Schnepf, B. D. Yacobucci, Renewable fuel standard (rfs): overview and issues, Library of Congress, Congressional Research Service, 2013. p. 6

[44] S. Afionis, L. C. Stringer, European union leadership in biofuels regulation: Europe as a normative power?, Journal of Cleaner Production 32 (2012) 114–123. p. 6

[45] H. Long, X. Li, H. Wang, J. Jia, Biomass resources and their bioenergy potential estimation: A review, Renewable and Sustainable Energy Reviews 26 (2013) 344–352. p. 6

[46] R. A. Sheldon, Green and sustainable manufacture of chemicals from biomass: state of the art, Green Chemistry 16 (3) (2014) 950–963. p. 6

[47] S. Nitayavardhana, S. K. Khanal, Biofuel residues/wastes: ban or boon?, Critical reviews in environmental science and technology 42 (1) (2012) 1–43. p. 7

[48] W. Institute, Biofuels for transport: global potential and implications for sustainable energy and agriculture, Earthscan, 2012. p. 7

[49] T. Bhaskar, A. Pandey, Advances in thermochemical conversion of biomass−introduction, in: Recent Advances in Thermo-Chemical Conversion of Biomass, Elsevier, 2015, pp. 3–30. p. 7, 13

[50] M. Pauly, K. Keegstra, Cell-wall carbohydrates and their modification as a resource for biofuels, The Plant Journal 54 (4) (2008) 559–568. p. 8

[51] J. L. McCarthy, Lignin chemistry, technology, and utilization: a brief history, Lignin: historical, biological, and material perspectives (2000) 2–99. p. 8

[52] D. Fengel, G. Wegener, Wood: chemistry, ultrastructure, reactions, Walter de Gruyter, 2011. p. 8

[53] F. Cherubini, The biorefinery concept: Using biomass instead of oil for producing energy and chemicals, Energy Conversion and Management 51 (7) (2010) 1412 – 1421. doi:https://doi.org/10.1016/j.enconman.2010.01.015. URL http://www.sciencedirect.com/science/article/pii/S0196890410000373 p. 10, 13

[54] C. Conde-Mejia, A. Jimenez-Gutierrez, M. El-Halwagi, A comparison of pretreatment methods for bioethanol production from lignocellulosic materials, Process Safety and Environmental Protection 90 (3) (2012) 189–202. p. 10

[55] E. Triwahyuni, Y. Sudiyani, H. Abimanyu, et al., The effect of substrate loading on simultaneous saccharification and fermentation process for bioethanol production from oil palm empty fruit bunches, Energy Procedia 68 (2015) 138–146. p. 10

[56] P. Haro, P. Ollero, A. V. Perales, A. Gómez-Barea, Thermochemical biorefinery based on dimethyl ether as intermediate: Technoeconomic assessment, Applied energy 102 (2013) 950–961. p. 11

[57] P. Haro, P. Ollero, A. L. Villanueva Perales, F. Vidal-Barrero, Potential routes for thermochemical biorefineries, Biofuels, Bioproducts and Biorefining 7 (5) (2013) 551–572. p. 11

[58] R. Navarro, M. Sanchez-Sanchez, M. Alvarez-Galvan, F. Del Valle, J. Fierro, Hydrogen production from renewable sources: biomass and photocatalytic opportunities, Energy & Environmental Science 2 (1) (2009) 35–54. p. 12

[59] D. Mohan, C. U. Pittman, P. H. Steele, Pyrolysis of wood/biomass for bio-oil: a critical review, Energy & fuels 20 (3) (2006) 848–889. p. 12

[60] J. Piskorz, D. Scott, D. Radlein, Composition of oils obtained by fast pyrolysis of different woods, in: ACS Symposium Series, Vol. 376, AMER CHEMICAL SOC 1155 16TH ST, NW, WASHINGTON, DC 20036, 1988, pp. 167–178. p. 12, 26

[61] J. Lehmann, S. Joseph, Biochar for environmental management: science, technology and implementation, Routledge, 2015. p. 12, 50

[62] S. Hunt, R. Drigo, review of the current state of bioenergy development in G8+ 5 countries, Global Bioenergy Partnership, Rome, IT. p. 13

[63] O. Jönsson, M. Persson, Biogas as transportation fuel, Fachtagung 2003 (2003) 99–111. p. 13

[64] E. D. Larson, A review of life-cycle analysis studies on liquid biofuel systems for the transport sector, Energy for sustainable development 10 (2) (2006) 109–126. p. 13

[65] J.-P. Lange, Lignocellulose conversion: an introduction to chemistry, process and economics, Biofuels, Bioproducts and Biorefining: Innovation for a sustainable economy 1 (1) (2007) 39–48. p. 13

[66] M. Basili, F. Fontini, Biofuel from jatropha curcas: environmental sustainability and option value, Ecological Economics 78 (2012) 1–8. p. 13

[67] D. P. Ho, H. H. Ngo, W. Guo, A mini review on renewable sources for biofuel, Bioresource technology 169 (2014) 742–749. p. 13

[68] S. N. Naik, V. V. Goud, P. K. Rout, A. K. Dalai, Production of first and second generation biofuels: a comprehensive review, Renewable and sustainable energy reviews 14 (2) (2010) 578–597. p. 13, 36

[69] L. Shen, J. Haufe, M. K. Patel, Product overview and market projection of emerging bio-based plastics pro-bip 2009, Report for European polysaccharide network of excellence (EPNOE) and European bioplastics 243. p. 13

[70] J. J. Bozell, G. R. Petersen, Technology development for the production of biobased products from biorefinery carbohydrates—the us department of energy's "Top 10" revisited, Green Chemistry 12 (4) (2010) 539–554. p. 13

[71] P. F. Harmsen, M. M. Hackmann, H. L. Bos, Green building blocks for bio-based plastics, Biofuels, Bioproducts and Biorefining 8 (3) (2014) 306–324. p. 14

[72] C. E. Manfio, S. Y. Motoike, M. D. V. de Resende, C. E. M. dos Santos, A. Y. Sato, Avaliação de progênies de macaúba na fase juvenil e estimativas de parâmetros genéticos e diversidade genética, Pesquisa Florestal Brasileira 32 (69) (2012) 63. p. 14

[73] G. T. Bertoni, El mbocayá o coco del paraguay (Acrocomia totai mart.), Revista de Agricultura (Asunción) 1 (1941) 36–50. p. 15

[74] K. S. Markley, The mbocayá palm: An economic oil plant of Paraguay, Journal of the American Oil Chemists Society 32 (7) (1955) 405–414. p. 15, 17

[75] M. J. McDonald, Revisión de la Situación Actual de Mbokaja (Acrocomia totai) en Paraguay, Informe Final, 2007. p. 17, 18

[76] A. Margeot, B. Hahn-Hagerdal, M. Edlund, R. Slade, F. Monot, New improvements for lignocellulosic ethanol, Current opinion in biotechnology 20 (3) (2009) 372–380. p. 21

[77] P. S. Nigam, A. Singh, Production of liquid biofuels from renewable resources, Progress in energy and combustion science 37 (1) (2011) 52–68. p. 21

[78] N. S. Mosier, R. Hendrickson, M. Brewer, N. Ho, M. Sedlak, R. Dreshel, G. Welch, B. S. Dien, A. Aden, M. R. Ladisch, Industrial scale-up of pH-controlled liquid hot water pretreatment of corn fiber for fuel ethanol production, Applied biochemistry and biotechnology 125 (2) (2005) 77–97. p. 23

[79] R. Kataki, R. S. Chutia, M. Mishra, N. Bordoloi, R. Saikia, T. Bhaskar, Feedstock suitability for thermochemical processes, in: Recent Advances in Thermo-Chemical Conversion of Biomass, Elsevier, 2015, pp. 31–74. p. 23, 31

[80] G. Almeida, J. Brito, P. Perré, Alterations in energy properties of eucalyptus wood and bark subjected to torrefaction: the potential of mass loss as a synthetic indicator, Bioresource technology 101 (24) (2010) 9778–9784. p. 24

[81] J. Zakzeski, P. C. Bruijnincx, A. L. Jongerius, B. M. Weckhuysen, The catalytic valorization of lignin for the production of renewable chemicals, Chemical reviews 110 (6) (2010) 3552–3599. p. 26

[82] A. Demirbas, Relationships between heating value and lignin, moisture, ash and extractive contents of biomass fuels, Energy Exploration & Exploitation 20 (1) (2002) 105–111. p. 26

[83] J. Rencoret, J. Ralph, G. Marques, A. Gutiérrez, A. T. Martínez, j. v. n. p. y. p. Del Río, José C, Structural characterization of lignin isolated from coconut (Cocos nucifera) coir fibers. p. 26, 71

[84] A. E. Harman-Ware, M. Crocker, R. B. Pace, A. Placido, S. Morton, S. DeBolt, Characterization of endocarp biomass and extracted lignin using pyrolysis and spectroscopic methods, BioEnergy Research 8 (1) (2015) 350–368. p. 26, 71

[85] T. P. Vispute, H. Zhang, A. Sanna, R. Xiao, G. W. Huber, Renewable chemical commodity feedstocks from integrated catalytic processing of pyrolysis oils, Science 330 (6008) (2010) 1222–1227. p. 26

[86] A. Zheng, Z. Zhao, S. Chang, Z. Huang, F. He, H. Li, Effect of torrefaction temperature on product distribution from two-staged pyrolysis of biomass, Energy & Fuels 26 (5) (2012) 2968–2974. p. 26, 58

[87] W. Emrich, Handbook of charcoal making: the traditional and industrial methods, Vol. 7, Springer Science & Business Media, 2013. p. 26

[88] J. Bourke, M. Manley-Harris, C. Fushimi, K. Dowaki, T. Nunoura, M. J. Antal, Do all carbonized charcoals have the same chemical structure? 2. A model of the chemical structure of carbonized charcoal, Industrial & Engineering Chemistry Research 46 (18) (2007) 5954–5967. p. 26, 28, 66, 74, 76, 82

[89] K. Mochidzuki, F. Soutric, K. Tadokoro, M. J. Antal, M. Tóth, B. Zelei, G. Várhegyi, Electrical and physical properties of carbonized charcoals, Industrial & Engineering Chemistry Research 42 (21) (2003) 5140–5151. p. 26, 66

[90] P. Basu, Biomass gasification, pyrolysis and torrefaction: practical design and theory, Academic press, 2018. p. 26, 28, 31, 41, 106

[91] D. Özçimen, A. Ersoy-Meriçboyu, Characterization of biochar and bio-oil samples obtained from carbonization of various biomass materials, Renewable Energy 35 (6) (2010) 1319–1324. p. 28

[92] W.-H. Chen, B.-J. Lin, B. Colin, J.-S. Chang, A. Pétrissans, X. Bi, M. Pétrissans, Hygroscopic transformation of woody biomass torrefaction for carbon storage, Applied Energy 231 (2018) 768 – 776. doi:https://doi.org/10.1016/j.apenergy.2018.09.135.
URL http://www.sciencedirect.com/science/article/pii/S0306261918314466 p. 28

[93] M. Pétrissans, P. Gérardin, M. Serraj, et al., Wettability of heat-treated wood, Holzforschung 57 (3) (2003) 301–307. p. 28

[94] Standard Practice for General Techniques of Thermogravimetric Analysis (TGA) Coupled With Infrared Analysis (TGA/IR), Standard, ASTM International, West Conshohocken, PA, www.astm.org (Mar. 2016). p. 28

[95] S. Singh, C. Wu, P. T. Williams, Pyrolysis of waste materials using TGA-MS and TGA-FTIR as complementary characterisation techniques, Journal of Analytical and Applied Pyrolysis 94 (2012) 99–107. p. 28

[96] F. Nsaful, F.-X. Collard, M. Carrier, J. F. Görgens, J. H. Knoetze, Lignocellulose pyrolysis with condensable volatiles quantification by thermogravimetric analysis−Thermal desorption/gas chromatography–mass spectrometry method, Journal of analytical and applied pyrolysis 116 (2015) 86–95. p. 28

[97] J. Cai, D. Xu, Z. Dong, X. Yu, Y. Yang, S. W. Banks, A. V. Bridgwater, Processing thermogravimetric analysis data for isoconversional kinetic analysis of lignocellulosic biomass pyrolysis: Case study of corn stalk, Renewable and Sustainable Energy Reviews 82 (2018) 2705–2715. p. 28

[98] F. Shafizadeh, P. P. Chin, Thermal deterioration of wood, Wood technology: chemical aspects 43 (1977) 57–81. p. 30

[99] C. Di Blasi, Heat, momentum and mass transport through a shrinking biomass particle exposed to thermal radiation, Chemical engineering science 51 (7) (1996) 1121–1132. p. 30

[100] A. Anca-Couce, Reaction mechanisms and multi-scale modelling of lignocellulosic biomass pyrolysis, Progress in Energy and Combustion Science 53 (2016) 41–79. p. 30, 86, 87

[101] S. R. Turns, et al., An introduction to combustion, Vol. 287, McGraw-hill New York, 1996. p. 30, 31, 33, 34, 37, 38, 61

[102] D. Wissmiller, Pyrolysis oil combustion characteristics and exhaust emissions in a swirl-stabilized flame. p. 31

[103] G. L. Borman, K. W. Ragland, Combustion engineering, 1998. p. 31

[104] F. El-Mahallawy, S.-D. Habik, Fundamentals and technology of combustion, Elsevier, 2002. p. 32

[105] G. Andrews, D. Bradley, Determination of burning velocity by double ignition in a closed vessel, Combustion and Flame 20 (1) (1973) 77–89. p. 33

[106] G. Yu, C. K. Law, C. Wu, Laminar flame speeds of hydrocarbon+ air mixtures with hydrogen addition, Combustion and flame 63 (3) (1986) 339–347. p. 33

[107] T. Poinsot, D. Veynante, Theoretical and numerical combustion. 2005, RT Edwards. p. 33

[108] J. T. Farrell, R. Johnston, I. Androulakis, Molecular structure effects on laminar burning velocities at elevated temperature and pressure, SAE transactions (2004) 1404–1425. p. 33

[109] K. P. Somers, J. M. Simmie, F. Gillespie, U. Burke, J. Connolly, W. K. Metcalfe, F. Battin-Leclerc, P. Dirrenberger, O. Herbinet, P.-A. Glaude, et al., A high temperature and atmospheric pressure experimental and detailed chemical kinetic modelling study of 2-methyl furan oxidation, Proceedings of the Combustion Institute 34 (1) (2013) 225–232. p. 33, 34

[110] K. E. Far, F. Parsinejad, H. Metghalchi, Flame structure and laminar burning speeds of jp-8/air premixed mixtures at high temperatures and pressures, Fuel 89 (5) (2010) 1041–1049. p. 33

[111] T. Kitagawa, T. Nakahara, K. Maruyama, K. Kado, A. Hayakawa, S. Kobayashi, Turbulent burning velocity of hydrogen–air premixed propagating flames at elevated pressures, International Journal of Hydrogen Energy 33 (20) (2008) 5842–5849. p. 33

[112] S. Liao, D. Jiang, Z. Huang, K. Zeng, Q. Cheng, Determination of the laminar burning velocities for mixtures of ethanol and air at elevated temperatures, Applied Thermal Engineering 27 (2) (2007) 374–380. p. 33

[113] M. Lawes, M. Ormsby, C. Sheppard, R. Woolley, Variation of turbulent burning rate of methane, methanol, and iso-octane air mixtures with equivalence ratio at elevated pressure, Combust. Sci. and Tech. 177 (7) (2005) 1273–1289. p. 33

[114] R. Amirante, E. Distaso, P. Tamburrano, R. D. Reitz, Laminar flame speed correlations for methane, ethane, propane and their mixtures, and natural gas and gasoline for spark-ignition engine simulations, International Journal of Engine Research 18 (9) (2017) 951–970. p. 33

[115] M. Orain, Y. Hardalupas, Effect of fuel type on equivalence ratio measurements using chemiluminescence in premixed flames, Comptes Rendus Mecanique 338 (5) (2010) 241–254. p. 33

[116] L. Sileghem, V. Alekseev, J. Vancoillie, K. Van Geem, E. J. Nilsson, S. Verhelst, A. Konnov, Laminar burning velocity of gasoline and the gasoline surrogate components iso-octane, n-heptane and toluene, Fuel 112 (2013) 355–365. p. 33, 61

[117] A. H. Lefebvre, W. G. Freeman, L. H. Cowell, Spontaneous ignition delay characteristics of hydrocarbon fuel-air mixtures. p. 34

[118] J. Hernandez, J. Sanz-Argent, J. Carot, J. Jabaloyes, Ignition delay time correlations for a diesel fuel with application to engine combustion modelling, International Journal of Engine Research 11 (3) (2010) 199–206. p. 34

[119] C. Allen, D. Valco, E. Toulson, T. Edwards, T. Lee, Ignition behavior and surrogate modeling of jp-8 and of camelina and tallow hydrotreated renewable jet fuels at low temperatures, Combustion and Flame 160 (2) (2013) 232–239. p. 34

[120] X. Hui, K. Kumar, C.-J. Sung, T. Edwards, D. Gardner, Experimental studies on the combustion characteristics of alternative jet fuels, Fuel 98 (2012) 176–182. p. 34

[121] H. Wang, M. A. Oehlschlaeger, Autoignition studies of conventional and fischer–tropsch jet fuels, Fuel 98 (2012) 249–258. p. 34

[122] Y. Zhu, S. Li, D. F. Davidson, R. K. Hanson, Ignition delay times of conventional and alternative fuels behind reflected shock waves, Proceedings of the Combustion Institute 35 (1) (2015) 241–248. p. 34

[123] M. M. Holton, Autoignition delay time measurements for natural gas fuel components and their mixtures, Ph.D. thesis (2008). p. 34

[124] J. R. Pier, Comparisons of biofuels in high-speed turbine locomotives: Emissions, energy use, and cost, Transportation research record 1691 (1) (1999) 24–32. p. 36

[125] B. Barnwal, M. Sharma, Prospects of biodiesel production from vegetable oils in india, Renewable and sustainable energy reviews 9 (4) (2005) 363–378. p. 36

[126] Y. Sharma, B. Singh, S. Upadhyay, Advancements in development and characterization of biodiesel: a review, Fuel 87 (12) (2008) 2355–2373. p. 36

[127] G. Astbury, A review of the properties and hazards of some alternative fuels, Process safety and environmental protection 86 (6) (2008) 397–414. p. 36

[128] Z. Habib, R. Parthasarathy, S. Gollahalli, Performance and emission characteristics of biofuel in a small-scale gas turbine engine, Applied energy 87 (5) (2010) 1701–1709. p. 36

[129] G. L. Juste, J. S. Monfort, Preliminary test on combustion of wood derived fast pyrolysis oils in a gas turbine combustor, Biomass and Bioenergy 19 (2) (2000) 119–128. p. 36

[130] D. Agarwal, A. K. Agarwal, Performance and emissions characteristics of jatropha oil (preheated and blends) in a direct injection compression ignition engine, Applied thermal engineering 27 (13) (2007) 2314–2323. p. 36

[131] S. Sundarapandian, G. Devaradjane, Theoretical investigation of the performance of vegetable oil operated ci engine for various equivalence ratios, Tech. rep., SAE Technical Paper (2009). p. 36

[132] K. Gupta, A. Rehman, R. Sarviya, Evaluation of soya bio-diesel as a gas turbine fuel, Iranica Journal of Energy & Environment 1 (3) (2010) 205–210. p. 36

[133] M. A. Rendón, M. A. Do Nascimento, P. P. Mendes, Analyzing the impact of using biodiesel in the parameters of a 30 kw micro-turbine control model, in: ASME Turbo Expo 2006: Power for Land, Sea, and Air, American Society of Mechanical Engineers, 2006, pp. 467–476. p. 36

[134] N. Hashimoto, Y. Ozawa, N. Mori, I. Yuri, T. Hisamatsu, Fundamental combustion characteristics of palm methyl ester (pme) as alternative fuel for gas turbines, Fuel 87 (15-16) (2008) 3373–3378. p. 36

[135] V. Lupandin, R. Thamburaj, A. Nikolayev, Test results of the ogt2500 gas turbine engine running on alternative fuels: biooil, ethanol, biodiesel and crude oil, in: ASME Turbo Expo 2005: Power for land, sea, and air, American Society of Mechanical Engineers Digital Collection, 2005, pp. 421–426. p. 36

[136] A. Oasmaa, B. Van De Beld, P. Saari, D. C. Elliott, Y. Solantausta, Norms, standards, and legislation for fast pyrolysis bio-oils from lignocellulosic biomass, Energy & Fuels 29 (4) (2015) 2471–2484. p. 35

[137] N. Darabiha, S. Candel, V. Giovangigli, M. Smooke, Extinction of strained premixed propane-air flames with complex chemistry, Combustion science and technology 60 (4-6) (1988) 267–285. p. 37

[138] C. K. Westbrook, F. L. Dryer, Chemical kinetic modeling of hydrocarbon combustion, Progress in Energy and Combustion Science 10 (1) (1984) 1 – 57. doi:10.1016/0360-1285(84)90118-7.
URL http://www.sciencedirect.com/science/article/pii/0360128584901187 p. 38

[139] S. Candel, D. Thevenin, N. Darabiha, D. Veynante, Progress in numerical combustion, Combustion Science and Technology 149 (1-6) (1999) 297–337. p. 39

[140] M. Stas, D. Kubick, J. Chudoba, M. Pospísil, Overview of analytical methods used for chemical characterization of pyrolysis bio-oil, Energy & Fuels 28 (1) (2014) 385–402. p. 39, 56

[141] J. Lehto, A. Oasmaa, Y. Solantausta, M. Kyto, D. Chiaramonti, Review of fuel oil quality and combustion of fast pyrolysis bio-oils from lignocellulosic

biomass, Applied Energy 116 (2014) 178 – 190. doi:https://doi.org/10.1016/j.apenergy.2013.11.040. p. 39, 118

[142] S. Czernik, A. Bridgwater, Overview of applications of biomass fast pyrolysis oil, Energy & fuels 18 (2) (2004) 590–598. p. 39, 55

[143] A. Oasmaa, D. Meier, Characterisation, analysis, norms & standards, in: Fast pyrolysis of biomass: a handbook, 2005, pp. 19–60. p. 39, 55

[144] M. Wu, S. Yang, Combustion characteristics of multi-component cedar bio-oil/kerosene droplet, Energy 113 (2016) 788 – 795. doi:https://doi.org/10.1016/j.energy.2016.07.097. p. 39

[145] S. Yang, M. Wu, T. Hsu, Experimental and numerical simulation study of oxy-combustion of fast pyrolysis bio-oil from lignocellulosic biomass, Energy 126 (2017) 854 – 867. doi:https://doi.org/10.1016/j.energy.2017.03.084. p. 39

[146] S. Yang, M. Wu, The droplet combustion and thermal characteristics of pinewood bio-oil from slow pyrolysis, Energy 141 (2017) 2377 – 2386. doi:https://doi.org/10.1016/j.energy.2017.11.119. p. 40

[147] T. Maneerung, J. Liew, Y. Dai, S. Kawi, C. Chong, C.-H. Wang, Activated carbon derived from carbon residue from biomass gasification and its application for dye adsorption: kinetics, isotherms and thermodynamic studies, Bioresource technology 200 (2016) 350–359. p. 40, 105

[148] J. L. Figueiredo, J. A. Moulijn, Carbon and coal gasification: science and technology, Vol. 105, Springer Science & Business Media, 2012. p. 40, 42

[149] H. A. Arafat, K. Jijakli, Modeling and comparative assessment of municipal solid waste gasification for energy production, Waste management 33 (8) (2013) 1704–1713. p. 41

[150] C. Higman, M. van der Burgt, Chapter 2 - the thermodynamics of gasification, in: C. Higman, M. van der Burgt (Eds.), Gasification (Second Edition), second edition Edition, Gulf Professional Publishing, Burlington, 2008, pp. 11 – 31. doi:https://doi.org/10.1016/B978-0-7506-8528-3.00002-X. URL http://www.sciencedirect.com/science/article/pii/B978075068528300002X p. 41

[151] C. Higman, M. van der Burgt, Chapter 1 - introduction, in: C. Higman, M. van der Burgt (Eds.), Gasification (Second Edition), second edition Edition, Gulf Professional Publishing, Burlington, 2008, pp. 1 – 9. doi:https://doi.org/10.1016/B978-0-7506-8528-3.00001-8. URL http://www.sciencedirect.com/science/article/pii/B9780750685283000018 p. 41

[152] C. Higman, Chapter 11 - gasification, in: B. G. Miller, D. A. Tillman (Eds.), Combustion Engineering Issues for Solid Fuel Systems, Academic Press, Burlington, 2008, pp. 423 – 468. doi:https://doi.org/10.1016/B978-0-12-373611-6.00011-2. URL http://www.sciencedirect.com/science/article/pii/B9780123736116000112 p. 42

[153] F. Rodriguez-Reinoso, M. Molina-Sabio, Activated carbons from lignocellulosic materials by chemical and/or physical activation: an overview, Carbon 30 (7) (1992) 1111–1118. p. 42

[154] T. J. Hilbers, Z. Wang, B. Pecha, R. J. Westerhof, S. R. Kersten, M. R. Pelaez-Samaniego, M. Garcia-Perez, Cellulose-lignin interactions during slow and fast pyrolysis, Journal of Analytical and Applied Pyrolysis 114 (2015) 197 – 207. doi:http://dx.doi.org/10.1016/j.jaap.2015.05.020.
URL http://www.sciencedirect.com/science/article/pii/S016523701530053X p. 42, 66

[155] C. D. Blasi, Modeling chemical and physical processes of wood and biomass pyrolysis, Progress in Energy and Combustion Science 34 (1) (2008) 47 – 90. doi:http://dx.doi.org/10.1016/j.pecs.2006.12.001.
URL http://www.sciencedirect.com/science/article/pii/S0360128507000214 p. 42, 66, 76, 94

[156] C. D. Blasi, Numerical simulation of cellulose pyrolysis, Biomass and Bioenergy 7 (1) (1994) 87 – 98. doi:http://dx.doi.org/10.1016/0961-9534(94)00040-Z.
URL http://www.sciencedirect.com/science/article/pii/096195349400040Z p. 42, 66

[157] K. S. Markley, Mbocayá or Paraguay coco palm – an important source of oil, Economic Botany 10 (1) (1956) 3–32. p. 46

[158] F. P. d. Amaral, Estudo das características físico-químicas dos óleos da amêndoa e polpa da macaúba [acrocomia aculeata (jacq.) lodd. ex mart]. p. 46

[159] J. d. C. e. SILVA, L. E. G. Barrichelo, J. O. Brito, Endocarpos de babaçu e de macaúba comparados a madeira de eucalyptus grandis para a produção de carvão vegetal, Ipef 34 (1986) 31–34. p. 46, 71, 74, 79

[160] E. S. DE OLIVEIRA, Gaseificação da macaúba., Pós-Graduação de Mestrado em Engenharia de Alimentos, Universidade Estadual do Sudoeste da Bahia. p. 46

[161] T. M. Farias, Biometria e processamento dos frutos da macaúba (acrocomia ssp) para a produção de óleos. p. 46

[162] J. C. del Río, J. Rencoret, A. Gutiérrez, H. Kim, J. Ralph, Hydroxystilbenes are monomers in palm fruit endocarp lignins, Plant physiology 174 (4) (2017) 2072–2082. p. 46

[163] J. Cai, Y. He, X. Yu, S. W. Banks, Y. Yang, X. Zhang, Y. Yu, R. Liu, A. V. Bridgwater, Review of physicochemical properties and analytical characterization of lignocellulosic biomass, Renewable and Sustainable Energy Reviews 76 (2017) 309–322. p. 45, 47, 48

[164] L. Wang, Sustainable bioenergy production, CRC Press, 2014. p. 48

[165] B. Z. Jankovic, M. M. Jankovic, Pyrolysis of pine and beech wood samples under isothermal experimental conditions. the determination of kinetic triplets, Cell Chem Technol 47 (2013) 681–697. p. 50

[166] R. K. Sharma, J. B. Wooten, V. L. Baliga, X. Lin, W. G. Chan, M. R. Hajaligol, Characterization of chars from pyrolysis of lignin, Fuel 83 (11-12) (2004) 1469–1482. doi:10.1016/j.fuel.2003.11.015.
URL http://dx.doi.org/10.1016/j.fuel.2003.11.015 p. 51, 68, 76, 78

[167] Q. Xu, S. Pang, T. Levi, Reaction kinetics and producer gas compositions of steam gasification of coal and biomass blend chars, part 1: Experimental

investigation, Chemical engineering science 66 (10) (2011) 2141–2148. p. 51, 77

[168] S. Brunauer, P. H. Emmett, E. Teller, Adsorption of gases in multimolecular layers, Journal of the American chemical society 60 (2) (1938) 309–319. p. 52

[169] K. S. Sing, Reporting physisorption data for gas/solid systems with special reference to the determination of surface area and porosity (recommendations 1984), Pure and applied chemistry 57 (4) (1985) 603–619. p. 52, 82

[170] D. Chen, Z. Zheng, K. Fu, Z. Zeng, J. Wang, M. Lu, Torrefaction of biomass stalk and its effect on the yield and quality of pyrolysis products, Fuel 159 (2015) 27–32. p. 55

[171] J. Meng, J. Park, D. Tilotta, S. Park, The effect of torrefaction on the chemistry of fast-pyrolysis bio-oil, Bioresource technology 111 (2012) 439–446. p. 55, 59, 121

[172] A. Zheng, Z. Zhao, S. Chang, Z. Huang, X. Wang, F. He, H. Li, Effect of torrefaction on structure and fast pyrolysis behavior of corncobs, Bioresource Technology 128 (2013) 370 – 377. doi:https://doi.org/10.1016/j.biortech.2012.10.067. p. 55, 118

[173] F. Pierre, G. Almeida, J. Colin, P. Perré, Reduction of biomass resilience by torrefaction: apparent stiffness during failure (asf) and specific failure energy (sfe) assessed by a custom impact device, Holzforschung 71 (11) (2017) 863–872. p. 55

[174] D. Meier, New methods for chemical and physical characterization and round robin testing, Fast pyrolysis of biomass: a handbook 1 (1999) 92–101. p. 56

[175] K. Sipilä, E. Kuoppala, L. Fagernäs, A. Oasmaa, Characterization of biomass-based flash pyrolysis oils, Biomass and Bioenergy 14 (2) (1998) 103–113. p. 56

[176] A. Oasmaa, E. Kuoppala, Y. Solantausta, Fast pyrolysis of forestry residue. 2. physicochemical composition of product liquid, Energy & fuels 17 (2) (2003) 433–443. p. 56

[177] S. Coronel, R. Mével, P. Vervish, P. Boettcher, V. Thomas, N. Chaumeix, N. Darabiha, J. Shepherd, Laminar burning speed of n-hexane-air mixtures, in: 8th US National Combustion Meeting 2013, Vol. 3, 2013, pp. 2568–2583. p. 57

[178] D. Alviso, Experimental and numerical characterization of the biodiesel combustion in a counterflow burner, Ph.D. thesis, École Centrale Paris - Universidad Nacional de Asunción (2013). p. 57, 59

[179] C. Marchal, J.-L. Delfau, C. Vovelle, G. Moréac, C. Mounaı, F. Mauss, et al., Modelling of aromatics and soot formation from large fuel molecules, Proceedings of the Combustion Institute 32 (1) (2009) 753–759. p. 57

[180] M. Frenklach, H. Wang, M. J. Rabinowitz, Optimization and analysis of large chemical kinetic mechanisms using the solution mapping method–combustion of methane, Progress in Energy and Combustion Science 18 (1) (1992) 47–73. p. 57

[181] J. M. Simmie, Detailed chemical kinetic models for the combustion of hydrocarbon fuels, Progress in energy and combustion science 29 (6) (2003) 599–634. p. 57

[182] H. Yang, R. Yan, H. Chen, D. H. Lee, C. Zheng, Characteristics of hemicellulose, cellulose and lignin pyrolysis, Fuel 86 (12) (2007) 1781 – 1788. doi:https://doi.org/10.1016/j.fuel.2006.12.013. p. 58, 124

[183] D. Alviso, P. Scouflaire, D. Lacoste, N. Darabiha, J. Rolon, Experimental and numerical characterization of the methyl decanoate combustion in laminar counterflow spray premixed flames, in: ASME Turbo Expo 2013: Turbine Technical Conference and Exposition, American Society of Mechanical Engineers, 2013, pp. V002T03A018–V002T03A018. p. 58

[184] C. J. Mueller, W. J. Cannella, T. J. Bruno, B. Bunting, H. D. Dettman, J. A. Franz, M. L. Huber, M. Natarajan, W. J. Pitz, M. A. Ratcliff, et al., Methodology for formulating diesel surrogate fuels with accurate compositional, ignition-quality, and volatility characteristics, Energy & Fuels 26 (6) (2012) 3284–3303. p. 59

[185] D. Chen, J. Zhou, Q. Zhang, Effects of torrefaction on the pyrolysis behavior and bio-oil properties of rice husk by using tg-ftir and Py-GC/MS, Energy & Fuels 28 (9) (2014) 5857–5863. p. 59, 121

[186] J. Andrae, Comprehensive chemical kinetic modeling of toluene reference fuels oxidation, Fuel 107 (2013) 740 – 748. doi:https://doi.org/10.1016/j.fuel.2013.01.070. p. 59, 61

[187] B. Kerschgens, L. Cai, H. Pitsch, A. Janssen, M. Jakob, S. Pischinger, Surrogate fuels for the simulation of diesel engine combustion of novel biofuels, International Journal of Engine Research 16 (4) (2015) 531–546. p. 59

[188] S. W. Wagnon, S. Thion, E. J. Nilsson, M. Mehl, Z. Serinyel, K. Zhang, P. Dagaut, A. A. Konnov, G. Dayma, W. J. Pitz, Experimental and modeling studies of a biofuel surrogate compound: laminar burning velocities and jet-stirred reactor measurements of anisole, Combustion and Flame 189 (2018) 325–336. p. 59

[189] M. K. Ghosh, M. S. Howard, Y. Zhang, K. Djebbi, G. Capriolo, A. Farooq, H. J. Curran, S. Dooley, The combustion kinetics of the lignocellulosic biofuel, ethyl levulinate, Combustion and Flame 193 (2018) 157–169. p. 59

[190] N. Darabiha, S. Candel, V. Giovangigli, M. Smooke, Extinction of strained premixed propane-air flames with complex chemistry, Combustion Science and Technology 60 (1988) 267 – 285. p. 60, 61, 63, 119, 130

[191] B. Franzelli, B. Fiorina, N. Darabiha, A tabulated chemistry method for spray combustion, Proceedings of the Combustion Institute 34 (1) (2013) 1659 – 1666. p. 60, 119, 130

[192] W. H. Press, S. A. Teukolsky, B. P. Flannery, W. T. Vetterling, Numerical recipes in Fortran 77: volume 1, volume 1 of Fortran numerical recipes: the art of scientific computing, Cambridge university press, 1992. p. 61

[193] E. Ranzi, A. Frassoldati, R. Grana, A. Cuoci, T. Faravelli, A. Kelley, Hierarchical and comparative kinetic modeling of laminar flame speeds of hydrocarbon and oxygenated fuels, Prog. Energy Combust. Sci. 38 (2012) 468–501. p. 61

[194] H. Takashi, T. Kimitoshi, Laminar flame speeds of ethanol, n-heptane, isooctane air mixture. department of mechanical engineering, Oita University, Japan. p. 61

[195] P. Versaevel, Combustion laminaire diphasique: Etude theorique et experimentale, PhD. thesis, Ecole Centrale Paris. p. 62

[196] M. Ikura, M. Stanciulescu, E. Hogan, Emulsification of pyrolysis derived bio-oil in diesel fuel, Biomass and Bioenergy 24 (3) (2003) 221 – 232. doi:https://doi.org/10.1016/S0961-9534(02)00131-9. p. 63, 118

[197] P. Weerachanchai, C. Tangsathitkulchai, M. Tangsathitkulchai, Phase behaviors and fuel properties of bio-oil-diesel-alcohol blends, World Academy of Science, Engineering and Technology 56 (2009) 387 – 393. p. 63, 118

[198] N. Darabiha, F. Lacas, J. Rolon, S. Candel, Laminar counterflow spray diffusion flames: A comparison between experimental results and complex chemistry calculations, Combustion and Flame 95 (3) (1993) 261 – 275. doi:10.1016/0010-2180(93)90131-L.
URL http://www.sciencedirect.com/science/article/pii/001021809390131L p. 63, 119, 130

[199] B. Franzelli, B. Fiorina, N. Darabiha, A tabulated chemistry method for spray combustion, Proceedings of the Combustion Institute 34 (1) (2013) 1659 – 1666. doi:http://dx.doi.org/10.1016/j.proci.2012.06.013.
URL http://www.sciencedirect.com/science/article/pii/S1540748912001216 p. 63

[200] M. Keiluweit, P. S. Nico, M. G. Johnson, M. Kleber, Dynamic molecular structure of plant biomass-derived black carbon (biochar), Environmental Science & Technology 44 (4) (2010) 1247–1253. p. 66

[201] G. Almeida, J. Brito, P. Perré, Alterations in energy properties of eucalyptus wood and bark subjected to torrefaction: The potential of mass loss as a synthetic indicator, Bioresource Technology 101 (24) (2010) 9778 – 9784. doi:http://dx.doi.org/10.1016/j.biortech.2010.07.026.
URL http://www.sciencedirect.com/science/article/pii/S0960852410012149 p. 67

[202] C. Couhert, J.-M. Commandre, S. Salvador, Is it possible to predict gas yields of any biomass after rapid pyrolysis at high temperature from its composition in cellulose, hemicellulose and lignin?, Fuel 88 (3) (2009) 408–417. doi:10.1016/j.fuel.2008.09.019.
URL http://dx.doi.org/10.1016/j.fuel.2008.09.019 p. 68

[203] A. Gani, I. Naruse, Effect of cellulose and lignin content on pyrolysis and combustion characteristics for several types of biomass, Renewable Energy 32 (4) (2007) 649–661. doi:10.1016/j.renene.2006.02.017.
URL http://dx.doi.org/10.1016/j.renene.2006.02.017 p. 68, 71

[204] D. Lv, M. Xu, X. Liu, Z. Zhan, Z. Li, H. Yao, Effect of cellulose, lignin, alkali and alkaline earth metallic species on biomass pyrolysis and gasification, Fuel Processing Technology 91 (8) (2010) 903–909. doi:10.1016/j.fuproc.2009.09.014.
URL http://dx.doi.org/10.1016/j.fuproc.2009.09.014 p. 68

[205] C. A. S. Hill, J. Ramsay, B. Keating, K. Laine, L. Rautkari, M. Hughes, B. Constant, The water vapour sorption properties of thermally modified and densified wood, Journal of Materials Science 47 (7) (2012) 3191–3197. doi:10.1007/s10853-011-6154-8.
URL http://dx.doi.org/10.1007/s10853-011-6154-8 p. 69

[206] J. Wannapeera, B. Fungtammasan, N. Worasuwannarak, Effects of temperature and holding time during torrefaction on the pyrolysis behaviors of woody biomass, Journal of Analytical and Applied Pyrolysis 92 (1) (2011) 99 – 105. doi:http://dx.doi.org/10.1016/j.jaap.2011.04.010.
URL http://www.sciencedirect.com/science/article/pii/S0165237011000805 p. 70

[207] M. J. Prins, K. J. Ptasinski, F. J. Janssen, Torrefaction of wood: Part 2. analysis of products, Journal of Analytical and Applied Pyrolysis 77 (1) (2006) 35 – 40. doi:http://dx.doi.org/10.1016/j.jaap.2006.01.001.
URL http://www.sciencedirect.com/science/article/pii/S0165237006000167 p. 70

[208] A. G. Bradbury, Y. Sakai, F. Shafizadeh, A kinetic model for pyrolysis of cellulose, Journal of Applied Polymer Science 23 (11) (1979) 3271–3280. p. 70

[209] J. Piskorz, D. S. A. Radlein, D. S. Scott, S. Czernik, Pretreatment of wood and cellulose for production of sugars by fast pyrolysis, Journal of Analytical and Applied Pyrolysis 16 (2) (1989) 127–142. p. 70

[210] J. L. Banyasz, S. Li, J. L. Lyons-Hart, K. H. Shafer, Cellulose pyrolysis: the kinetics of hydroxyacetaldehyde evolution, Journal of Analytical and Applied Pyrolysis 57 (2) (2001) 223–248. p. 70

[211] E. Jakab, Chapter 3 - Analytical Techniques as a Tool to Understand the Reaction Mechanism, in: A. Pandey, T. Bhaskar, M. Stocker, R. K. Sukumaran (Eds.), Recent Advances in Thermo-Chemical Conversion of Biomass, Elsevier, Boston, 2015, pp. 75 – 108. doi:http://dx.doi.org/10.1016/B978-0-444-63289-0.00003-X.
URL http://www.sciencedirect.com/science/article/pii/B978044463289000003X p. 71, 99

[212] P. Lv, G. Almeida, P. Perré, TGA-FTIR Analysis of Torrefaction of Lignocellulosic Components (cellulose, xylan, lignin) in Isothermal Conditions over a Wide Range of Time Durations, BioResources 10 (3) (2015) 4239–4251. p. 71, 99

[213] H. Yang, R. Yan, H. Chen, D. H. Lee, C. Zheng, Characteristics of hemicellulose, cellulose and lignin pyrolysis, Fuel 86 (12-13) (2007) 1781–1788. doi:10.1016/j.fuel.2006.12.013.
URL http://dx.doi.org/10.1016/j.fuel.2006.12.013 p. 71

[214] V. Mendu, A. E. Harman-Ware, M. Crocker, J. Jae, J. Stork, S. Morton, A. Placido, G. Huber, S. DeBolt, Identification and thermochemical analysis of high-lignin feedstocks for biofuel and biochemical production, Biotechnology for biofuels 4 (1) (2011) 43. p. 71

[215] J. Ralph, Hydroxycinnamates in lignification, Phytochemistry Reviews 9 (1) (2010) 65–83. p. 71

[216] P. H. G. Cademartori, P. S. d. Santos, L. Serrano, J. Labidi, D. A. Gatto, Effect of thermal treatment on physicochemical properties of gympie messmate wood, Industrial Crops and Products 45 (2013) 360–366. doi:10.1016/j.indcrop.2012.12.048.
URL http://dx.doi.org/10.1016/j.indcrop.2012.12.048 p. 71

[217] T. Sonobe, N. Worasuwannarak, Kinetic analyses of biomass pyrolysis using the distributed activation energy model, Fuel 87 (3) (2008) 414–421. p. 71

[218] M. I. Al-Wabel, A. Al-Omran, A. H. El-Naggar, M. Nadeem, A. R. Usman, Pyrolysis temperature induced changes in characteristics and chemical composition of biochar produced from conocarpus wastes, Bioresource technology 131 (2013) 374–379. p. 74

[219] S. Yaman, Pyrolysis of biomass to produce fuels and chemical feedstocks, Energy conversion and management 45 (5) (2004) 651–671. p. 74

[220] M. J. Antal, E. Croiset, X. Dai, C. DeAlmeida, W. S.-L. Mok, N. Norberg, J.-R. Richard, M. Al Majthoub, High-yield biomass charcoal, Energy & Fuels 10 (3) (1996) 652–658. p. 74, 75

[221] L. Wang, M. Trninic, Ø. Skreiberg, M. Gronli, R. Considine, M. J. Antal Jr, Is elevated pressure required to achieve a high fixed-carbon yield of charcoal from biomass? part 1: Round-robin results for three different corncob materials, Energy & Fuels 25 (7) (2011) 3251–3265. p. 74

[222] L. Wang, Ø. Skreiberg, M. Gronli, G. P. Specht, M. J. Antal Jr, Is elevated pressure required to achieve a high fixed-carbon yield of charcoal from biomass? part 2: The importance of particle size, Energy & Fuels 27 (4) (2013) 2146–2156. p. 74

[223] J. J. Chew, V. Doshi, Recent advances in biomass pretreatment–torrefaction fundamentals and technology, Renewable and Sustainable Energy Reviews 15 (8) (2011) 4212–4222. p. 74

[224] S. Cavagnol, J. F. Roesler, E. Sanz, W. Nastoll, P. Lu, P. Perré, Exothermicity in wood torrefaction and its impact on product mass yields: From micro to pilot scale, The Canadian Journal of Chemical Engineering 93 (2) (2015) 331–339. p. 74

[225] W. Willems, C. Mai, H. Militz, Thermal wood modification chemistry analysed using van krevelen's representation, International Wood Products Journal 4 (3) (2013) 166–171. p. 76

[226] V. Baliga, R. Sharma, D. Miser, T. McGrath, M. Hajaligol, Physical characterization of pyrolyzed tobacco and tobacco components, Journal of Analytical and Applied Pyrolysis 66 (1âĂŞ2) (2003) 191 – 215. doi:http://dx.doi.org/10.1016/S0165-2370(02)00114-6.
URL http://www.sciencedirect.com/science/article/pii/S0165237002001146 p. 76

[227] Y. Zhang, S. Kajitani, M. Ashizawa, K. Miura, Peculiarities of rapid pyrolysis of biomass covering medium-and high-temperature ranges, Energy & fuels 20 (6) (2006) 2705–2712. p. 76

[228] D. Dayton, A review of the literature on catalytic biomass tar destruction, US DOE NREL Report Golden, CO (2002) 510–32815. p. 76

[229] C. A. Hill, A. N. Papadopoulos, A review of methods used to determine the size of the cell wall microvoids of wood, Journal-Institute of Wood Science 15 (6; ISSU 90) (2001) 337–345. p. 77, 82

[230] H. C. Mazzottini-dos Santos, L. M. Ribeiro, M. O. Mercadante-Simões, B. F. Sant'Anna-Santos, Ontogenesis of the pseudomonomerous fruits of Acrocomia aculeata (Arecaceae): a new approach to the development of pyrenarium fruits, Trees 29 (1) (2015) 199–214. doi:10.1007/s00468-014-1104-0. URL http://dx.doi.org/10.1007/s00468-014-1104-0 p. 78, 86

[231] E. T. Engelund, L. G. Thygesen, S. Svensson, C. A. S. Hill, A critical discussion of the physics of woodâĂŞwater interactions, Wood Science and Technology 47 (1) (2013) 141–161. doi:10.1007/s00226-012-0514-7. URL http://dx.doi.org/10.1007/s00226-012-0514-7 p. 79

[232] S. Brunauer, L. S. Deming, W. E. Deming, E. Teller, On a theory of the van der waals adsorption of gases, Journal of the American Chemical Society 62 (7) (1940) 1723–1732. p. 80

[233] Z. Jalaludin, C. A. Hill, Y. Xie, H. W. Samsi, H. Husain, K. Awang, S. F. Curling, Analysis of the water vapour sorption isotherms of thermally modified acacia and sesendok, Wood Material Science and Engineering 5 (3-4) (2010) 194–203. p. 81

[234] C. A. S. Hill, A. Norton, G. Newman, The water vapor sorption behavior of natural fibers, Journal of Applied Polymer Science 112 (3) (2009) 1524–1537. doi:10.1002/app.29725. URL http://dx.doi.org/10.1002/app.29725 p. 82

[235] W. Pattaraprakorn, R. Nakamura, T. Aida, H. Niiyama, Adsorption of CO_2 and N_2 onto charcoal treated at different temperatures, Journal of Chemical Engineering of Japan 38 (5) (2005) 366–372. p. 82

[236] A. Harding, N. Foley, P. Norman, D. Francis, K. Thomas, Diffusion barriers in the kinetics of water vapor adsorption/desorption on activated carbons, Langmuir 14 (14) (1998) 3858–3864. p. 82

[237] P. Lodewyckx, The effect of water uptake in ultramicropores on the adsorption of water vapour in activated carbon, Carbon 48 (9) (2010) 2549–2553. p. 82

[238] S. Duarte, P. Lv, G. Almeida, J. C. Rolón, P. Perre, Alteration of physicochemical characteristics of coconut endocarp–acrocomia aculeata–by isothermal pyrolysis in the range 250–550 °C, Journal of Analytical and Applied Pyrolysis 126 (2017) 88–98. p. 86, 118

[239] S. Vyazovkin, Isoconversional kinetics of thermally stimulated processes, Springer, 2015. p. 86

[240] S. Cavagnol, E. Sanz, W. Nastoll, J. F. Roesler, V. Zymla, P. Perré, Inverse analysis of wood pyrolysis with long residence times in the temperature range 210–290 c: Selection of multi-step kinetic models based on mass loss residues, Thermochimica acta 574 (2013) 1–9. p. 87, 88, 89, 90, 91, 92, 94, 154, 162

[241] J. Cai, W. Wu, R. Liu, An overview of distributed activation energy model and its application in the pyrolysis of lignocellulosic biomass, Renewable and Sustainable Energy Reviews 36 (2014) 236–246. p. 87, 90, 91, 95

[242] W. W. Wendlandt, Thermal analysis, Vol. 19, Wiley-Interscience, 1986. p. 88

[243] G. Varhegyi, E. Jakab, M. J. Antal Jr, Is the broido-shafizadeh model for cellulose pyrolysis true?, Energy & fuels 8 (6) (1994) 1345–1352. p. 88, 92

[244] J. Cai, W. Wu, R. Liu, G. W. Huber, A distributed activation energy model for the pyrolysis of lignocellulosic biomass, Green Chem. 15 (2013) 1331–1340. doi:10.1039/C3GC36958G.
URL http://dx.doi.org/10.1039/C3GC36958G p. 88

[245] G. Várhegyi, H. Chen, S. Godoy, Thermal decomposition of wheat, oat, barley, and brassica carinata straws. a kinetic study, Energy & Fuels 23 (2) (2009) 646–652. arXiv:https://doi.org/10.1021/ef800868k, doi:10.1021/ef800868k.
URL https://doi.org/10.1021/ef800868k p. 88

[246] E. Suuberg, Approximate solution technique for nonisothermal, Gaussian distributed activation energy models, Combustion and Flame 50 (1983) 243–245. p. 90

[247] J. Cai, C. Jin, S. Yang, Y. Chen, Logistic distributed activation energy model–part 1: Derivation and numerical parametric study, Bioresource technology 102 (2) (2011) 1556–1561. p. 90

[248] L. Kolar-Anić, S. Veljković, S. Kapor, B. Dubljević, Weibull distribution and kinetics of heterogeneous processes, The Journal of Chemical Physics 63 (2) (1975) 663–668. p. 90

[249] L. Kolar-Anić, S. Veljković, Statistical foundations of heterogeneous kinetics, The Journal of Chemical Physics 63 (2) (1975) 669–673. p. 90

[250] A. K. Burnham, R. L. Braun, Global kinetic analysis of complex materials, Energy & Fuels 13 (1) (1999) 1–22. p. 90

[251] S. Vyazovkin, A. K. Burnham, L. Favergeon, N. Koga, E. Moukhina, L. A. Pérez-Maqueda, N. Sbirrazzuoli, Ictac kinetics committee recommendations for analysis of multi-step kinetics, Thermochimica Acta (2020) 178597. p. 90

[252] T. Mani, P. Murugan, N. Mahinpey, Determination of distributed activation energy model kinetic parameters using simulated annealing optimization method for nonisothermal pyrolysis of lignin, Industrial & Engineering Chemistry Research 48 (3) (2009) 1464–1467. p. 90

[253] J. Cai, R. Liu, New distributed activation energy model: numerical solution and application to pyrolysis kinetics of some types of biomass, Bioresource technology 99 (8) (2008) 2795–2799. p. 91

[254] J. Cai, W. Wu, R. Liu, G. W. Huber, A distributed activation energy model for the pyrolysis of lignocellulosic biomass, Green Chemistry 15 (5) (2013) 1331–1340. p. 98, 99

[255] G. Várhegyi, B. Bobály, E. Jakab, H. Chen, Thermogravimetric study of biomass pyrolysis kinetics. a distributed activation energy model with prediction tests, Energy & Fuels 25 (1) (2011) 24–32. p. 99

[256] Ö. Şahin, C. Saka, A. A. Ceyhan, O. Baytar, Preparation of high surface area activated carbon from elaeagnus angustifolia seeds by chemical activation with zncl2 in one-step treatment and its iodine adsorption, Separation Science and Technology 50 (6) (2015) 886–891. p. 105

[257] L. Rong, T. Maneerung, J. C. Ng, K. G. Neoh, B. H. Bay, Y. W. Tong, Y. Dai, C.-H. Wang, Co-gasification of sewage sludge and woody biomass in a fixed-bed downdraft gasifier: toxicity assessment of solid residues, Waste management 36 (2015) 241–255. p. 105

[258] M. Barrio, B. Gøbel, H. Risnes, U. Henriksen, J. Hustad, L. Sørensen, Steam gasification of wood char and the effect of hydrogen inhibition on the chemical kinetics, Progress in thermochemical biomass conversion 1 (2001) 32–46. p. 106

[259] R. F. Probstein, R. E. Hicks, Synthetic fuels, Courier Corporation, 2006. p. 106

[260] V. Minkova, S. Marinov, R. Zanzi, E. Björnbom, T. Budinova, M. Stefanova, L. Lakov, Thermochemical treatment of biomass in a flow of steam or in a mixture of steam and carbon dioxide, Fuel Processing Technology 62 (1) (2000) 45–52. p. 106

[261] D. Savova, E. Apak, E. Ekinci, F. Yardim, N. Petrov, T. Budinova, M. Razvigorova, V. Minkova, Biomass conversion to carbon adsorbents and gas, Biomass and Bioenergy 21 (2) (2001) 133–142. p. 106

[262] P. Giudicianni, G. Cardone, R. Ragucci, Cellulose, hemicellulose and lignin slow steam pyrolysis: Thermal decomposition of biomass components mixtures, Journal of Analytical and Applied Pyrolysis 100 (2013) 213–222. p. 106

[263] L. Khezami, A. Chetouani, B. Taouk, R. Capart, Production and characterisation of activated carbon from wood components in powder: cellulose, lignin, xylan, Powder Technology 157 (1-3) (2005) 48–56. p. 106

[264] E. P. Önal, B. B. Uzun, A. E. Pütün, Steam pyrolysis of an industrial waste for bio-oil production, Fuel Processing Technology 92 (5) (2011) 879–885. p. 107

[265] A. E. Pütün, E. Apaydin, E. Pütün, Bio-oil production from pyrolysis and steam pyrolysis of soybean-cake: product yields and composition, Energy 27 (7) (2002) 703–713. p. 107

[266] V. Minkova, M. Razvigorova, E. Bjornbom, R. Zanzi, T. Budinova, N. Petrov, Effect of water vapour and biomass nature on the yield and quality of the pyrolysis products from biomass, Fuel Processing Technology 70 (1) (2001) 53–61. p. 107, 110

[267] D. K. Seo, S. S. Park, Y. T. Kim, J. Hwang, T.-U. Yu, Study of coal pyrolysis by thermo-gravimetric analysis (tga) and concentration measurements of the evolved species, Journal of Analytical and Applied Pyrolysis 92 (1) (2011) 209–216. p. 108

[268] K. Jayaraman, I. Gokalp, Thermogravimetric and evolved gas analyses of high ash indian and turkish coal pyrolysis and gasification, Journal of Thermal Analysis and Calorimetry 121 (2) (2015) 919–927. p. 109

[269] D. R. Mehandjiev, R. N. Nickolov, R. B. Ioncheva, Determination of nitrogen structures on activated carbon surfaces by a chemical method, Fuel 76 (5) (1997) 381–384. p. 110

[270] R. Nickolov, D. Mehandjiev, Application of the simplified equation for micropore size distribution to the study of water vapour adsorption on activated carbon, Adsorption Science & Technology 12 (3) (1995) 203–209. p. 110

[271] F. Mermoud, F. Golfier, S. Salvador, L. Van de Steene, J.-L. Dirion, Experimental and numerical study of steam gasification of a single charcoal particle, Combustion and flame 145 (1-2) (2006) 59–79. p. 112

[272] H. Fatehi, X.-S. Bai, Structural evolution of biomass char and its effect on the gasification rate, Applied Energy 185 (2017) 998–1006. p. 112, 113

[273] W. M. A. W. Daud, W. S. W. Ali, Comparison on pore development of activated carbon produced from palm shell and coconut shell, Bioresource Technology 93 (1) (2004) 63 – 69. doi:https://doi.org/10.1016/j.biortech.2003.09.015.
URL http://www.sciencedirect.com/science/article/pii/S0960852403002955 p. 113

[274] Z. Hu, M. P. Srinivasan, Y. Ni, Preparation of mesoporous high-surface-area activated carbon, Advanced materials 12 (1) (2000) 62–65. p. 113

[275] J. Meng, J. Park, D. Tilotta, S. Park, The effect of torrefaction on the chemistry of fast-pyrolysis bio-oil, Bioresource Technology 111 (2012) 439 – 446. doi:https://doi.org/10.1016/j.biortech.2012.01.159. p. 118

[276] R. Brown, Thermochemical processing of biomass: conversion into fuels, chemicals and power, Chichester: John Wiley Sons, Ltd. p. 118

[277] A. Bridgwater, Upgrading fast pyrolysis liquids, Brown RC, editor. Thermochem. process. biomass convers. into fuels, chem. power. Chichester: John Wiley Sons, Ltd (2011) 99 – 157. p. 118

[278] A. Krutof, K. Hawboldt, Blends of pyrolysis oil, petroleum, and other bio-based fuels: A review, Renewable and Sustainable Energy Reviews 59 (2016) 406 – 419. doi:https://doi.org/10.1016/j.rser.2015.12.304. p. 118

[279] D. Nguyen, D. Honnery, Combustion of bio-oil ethanol blends at elevated pressure, Fuel 87 (2) (2008) 232 – 243. doi:https://doi.org/10.1016/j.fuel.2007.04.023. p. 119

[280] D. Alviso, J. Rolon, P. Scouflaire, N. Darabiha, Experimental and numerical studies of biodiesel combustion mechanisms using a laminar counterflow spray premixed flame, Fuel 153 (2015) 154 – 165. doi:http://dx.doi.org/10.1016/j.fuel.2015.02.079. p. 119, 130

[281] D. Alviso, F. Krauch, R. Roman, H. Maldonado, R. G. dos Santos, J. Rolon, N. Darabiha, Development of a diesel-biodiesel-ethanol combined chemical scheme and analysis of reactions pathways, Fuel 191 (2017) 411–426. p. 119, 130

[282] Grupo cavallaro s.a.c.i., https://www.cavallaro.com.py/. p. 119

[283] M. Stas, D. Kubicka, J. Chudoba, M. P. sil, Overview of analytical methods used for chemical characterization of pyrolysis bio-oil, Energy & Fuels 28 (1) (2014) 385–402. arXiv:https://doi.org/10.1021/ef402047y, doi:10.1021/ef402047y.
URL https://doi.org/10.1021/ef402047y p. 121

[284] K. Sipila, E. Kuoppala, L. Fagernas, A. Oasmaa, Characterization of biomass-based flash pyrolysis oils, Biomass and Bioenergy 14 (2) (1998) 103 – 113. doi:https://doi.org/10.1016/S0961-9534(97)10024-1. p. 121

[285] A. Oasmaa, E. Kuoppala, Y. Solantausta, Fast pyrolysis of forestry residue. 2. physicochemical composition of product liquid, Energy & Fuels 17 (2) (2003) 433–443. arXiv:https://doi.org/10.1021/ef020206g, doi:10.1021/ef020206g.
URL https://doi.org/10.1021/ef020206g p. 121

[286] A. Zheng, Z. Zhao, S. Chang, Z. Huang, F. He, H. Li, Effect of torrefaction temperature on product distribution from two-staged pyrolysis of biomass, Energy & Fuels 26 (5) (2012) 2968–2974. arXiv:https://doi.org/10.1021/ef201872y, doi:10.1021/ef201872y.
URL https://doi.org/10.1021/ef201872y p. 124

[287] E. Kantarelis, W. Yang, W. Blasiak, Production of liquid feedstock from biomass via steam pyrolysis in a fluidized bed reactor, Energy & Fuels 27 (8) (2013) 4748–4759. arXiv:https://doi.org/10.1021/ef400580x, doi:10.1021/ef400580x.
URL https://doi.org/10.1021/ef400580x p. 124

[288] M. Mehl, O. Herbinet, P. Dirrenberger, R. Bounaceur, P.-A. Glaude, F. Battin-Leclerc, W. J. Pitz, Experimental and modeling study of burning velocities for alkyl aromatic components relevant to diesel fuels, Proceedings of the Combustion Institute 35 (1) (2015) 341 – 348. doi:https://doi.org/10.1016/j.proci.2014.06.064. p. 125

[289] J. L. Emdee, K. Brezinsky, I. Glassman, A kinetic model for the oxidation of toluene near 1200 k, The Journal of Physical Chemistry 96 (5) (1992) 2151–2161. arXiv:https://doi.org/10.1021/j100184a025, doi:10.1021/j100184a025.
URL https://doi.org/10.1021/j100184a025 p. 125

[290] R. P. Lindstedt, L. Q. Maurice, Detailed kinetic modelling of toluene combustion, Combustion Science and Technology 120 (1-6) (1996) 119–167. arXiv:https://doi.org/10.1080/00102209608935571, doi:10.1080/00102209608935571.
URL https://doi.org/10.1080/00102209608935571 p. 125, 127

[291] P. Dagaut, G. Pengloan, A. Ristori, Oxidation, ignition and combustion of toluene: Experimental and detailed chemical kinetic modeling, Phys. Chem. Chem. Phys. 4 (2002) 1846–1854. doi:10.1039/B110282F.
URL http://dx.doi.org/10.1039/B110282F p. 126, 127

[292] W. K. Metcalfe, S. Dooley, F. L. Dryer, Comprehensive detailed chemical kinetic modeling study of toluene oxidation, Energy & Fuels 25 (11) (2011) 4915–4936. arXiv:https://doi.org/10.1021/ef200900q, doi:10.1021/ef200900q.
URL https://doi.org/10.1021/ef200900q p. 126, 127

[293] L. Cai, H. Pitsch, Optimized chemical mechanism for combustion of gasoline surrogate fuels, Combustion and Flame 162 (5) (2015) 1623 – 1637. doi:http://dx.doi.org/10.1016/j.combustflame.2014.11.018. p. 126, 127

[294] R. Sivaramakrishnan, R. S. Tranter, K. Brezinsky, High pressure pyrolysis of toluene. 1. experiments and modeling of toluene decomposition, The Journal of Physical Chemistry A 110 (30) (2006) 9388–9399, pMID: 16869688.

arXiv:https://doi.org/10.1021/jp060820j, doi:10.1021/jp060820j.
URL https://doi.org/10.1021/jp060820j p. 127

[295] M. Colket, D. Seery, Reaction mechanisms for toluene pyrolysis, Symposium (International) on Combustion 25 (1) (1994) 883 – 891, twenty-Fifth Symposium (International) on Combustion. doi:https://doi.org/10.1016/S0082-0784(06)80723-X. p. 127

[296] J. L. Emdee, K. Brezinsky, I. Glassman, A kinetic model for the oxidation of toluene near 1200 k, The Journal of Physical Chemistry 96 (5) (1992) 2151–2161. arXiv:https://doi.org/10.1021/j100184a025, doi:10.1021/j100184a025.
URL https://doi.org/10.1021/j100184a025 p. 127

[297] N. Leplat, J. Vandooren, Numerical and experimental study of the combustion of acetic acid in laminar premixed flames, Combustion and Flame 159 (2) (2012) 493 – 499. doi:https://doi.org/10.1016/j.combustflame.2011.08.007. p. 127, 128

[298] N. M. Marinov, A detailed chemical kinetic model for high temperature ethanol oxidation, shock 3 (2) (1999) 257–263. p. 127, 128

[299] P. Saxena, F. A. Williams, Numerical and experimental studies of ethanol flames, Proceedings of the Combustion Institute 31 (1) (2007) 1149–1156. p. 127, 128

[300] L. Cancino, M. Fikri, A. Oliveira, C. Schulz, Measurement and chemical kinetics modeling of shock-induced ignition of ethanol- air mixtures, Energy & Fuels 24 (5) (2010) 2830–2840. p. 127, 128

[301] N. Leplat, P. Dagaut, C. Togbé, J. Vandooren, Numerical and experimental study of ethanol combustion and oxidation in laminar premixed flames and in jet-stirred reactor, Combustion and Flame 158 (4) (2011) 705–725. p. 127, 128

[302] X. Zhen, Y. Wang, D. Liu, An overview of the chemical reaction mechanisms for gasoline surrogate fuels, Applied Thermal Engineering 124 (2017) 1257 – 1268. doi:https://doi.org/10.1016/j.applthermaleng.2017.06.101. p. 126

[303] J. Hernandez, J. Sanz-Argent, J. Benajes, S. Molina, Selection of a diesel fuel surrogate for the prediction of auto-ignition under {HCCI} engine conditions, Fuel 87 (6) (2008) 655 – 665. doi:http://dx.doi.org/10.1016/j.fuel.2007.05.019. p. 146

[304] J. J. Hernandez, J. Sanz-Argent, E. Monedero-Villalba, A reduced chemical kinetic mechanism of a diesel fuel surrogate (n-heptane/toluene) for {HCCI} combustion modelling, Fuel 133 (2014) 283 – 291. doi:http://dx.doi.org/10.1016/j.fuel.2014.05.029. p. 146

[305] J. Luo, M. Yao, H. Liu, B. Yang, Experimental and numerical study on suitable diesel fuel surrogates in low temperature combustion conditions, Fuel 97 (2012) 621 – 629. doi:http://dx.doi.org/10.1016/j.fuel.2012.02.057. p. 146